Large Space Systems Technology - 1980

Volume II - Base Technology

NASA

Large Space Systems Technology - 1980

Volume II - Base Technology

Compiled by
Frank Kopriver III
Systems Management Associates
Hampton, Virginia

PREFACE

This publication is a compilation of the papers presented at the Second Annual Large Space Systems Technology (LSST) Technical Review conducted at NASA Langley Research Center on November 18-20, 1980. The Review provided personnel of government, university, and industry with an opportunity to exchange information, to assess the present status of technology developments on the LSST Program, and to plan the development of new technology for large space systems.

The papers describe technological or developmental efforts that were accomplished during Fiscal Year 1980 in support of the LSST Program and were prepared by those in government, university, and industry who performed the work. These papers were divided into three major areas of interest: (1) technology pertinent to large antenna systems, (2) technology related to large space systems, and (3) activities that support both antenna and platform systems.

This publication is divided into two volumes. Volume I, entitled "Systems Technology", includes research activities sponsored through the LSST Program Office. Volume II, entitled "Base Technology", covers research activities sponsored through the Materials and Structures Section, Research and Technology Division, of the Office of Aeronautics and Space Technology.

This compilation provides the participants and their organizations with the papers presented at the Review in a referenceable format. Also, users of large space systems technology can follow the development progress with this document along with proceedings of previous and future LSST Technical Reviews. (See NASA CP-2118, 1980.) The LSST Program Office, Langley Research Center, which hosted the Review, will use this information as an aid in measuring performance and in planning future tasks. The historical background of the LSST Program is given in the introduction to NASA CP-2035, 1978, which covers a NASA/industry seminar that provided ideas and plans to the Program Office for its initial year of operation.

This publication was expedited and enhanced through the efforts of the staff of the Scientific and Technical Information Programs Division, Langley Research Center.

The use of trade names or manufacturer's names in this publication does not constitute endorsement, either expressed or implied, by the National Aeronautics and Space Administration.

CONTENTS

VOLUME I – SYSTEMS TECHNOLOGY*

*Contents for Volume I is included for convenience.

VOLUME II - BASE TECHNOLOGY

SUPPORTING ACTIVITIES

SPACE PLATFORMS

SPACE ANTENNAS

BASE TECHNOLOGY OVERVIEW

Michael F. Card
NASA Langley Research Center
Hampton, Virginia

Large Space Systems Technology - 1980
Second Annual Technical Review
November 1980

BASE TECHNOLOGY OVERVIEW

Michael F. Card
NASA Langley Research Center

The work reported in this volume has been sponsored by the Materials and Structures Division of NASA's Office of Aeronautics and Space Technology. It represents work on base technology for large space structures. As the illustration indicates, the work in the structures area is very broad and is focused on development of various options for spacecraft building blocks. The effort has included development of advanced concepts for deployable or erectable platforms and antennas, and has involved both analysis and test of structural member, joints and subcomponents.

The role of base activities in large space structures is to cultivate longer range ideas and explore high-risk/high-payoff areas. In doing so, new configurations often pose new technical problems which require advanced analysis techniques to provide insight into structural response. Further, there is usually a need to provide baseline materials and structures data to confirm analysis and provide standards of comparison. Finally, a major role of base technology studies is to generate an in-depth understanding and perspective on competing ideas, so they may be brought into technical focus.

In this status report of ongoing base research, materials data on the durability of composite materials will be presented. Structural studies on loads in deployable trusses, results of sizing studies of large generic truss structures and new perspectives on concepts for large, accurate antenna reflectors will be reviewed. In addition, new theoretical results will be presented for buckling and vibration of lattice structures, as well as preliminary studies of damping augmentation and adaptive control of large structures.

SPACECRAFT BUILDING BLOCKS
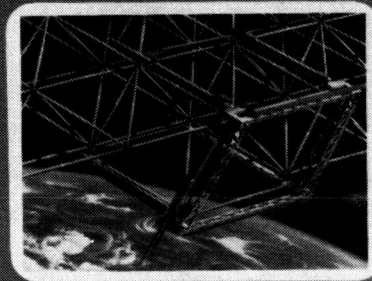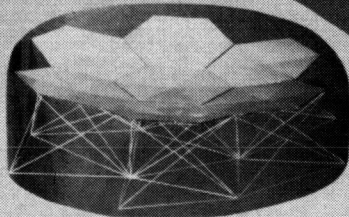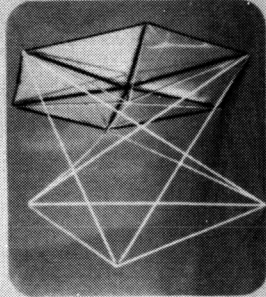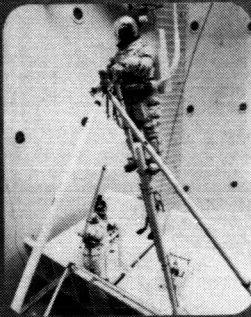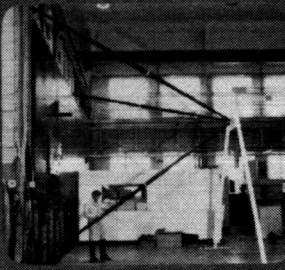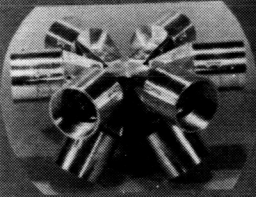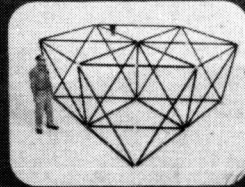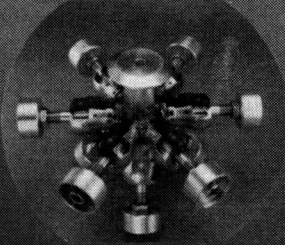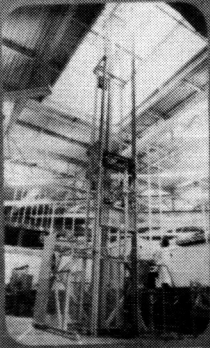
OPTIMUM DAMPER LOCATIONS FOR A FREE-FREE BEAM

G. C. Horner
Langley Research Center
Hampton, Virginia

RESEARCH ISSUES IN STRUCTURAL DYNAMICS
AND CONTROL OF LARGE SPACE STRUCTURES

An in-house research team has been formed to address some key issues in the dynamics and control of large space structures. Contracts and grants are used to supplement the in-house research effort.

One technical issue under research is structural modeling of large space structures. One difficulty is the large number of degrees of freedom and how to reduce the equations of motion to a manageable size. One promising technique for achieving this appears to be the continuum approach. System identification techniques will have to be developed so that space borne structures may be analyzed and characterized.

The placement of actuators and sensors in optimal locations is of technical interest. The most effective locations for achieving a certain control objective must be identified. The issue of colocated versus noncolocated sensors and actuators should be investigated in terms of performance and stability.

Another issue is adaptive/learning control systems for large space structures. Some classes of structures such as deployable and erectable structures may require control at an intermediate stage before the final configuration is achieved. To control these systems an algorithm which can identify the pertinent dynamics in real time will be needed.

O   MODELING AND IDENTIFICATION PROCEDURES FOR DYNAMIC ANALYSIS AND CONTROL

O   OPTIMUM ACTUATOR AND SENSOR PLACEMENT AND DESIGN

O   DISTRIBUTED SENSING AND ACTUATION VERSUS COLOCATED SENSING AND ACTUATION

O   ADAPTIVE/LEARNING CONTROL SYSTEMS FOR STRUCTURAL SYSTEMS

O   REDUNDANT MANAGEMENT TECHNIQUES FOR STRUCTURAL SYSTEMS

Figure 1

OPTIMUM DAMPER LOCATIONS FOR A FREE-FREE BEAM

The objectives of this research are to identify optimum locations for sensors and actuators on large space structures. If it is assumed that large platforms and antennae will have many potential actuator/sensor locations, we may logically ask "Where should actuators and sensors be placed?" Not only should the optimum placement be determined, but also the dynamic characteristics of actuators may also be necessary.

OBJECTIVES

o DEVELOP ALGORITHMS TO OPTIMALLY LOCATE AND DESIGN DAMPERS FOR LARGE SPACE STRUCTURES

o DETERMINE REQUIREMENTS FOR DISTRIBUTED SENSING AND ACTUATION (AS OPPOSED TO COLOCATED SENSOR AND ACTUATOR) IN CONTROL OF STRUCTURAL SYSTEMS

APPROACH

o USE MATHEMATICAL PROGRAMMING TO SOLVE FOR OPTIMUM DAMPING RATE AND LOCATION.

o CONSIDER ACTUATOR DYNAMICS TO SOLVE FOR OPTIMUM ACTUATOR MASS.

Figure 2

DAMPING CHARACTERISTICS OF A FREE-FREE BEAM

     To get an understanding of the behavior of large space structures, we first look at the damping characteristics of a uniform beam. A dash pot is located at one end of a free-free beam. This is an ideal dash pot which is characterized by a damping rate, C, and no other dynamic characteristics. In figure 3 it is seen that for small values of C ($<$.005), the damping ratio, ζ, and damping rate are linearily related. This is denoted as perturbation theory. As the damping rate is increased, the damping ratio reaches a peak value and then decreases. The peak value of the damping ratio is about 0.2 for the first flexible mode. Suppose a design problem were stated which required that the first mode have a damping ratio greater than 0.2. This requirement may be a result of mission performance specifications. To achieve more than the 0.2 damping ratio in the first mode, one or more dash pots are required. Since the design problem being addressed here is one in which the damping ratio is prescribed for each mode to be damped, the damping rate of the dash pots is determined.
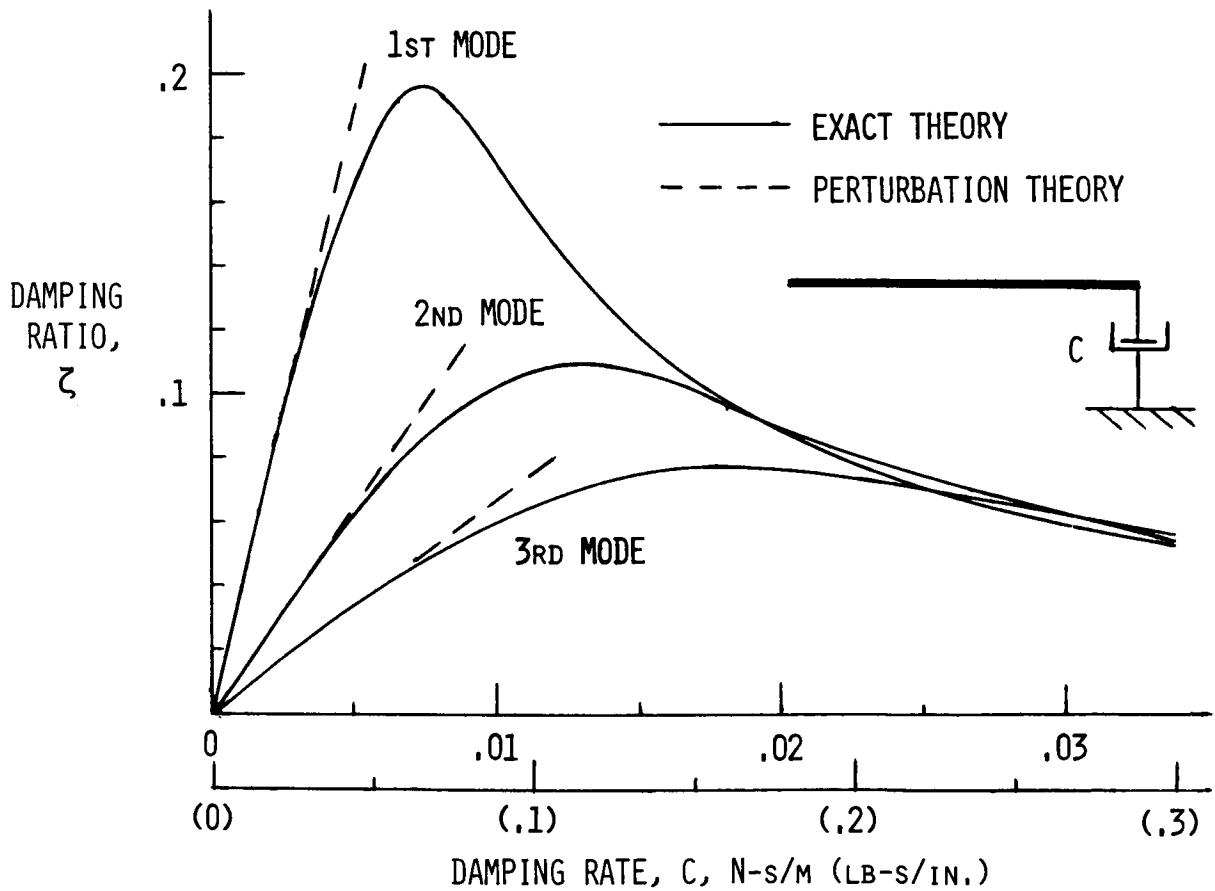
Figure 3

DAMPING CHARACTERISTICS OF A CLAMPED-FREE BEAM

The results are essentially the same as for the free-free beam in figure 3.
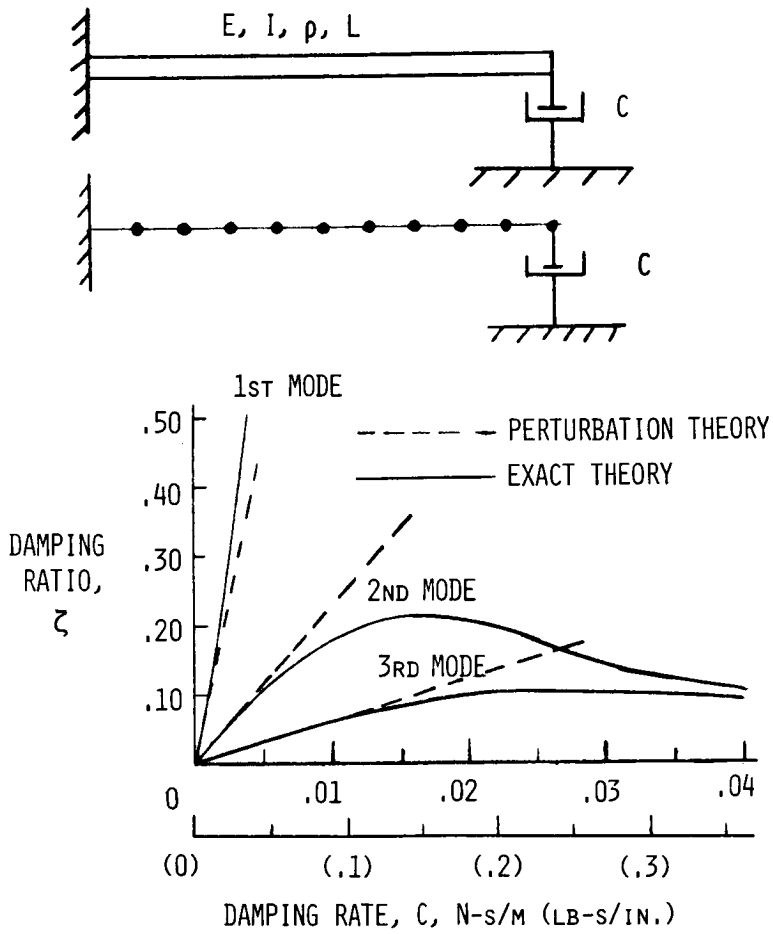
Figure 4

NONLINEAR OPTIMIZATION PROBLEM

A design problem is posed which states that given the prescribed modal damping ratio for N modes, what are the optimum damping locations and sizes? The design problem is now cast as a nonlinear optimization problem. Since it is not known where the dash pots should be located on a structure, the initial step is to put a dash pot at every location of the beam. The objective function is to minimize the total dissipative effort. The constraints are that the actual computed modal damping ratios must be greater than or equal to the prescribed value. Another constraint is that the damping rate must be positive. This guarantees stability.

0   FOR PRESCRIBED MODAL DAMPING RATIO IN N MODES, WHAT ARE THE BEST DAMPING SIZES AND LOCATIONS?

0   OBJECTIVE

MINIMIZE TOTAL DISSIPATION $\text{MIN} \sum_i C_i$

C_i
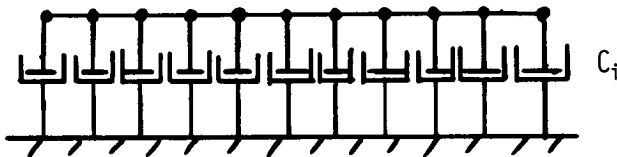
0   CONSTRAINTS

(COMPUTED MODAL DAMPING RATIO)$_j \geq$ (DESIGN VALUE)$_j$
C_i MUST BE POSITIVE

Figure 5

OPTIMUM DAMPING LOCATIONS AND SIZES FOR A FREE-FREE BEAM

Some results are presented in figure 6 for a free-free beam. The design problem consisted of prescribing a modal damping ratio of 0.5 in N modes. The results are shown for N = 1, 2, 3, 4. The results are also split between symmetric solutions and nonsymmetric solutions. The symmetric solutions are obtained by minimizing the total dissipation while imposing symmetry in the solution. The horizontal lines represent the length of the beam. The vertical lines are proportional to the magnitude of the damping rate at the location shown on the beam axis. The nonsymmetric solution is obtained by removing the symmetry requirement and the smallest damper location. Thus, nonsymmetric solutions will have no more than one fewer dampers than the symmetric case. In some cases the objective function for the nonsymmetric solution is less than that for the symmetric case.
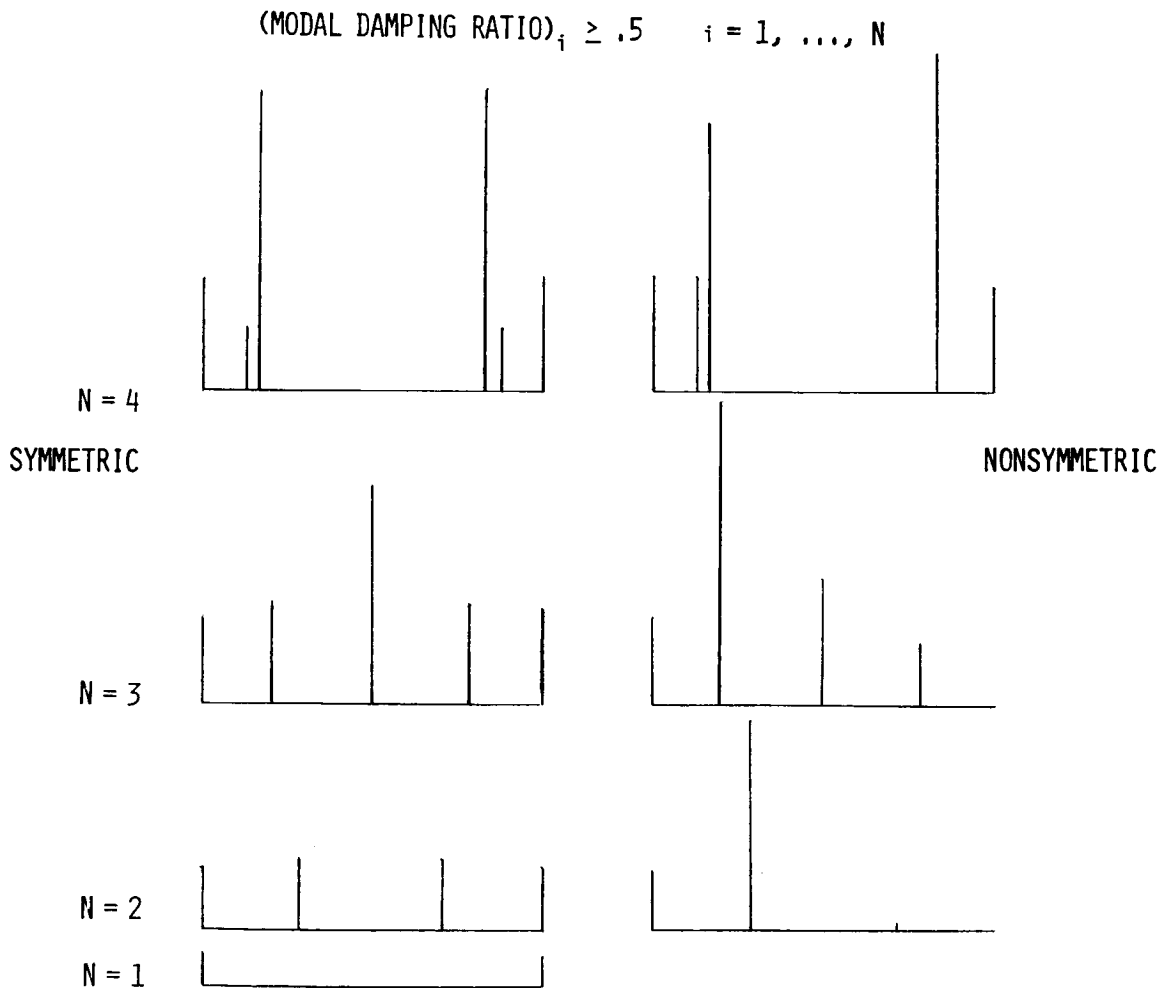
$(\text{MODAL DAMPING RATIO})_i \geq .5 \quad i = 1, ..., N$

Figure 6

The results shown in figure 7 are similar to those in figure 6.

$(\text{MODAL DAMPING RATIO})_i \geq .5 \quad i = 1, \ldots, N$
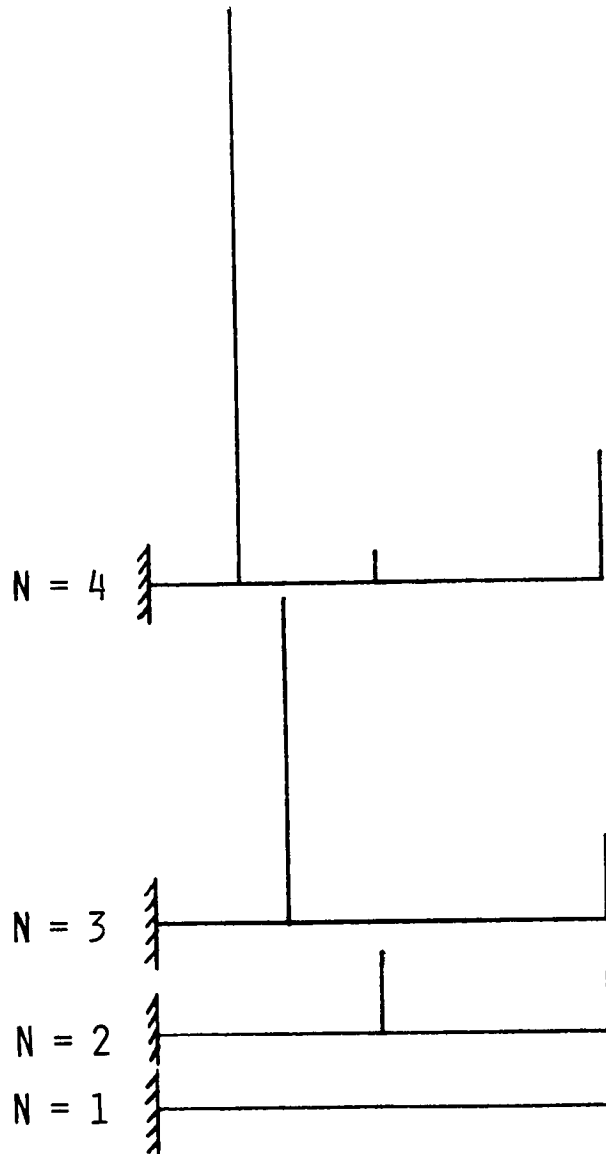
Figure 7

FUTURE RESEARCH

The future research thrusts will involve the addition of actuator dynamics to the structural dynamic models. This will allow the mass and stiffness as well as the damping rate of the damper to be design variables. Thus this will be the actuator design phase.

Next, a 2-dimensional structural model which has a higher modal density will be developed.

O NONCOLOCATED SENSORS AND ACTUATORS

O ADDITION OF ACTUATOR DYNAMICS

O 2-DIMENSIONAL STRUCTURAL MODEL

Figure 8

NONCOLOCATED SENSORS AND ACTUATORS

One possible configuration of sensors and actuators is shown by the damping matrix. As seen by the matrix, each sensor "talks" to each actuator which gives rise to the fully populated matrix. This is in contrast to colocation which would give a diagonal matrix. By enforcing the three inequalities, stability will be guaranteed a priori.

o   ONE POSSIBLE CONFIGURATION
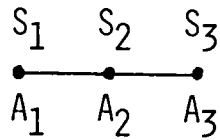
$$S_1 \quad S_2 \quad S_3$$
$$A_1 \quad A_2 \quad A_3$$

S = VELOCITY SENSOR
A = FORCE ACTUATOR

DAMPING MATRIX

$$
\begin{bmatrix} A_1 \\ A_2 \\ A_3 \end{bmatrix}
=
\begin{bmatrix}
C_{11} & -C_{12} & -C_{13} \\
-C_{12} & C_{22} & -C_{23} \\
-C_{13} & -C_{23} & C_{33}
\end{bmatrix}
\begin{bmatrix} S_1 \\ S_2 \\ S_3 \end{bmatrix}
$$

FOR A STABLE SYSTEM

$$C_{11} - C_{12} - C_{13} > 0$$

$$-C_{12} + C_{22} - C_{23} > 0$$

$$-C_{13} - C_{23} + C_{33} > 0$$

Figure 9

LaRC FLEXIBLE BEAM EXPERIMENT

To verify some of the optimization results and other control algorithms, a flexible beam experiment has been initiated at LaRC. In figure 10, the flexible beam experiment consists of a 3.66 m (12 ft) long aluminum beam with a 4.76 mm (3.16 in.) by 15 cm (6 in.) cross section. The beam is suspended by two small flexible cables so that free-free end conditions are approximated. Located in front of the beam are four electromagnetic shakers (actuators) which can be repositioned along the beam by sliding them along the platform which supports them. The console on the left contains the power amplifiers for the shakers.
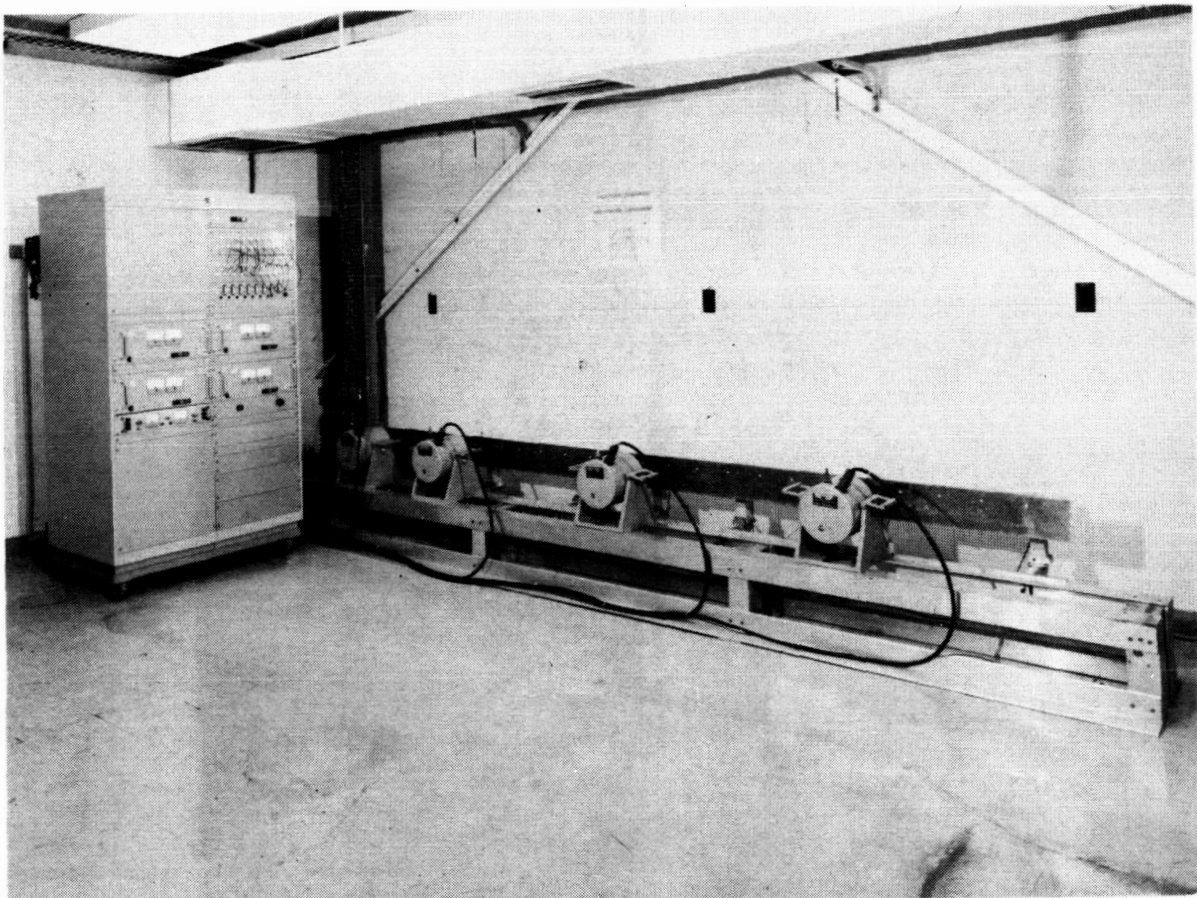
Figure 10

LaRC FLEXIBLE BEAM EXPERIMENT
(Continued)

Figure 11 shows another picture of the experimental setup. On one side of the beam the four shakers are located and on the other side of the beam there are nine noncontacting displacement probes. With the experiment being tied in with the CDC Cyber 175 computer, real-time calculations may be made. For example, the output of the displacement probes can be made available to the computer. Using state estimation, the velocity at the shaker locations can be approximated. Knowing the damping rate or gain from the optimization program and the velocity, the desired force output of the shakers can be calculated.
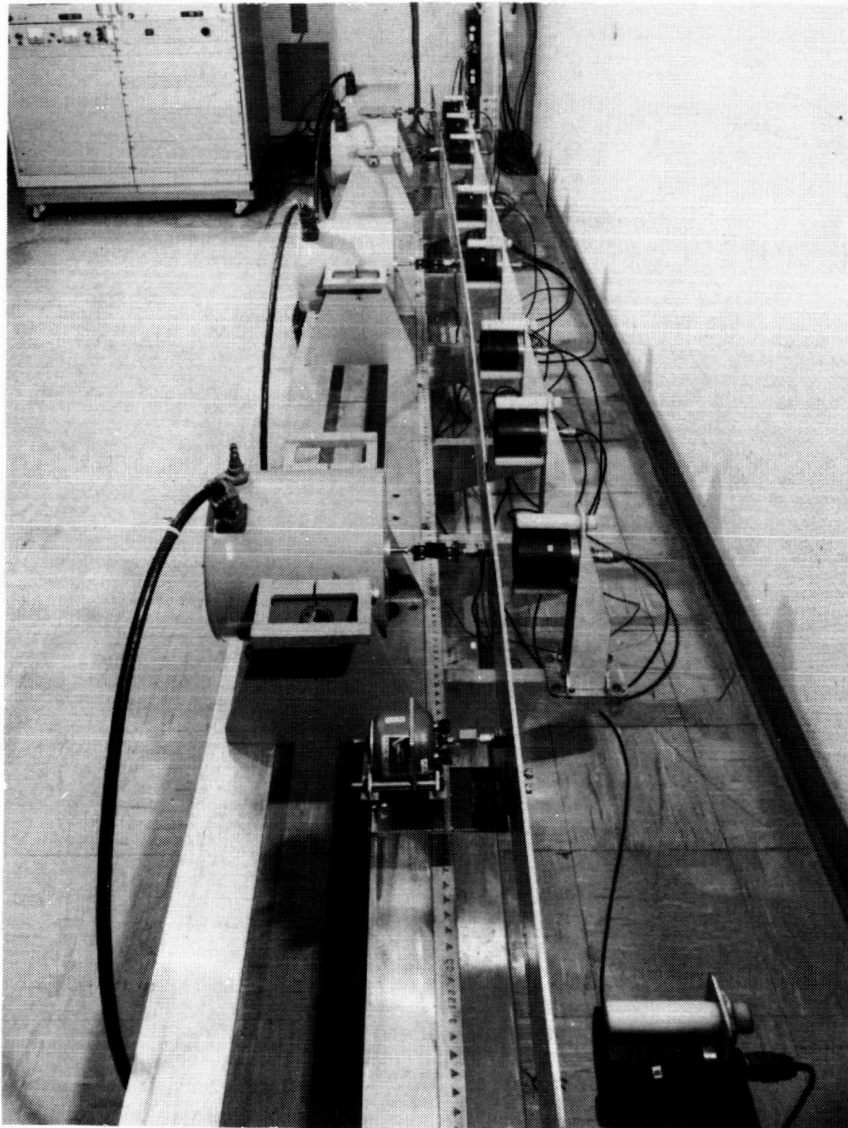
Figure 11

CONTROL THEORETICS FOR LARGE

STRUCTURAL SYSTEMS

Raymond C. Montgomery
NASA Langley Research Center

RESEARCH ISSUES IN STRUCTURAL DYNAMICS AND CONTROL OF LARGE SPACE STRUCTURES

At Langley Research Center, we are addressing the issue of structural dynamics and control with experimentation and theoretical development. Figure 1 lists the areas of research being addressed including modeling identification for both the purposes of analysis and controls, design of structural control systems actuator sensor placement, and distributed sensing and actuation as opposed to co-located sensor and actuators. Also, we will be looking at adaptive/learning processes that could more specifically be refered to as inflight testing procedures where a structure is tested during its deployment or assembly and during its orbital life at specific points where we identify the characteristics of the structure for the purpose of tuning the control system. Another area is redundancy management techniques for structural systems. This is important because of the relaibility issue for managing multiple very large numbers of sensors and actuators. The management approach is indicated on figure 2.

0 MODELING AND IDENTIFICATION PROCEDURES FOR DYNAMIC ANALYSIS AND CONTROL

0 OPTIMUM ACTUATOR AND SENSOR PLACEMENT AND DESIGN

0 DISTRIBUTED SENSING AND ACTUATION VERSUS COLOCATED SENSING AND ACTUATION

0 ADAPTIVE/LEARNING CONTROL SYSTEMS FOR STRUCTURAL SYSTEMS

0 REDUNDANT MANAGEMENT TECHNIQUES FOR STRUCTURAL SYSTEMS

Figure 1

APPROACH - THEORY

Our in-house effort involves research in adaptive/learning by myself; research in basic design of structural control systems actuator placement and sensor placement by Garnett Horner; and research in the application of the coupling theory to structural control by Al Hamer. NASA has a contract to Honeywell, Inc., in Minneapolis, MN, to do studies on closed loop control of the space shuttle orbiter attached to a payload using the RMS arm and to look at measures of parameter identification performance relative to real time identification of structural systems. We have another contract with Vigyan Research Associates to conduct studies on the application of modern control theory, mainly linear quadratic gaussian control techniques, to structural dynamics systems. In research grants, Stanford University is studying the problem of structural dynamics and control design with particular emphasis on the placement of actuators and sensors. MIT has a grant to study reliability issues--the problem of designing the basic control systems considering that the components have a finite reliability and may fail during operation considering large numbers of actuators and sensors. The University of Houston is pursuing the problem of vibrational systems and developing algorithms that are extremely efficient for decoupling of structural models for very large order systems. The City University of New York is conducting research on adaptive/learning control systems. Howard University is dealing with the problem of modeling large structural systems in orbit accounting for the orbital dynamics para-meters. North Carolina State A&T University is studying the problem of modeling large structural systems for both analysis and control. The remainder of the talk will concern further detail on the items which have the bullets by them. This is because of my familiarity with those particular subjects. For information regarding the other subjects, one should consult with the principal investigators of those specific grants or contracts.

IN-HOUSE • MONTGOMERY - ADAPTIVE/LEARNING
               HORNER - FREE-FREE ACTUATION, PLACEMENT, DESIGN
               HAMER - DECOUPLING THEORY

CONTRACTS • HONEYWELL - ACTIVE CLOSED LOOP CONTROL AND PARAMETER ID
               VIGYAN RESEARCH ASSOCIATES, INC. - CONTROLLER DESIGN
                 METHODOLOGY

GRANTS   • STANFORD - PLACEMENT, DESIGN
           • MIT - RELIABILITY ISSUES
             U. HOUSTON - DECOUPLING STRUCTURAL MODELS
          • CUNY - ADAPTIVE/LEARNING
             VPI&SU - ADAPTIVE, PAR ID, MODELING
             HOWARD UNIVERSITY - MODELING OF ORBITING PLATFORMS
          • NC A&T - MODELING OF LARGE FLEXIBLE STRUCTURES

Figure 2

Langley has just completed a workshop where the specific items which had bullets attached to them in the previous slide were discussed. Now I would like to give you an overview of some of the results which were presented at that workshop. The first item I have chosen to discuss is research which is being undertaken by Prof. Cannon at Stanford University. Prof. Cannon is considering the problem of sensor and actuator placement and, in particular, is investigating the problem of non-colocated feedback. Figure 3 presents a discription of some of that research. On the left of the slide, we have a schematic diagram indicating a feedback from a structural dynamics system which is a series of discs which are connected by a wire that can transmit torsion. Note that the angle θ is measured as the lower disc and is then processed by a compensator which generates a moment applied at another disc. The significant point of this research is that in certain conditions the system becomes a nonminimum phase system which means that in control system jargon, the system will be conditionally stable. That is, it may be stable at one value of feedback gain on the compensator and unstable at another. To assure that you will have a stable system requires precise modeling.
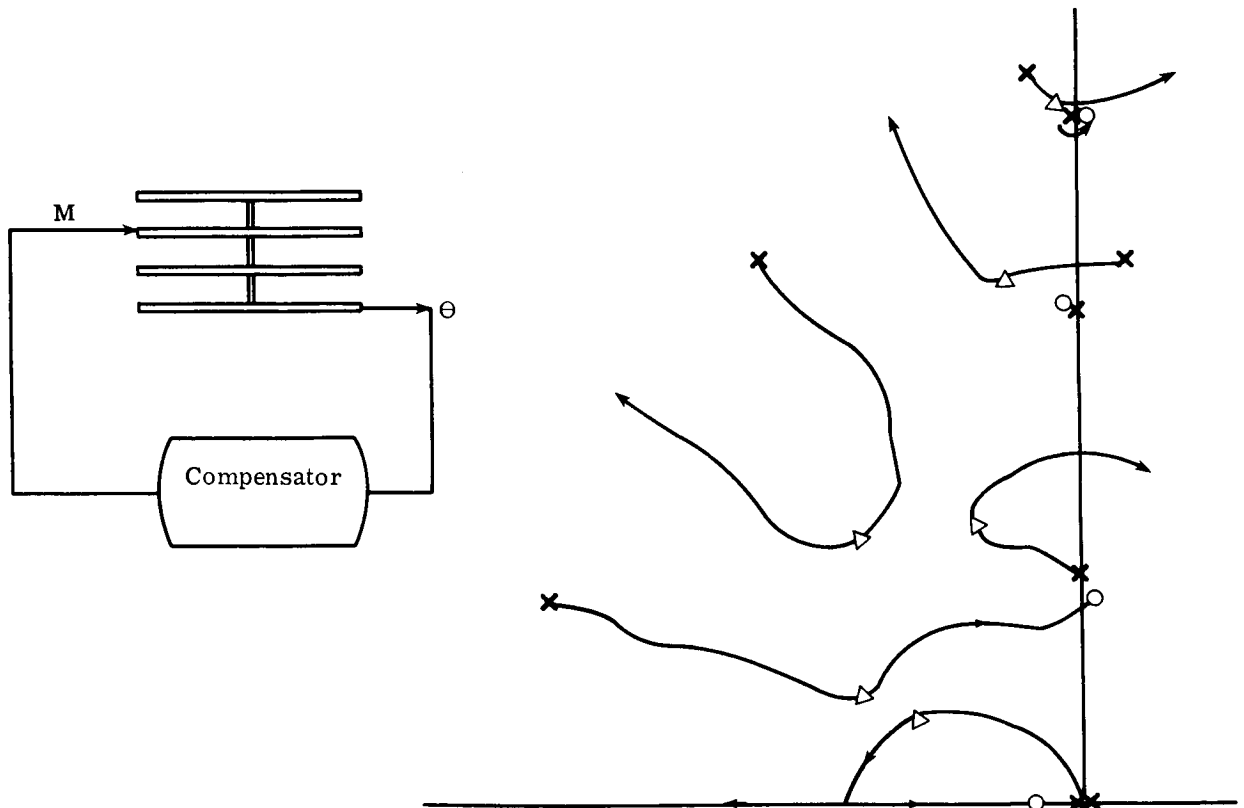
Figure 3

WHY DO WE NEED TO CONSIDER COMPONENT UNRELIABILITY?

The MIT research effort involves reliability issues for large structures. Figure 4 lists reasons that we need to consider component reliability or unreliability as the case may be. Large lightweight structures in space may need active damping because of the tradeoffs in delivering mast orbit versus the cost of providing active control. Also, to effect control of many modes for large platforms being conceived will involve many sensors and actuators, possibly hundreds of them. The next point is that, even if these systems are serviced in orbit, we would like for the service interval to be very long. It is unfortunate that the mean time between failures that can reasonably be anticipated will still dictate some means of automatic system reconfiguration because of the number of components which may fail during one year.

° A LARGE, LIGHTWEIGHT STRUCTURE IN SPACE WILL DISPLAY MANY VIBRATORY MODES WHICH MAY HAVE TO BE ACTIVELY DAMPED TO ASSURE MISSION SUCCESS.

° EFFECTIVE CONTROL OF THESE MANY MODES WILL REQUIRE USE OF A LARGE NUMBER OF SENSORS AND ACTUATORS—POSSIBLY HUNDREDS OF THEM.

° EVEN IF THESE CONTROL SYSTEMS ARE SERVICED IN ORBIT, ONE WOULD LIKE THE SERVICE INTERVAL TO BE LONG—AT LEAST ONE YEAR.

° WITH COMPONENT MEAN TIME BETWEEN FAILURES WHICH CAN REASONABLY BE ANTICIPATED, ONE MUST EXPECT MANY OF THE CONTROL SYSTEM COMPONENTS TO FAIL IN THE COURSE OF A YEAR.

Figure 4

Figure 5 is a graph of expected number of failures which may occur in one year versus component mean time between failure. The 100,000 hour point on the graph in component mean time between failure corresponds to approximately 12 years. Note that if we have 200 components and for each we expect 12 years mean time between failure, then we can expect to have about 20 failures during the course of one year. This dictates automatic system reconfiguration to account for failures. This implies, however, that the designers of the structure consider the reliability issue and automatic reconfiguration limitations.
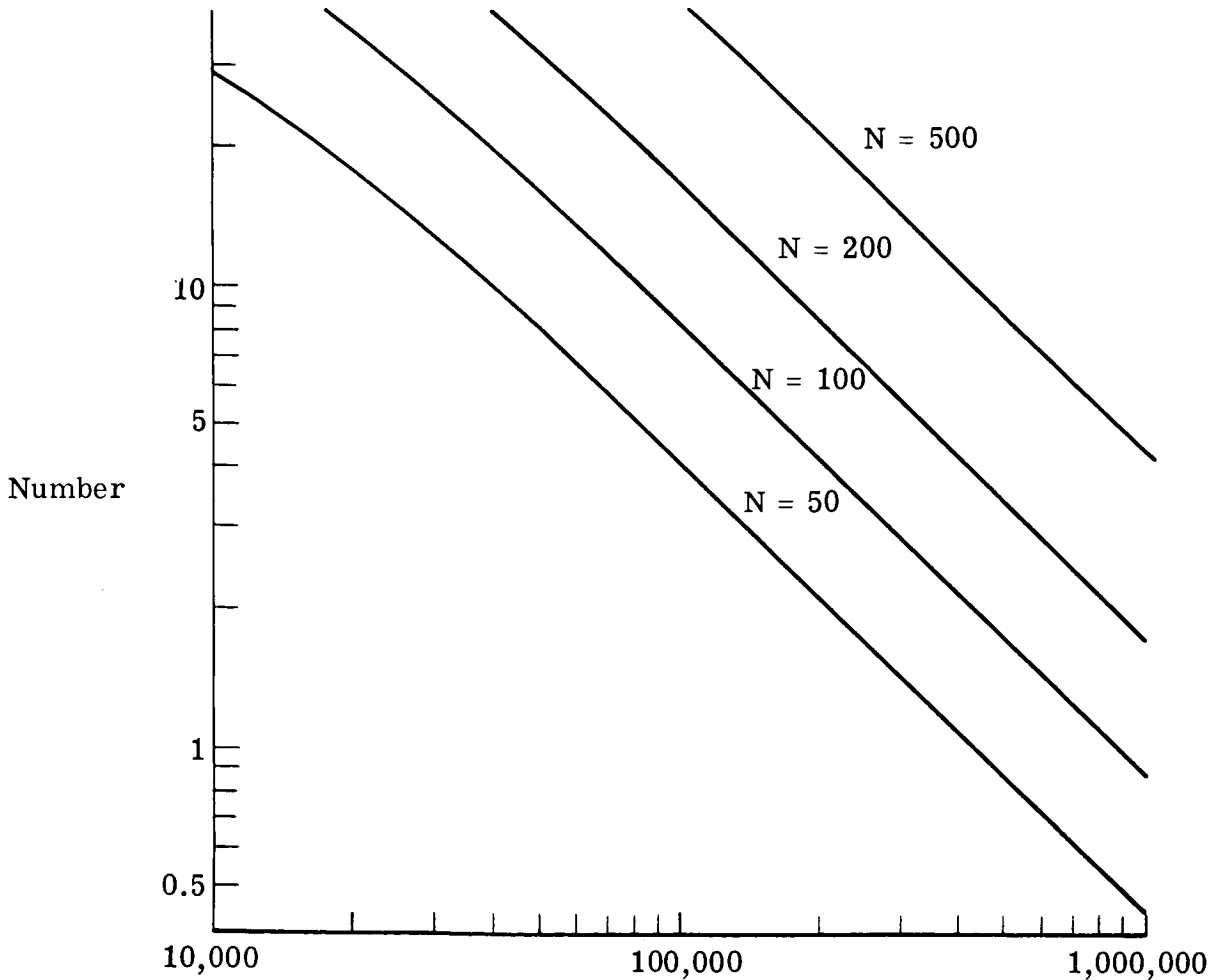
Figure 5

DETECTION FILTER

One mechanism for detecting failures has been developed at MIT which is called the failure detection filter. This filter is shown in figure 6 and is quite similar to the Kalman filter except that the system matrices are selected in order that failures be amplified. If a failure does occur, the output error on the slide readily indicates the type of failure that has occured.
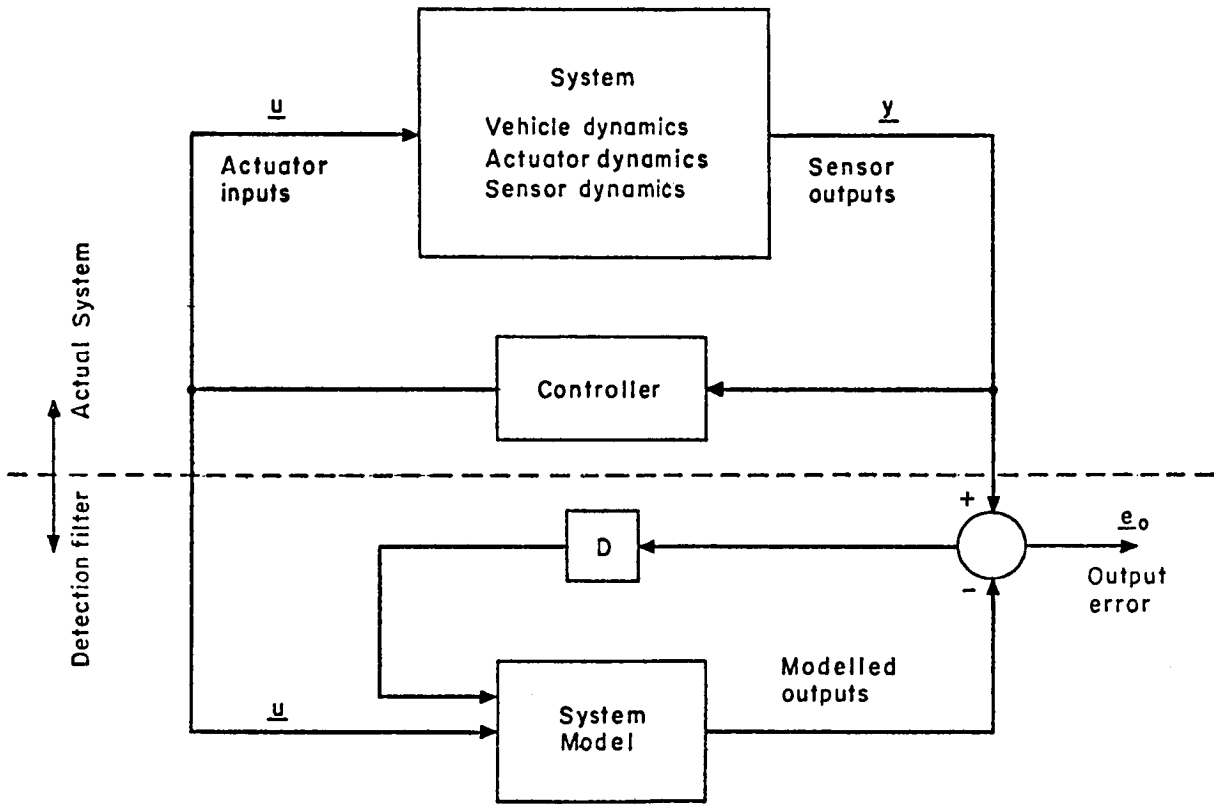
Figure 6

The Honeywell research involves determining performance measures of models for distributed parameter systems. Figure 7 summarizes the research involved. The equation which is at the top of the slide indicates the form of a model which is being considered where parameters A, B, L and C would have to be identified in real time. The model from which measurements Z were generated is called the truth model and the parameters A, B, etc., take on values which have a star on them. The model which is used in the control process, however, may use values of A, B, and C which are subscripted with an alpha. The truth model is really not known to the onboard control system and must be identified. For finite dimensional systems the truth model can be in the same class as the model stored on the computer but for distributed systems or structural dynamics systems the truth model cannot be represented by model of finite dimension. Therefore, one cannot compare, in an elementary context, the model which is used for onboard computation with the actual distributed parameter model. One breakthrough in this research allows one to obtain a measure of distance from the computational model, represented by M_α, and the truth model which is

represented by M_* has been accomplished at MIT by Yoram Baram and later extended by Yared allowing one to obtain measures of modeling performance of this type of problem. The Honeywell will test these measures to determine their suitability on realistic problems involving the space shuttle coupled to a payload using the RMS arm.

$$X(K+1) = A_* X(T) + B_* U(T) + L_* \zeta(T)$$
$$Z(T) = C_* X(T) + \Theta(T)$$

TRUTH: $M_* = \{A_*, B_*, C_*, L_*, \Xi_*, \Theta_*\}$

MODEL: $M_\alpha = \{A_\alpha, B_\alpha, C_\alpha, L_\alpha, \Xi_\alpha, \Theta_\alpha\}$

GOAL: FIND MODEL M_α "CLOSEST" TO M_*.

CLOSEST = MINIMIZE THE NEGATIVE LOG LIKELIHOOD FUNCTION
(COMPUTED FROM KBF FOR M_α)

Figure 7

DISTANCE MEASURE

Figure 8 is a graph of this measure of performance of a structural dynamics model versus one of the model's parameters. In this case, the true value of the parameter produces a minimum value of the measure for which one would hope. However, for using a computational algorithm to solve for the minimum value of the measure, and if we use a gradient-type algorithm, one can see that if our initial guess of estimate of parameter W_1 is two, then we will diverge

from the true value of the model. This slide indicates that research is needed both in obtaining the distance measure and in obtaining the optimal estimates of the onboard computational or parameter identification process.

$I(*, \alpha)$ = Distance from true system to model α.
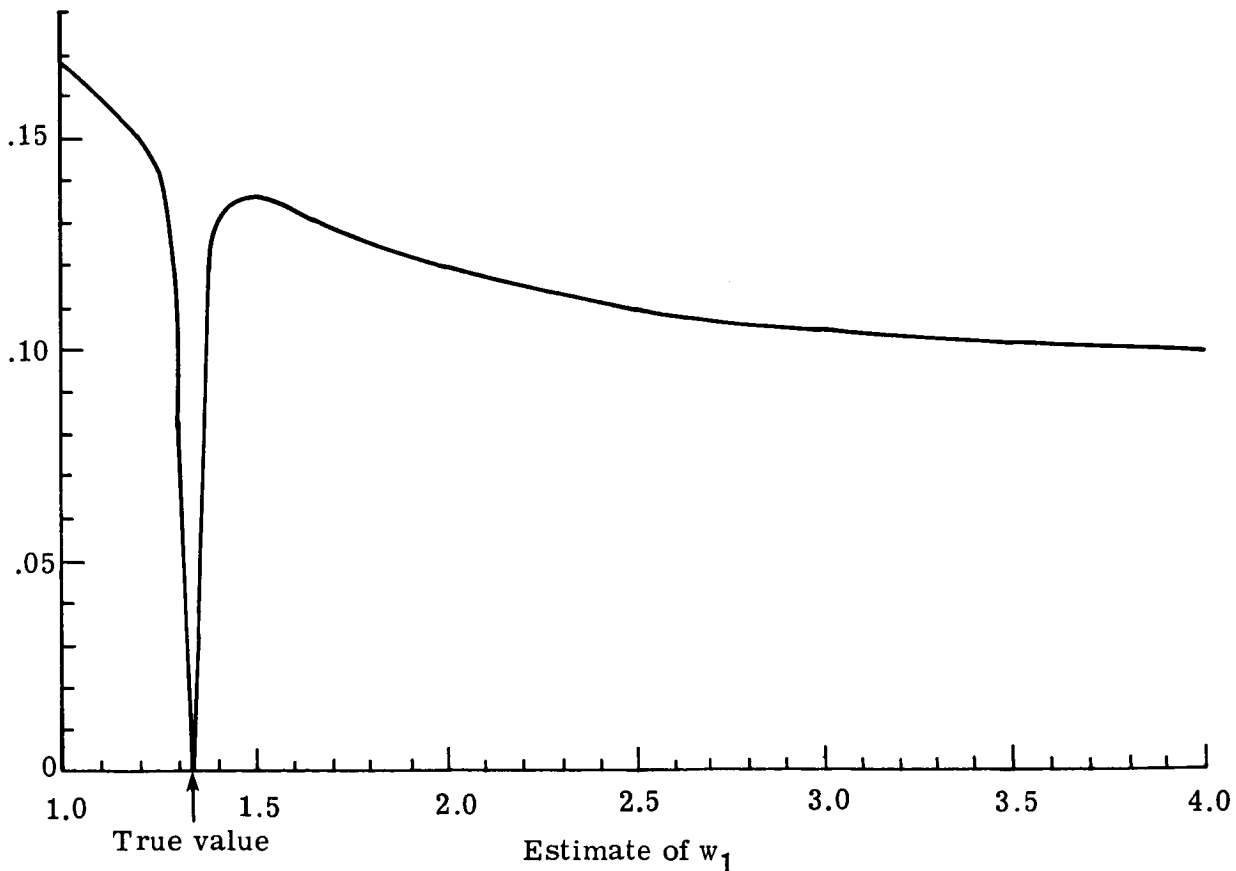
Figure 8

The next several figures will concern an area of research which is being undertaken in-house at Langley Research Center--adaptive/learning control. This effort is also being undertaken at CUNY with Prof. Frederick Thau as the principal investigator. Figure 9 shows a physical model of the solar electric propulsion array which has been modeled analytically at LaRC and NC A&T by Prof. Elias Abu-Saba using the SPAR computer program which was generated by Lockheed. The model is a full six-degree-of-freedom model which involves bending elements and axial force elements of the astromast. The SEP array will be deployed from the space shuttle orbiter from its payload bay in orbit.

PHYSICAL MODEL
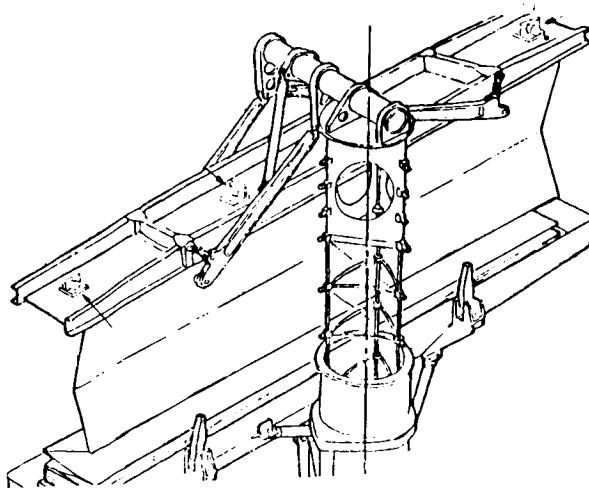
SPAR MODEL
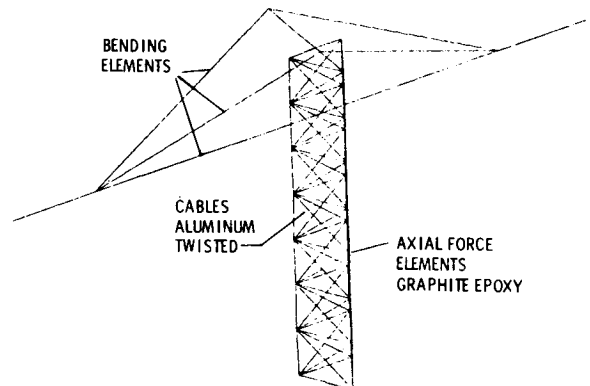
Figure 9

SEP REMOTE SENSING CONCEPT

Figure 10 shows a view of the space shuttle orbiter with the SEP array deployed. It also indicates a sensing concept which has been used in the simulation of the motion of the SEP as attached to the shuttle orbiter. The sensing concept involves targets which can be viewed by cameras mounted at the four corners of the shuttle payload bay (left side of the figure). The sensor targets are perceived by each camera and are registered in the digital computer and by triangulation, the motion of each of the sensor targets is determined.
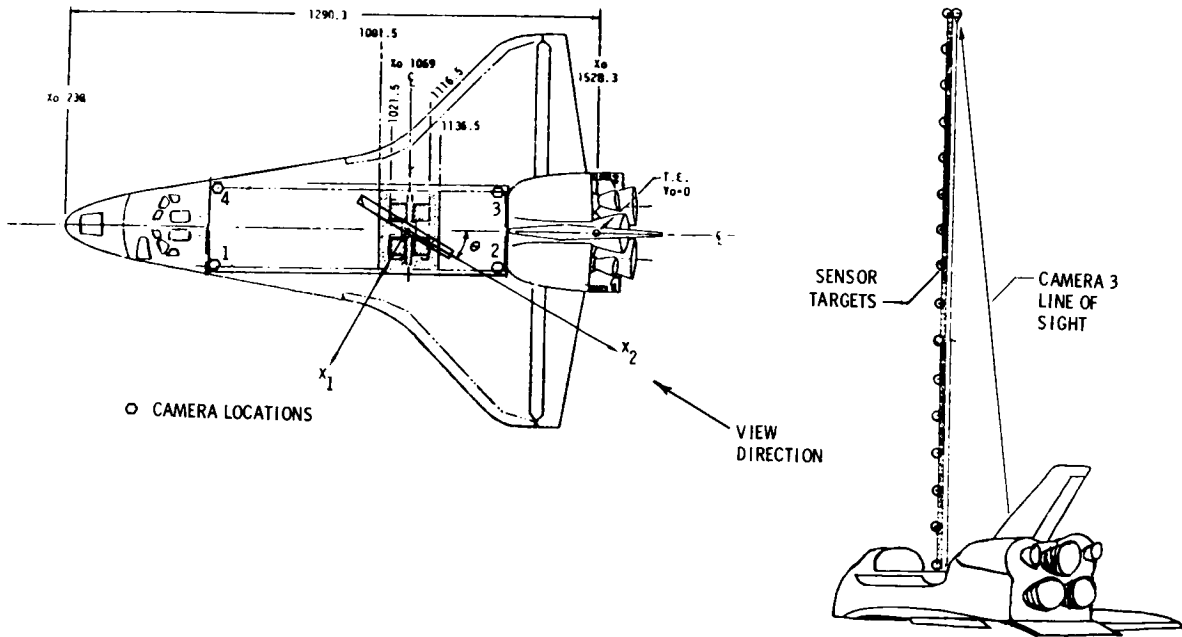
Figure 10

Figure 11 indicates the raster components of the motions of one of the targets located mid-way up the mast as perceived by Cameras 1 and 2. This is a 10 second batch simulation using the CYBER 175 computer system. At each instant in time, this measurement data is processed by first fitting the measurements to a set of approximation functions stored in an onboard digital flight computer. This produces a set of modal amplitudes which are then processed in parallel to identify frequency and control characteristics of modal amplitudes in real time. Thus, a bank of parallel second order identification processors, amenable to microcomputer implementation, is the main element in the system identification logic.
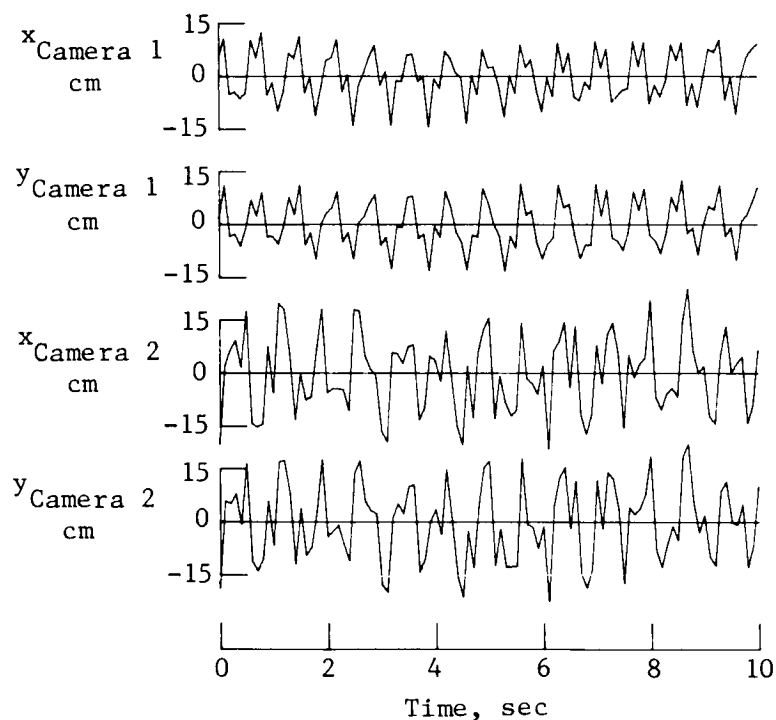
Figure 11

MODE 2 ESTIMATION AND INDENTIFICATION RESULTS

Figure 12 is the output of one element of the bank of processors for Mode 2. The top graph is the estimate of the modal amplitude of the second approxima-tion function. The next two lower graphs on this slide are two parameters which indicate the frequency and damping of Mode 2. It is seen from the graph that convergence of the two parameters occurs in approximately one quarter of the cycle of Mode 2. The next figure will amplify on this char-acteristic for Mode 10.

Figure 12

Figure 13 shows results from the processing of one processor of the parallel
banks of identification processes in simulated real time. This is for the
10th mode and the upper graph shows the estimate of the modal amplitude of
the 10 mode as perceived by the measurement system. The next curve is the
error in the 10th mode and you can see that there is some correlated error
in time for the estimate of that mode. The next lower graphs are parameters
which indicate the frequency of mode 10. Convergence of the parameters A_1
and A_2 for mode 10, in the real time identification process, is seen to
occur in approximately one quarter of the cycle of the amplitude of mode 10
at the top of the graph. This, however, is a perceived oscillation since
the simulated flight computer is digital and samples the motion at intervals
taken at 1/32 of a second. In fact, mode 10 is a very high frequency oscilla-
tion but the perceived frequency, readily apparent from the graph at the top
of the page, is much lower. One of the significant outputs of the research
is that the time required to identify a mode is about 1/4 the period of the
perceived frequency, not the actual model frequency.
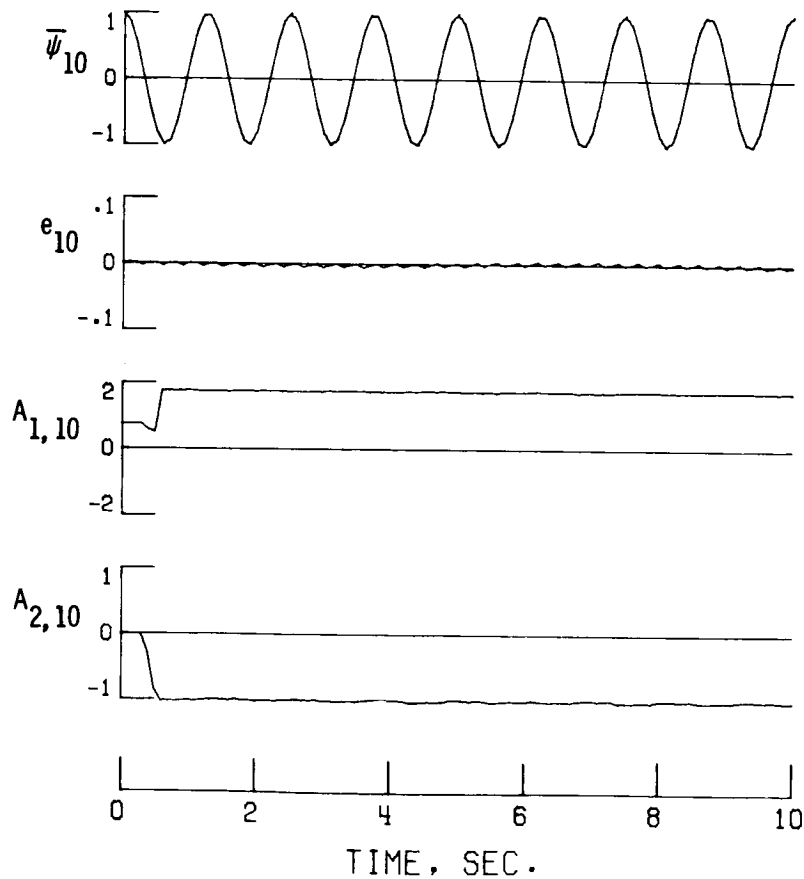
Figure 13

BEAM EXPERIMENTAL APPARATUS

The theoretical concepts which have been discussed, in addition to others, will be tested using an experimental apparatus described earlier by Dr. Horner which I will now describe in a little more detail. The experimental facility consists of a beam as shown in figure 14 where noncontacting sensors measure the deflection of the beam and piezotrons, attached to the actuator arms measure the load input to the beam. Signals from the sensors and the piezotrons are transmitted using the signal distribution system to the Cyber 175 real time digital computer system at Langley.
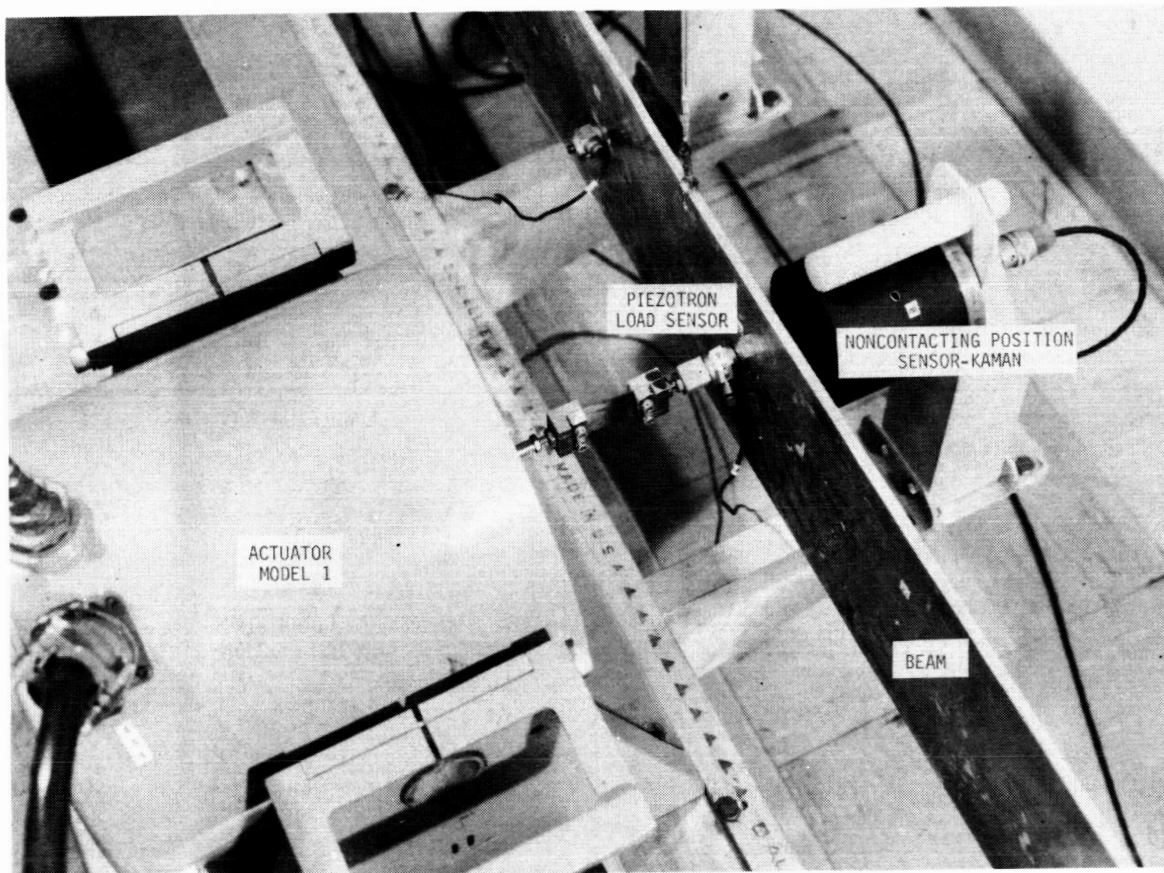
Figure 14

The real time signal distribution system is schematically indicated in
figure 15. The beam experimental apparatus is located in Building 1232 and
is interfaced through an EAI 690 Hybrid computer system to the main signal
distribution system of this Center. The signals are then sent to DASS 1 or
DASS 2 which are the digital real time interfaces for the Cyber 175 which are
to be used to control the beam.
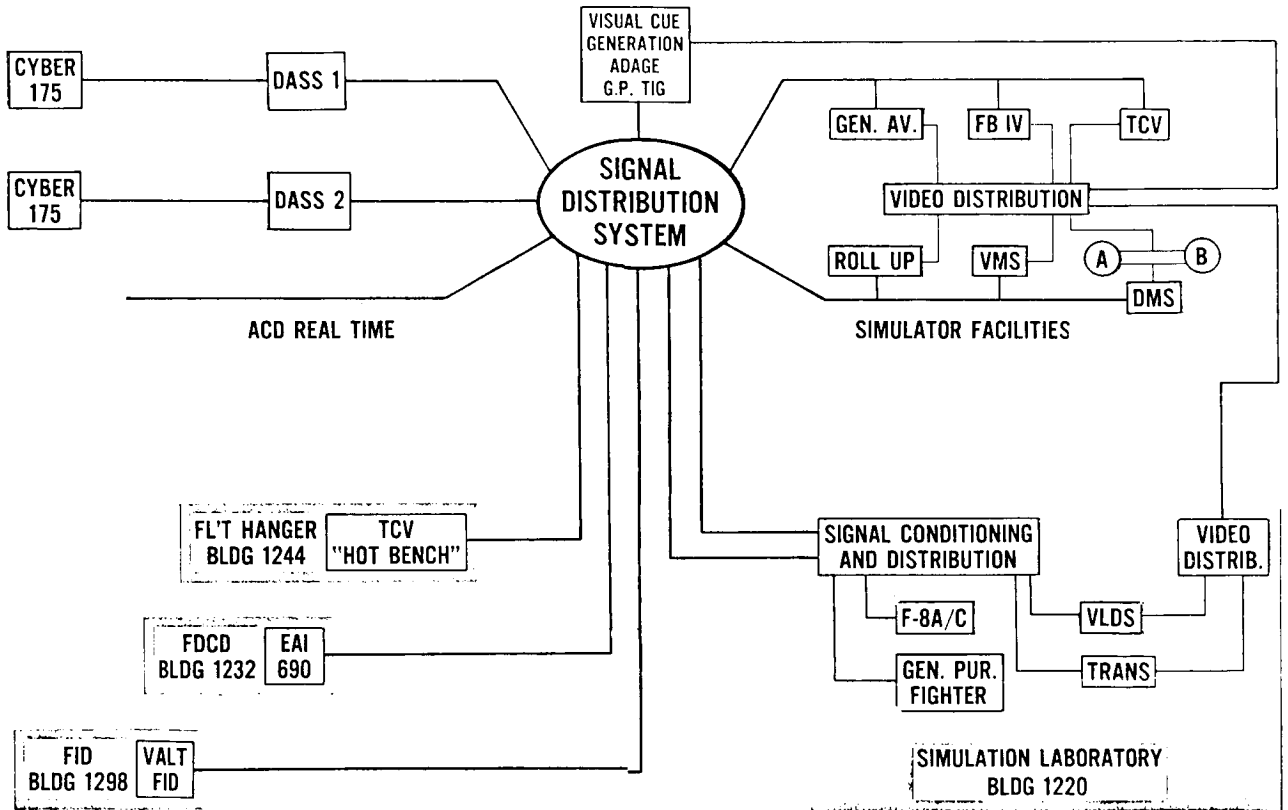
Figure 15

SIGNAL AND POWER DISTRIBUTION OVERVIEW

Figure 16 shows a diagram of the signal distribution of the experimental apparatus. The sensor outputs of the Kaman probes (noncontacting sensors) are sent through the signal buffer to the Cyber RTS interface. The Cyber computer processes the signals and determines commands to the actuators which were shown in Slide 10-L. The Pacer Hybrid interface is used for analog processing of these signals and for processing of an optical scanning sensor which will be included in the apparatus at a later time.
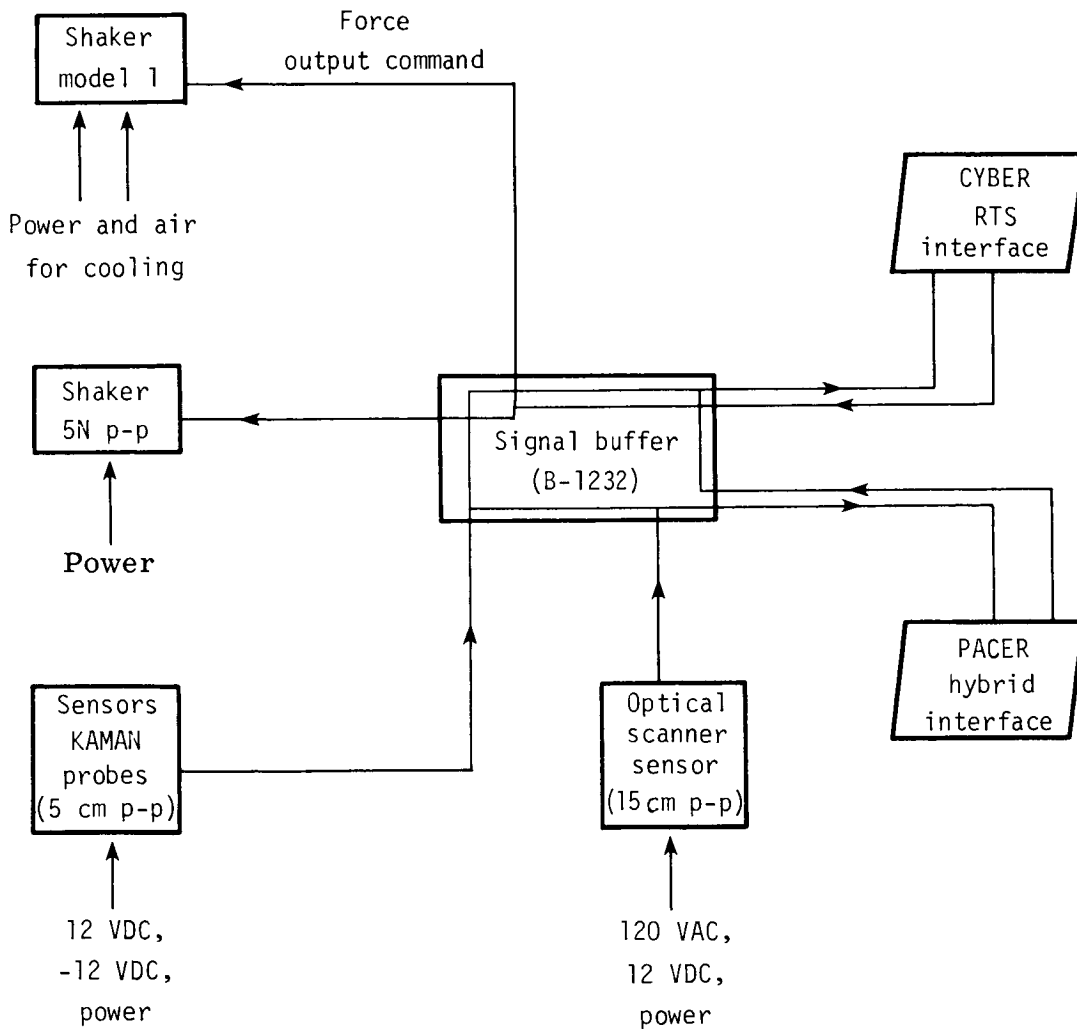
Figure 16

Figure 17 is a batch simulation of the motion of the beam. Each of the graphs is a plot of the horizontal deflection of the beam versus the beam longitudinal axis coordinate x-3. Along the abscissa of each graph is a series of arrows which indicate the locations of the actuators used in the beam apparatus. The triangles which appear on the graphs are the locations and the outputs of the Kaman probes. This particular set of graphs is the free response characteristics of the beam with an initial condition as shown at t=0. In five seconds using a 10 Mode simulation obtained from the SPAR computer program, the motion evolves as is shown in the second graph. This is continued to 10 seconds on the third and final graph. The same program which was used to generate the system identification used for the SEP array has also been used for the beam. The performance of the parallel bank of system identification modules for the beam simulation is similar to that for the SEP array. This same algorithm will be tested using the experimental apparatus when it becomes operational. The experimental apparatus will also provide the capability of studying the effects of failures in actuators and sensors. It will be used to develop and test algorithms for auto- matic system reconfiguration in real time parameter identification and control of structural systems. Current plans call for another structure more representa- tive of the problems of large structural systems in space to be substituted for the beam at a later date.

Beam long axis X3, cm
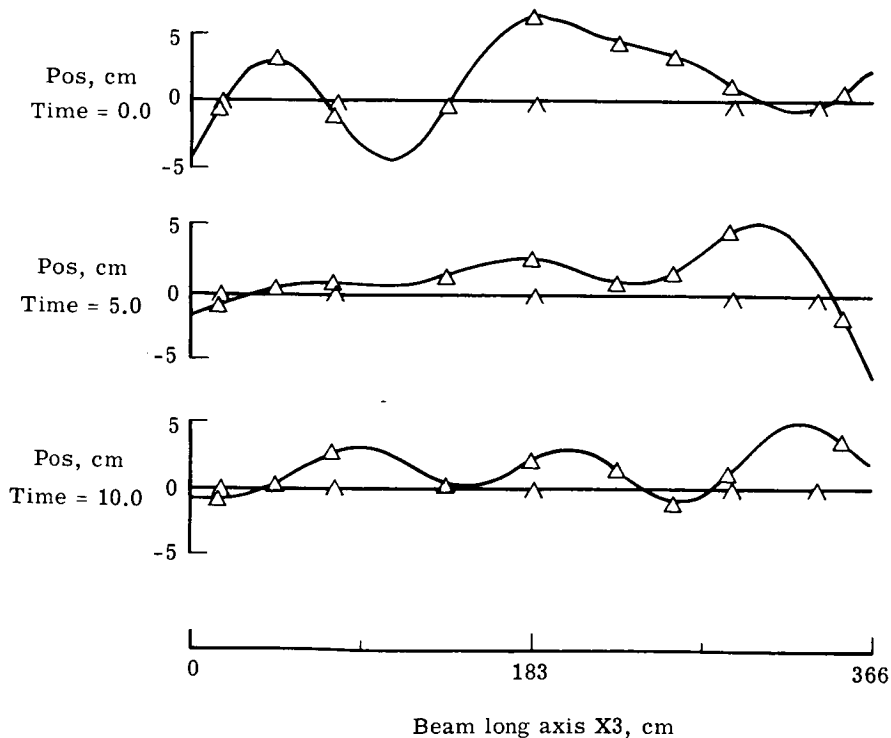
Figure 17

BUCKLING AND VIBRATION OF PERIODIC LATTICE STRUCTURES

Melvin S. Anderson
NASA Langley Research Center
Hampton,Virginia

INTRODUCTION

Proposed concepts for large space structures are typified in the two photos of figure 1. Lattice booms and platforms composed of flexible members or large diameter rings which may be stiffened by cables in order to support membrane-like antennas or reflector surfaces are the main components of these large space structures. Analysis of these structures with a complete finite element model may be prohibitively expensive or impractical. However, the nature of these structures (repetitive geometry with few different members) makes possible relatively simple solutions for buckling and vibration of a certain class of these structures. This theory along with typical results will be discussed in this paper.
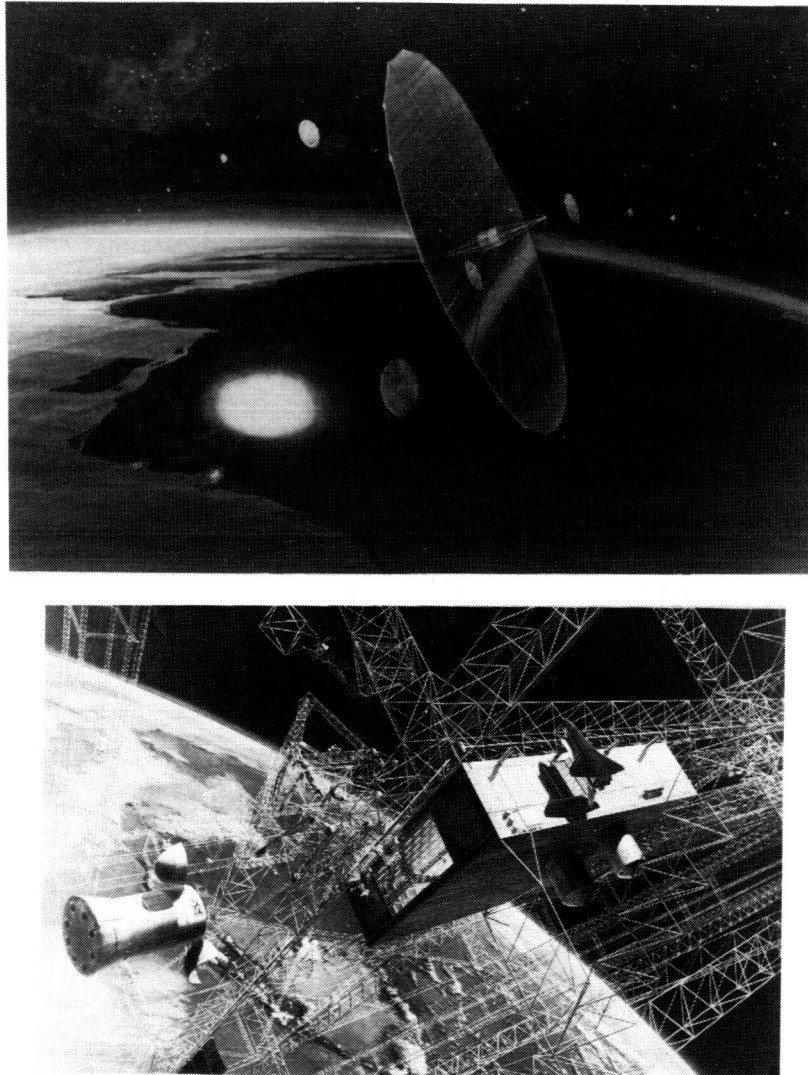
Figure 1

PERIODIC LATTICE CONFIGURATIONS ANALYZED

Exact buckling and vibration solutions have been obtained for the configurations shown in figure 2. The theory for buckling was developed in reference 1 and a simple extension yields vibration results as well. The column configurations are loaded with uniform axial load and are simply supported at the ends. If the ring is cable stiffened, the attachment point at the central mast must be assumed rigid. The flexibility of the mast may be included at the expense of increasing the problem size.
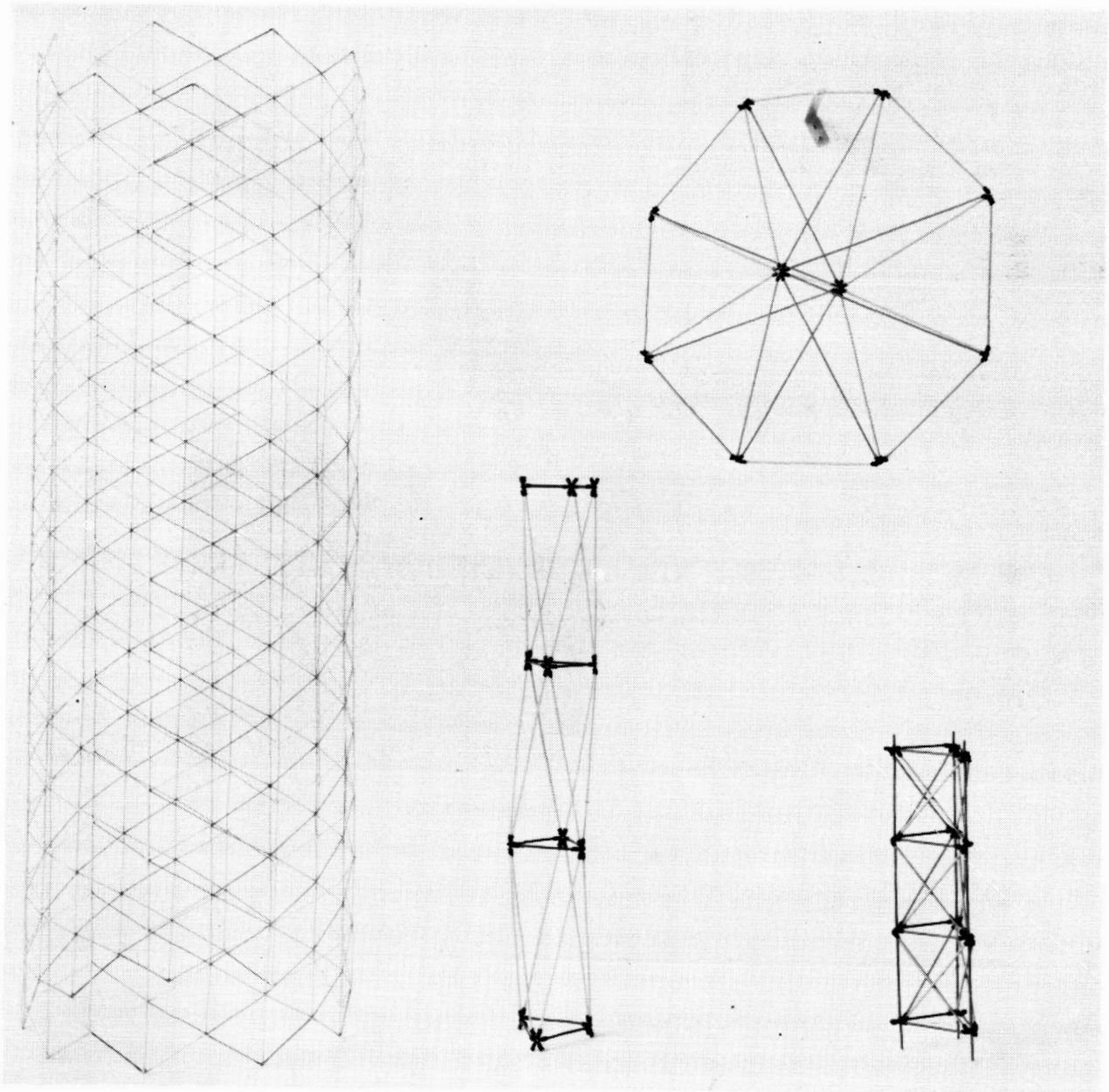
Figure 2

The theory in its simplest form is applicable to any configuration where the relative geometric relationship between nodes is identical for all nodes. This relation is true for all the configurations of figure 2. (The nodes at the ends of the mast of the ring configuration are assumed to have zero displacement, so they do not enter in the analysis.) Each member is represented by a stiffness matrix derived from the exact solution of the beam column equation. This transendental matrix gives the current member stiffness at any end load or frequency. It is not necessary to have intermediate nodes to insure accuracy. Using conventional finite element techniques, equilibrium equations can be written involving displacements and rotations of a typical node and its neighbors. The assumptions of a simple trigonometric mode shape is found to satisfy these equations exactly; thus the entire problem is governed by just one 6 x 6 matrix equation involving the amplitude of the displacement and rotation mode shapes. The boundary conditions implied by this solution are simple supported ends for the column type configurations.

- EACH NODE HAVING IDENTICAL GEOMETRICAL RELATIONSHIP WITH ITS NEIGHBORS

- STIFFNESS OF EACH MEMBER REPRESENTED BY "EXACT" FINITE ELEMENT MODEL THAT ACCOUNTS FOR FREQUENCY AND BEAM COLUMN EFFECT

- PERIODIC MODE SHAPE

- EIGENVALUES OF 6 x 6 DETERMINANT FOR BUCKLING OR VIBRATION

Figure 3

BUCKLING OF LATTICE ISOGRID CYLINDER

A simple approach to analysis of lattice structures containing a large number of members is to develop equivalent beam, plate, or shell stiffness so that they may be analyzed with a continuum theory. The present discrete lattice theory can be used to evaluate the accuracy of such an approach. In the example given in figure 4, the buckling load of an isogrid cylinder similar to that shown in figure 2 is given in terms of the slenderness ratio of an individual member. The load is normalized by the load obtained from continuum theory; thus, a value of 1 means agreement between the two approaches. Two orientations of the isogrid are shown, one with one set of members aligned axially and the other orientation has one set aligned circumferentially. For each orientation two curves are given, one for all members straight, the other applicable to configurations having helical members curved to lie in the surface of the circular cylinder containing the vertices. The results of the figure show the following: (1) as member slenderness ratio increases, the discretness effect compared to continuum theory is much more significant; (2) the highest load capability is for straight members having a principal direction in the circumferential direction. This orientation results in lower individual member loads for a given end load and thus greater resistance to buckling; (3) buckling loads are further reduced if helical members are curved. If there is a compressive force in the curved member which occurs for the $\pm 30°$, $90°$ configurations the reduction in buckling load is the greatest.
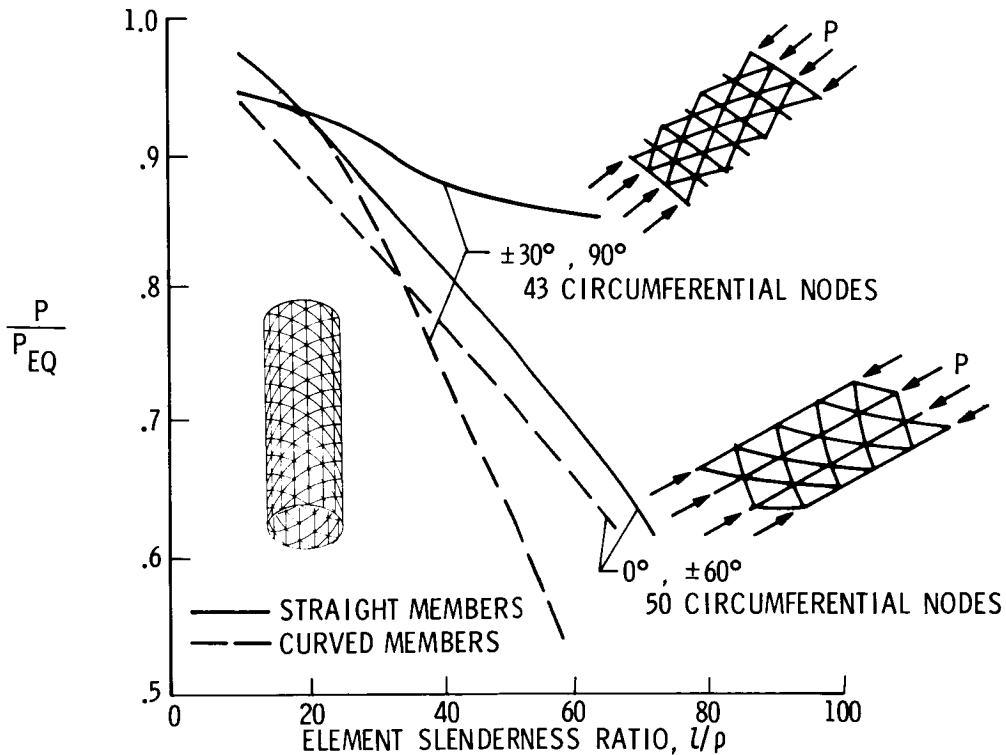
Figure 4

BUCKLING OF TRIELEMENT BEAM

    A beam configuration that has been proposed for many applications because of its structural efficiency for carrying axial load consists of three longerons with cross-braced diagonals. The buckling characteristics for a simply supported three element beam loaded in axial compression are shown in figure 5. The buckling load is plotted as a function of buckle length. Three different modes are possible. Buckling of an individual member as an Euler column supported at the joint locations is illustrtated on the left. The load for all buckle lengths has been normalized with respect to the local buckling load corresponding to a buckle length equals bay length ℓ. If the column is sufficiently long, in this case somewhat greater than 17 bays, it will buckle in an overall column mode. The classical Euler load based on continuum stiffnesses is shown dashed and indicates some effect of the shear flexibility of the diagonals. A third mode is possible when the diagonals are small with respect to the longerons. In this case, a moderate length buckle involving movement of the diagonals can result in lower loads than assuming the diagonal force nodes. The discrete lattice buckling theory gives all these results from the same analysis as a function of the wavelength parameters.
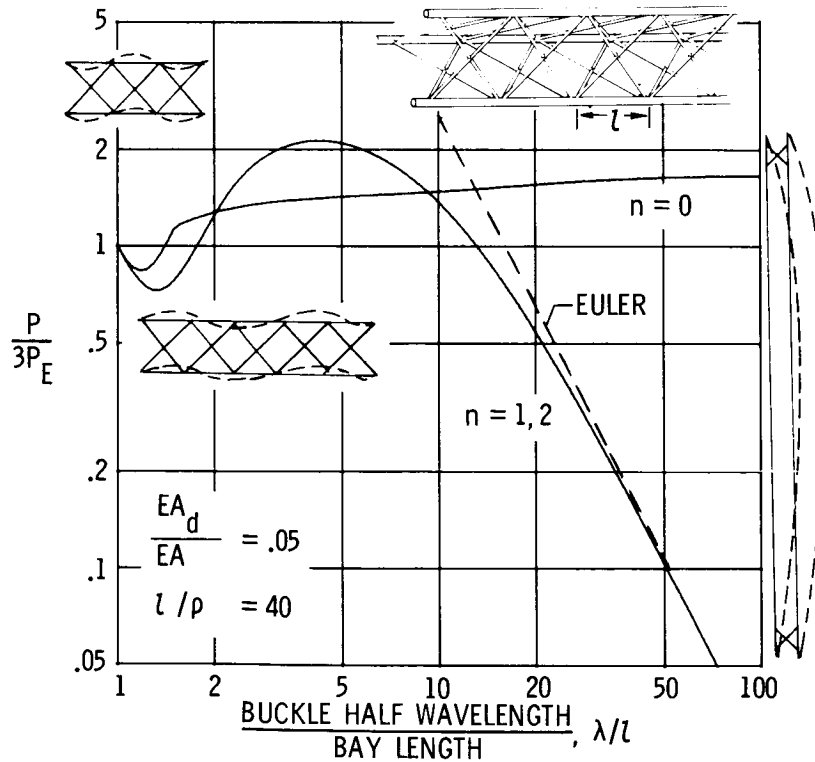
Figure 5

STRUCTURAL EFFICIENCY OF COLUMN CONFIGURATIONS

A study was made of the column mass required to sustain a given load for the three element column discussed in the previous slide. Another column configuration sometimes referred to as a geodesic beam is also shown in figure 2. The configuration is somewhat unusual in that there are no pure axial members. The load carrying members are inclined to the axis of the column and provide the transverse shear stiffness as well as contribute to the buckling stiffness. The battens are loaded in tension when axial compression is applied. A comparison of the mass of the two different configurations is shown in figure 6. The mass parameter is plotted against a compressive loading index. The results were obtained by systematically varying proportions in the buckling analysis and observing the minimum mass required for a given end load. The minimum mass conventional three element beam with diagonal bracing is significantly lighter than the geodesic beam. However, the proportions for minimum weight are much different. The area of the diagonal stiffeners is less than 1% of the longerons whereas the geodesic beam has all areas essentially equal. An optimum configuration with equal areas would be of advantage for small loads that lead to minimum size members. The upper curve is for the trielement beam with all members equal area. In this case, it is much heavier than the geodesic beam.
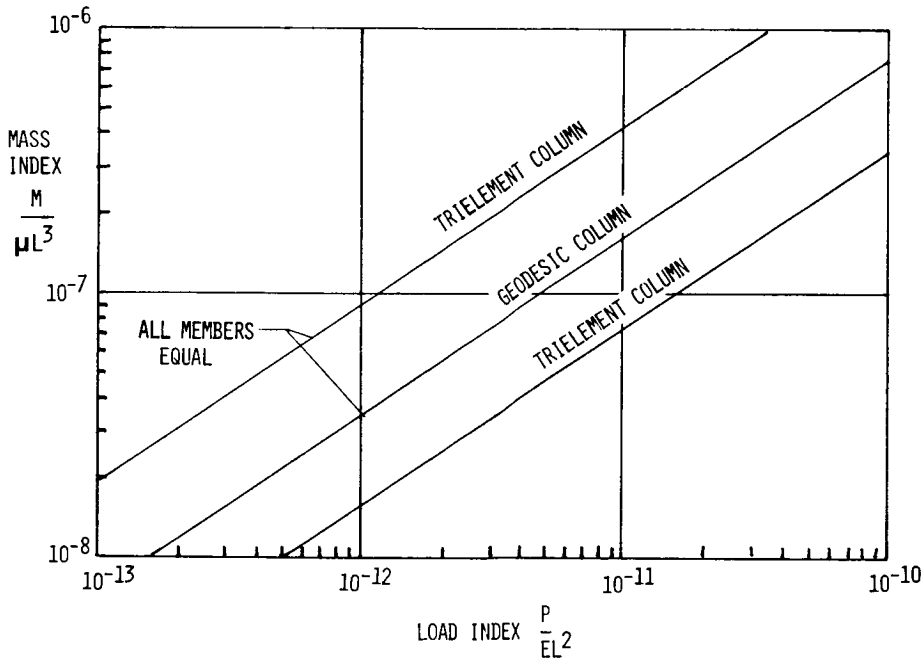
Figure 6

BUCKLING OF CABLE STIFFENED RING

The polygonal ring configuration with central mast used to attach cable stiffening has been proposed to support thin reflector or antenna surfaces The pretension of the cable puts the ring members in compression; additional compression is caused from the inward radial loads due to stretching a membrane like surface in the interior of the ring. For very large structures, the prevention of ring buckling can be a significant design requirement. The buckling problem for this configuration has been solved and typical results shown in figure 7. The radial buckling load Q which is applied at each vertex is plotted against a parameter proportional to the pretension in the cables. Also shown is the internal force in the ring, P. Both P and Q are expressed in terms of classical ring buckling parameters. The dashed line at the lower part of the figure indicates the load capability without cable stiffening. As pretension is increased, the buckling load increases. The single line on the left represents the point at which the cables go slack. The maximum load is reached when a general mode appears even while cables are still in tension. For this case the critical mode has 5 circumferential waves. Note that the n=2 mode, which is the lowest for an unstiffened ring, is higher than the n = 5 mode. Once the general buckling mode occurs, further increases in pretension cause a slow drop in the buckling load Q but the force in the ring remains essentially constant.
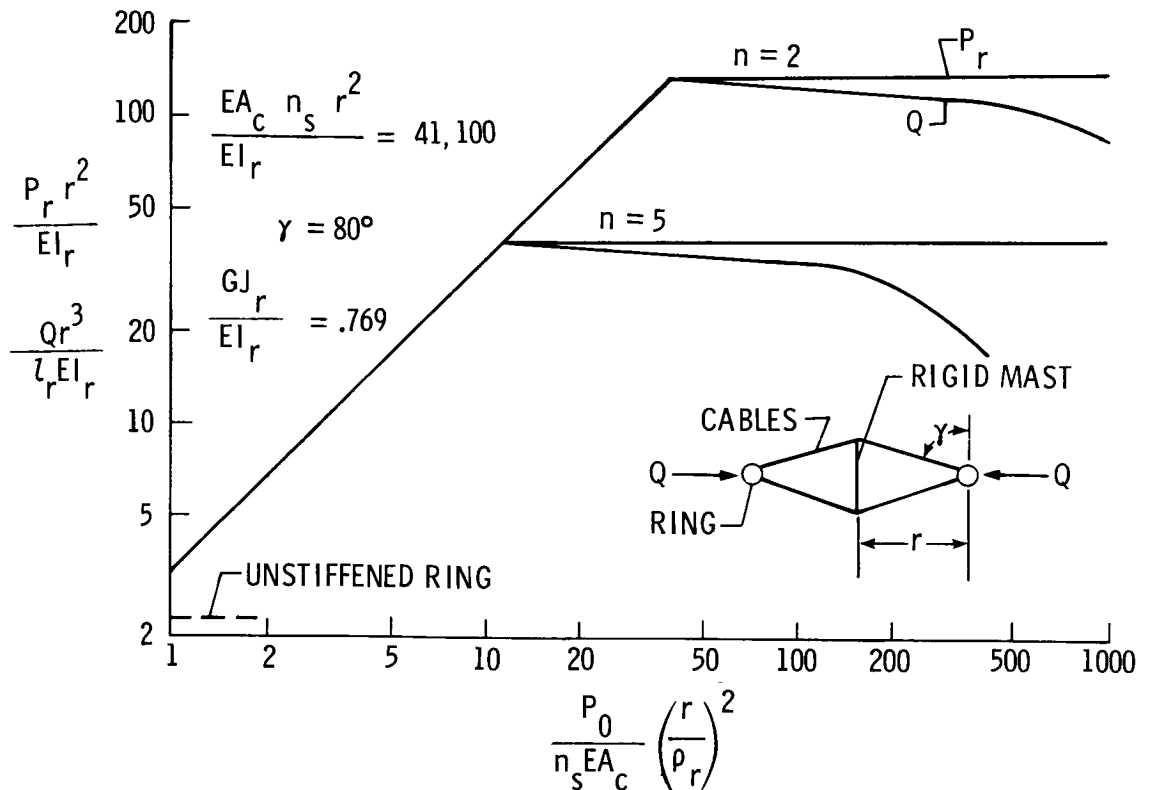
Figure 7

VIBRATION OF CABLE STIFFENED RING

The vibration characteristics of the same ring studied in figure 7 are shown in figure 8. Frequency is plotted against pretension for various values of the radial load Q. No frequency is shown at values of pretension lower than that required to prevent cables from going slack due to the load Q. The frequency then drops slowly until the buckling condition is approached. It drops very rapidly then to zero which represents the buckling solution of the previous figure. One effect that is missing from these calculations is the mass of the membane that is exerting the force Q. A method of including this effect is currently under development.
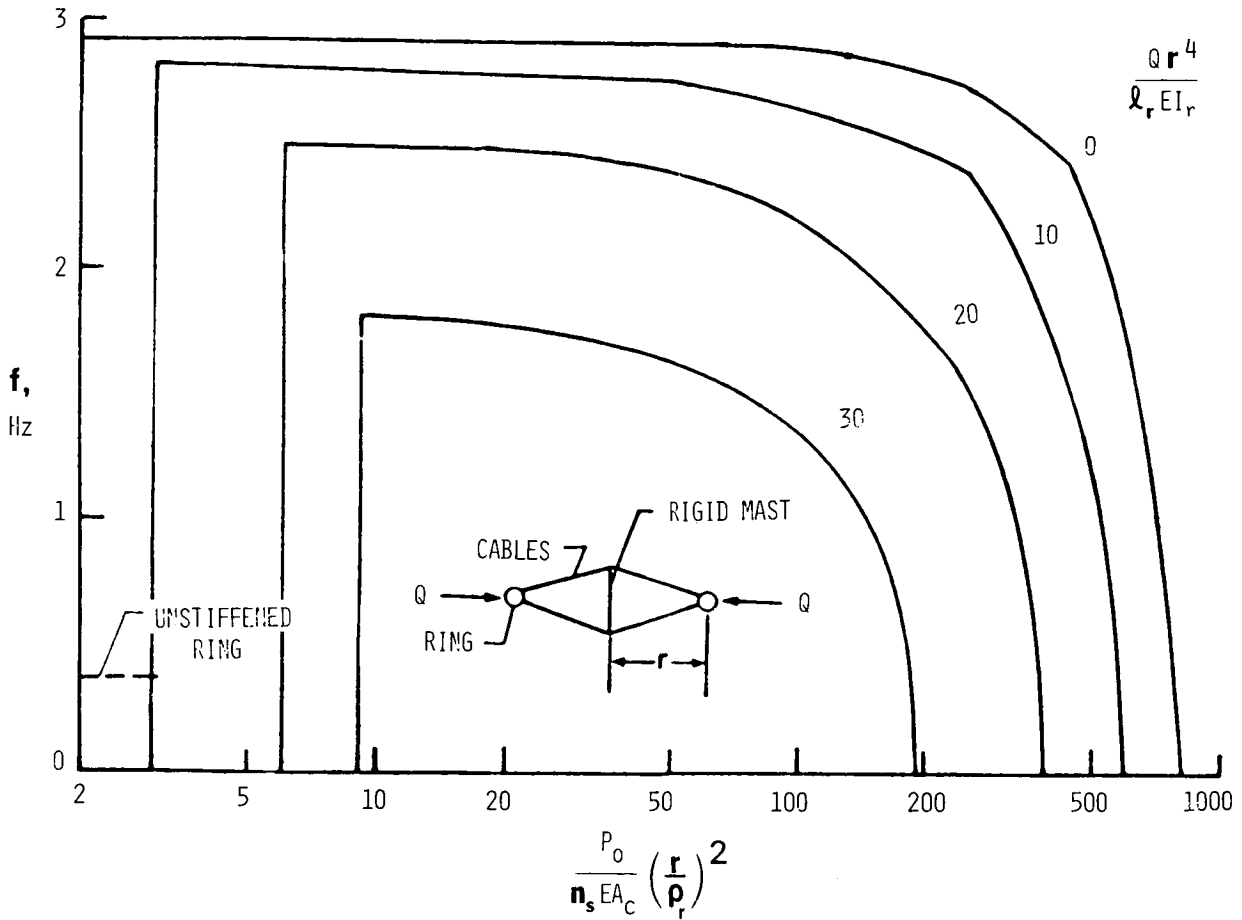
Figure 8

SUMMARY

An analysis for buckling and vibration of repetitive lattice structures has been developed. The results are essentially exact for ring configurations and for column configurations having simply supported ends. A wide variety of configurations are possible within the framework of one analysis. Results were given for typical configurations. In many areas, discrete effects not possible to determine with simple theory were identified. Yet the solution is no more complicated than the eigenvalues of a 6 x 6 matrix.

REFERENCE

1. Anderson, Melvin S.: Buckling of Periodic Lattice Structures. Presented at AIAA/ASME 21st Structures, Structural Dynamics, and Materials Conference Seattle, Washington. May 12-14, 1980. AIAA Paper No. 80-0681. To be published in AIAA Journal.

● ESSENTIALLY EXACT BUCKLING AND VIBRATION ANALYSIS DEVELOPED

● APPLICABLE TO A NUMBER OF LATTICE CONFIGURATIONS WITH REPETITIVE GEOMETRY

● COMPLEX BEHAVIOR ACCURATELY MODELED

● SOLUTION REQUIRES ONLY EIGENVALUES OF 6 X 6 MATRIX

Figure 9

STRUCTURAL SIZING CONSIDERATIONS FOR
LARGE SPACE STRUCTURES

Walter L. Heard, Jr., Harold G. Bush, and Joseph E. Walz
NASA   Langley Research Center
Structural Mechanics Division

INTRODUCTION AND OBJECTIVES

A number of missions for the Space Shuttle have been proposed which involve placing large truss platforms on-orbit (figure 1). These platforms range in size from tens of meters in span for reflector application to several thousand meters for solar power collector application. These proposed sizes and the operational requirements considered are unconventional in comparison to earthbound structures, and little information exists concerning efficient proportions of the structural elements forming the framework of the platforms. Such proportions are of major concern because they have a strong influence on the packaging efficiency and, thus, the transportation effectiveness of the Shuttle.

The present study is undertaken to: (1) identify efficient ranges of application of deployable and erectable platforms configured for Shuttle transport to orbit, and (2) determine sensitivity to key parameters of minimum mass deployable and erectable platform designs. The term "deployable" herein is limited to those structures that are manufactured, fully assembled, and folded for packaging in the Shuttle cargo bay on earth so that the complete structure can be unfolded on-orbit. "Erectable" structures would have the individual truss members manufactured and precisely set to length on earth, but not assembled into full platforms until orbit is achieved. Each of these concepts has its advantages and disadvantages, and it is important to know the sizes and applications that may be best suited to deployable construction and those where erectable structures may have the advantage.

Figure 1

46
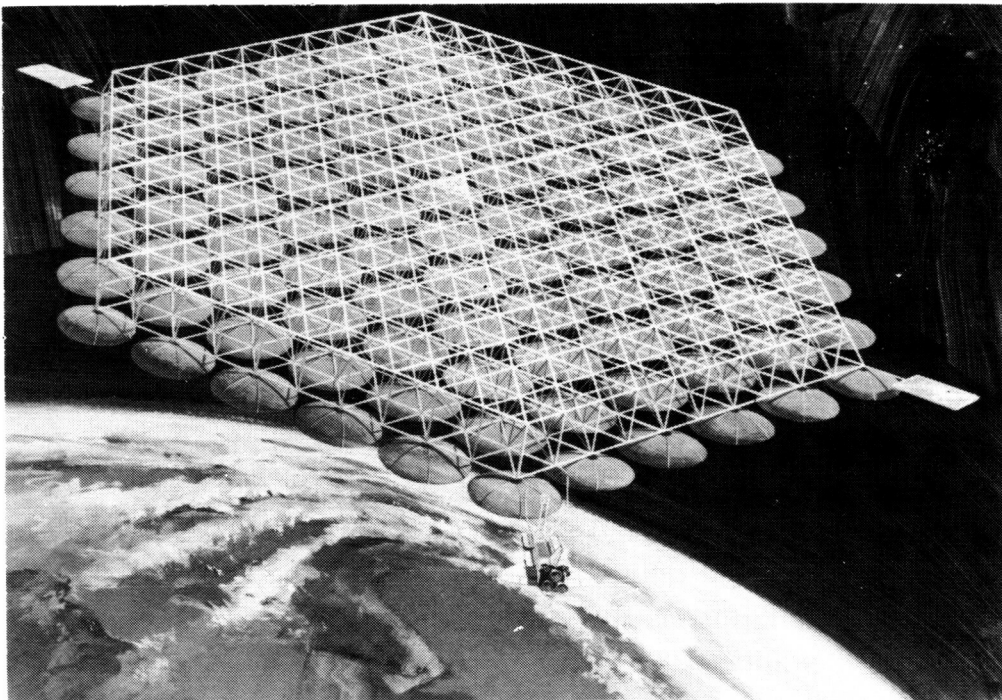
STRUCTURAL CONFIGURATION

To accomplish the objectives the tetrahedral truss was selected as the mathematical model because of its inherent low mass and high stiffness characteristics. Figure 2 describes the structure and the terminology used. The platform has a hexagonal planform of maximum span D. A distributed nonstructural (payload) mass may be attached to one surface. The expanded view in figure 2 shows a cutaway segment of the truss without the surface covering. The platform is constructed of face struts which are the members in the upper and lower surfaces of the platform, and core struts which are the intersurface members. The struts are interconnected by cluster joints which accommodate nine struts per node -- six face struts and three core struts. The face struts may have different geometric proportions than the core struts and may also be of different material. However, all results shown herein are for graphite-epoxy strut material and aluminum joints. Joint masses were assumed to be proportional to strut diameters with mass factors taken from actual laboratory specimens.

HEXAGONAL PLANFORM   TRUSS SEGMENT
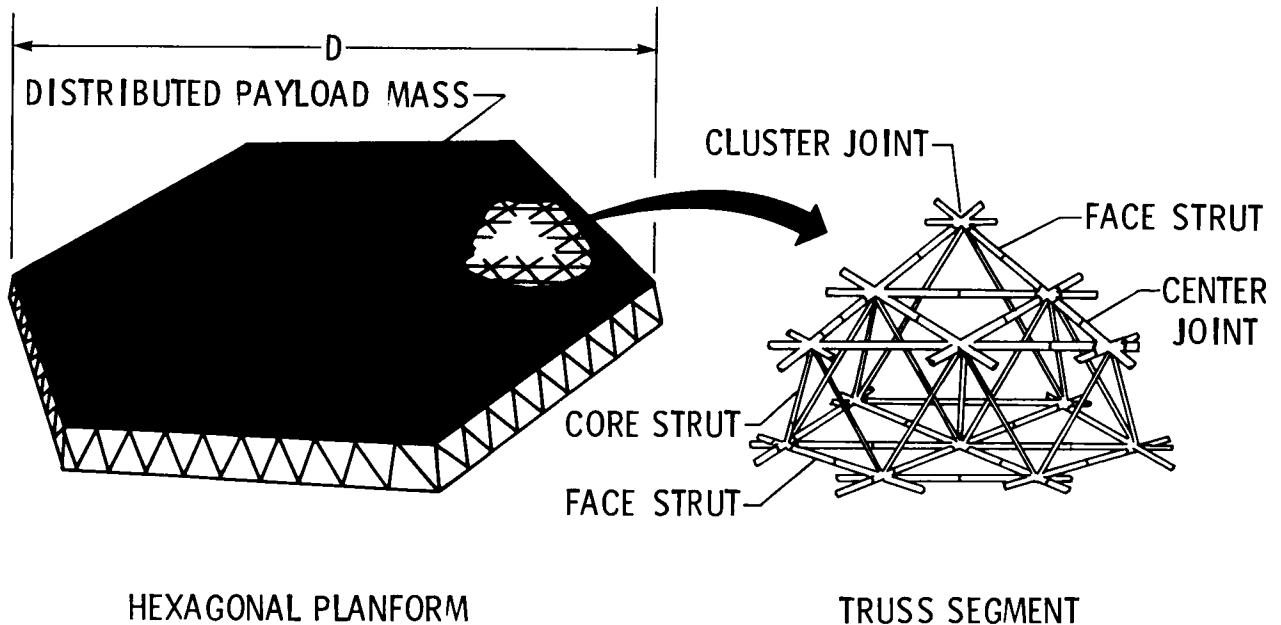
Figure 2

The packaging details for the deployable platform are shown in figure 3; the appropriate equations are presented in reference 1. The deployable platform is assumed to be constructed of cylindrical struts. The face struts are hinged at their centers to fold inward. The core struts are one piece. In this arrangement the face struts can never be longer than the core struts or interference will occur between upper and lower face struts in the folded configuration. The maximum allowable length of the package is taken to be 18 meters, the approximate length of the Shuttle cargo bay. This folding arrangement is usually more efficient than outward folding surface struts because it permits packaging of a deeper and thus a stiffer platform in the Shuttle cargo bay. The cross-sectional area and volume requirements for packaging are functions of six variables -- face strut diameter, length, and thickness, and core strut diameter, length, and thickness.

SIZING VARIABLES FOR
STRUCTURAL OPTIMIZATION

TOP VIEW SHOWING PACKAGED TRUSS GEOMETRY

PACKAGE WITH INWARD FOLDING FACE STRUTS
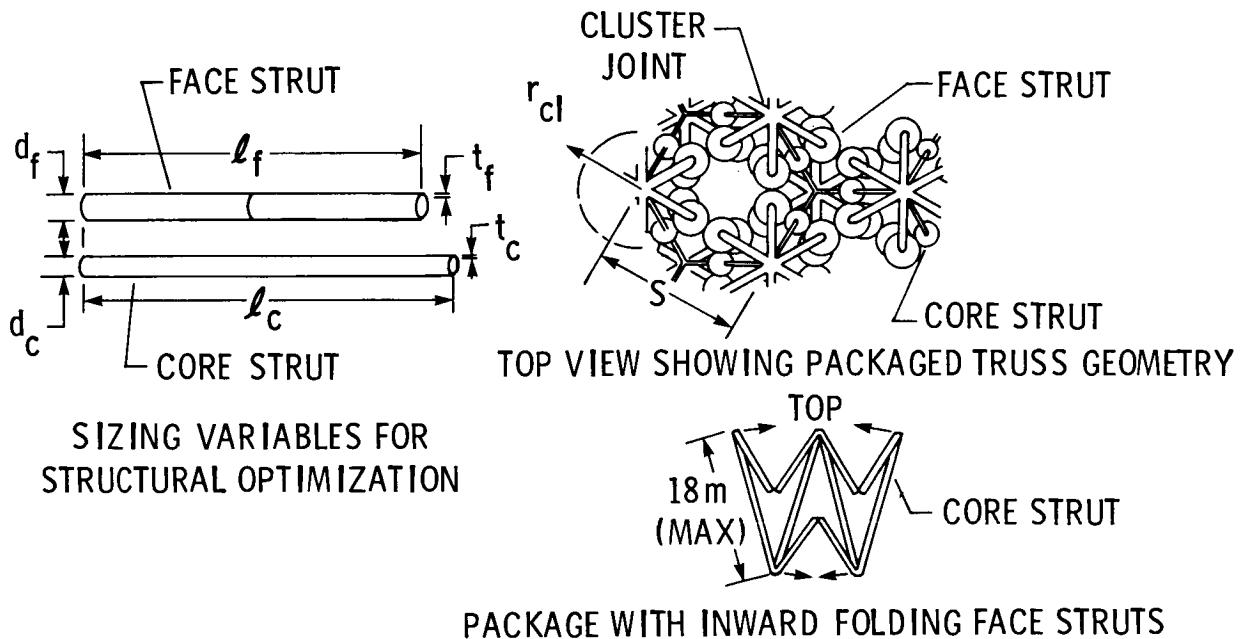
Figure 3

The packaging details for the erectable platform are shown in figure 4; the appropriate equations are presented in reference 1. The erectable platform truss is constructed of doubly tapered, nestable, struts which are assembled from two conical strut halves joined at their large ends. The strut halves are nested like ice-cream cones, packed in the Shuttle in stacks of strut halves, and assembled into full struts on-orbit. The stacks of strut halves may not exceed 18 meters in length. A square packing array is assumed for the cross-sectional packaging arrangement of the stacks so that the maximum diameters of the struts determine the approximate cross-sectional area required for stowage. The other variables that determine packaging requirements are thicknesses, lengths, and minimum diameters of the face and core struts -- eight variables in all.

SIZING VARIABLES FOR STRUCTURAL OPTIMIZATION

PACKAGED STACKS OF NESTED STRUT HALVES

SQUARE PACKING ARRAY ASSUMED

Figure 4

49
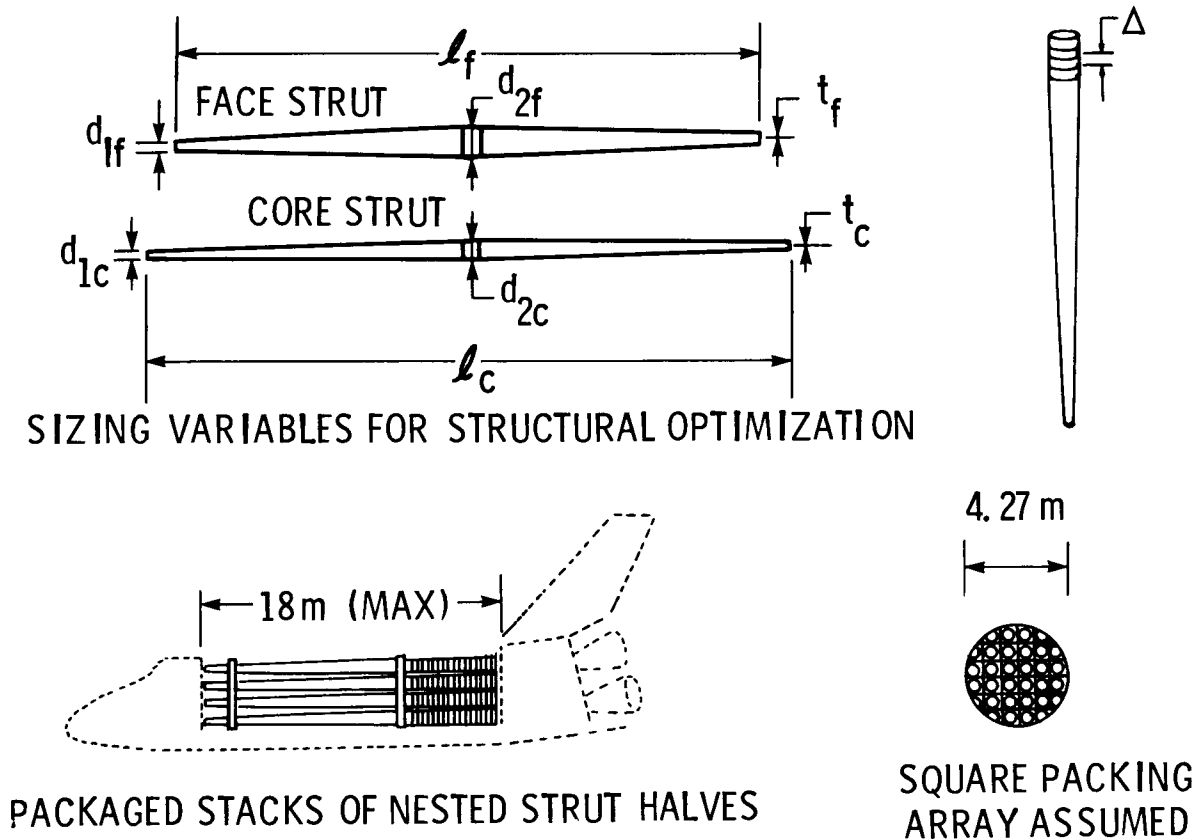
Figure 5 indicates the approach used to arrive at optimum designs. The objective is to minimize the structural mass per unit area of the platform (ref. 1) with respect to the strut proportions. The minimization takes place subject to any number of design requirements and constraints deemed pertinent to the problem and which can be written analytically. The CONMIN computer program (ref. 2) which uses mathematical programming techniques to solve nonlinear, constrained, optimization problems is used as the structural optimizer.

- **MINIMIZE PLATFORM STRUCTURAL MASS PER UNIT AREA,**

$$\left(\frac{M}{A}\right)_{PLATFORM} = \left(\frac{M}{A}\right)_{STRUTS} + \left(\frac{M}{A}\right)_{JOINTS}$$

- **WITH RESPECT TO STRUT PROPORTIONS,**

  THICKNESSES
  DIAMETERS
  LENGTHS

- **SUBJECT TO DESIGN REQUIREMENTS AND CONSTRAINTS.**

- **OPTIMIZER -- CONMIN COMPUTER PROGRAM.**

Figure 5

DESIGN CONSTRAINTS

Simple analytical relations are presented in reference 1 for the platform structural response. These relations become the constraints used to size the struts according to specified response standards. For instance, as shown in figure 6, the platform fundamental frequency can be constrained to be greater than or equal to a specified design frequency predetermined to insure sufficient platform stiffness for mission accomplishment. The fundamental frequency of the struts can also be constrained to some multiple value of the platform design frequency. In addition, strut loads arising from a variety of sources can be constrained to be less than or equal to the strut Euler buckling load. Other effects such as initial curvature of the strut axis and strut taper which affect strut axial stiffness and ultimately platform bending stiffness are also considered. Some selected numerical results for tetrahedral truss platforms optimized in this manner are shown in the next three figures.

STRUCTURAL RESPONSE	CONSTRAINT
● f_T, TRUSS FUNDAMENTAL FREQUENCY (FREE EDGES)	$f_T \geq f_d$
● f_s, STRUT FUNDAMENTAL FREQUENCY (SIMPLY SUPPORTED)	$f_s \geq k f_d$
● P, STRUT LOAD (SIMPLY SUPPORTED)	$P \leq P_E$

WHERE

$P = P_d$, CONSTANT DESIGN LOAD (ASS'Y, DOCKING, ETC.)

$= P_{gg}$, GRAVITY GRADIENT CONTROL LOAD

$= P_{ot}$, ORBITAL TRANSFER LOAD

Figure 6

PLATFORM DESIGN FREQUENCY EFFECTS

For the results in figure 7, a distributed payload mass of 0.1 kg/m^2 was assumed. Also, the strut fundamental frequency was required to be at least 10 times the platform design frequency. The results in the left-hand plot in figure 7 show that the mass per unit area of efficient deployable and erectable platforms is comparable over the range of design frequencies investigated, and that platform frequency has a very strong influence on the structural mass requirements (nearly proportional). Note also that the structural mass per unit area values for efficient platforms are very low -- on the order of a mesh reflector surface-covering.

The effect of platform design frequency on Shuttle transportation requirements is shown in the right-hand plot in figure 7. In the lower frequency range, the number of Shuttle flights required to orbit erectable and deployable platforms of a given size is similar. In the higher frequency range, Shuttle flights increase sharply for deployable platforms while erectables exhibit a more gradual increase. This is because at the lower frequencies, the packaged platforms are mass controlled Shuttle cargos. At higher frequencies erectable platforms remain mass controlled cargos, but the deployable platform packages become volume controlled cargos. These results indicate that for a given size platform, there is a practical design frequency (i.e. structural stiffness) upper limit for deployable platforms, above which transportation costs will become increasingly prohibitive.
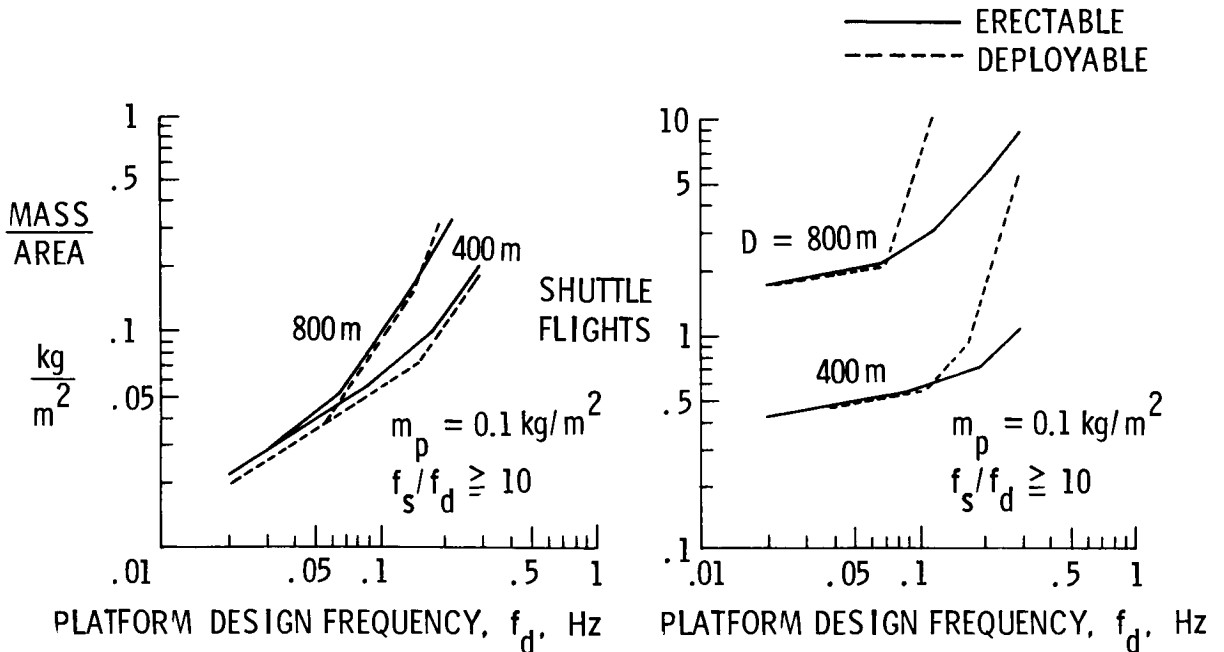
Figure 7

STRUT DESIGN FREQUENCY EFFECTS

For the results shown in figure 7 the strut frequency was specified to be at least ten times the platform design frequency. The effect of relaxing this requirement is presented in figure 8. Results are shown for both 800 and 400 meter erectable and deployable platforms, designed for a .1 Hz fundamental frequency. Again, the payload mass is assumed to be .1 kg/m^2. The left-hand plot in figure 8 shows that the mass per unit area requirements at the strut frequency factor of ten are approximately four-to-five times greater than that for a frequency factor of two. This indicates that strut frequency factor is a strong structural design driver (mass per unit area requirements are nearly proportional to strut frequency requirements). The right-hand plot shows that the Shuttle flights required by the 400 meter platforms are not greatly affected by the strut frequency factor over the range investigated. However, an abrupt increase in Shuttle flights occurs for the 800 meter deployable platform above a strut frequency factor of five indicating that practical limits for this parameter also exist for large deployable platforms.
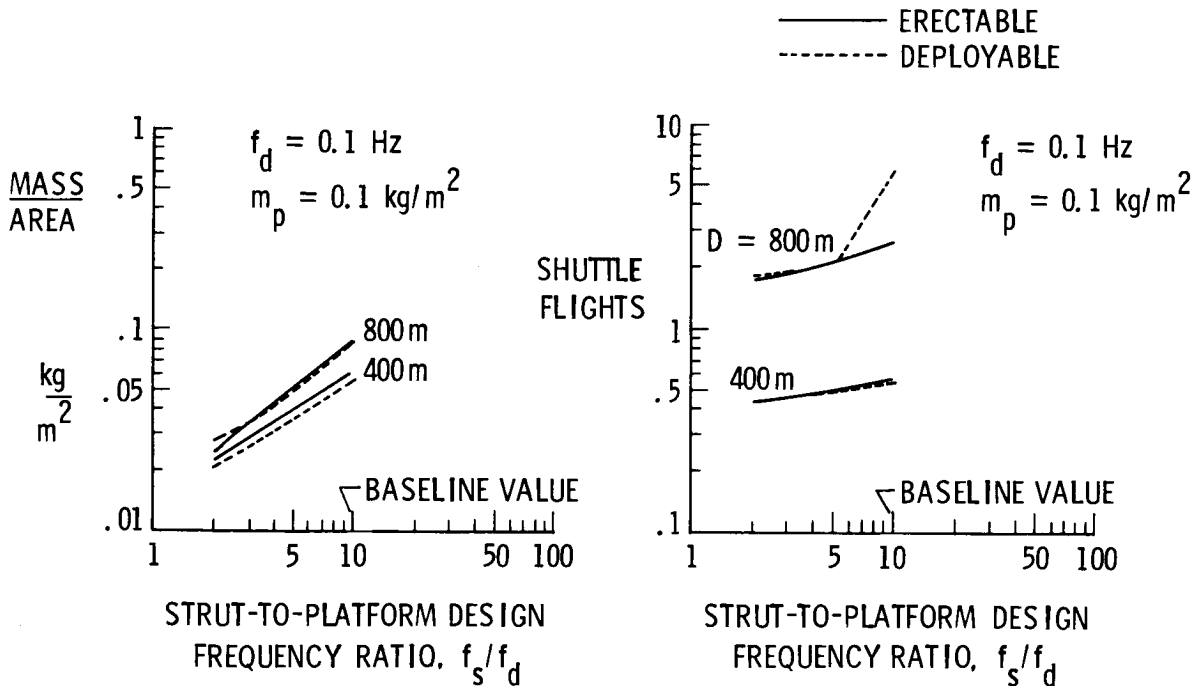
Figure 8

Figure 9 shows the effect of a constant strut design load on mass and transportation requirements. The range of design loads considered is from 10 to 400 Newtons. Again, calculations are for a payload mass of .1 kg/m^2, a .1 Hz platform design frequency, and a strut frequency factor of ten. The structural mass per unit area requirements shown in the left-hand plot in figure 9 are not greatly affected over the load range considered except for the 400 meter deployable platform which shows about a factor of two mass increase. The right-hand plot shows that Shuttle transportation for erectable platforms (solid lines) is also relatively unaffected over this load range. There is, however, a significant impact of strut design load on the Shuttle transportation for the 400 meter deployable platform. Transportation requirements increase from .5 flights, for essentially zero design load, to approximately four flights for a design load of 400 Newtons. (The increased strut cross-section required to carry the design loads causes a factor of eight packaging penalty on the 400 meter deployable platform). The transportation requirements for the 800 meter deployable platform indicate that the larger strut cross-sections required to satisfy frequency constraints are sufficient to carry strut loads up to approximately 80 Newtons. Above this value, strut cross-section increases significantly to carry the load, as shown by the increased Shuttle flight requirements -- about a factor of two over the range of loads investigated.
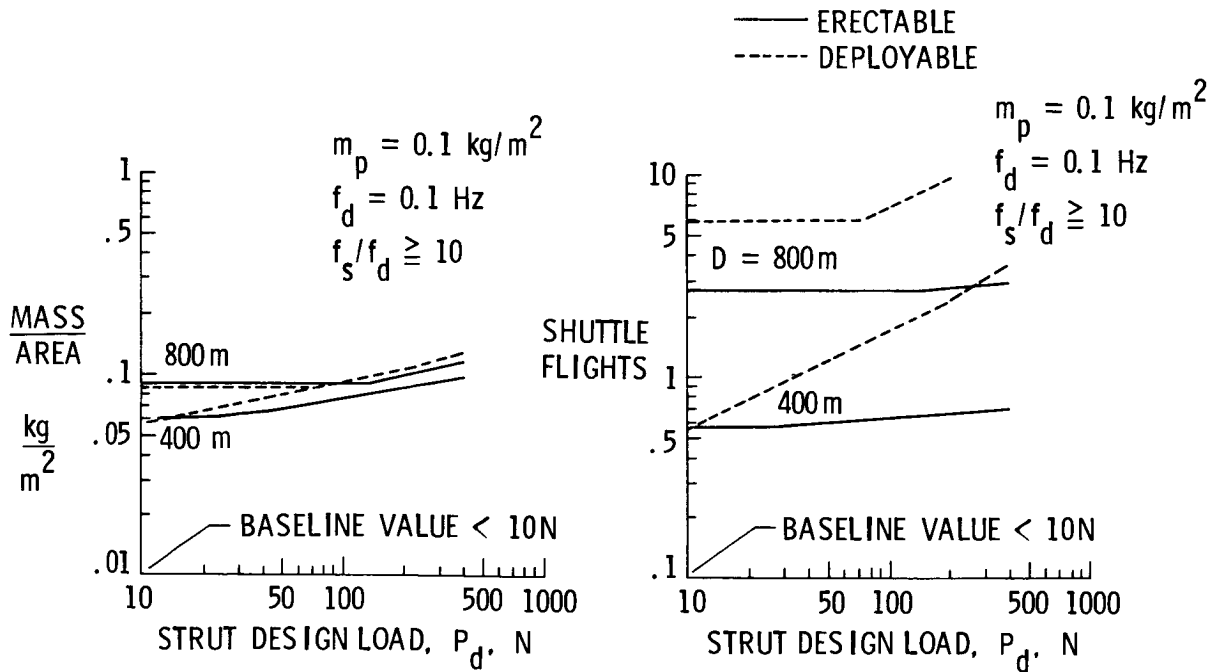
Figure 9

TRANSPORTABILITY OF SLENDER STRUT DEPLOYABLE PLATFORMS

The structural proportions which characterize minimum mass truss designs are extremely important, particularly for deployable trusses (ref. 3). Conventional truss structures typically employ struts having slenderness ratios (ratio of strut length to radius of gyration) less than 300. The platform designs presented herein exhibit strut slenderness ratios ranging from 600 to 4000, and still satisfy all imposed design requirements.

The benefits of slender strut construction are illustrated in figure 10, where the Shuttle flights required to orbit various size platforms are given as a function of the optimum strut slenderness ratio. For these calculations the payload mass, m_p, is .1 kg/m^2 and struts are constrained to have a fundamental frequency of at least ten times the platform fundamental design frequency. The curves for each platform size are the loci of minimum mass designs and encompass an approximate range of platform design frequencies from .04 Hz to .28 Hz. For a given size platform, as slenderness ratio increases (and frequency decreases) the Shuttle flights required to transport that platform to low earth orbit decrease rapidly. Each curve exhibits an abrupt change at an approximate slenderness ratio value of 1600. At slenderness ratios less than this value, Shuttle flights of deployable tetrahedral trusses are volume controlled; above this value they are mass controlled for the design requirements considered in this study. The potential benefit of reducing the number of Shuttle flights required to orbit a large deployable platform (e.g. antenna or collector surface) is sufficiently attractive to warrant a thorough investigation of slender strut construction of large truss platforms.
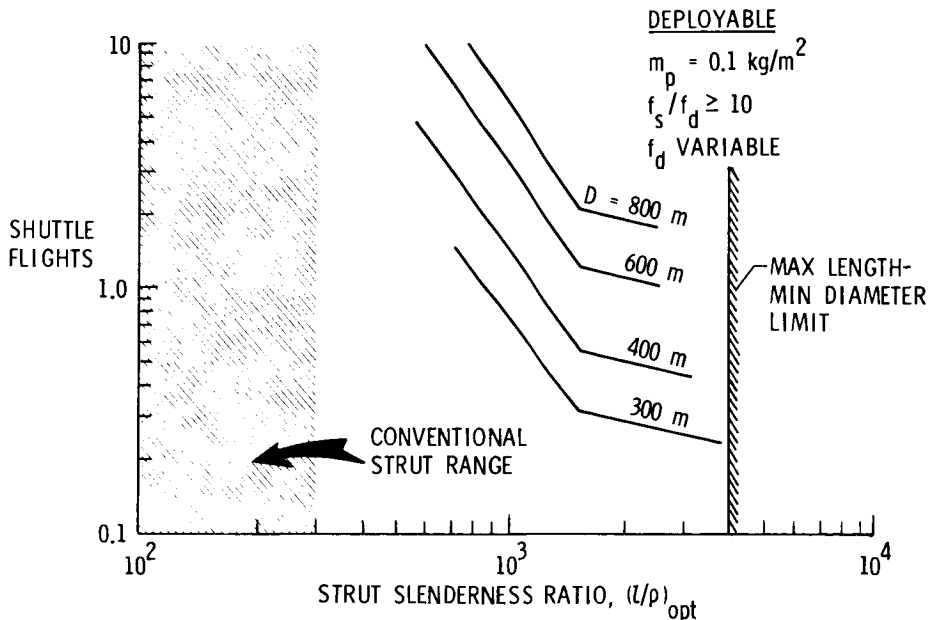
Figure 10

ORBITAL TRANSFER OF DEPLOYABLE PLATFORMS

All results shown in the previous figures have been for platforms sized for low earth orbit operation. If these platforms require subsequent transfer to geosynchronous orbit for mission accomplishment, they must be sized to withstand the acceleration loads for this maneuver. For an initial assessment of orbital transfer loads, the effects on deployable platform transportation requirements were examined and results are shown in figure 11. The study is limited to considering only constant thrust chemical propulsion systems. The propulsion system thrust load is applied normal to the surface of the platform at the three centermost cluster joints. Deployable platforms of 100, 150, and 200 meter spans are sized for thrust-to-weight ratios ranging from .001 to .1 g's. The results show only the number of Shuttle flights required to place a platform sized for these thrust loads into low earth orbit. The transportation requirements for orbiting the propulsion system to send the platform on to geosynchronous orbit are not shown. For the conditions specified, these results indicate that the maximum size platform that could be placed in GEO, using one Shuttle flight to LEO, is approximately 200 meters in span using a thrust-to-weight ratio of .01 g. The maneuver would take about 15 hours. A faster transport time for a 200 meter platform would require heavier struts to carry the larger acceleration loads, thus multiple Shuttle flight would be required to orbit the larger package.
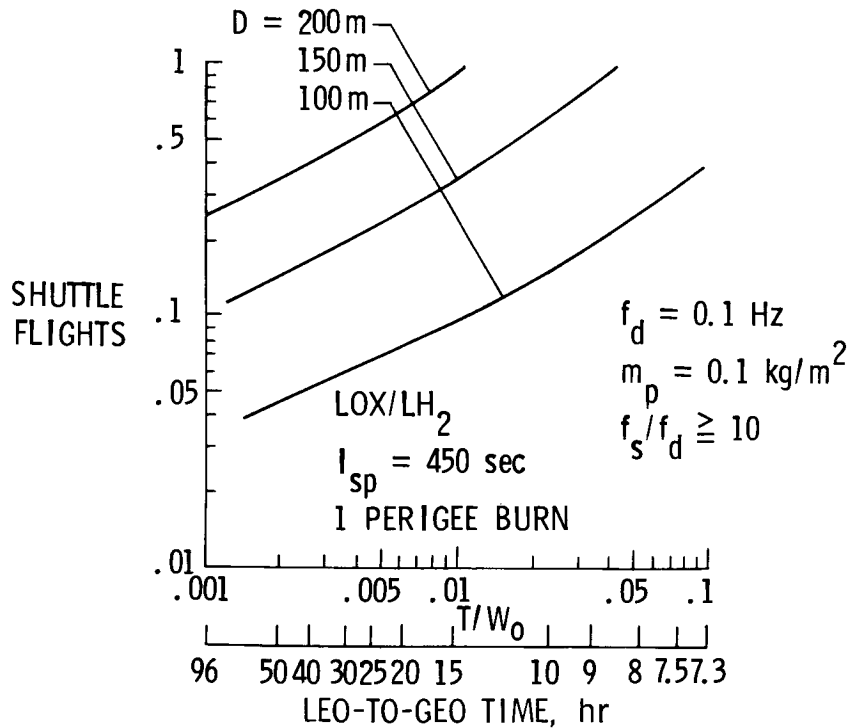
Figure 11

CONCLUDING REMARKS

Large deployable and erectable tetrahedral truss platforms are sized for minimum mass to meet a variety of practical design requirements using computerized mathematical programming techniques. These platform designs are characterizd by ultra-low structural mass per unit area which is equivalent to that of mesh reflector surfaces.

The struts for minimum mass deployable and erectable truss platforms are found to be much more slender than struts conventionally used for earthbound structural applications. The transportation efficiency exhibited by platforms constructed of these slender struts warrants a thorough investigation to determine the feasibility of fabricating spacecraft in this manner.

Platform fundamental frequency, which is a measure of overall structural stiffness, is shown to be a strong design driver, indicating a need to determine the minimum acceptable value of this parameter which will permit mission accomplishment. The severe effect on structural proportions of maintaining high strut frequency relative to platform frequency also indicates a need to determine the minimum value of this parameter required to prevent vibrational coupling between strut and platform.

Preliminary orbital transfer investigations indicate that deployable platforms of up to 200 m span may be placed in geosynchronous orbit with a single Shuttle flight using a constant thrust chemical propulsion system which limits initial acceleration to .01 g or less.

● EFFICIENT DESIGNS EXHIBIT ULTRA-LOW STRUCTURAL MASS

● STRUT SLENDERNESS RATIOS MUCH GREATER THAN CONVENTIONALLY USED FOR EARTHBOUND STRUCTURES

● PLATFORM AND STRUT FREQUENCY REQUIREMENTS ARE STRONG STRUCTURAL DESIGN DRIVERS

● HIGH STIFFNESS REQUIREMENTS LIMIT THE RANGE OF APPLICABILITY OF DEPLOYABLE PLATFORMS

● PLATFORMS OF UP TO 200 m SPAN, SIZED FOR ORBITAL TRANSFER TO GEO, REQUIRE ONE SHUTTLE FLIGHT TO LEO

Figure 12

REFERENCES

1. Heard, Walter L., Jr.; Bush, Harold G.; Walz, Joseph E.; and Rehder, John J.: Structural Sizing Considerations for Large Space Platforms. AIAA Paper No. 80-0680, presented at the AIAA/ASME 21st Structures, Structural Dynamics and Marterials Conference, Seattle, WA, May, 1980.

2. Vanderplaats, G. N.: CONMIN -- A FORTRAN Program for Constrained Function Minimization -- User's Manual. NASA TM X - 62282, Aug. 1973.

3. Bush, Harold G. and Heard, Walter L., Jr.: Recent Advances in Structural Technology for Large Deployable and Erectable Spacecraft. NASA TM - 81905, Oct. 1980.

DEPLOYMENT TESTS OF A 36-ELEMENT TETRAHEDRAL TRUSS MODULE

R. W. Herr and G. C. Horner
Langley Research Center
Hampton, Virginia

Second Annual Technical Review
November 18, 1980

DEPLOYABLE PLATFORM

OBJECTIVE:

DEVELOP BASIC STRUCTURAL TECHNOLOGY & TEST TECHNIQUES FOR LARGE DEPLOYABLE PLATFORMS

OUTLINE:

o GROUND DEPLOYMENT TEST METHODS FOR LARGE SPACE STRUCTURE

o SINGLE ELEMENT & 36 ELEMENT MODULE EXPERIMENTAL/ANALYTICAL RESULTS

o APPROX. ANALYSIS TO DETERMINE MAX. SIZE PLATFORM THAT CAN BE DEPLOYED IN GROUND TESTS

Figure 1.

36—ELEMENT DEPLOYABLE TRUSS

Photographs of the truss used in the deployment experiments are shown in figure 2. The upper surface is composed of twelve thin wall graphite-epoxy tubular elements foldable at their midpoints and hinged to a cluster joint at each end to form a hexagon. The nine element lower surface forms a triangle and is connected to the upper surface through thirteen non-folding inter-surface elements pinned at each end to a cluster joint. All elements were 38 mm in diameter by 2.134 m in length node to node and had a wall thickness of .6 mm. Surface elements were designed to fold outward forming a package 4.3 m in length by .3 m in diameter. Deployment energy was provided through the first half of the deployment cycle by a linear spring in each of the 21 surface elements. Surface elements were locked in the deployed position by a conventional spring loaded catch mechanism located on each knee-joint. Fifty-six percent of the 14.5 kg total truss mass was in the graphite-epoxy and the remainder in the aluminum joints and fittings. Several strain-gage bridges and accelerometers were installed on the truss to measure deployment loads.

DEPLOYED   PACKAGED
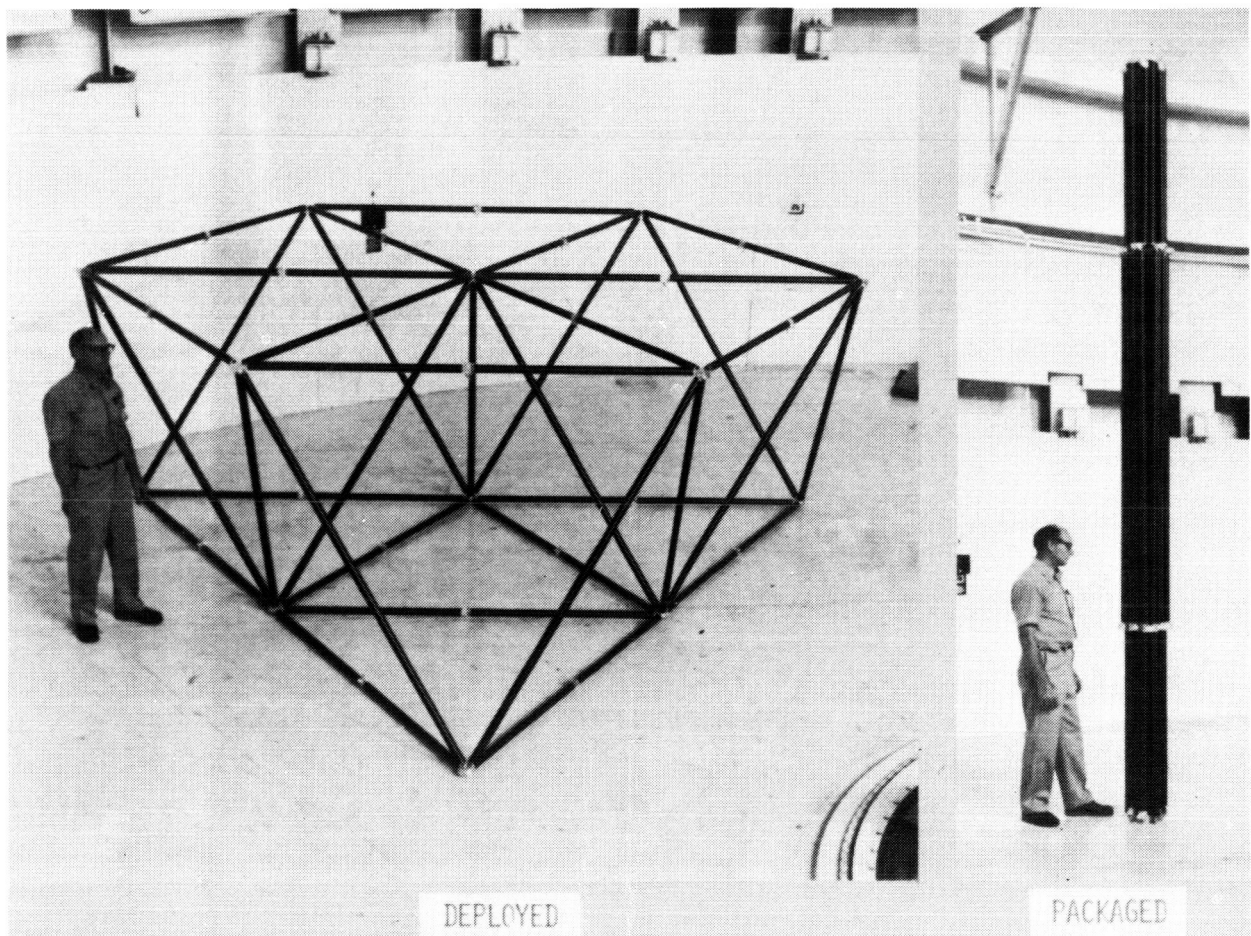
Figure 2.

MAXIMUM BENDING STRESS OF GRAPHITE-EPOXY ELEMENT

For a truss of the size shown in the previous figure, the principal deployment load (bending of a pinned-pinned beam) can be simulated without the use of deployment springs by testing a single surface element as indicated in figure 3. In this technique, a mass which is large relative to the mass of the element is fixed to each end of a foldable element and allowed to swing outward in pendulum fashion on long cables. The kinetic energy of the element at lockup can be accurately controlled by the separation at the upper end of the support cables. The maximum experimental bending stresses at lockup measured adjacent to the element knee-joint (open symbols) shows excellent agreement with stress predicted by the simple analytical expression given over a wide range of deployment energies. In the analytical expression d is the element diameter, E the modulus of elasticity, U_O the deployment energy, I the area moment-of-inertia, ℓ the element length, m the mass of the graphite/epoxy tube, and m_k the mass of the knee-joint.

$$\sigma_{MAX} = .933D\sqrt{\frac{3EU_O}{2I\ell}\left(\frac{1 + 2\frac{M_K}{M}}{1 + 3\frac{M_K}{M}}\right)}$$
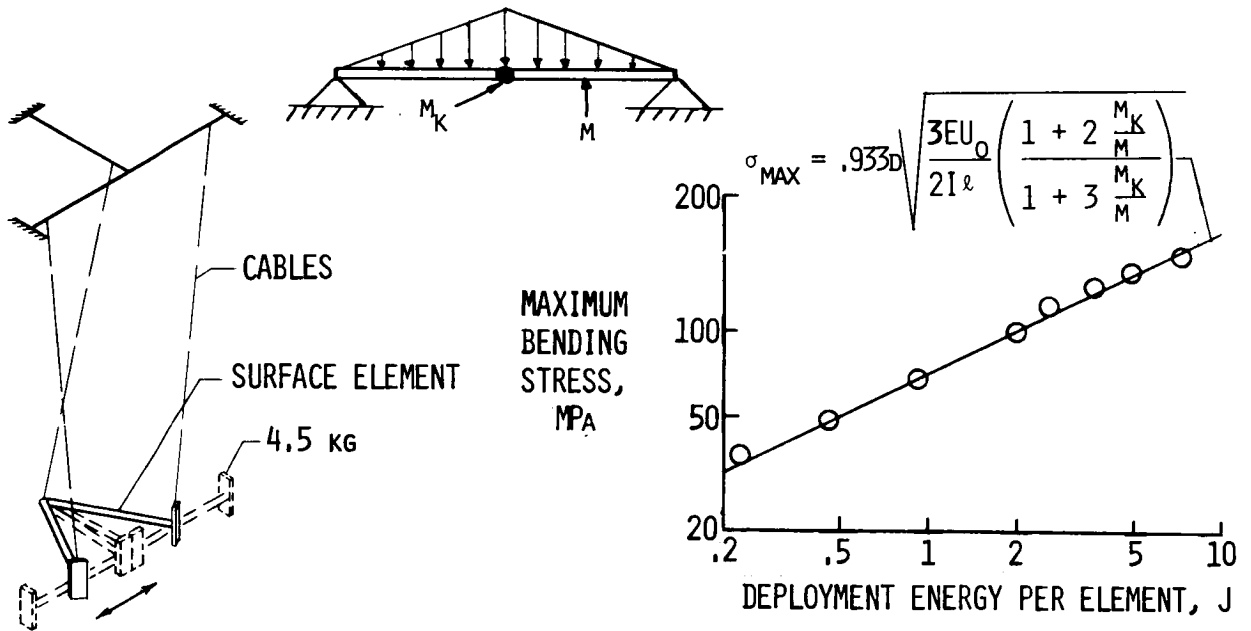
Figure 3.

TEST METHODS

In the past, models of deployable structures have been limited largely to small scale models which could be readily deployed by suspending the model on several soft shock cords. The scale of the deployable truss used in the present investigation precluded the use of this test technique as the gravity forces and moments are of the same order of magnitude as the deployment forces and moments. For these tests, the truss was deployed during free-fall in the LaRC 55' vacuum facility. Appreciably larger trusses could be deployed by lofting the packaged truss upward from the floor of the facility and allowing it to deploy during the upward as well as the downward portion of its trajectory, thus doubling the available test time. It must be realized, of course, that the mechanisms required to loft and decelerate such a large truss would be much more complex than those required for a straight drop.

O SOFT SUSPENSION

O STRAIGHT DROP

O LOFT AND DROP

Figure 4.

Deployment tests of the 36-element truss were conducted in the LaRC 55' vacuum facility as illustrated in figure 5. This facility is approximately 17 m in diameter and 18 m in height. The packaged truss was secured by a small diameter cable about its girth midway along its length. A pyrotechnic cable cutter was installed to sever the cable on command. Prior to a test, the 21 deployment springs were cocked and the packaged truss hoisted to the top of the facility by means of a 1.6 mm cable attached to the central cluster joint of the hexagonal surface. The support cable passed through a pulley at the top of the facility and was attached to a wall by means of a short loop of cable containing a pyrotechnic cable cutter. 8.2 m of slack cable was provided for free-fall as illustrated. Both pyrotechnic devices were actuated simultaneously, allowing the truss to deploy while in free-fall. After 1.3 seconds of free-fall, the 8.2 m of slack cable was used up and a wire energy absorbing device installed in the support cable just above the truss brought the deployed truss to a gentle halt. Signals from strain gage bridges and accelerometers were recorded on tape during deployment for later analysis.
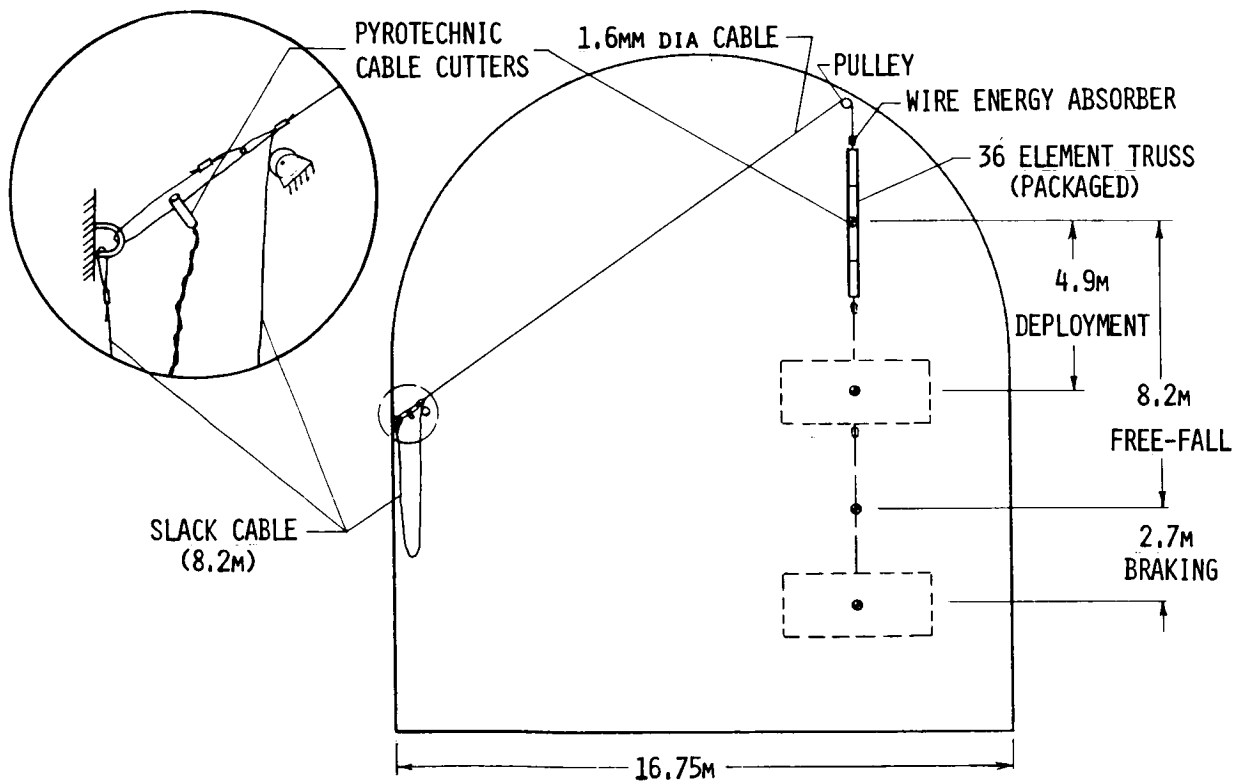
Figure 5.

WIRE ENERGY ABSORBER

After the free-fall test period, the deployed truss was brought to a gentle halt by means of the wire energy absorber depicted in figure 6. In this device a mild steel wire is pulled over a series of three pulleys yielding the wire in bending six times. The braking force is dependent upon the number and diameter of the pulleys and the diameter and yield strength of the wire. The energy absorber was designed for a drag force of 534 N thus limiting the load felt by the deployed truss to 3.75 g's.
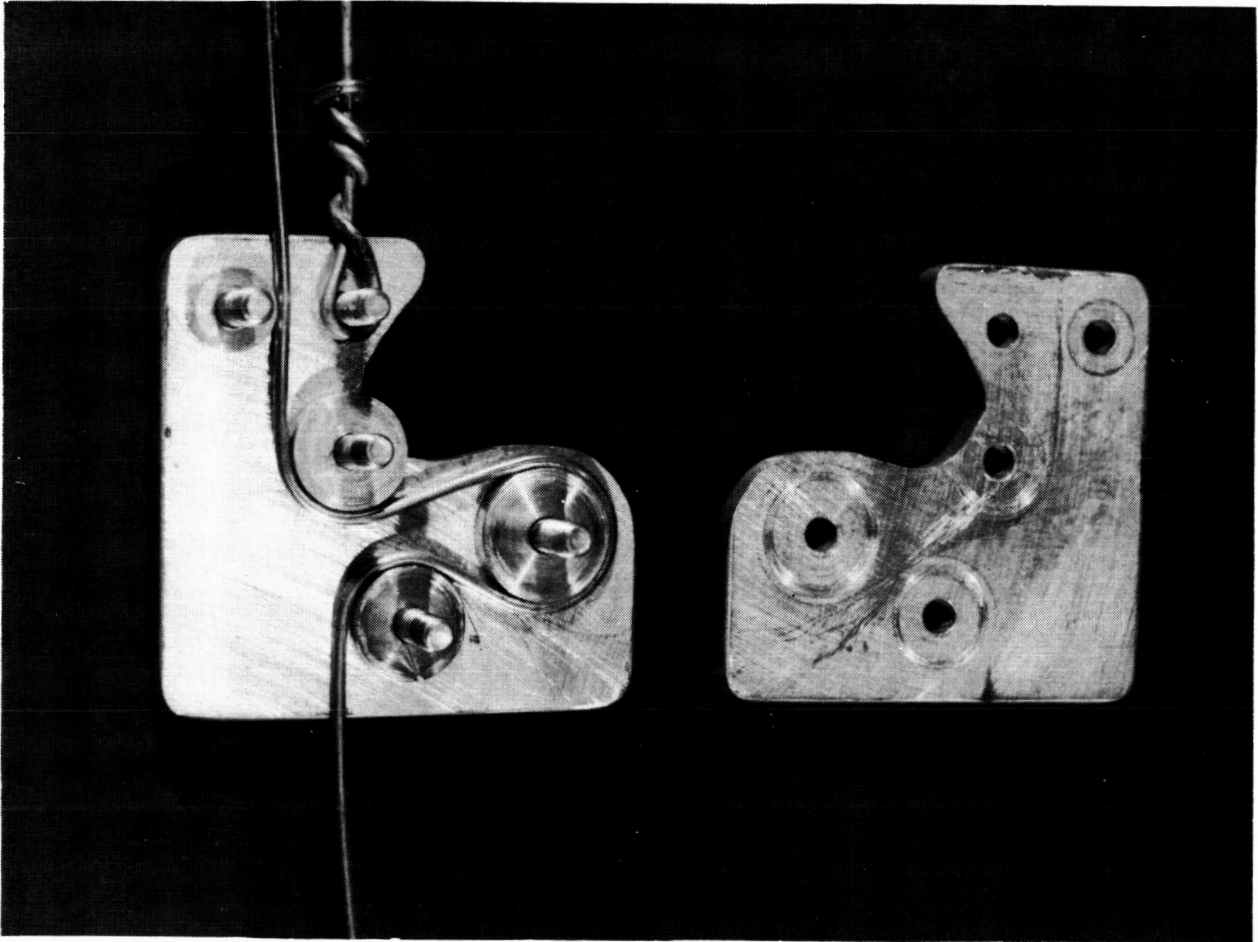
Figure 6.

EFFECT OF ATMOSPHERE ON VERTICAL ACCELERATION

A servo accelerometer mounted on one of the lower surfae cluster joints was oriented to measure the vertical acceleration. Figures 7(a) and 7(b) show time histories from this accelerometer during deployment tests conducted at atmospheric pressure and at 1/10th atmosphere, respectively. At atmospheric pressure, release occurs at time zero; lock-up at 1.1 seconds; braking from 1.4 to 2.0 seconds and bouncing on support cable from 2 seconds on. At 1/10th atmosphere, lockup and braking occurs .1 second earlier. The kinematic analysis indicated a deployment time of 1.05 seconds. For the tests at atmospheric pressure, the vertical acceleration is seen to drop initially to zero-g but increases (due to aerodynamic drag) to approximately .8g by the time the brake is applied. At 1/10th atmosphere, the acceleration between lockup and braking remains in the vicinity of zero-g.

(A) ATMOSPHERIC PRESSURE

(B) ONE-TENTH ATMOSPHERE
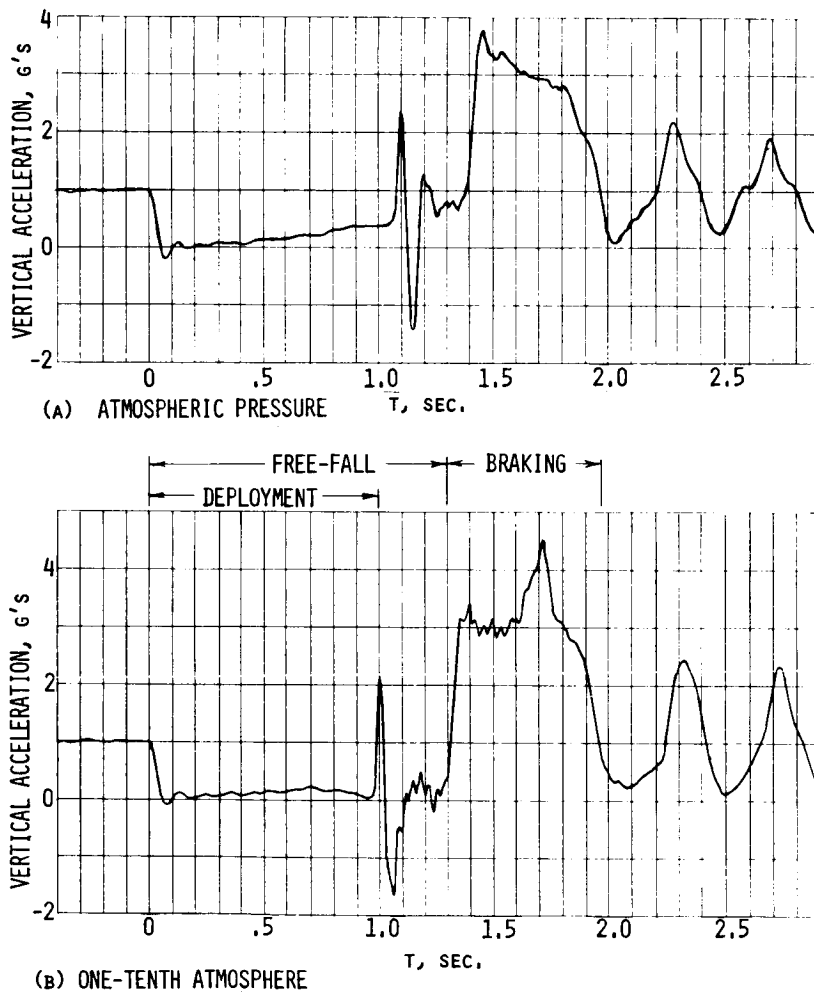
Figure 7.

RATIO OF MEASURED TO CALCULATED BENDING STRESS AT LOCKUP

Although the atmosphere had but a minor effect on deployment time, it was found to have a major effect on deployment loads. Strain gage bridges were located adjacent to the knee-joint of four surface elements (two on upper surface and two on the lower) to measure the bending stresses at lockup. In figure 8 the average of the stress measured on these four gages relative to the calculated stress of 107 MPa is tabulated for three deployment tests; two at atmospheric pressure and one at one-tenth atmosphere. For the tests conducted at atmospheric pressure, the average of the measured bending stresses was only 56% of calculated while at one-tenth atmosphere, the average of the measured bending stresses was the same as the calculated stress.

(CALCULATED STRESS = 107 MPa)

TEST NO.	TEST PRESSURE	STRESS EXP/CALC
1	1 ATMOS	.57
2	1 ATMOS	.55
3	1/10 ATMOS	1.00

Figure 8.

DIMENSIONLESS DEPLOYMENT TIME AS FUNCTION OF PLATFORM SIZE

The results of a simplified kinematic analysis are shown in figure 9 where the dimensionless deployment time is plotted as a function of the number of radial bays in the truss. In the dimensionless parameter, t represents the deployment time, U_o the deployment energy per element, ℓ the element length, and m_c the effective mass associated with each cluster joint. For values of N>4, the curves are essentially straight lines with a slope of 45°, indicating that the deployment time is proportional to N. The separation of the various curves show that deployment time is not only a function of the deployment energy but also how quickly that energy is delivered to the truss. It may be observed that the deployment time for a constant moment input is more than double that for an impulsive energy input. Since drop height for free-fall deployment tests varies as the square of the deployment time, the rapidity with which the deployment energy is put into the truss can become critical. The angle Θ represents half the included angle formed by the two halves of the foldable elements.
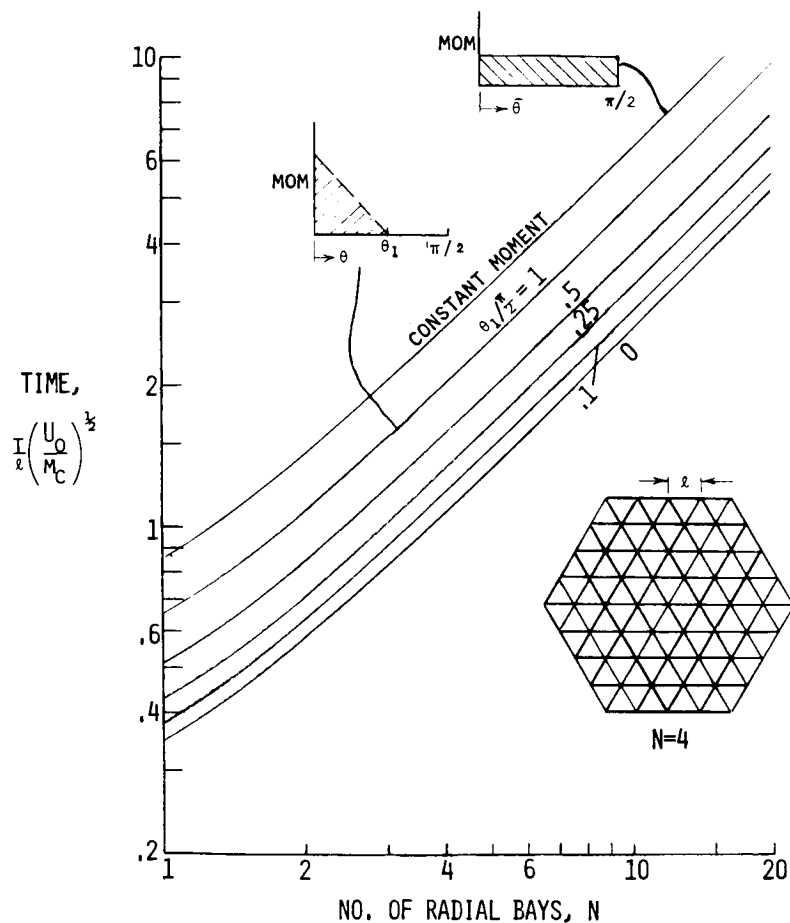

Figure 9.

FACILITY HEIGHT REQUIRED AS FUNCTION OF DEPLOYMENT ENERGY AND TRUSS SIZE

Utilizing the same truss elements as were used in the present deployment tests, figure 10 indicates the facility height required for deployment tests as a function of the deployment energy and the number of radial bays. The 18m working height of the LaRC 55' vacuum facility is indicated by the horizontal broken line. It is seen that in order to deploy a truss with two radial bays in this facility, the deployment energy of 2.3 J per element used in the present tests would have to be doubled and doubled again for N=3. Although the resulting bending stresses at these energy levels are not excessive, the design of the deployment spring and cocking mechanism may present some problems. An alternative test method which hypothetically doubles the test time is to loft the packaged truss upward from the floor of the facility and allow it to deploy during the upward as well as the downward portion of its trajectory. For a given height, this has the effect of cutting the energy requirements by a factor of four as indicated in the abcissa. Thus a truss having three radial bays could be deployed in the LaRC 55' vacuum cylinder using the same springs as were used in the present one bay test. The mechanism to loft and decelerate such a large truss would, of course, be much more complex.
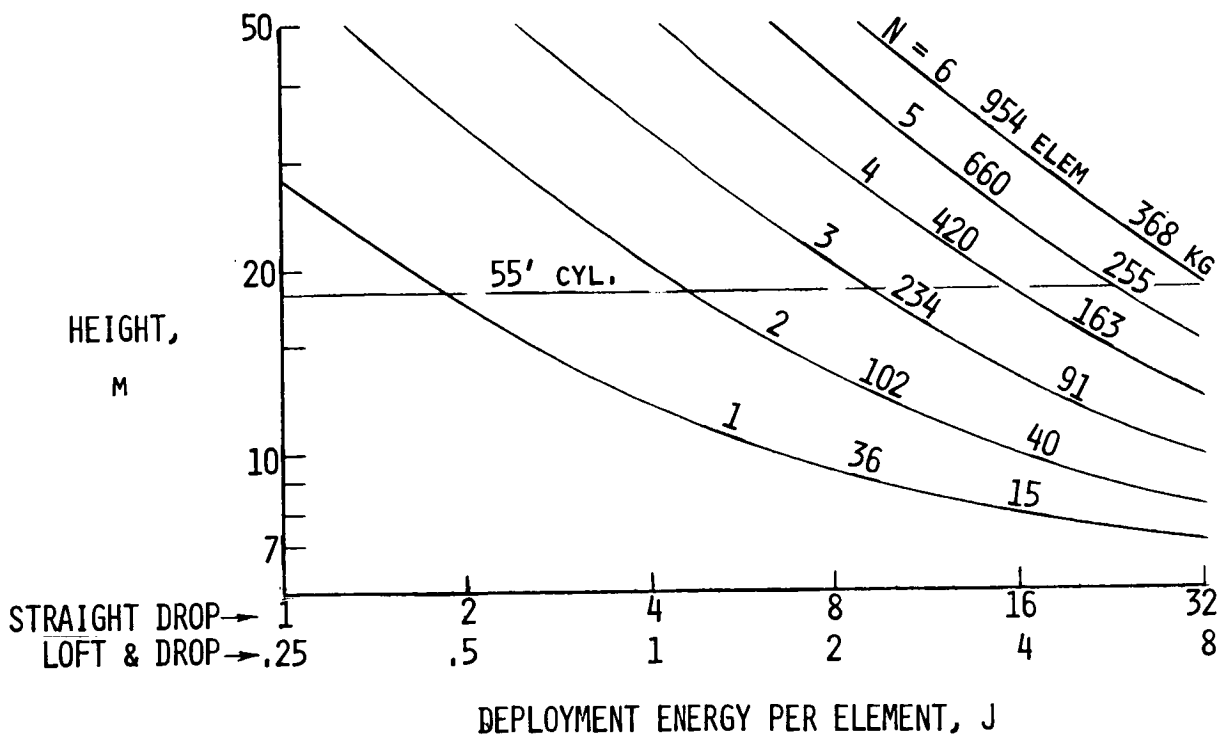

Figure 10.

AUTOMATED INSTALLATION OF

LARGE PLATFORM UTILITIES

R. M. Vernon

LOCKHEED MISSILES & SPACE COMPANY, INC.

Sunnyvale, California

LARGE PLATFORM ASSEMBLER-ORBITER MOUNTED CONFIGURATION

A contractual study of the "Development of Assembly and Joint Concepts for Erectable Space Structures" was undertaken by the Lockheed Missiles & Space Company, Inc., in January, 1979. This study was initiated by the NASA-LaRC and investigated the technology associated with the on-orbit assembly of tetrahedral truss platforms erected of composite tapered, nestable columns. The tetrahedral truss systems incorporate nine-member node joints; two types of these joints were designed and fabricated. Several concepts for assembly were investigated and a preferred concept, the gimballed parallelogram assembler, was developed. This assembly machine design provides fully automatic erection in either orbiter-attached or free-flying modes. For the free-flyer, construction materials (columns and node joints) are unloaded in canisters from the STS Orbiter. The design of machines for assembly of columns ranging in size from 4m to 20m was studied. The smaller machine, mounted on the Orbiter as shown in Figure 1, would be deployable and restowable. Concepts were also developed for STS packaging and transportation of construction materials and the assembler. An assessment of the effects of including non-structural systems in the assembly process was performed, and the effects on design and operation of the automated assembler evaluated. The results of the basic assembler studies are described in Reference 1.
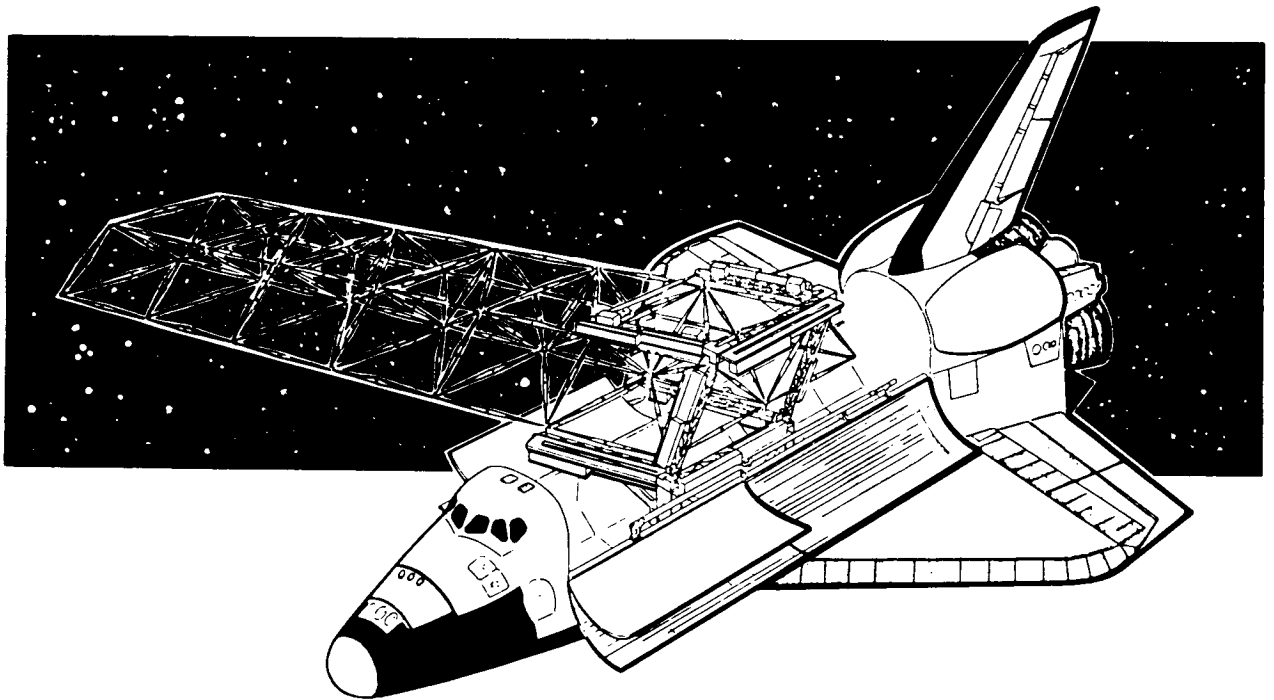

Figure 1

AUTOMATED ASSEMBLER DETAIL

The major structural features of the baseline automated assembler are
shown in the figure. This machine is designed to provide rapid assembly of
columns and node joints into a variety of platform shapes. It is also inher-
ently reliable, using simple, state-of-the-art mechanisms which perform sequen-
tial, repetitive operations. The machine consists of a four-sided main frame
having a gimbal joint at each corner. The relative position of the members is
controlled by a set of eight actuators which are used to align the frame with
the structure being constructed. Two pairs of swing arms, each pair connected
by a tie rod, provide for installation of columns in two parallel planes.
Supplies of node joints and half-columns are provided in special canisters;
node joint canisters are located on the rotating arms, while the half-column
canisters are contained in the column storage and assembly packages mounted on
one side of each member of the machine. The column assemblers transport com-
pleted columns to adjacent column insertion mechanisms which insert the column
ends into node joints held by the node retainers. The machine operates by
alternately attaching and releasing upper and lower node retainers as it moves
from node to node, inserting columns and dispensing node joints as it prog-
resses. In addition to the assembler structure and mechanisms, supporting sub-
systems are required for maneuver control, electrical power, command and
control, data handling and thermal control. For free-flying operation, three
additional subsystems are required. These are attitude control, communications,
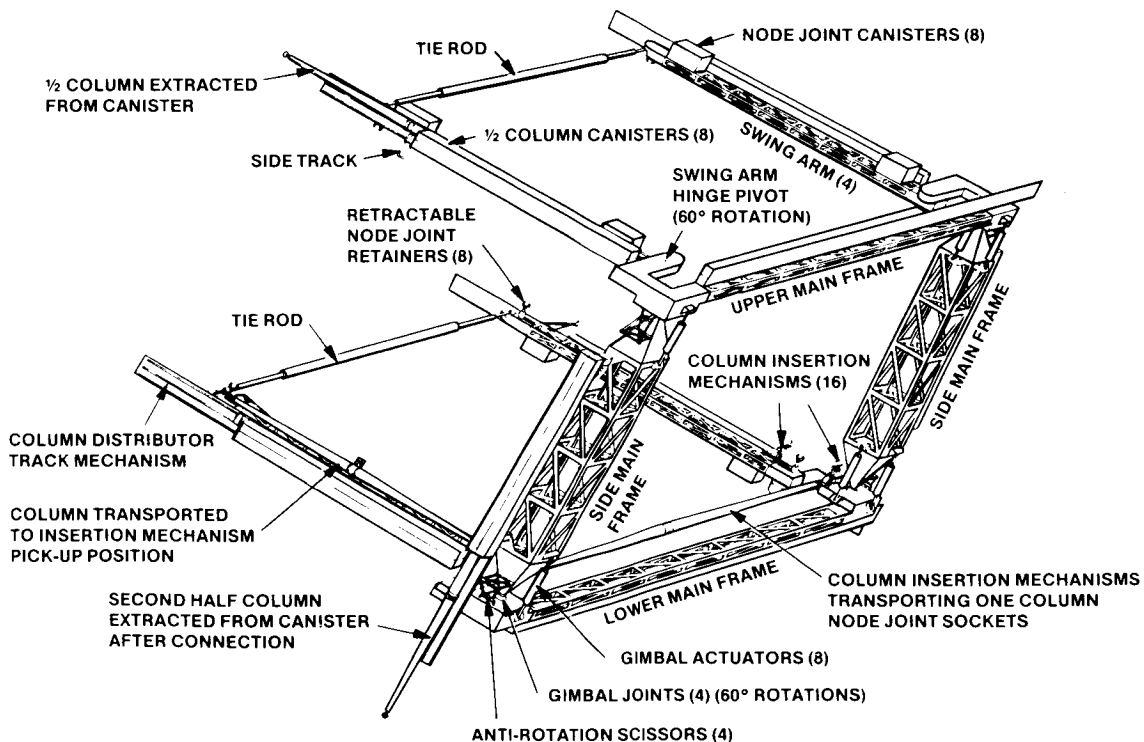and, for long-life missions, propulsion and reaction control.

Figure 2

SPACE PLATFORM GEOMETRY

The tetrahedral truss acts as a space platform on which a variety of components and equipment can be mounted. This truss is erected from tapered, composite half-columns which are coupled at their large ends to form full columns. A key feature of this truss is the nine-point node joint. These joints are identical, and each provides nine receptacles for installation of column end-fittings. A typical arrangement of an assembled space platform is shown schematically in Figure 3. The dimensions shown are based on a 4m column length. The upper surface of the platform is shown by the heavy solid lines, representing individual columns, and the filled circles which indicate node joints. The lower face of the platform is represented by the light solid lines and open circles. The dashed lines are core columns connecting the upper and lower platform faces. In general, core columns will have different dimensions than face columns. Platform planforms which can be constructed with the replicated tetrahedral structure include equilateral triangles, hexagons, rectangles, and a linear truss as shown in the figure. In addition, the basic structure can be used to generate hexagonal toroidal platforms, spherical surface segments and, of course, large area platforms.
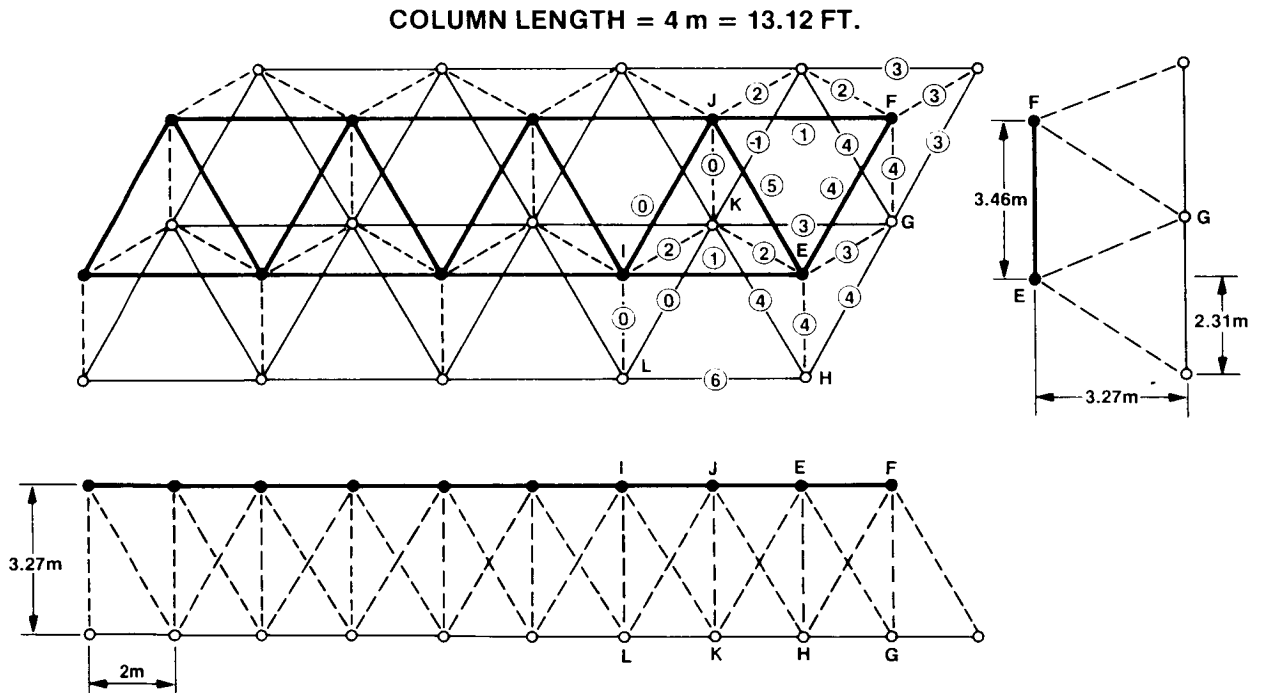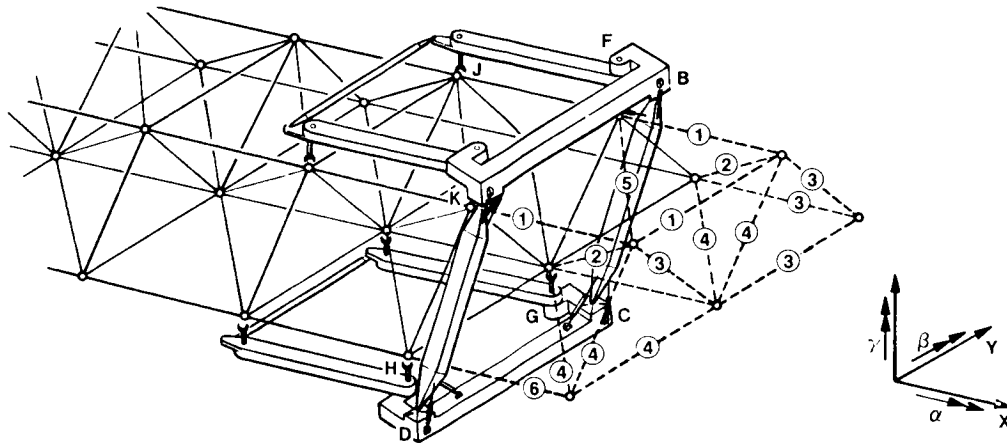
COLUMN LENGTH = 4 m = 13.12 FT.

Figure 3

ASSEMBLER OPERATION

As shown in Figure 4, the assembler is attached to the platform under construction by the node joint retainers; the machine maneuvers by releasing one or two pairs of node joints, rotating about the stationary joints, and capturing new pairs of node joints. In order to provide platform control, a maximum of four node joints can be released simultaneously. The assembler can then maneuver either laterally, forward or backward about the four held joints, inserting from one to eight columns at a time. Since the assembler is always outside the envelope of the platform being assembled, columns can be assembled and inserted simultaneously, thus minimizing construction time.

The assembler can utilize a variety of maneuver sequences depending on the shape of the platform being constructed. In constructing a large area platform, for example, the assembler advances along the edge of the platform by alternately swinging its arms about the two upper gimbals (rotation γ) and then about the two lower gimbals. Figure 4 illustrates the construction sequence for building a linear platform. The platform shown here has the minimum section which can be built by the assembler. The construction sequence consists of six steps per cycle during which 17 columns are inserted to advance the platform by one column length. The columns which are installed at each step are shown by the circled numbers. Note that steps 5 and 6 can be performed simultaneously, so that the 17 column cycle can be completed in 10.5 minutes, and a 2700 column shuttle load assembled in 27.8 hours.

STEPS 5 AND 6 CAN BE PERFORMED SIMULTANEOUSLY
SEVENTEEN 2M COLUMNS CAN BE INSERTED IN APPROXIMATELY 10.5 MIN
STD. 2700 COLUMN LOAD IN 27.8 HR.

STEP	ROTAT.	ABOUT	NO. COL.	ROT. TIM. MIN.	COL. INS. MIN.
1	β	C&D	3	1	1
2	α	A&B	2	1	1
3	β	A&B	5	1	1.25
4	α	A&B	5	1	1.25
5	γ	E&F	1	1	1
6	γ	H&G	1	1	1
TOTAL			17	6	6.5

Figure 4

SNAP LOCK NODE JOINT

Several node joint concepts have been derived for tetrahedral truss structures; one of these is shown in Figure 5. The joint is designed so that the column end fittings (having the sprocket-like toothed heads) are inserted laterally into the joint. The teeth on the end fitting are designed to engage a pin in the node-joint receptacle, thereby locking the column against torsion. During the assembly sequence, as the end fitting is guided into place it trips a cam latch which swings down to grasp the column end fitting. A spring-loaded locking finger drives itself along one of the cam surfaces, securing the latch in its locked position. Tests with the fabricated joint show that insertion can be performed with minimum effort and that the joint offers good rigidity in the locked configuration.
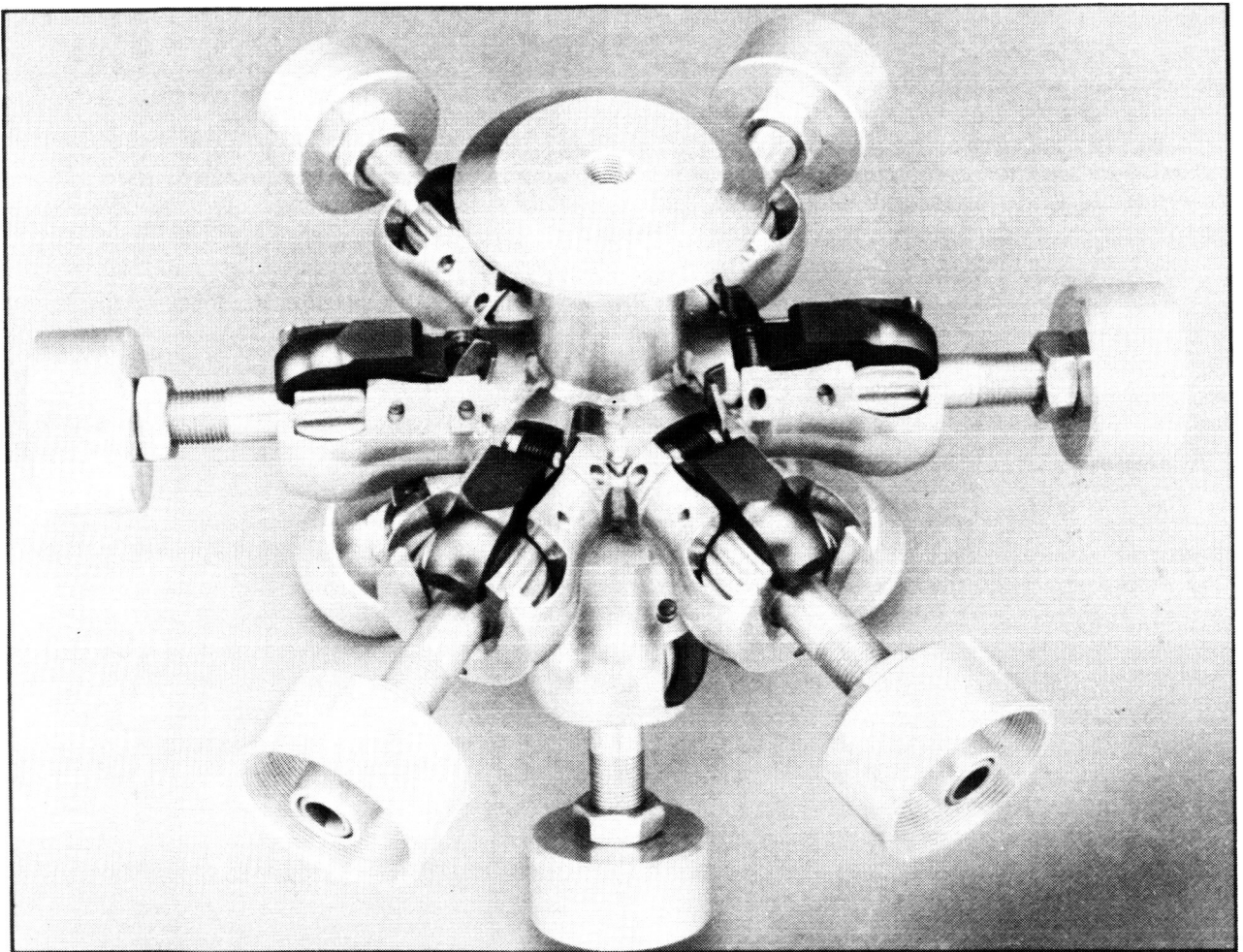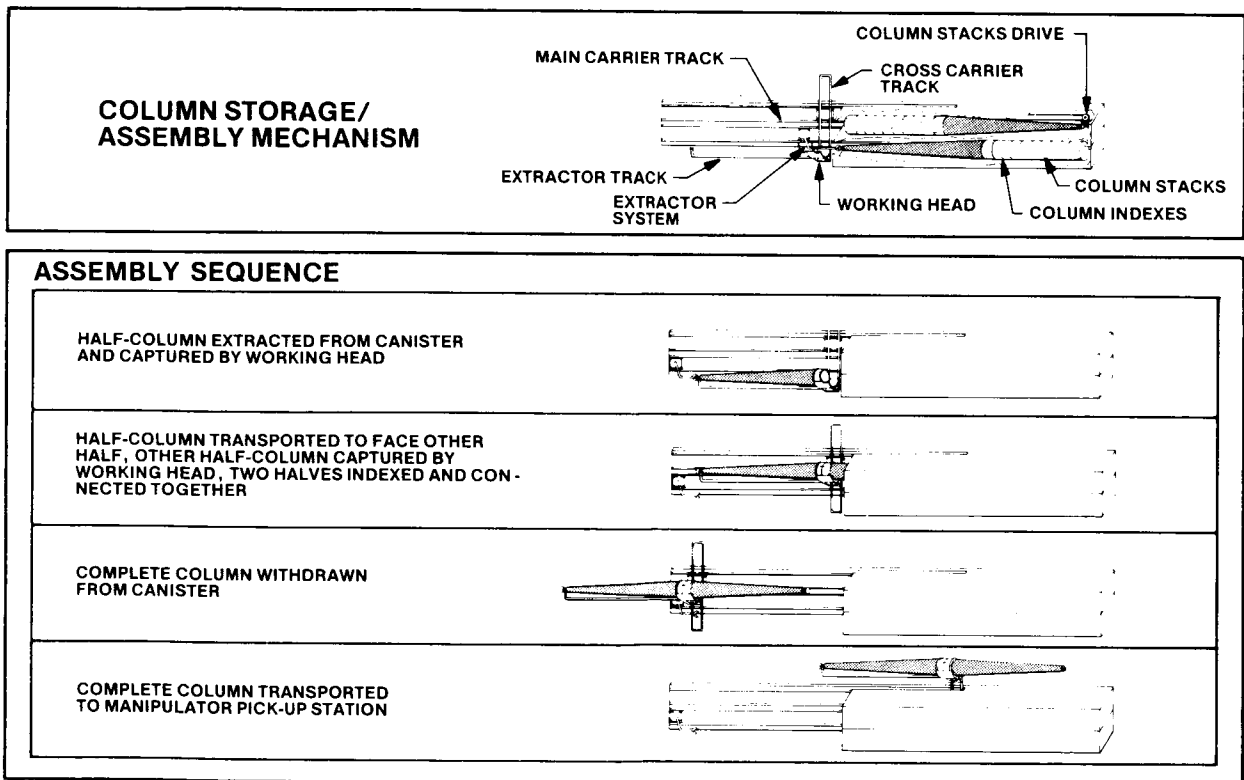

Figure 5

COLUMN STORAGE AND ASSEMBLY

A candidate design concept for column storage and assembly is shown in Figure 6. This half-column assembly machine consists essentially of a tracked column carrier and a double canister which contains two stacks of nested half-columns stored in opposite directions. The canisters are equipped with a driving mechanism designed to advance the column stacks one step at a time. This advance mechanism can be powered from the carrier track via a simple clutch system.

The carrier mechanism performs all the functions required to assemble and transport the half-columns to a position where they can be captured by the insertion mechanisms. The sequence of operation is shown in the figure. Designs for the working head, node retainers, node supply and column insertion mechanisms have also been developed in sufficient detail to verify concept feasibility.

Figure 6

BASELINE ASSEMBLER CAPABILITIES

Several features of the automatic assembler are summarized in Figure 7. As described earlier, the assembler can be adapted to operation in a free-flying or an Orbiter-mounted mode. In the latter case, rail-mounted operation can be used to minimize forces imposed on the Orbiter due to assembler maneuvers. Programming the assembler to construct various platform geometries is expected to require only software changes, except for the use of special column canisters for unequal length core and face columns such as would be used to generate spherical surfaces. It is estimated that the automatic assembler would be capable of assembling a shuttle load of 20-m columns in about 36 hours (free-flying mode). This estimate consists of eight hours for loading the assembler and 28 hours of actual construction time. The resulting platform would have an area of 0.1 sq km. For Orbiter-mounted operation, smaller platforms would be built with more complex interactions and interfaces with the STS. In addition to the availability of astronaut support by EVA, data handling, maneuver control and electrical power can be provided to the assembler by umbilical connections to the Orbiter.

ASSEMBLY MODES

- ORBITER MOUNTED
- FREE FLYING

ASSEMBLY PROGRAMMING

- VARIED SHAPES/SIZES
  - LINEAR TRUSS
  - LARGE AREA PLATFORMS
  - HEXAGONAL TORUS
  - SPHERICAL SURFACE
- ENLARGE/MODIFY STRUCTURES

CONSTRUCTION TIME

- 1.5 DAYS PER SHUTTLE LOAD

INTERFACES

- STS TRANSPORT
- AUTOMATIC MAIN-FRAME DEPLOYMENT, UTILITY INTERCONNECT
- ASSEMBLY UNDER PROGRAM OR ASTRONAUT CONTROL
- ASSEMBLER RAIL MOUNT FOR LARGE STRUCTURES
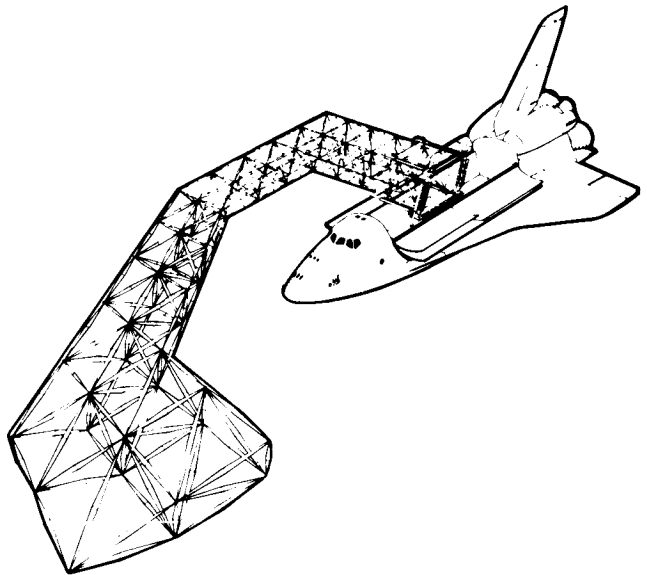- COLLAPSE/STOW WITH EVA ASSIST

Figure 7

AUTOMATED UTILITIES INSTALLATION

A major task in this study was the assessment of capabilities of the
assembler in installing non-structural platform systems. These systems include
electrical power distribution, heat transport, command and data signal trans-
mission, and payload data transmission. The objectives of this effort were to
evaluate the effects of including installation of utilities on the assembly
process and on the design, operation and performance of the assembler. In
addition, any special requirements on the assembler and/or the platform due
to the installation of utilities were to be identified. The chart shown in
Figure 8 lists these objectives, as well as the guidelines followed in this
task. The procedure followed was to define a set of candidate utility
characteristics and installation requirements, define and design installation
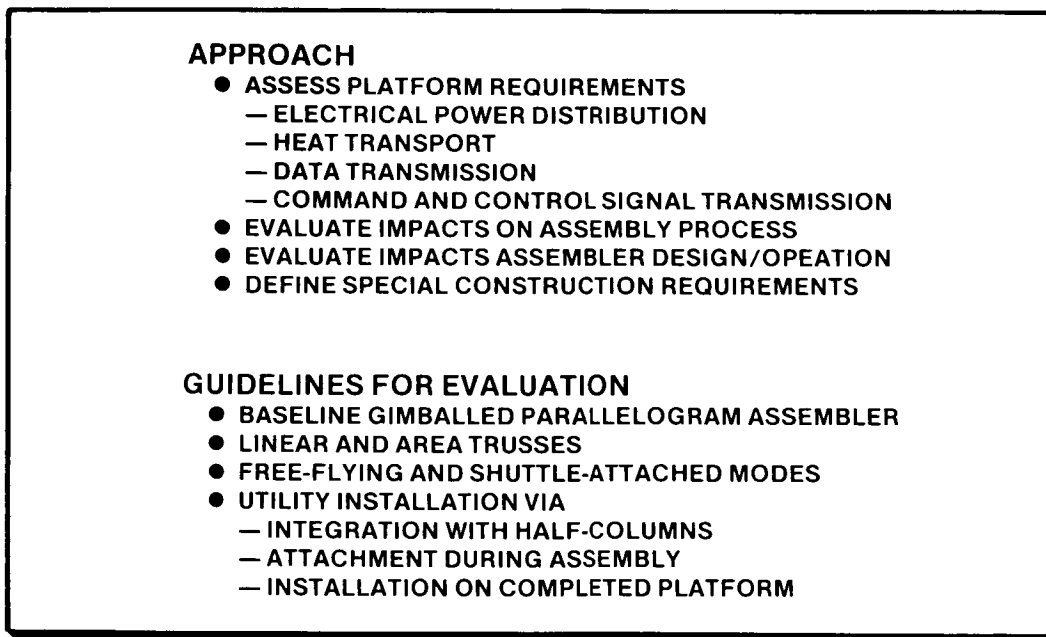concepts, and perform an assessment of impacts on the assembler and its
operation.

APPROACH
- ASSESS PLATFORM REQUIREMENTS
  - ELECTRICAL POWER DISTRIBUTION
  - HEAT TRANSPORT
  - DATA TRANSMISSION
  - COMMAND AND CONTROL SIGNAL TRANSMISSION
- EVALUATE IMPACTS ON ASSEMBLY PROCESS
- EVALUATE IMPACTS ASSEMBLER DESIGN/OPEATION
- DEFINE SPECIAL CONSTRUCTION REQUIREMENTS

GUIDELINES FOR EVALUATION
- BASELINE GIMBALLED PARALLELOGRAM ASSEMBLER
- LINEAR AND AREA TRUSSES
- FREE-FLYING AND SHUTTLE-ATTACHED MODES
- UTILITY INSTALLATION VIA
  - INTEGRATION WITH HALF-COLUMNS
  - ATTACHMENT DURING ASSEMBLY
  - INSTALLATION ON COMPLETED PLATFORM

Figure 8

BASELINE UTILITIES REQUIREMENTS

Candidate utilities considered in this task included those required for the following:

o Electrical power distribution

o Heat transport

o Data transmission

o Command and control signal transmission

Basic requirements for the distribution of these utilities were derived using published descriptions of space platform concept designs, as exemplified by References 2 and 3. In general, the larger platforms require larger total power and benefit most from high voltage distribution systems. A breakdown of utility distribution systems for four reference platforms (Rockwell P-1, MDAC A/B, SASP and ASASP) was constructed. From this summary, it was found that wire sizes for power distribution were much larger than those for data and signal transmission. Therefore, attention was directed toward requirements for power and coolant distribution, and definition of a baseline set of near-term requirements and an alternative set of requirements for an advanced platform. These requirements are summarized in Figure 9. Baseline power distribution was to be obtained in both the near-term and advanced platforms by the use of No. 4 AWG cables. The most stringent requirement for coolant distribution was that for the near-term platform, where 20 mm-diameter tubing was required.

PLATFORMS: NAR P-1, MDAC A/B, H, SASP-A, B, C, ASASP
DC LOADS: 5 TO 33.kW, 29 TO 168 V

FUNCTION	UTILITY REQUIREMENT	
	NEAR TERM	ADVANCED
POWER	NINE NO. 4 AWG WIRES OR FLAT CABLE, 0.020 IN. THICK	THIRTEEN NO. 4 AWG WIRES
DATA AND COMMUNICATIONS	FOUR R6143 COAX LINES	10 CHANNEL FIBER OPTIC LINE
COMMAND AND CONTROL	FOUR NO. 12 TSP LINES	FOUR NO. 12 TSP LINES
THERMAL CONTROL	PUMPED-FLUID HEAT PIPES OR FOUR 2 C-M DIA STEEL TUBES	LOCALIZED AT P/L MODULES

Figure 9 (Note: 1 in. = 2.54 cm.)
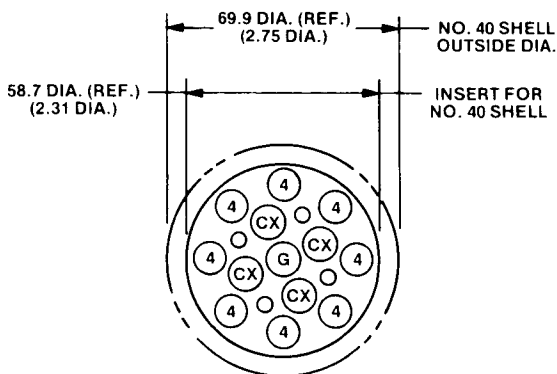
WIRE BUNDLE ARRANGEMENTS

For the purpose of this study, the electric cable configuration was assumed to consist of the following wires:

9 #4 AWG + 4 RG 143 coax + 4 #12 TSP lines

A bundle thus consists of 17 wires which may be organized either within a circular or a flat pattern (Fig. 10). The circular pattern can be used either with reel storage or as cable segments designed for straight storage in canisters either separately or with the half-columns. The flat pattern is designed to allow easy bending over reels, in which case a special device must be provided to straighten the cable before it is laid along the structure. A preliminary investigation indicates that the baseline set of cables will require a #40 connector shell which has a diameter of 59 mm. The connector nut is somewhat larger (~70 mm). The flat bundle concept may have multi-branches with connectors if reel stowage permits. A 1-m diameter reel having a .30-m core diameter will contain approximately 80 m of cable in the case where only the end connectors are needed. Multispool stowage will make it possible to provide within a single canister a continuous length of cable in multiples of 80 m. The round cable bundles may be stowed in reels or in linear canisters, either as a part of the half-column canisters or as separate specialized canisters. In this case, the cables are laid straight, each one in a tubular compartment of the length of the half-column canister. The cables are extracted from the canister at the time of column assembly and attached to the column.

CABLE CONNECTOR ARRANGEMENT IN STANDARD NO. 40 SHELL

1	9.5 DIA. GROUND AT CENTER
4	9.5 DIA. CO-AX ON 0.934 DIA.
8	9.5 DIA. NO. 4 ON 1.754 DIA.
4	4.8 DIA. NO. 12

WIRE BUNDLE ARRANGEMENTS

ALL INCLUDE:
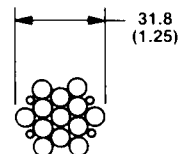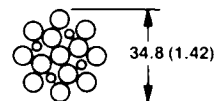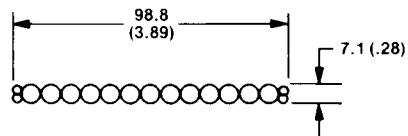| 1 | 7.1 DIA. GROUND |
4	7.1 DIA. CO-AX
8	7.1 DIA. NO. 4
4	3.1 DIA. NO. 12

Figure 10

TUBING CONFIGURATIONS

Several types of tubing design and material were considered:

1. Thin wall tubing - aluminum, stainless steel, graphite epoxy

2. Thin wall lenticular tubing - stainless steel, graphite epoxy

3. Inflatable - self-curing fiberglass tubing

4. Inflatable - fiberglass reinforced plastic tubing

They are shown schematically on Fig. 11. Tubing type 1 is a standard design needing no special development. Tubing type 2 consists of two thin metallic plates bent to a sinusoidal cross section and continuously welded together to a lenticular shape. This tubing is not capable of carrying high pressures due to high stresses at the welds, but it can be flattened out and rolled around a drum in a tight package of great deployed length. Tubing type 3 consists of a fiberglass tube bonded inside plastic tubing. The fiberglass is impregnated with an epoxy resin and will remain pliable until such time as a catalyst is brought in contact with it. In this condition, a considerable length of tubing can be flattened and wound on a spool in a very tight package. After the flattened hose has been laid-up and all connections secured, it is inflated with the catalyst, allowed to cure, vented and flushed with compressed air. Tubing type 4 is a continuous plastic tube reinforced by a braided fiberglass casing bonded with a flexible agent. Such a tubing could be flattened to be wound over a drum or reel and dispensed in the same manner as tubing No. 3.
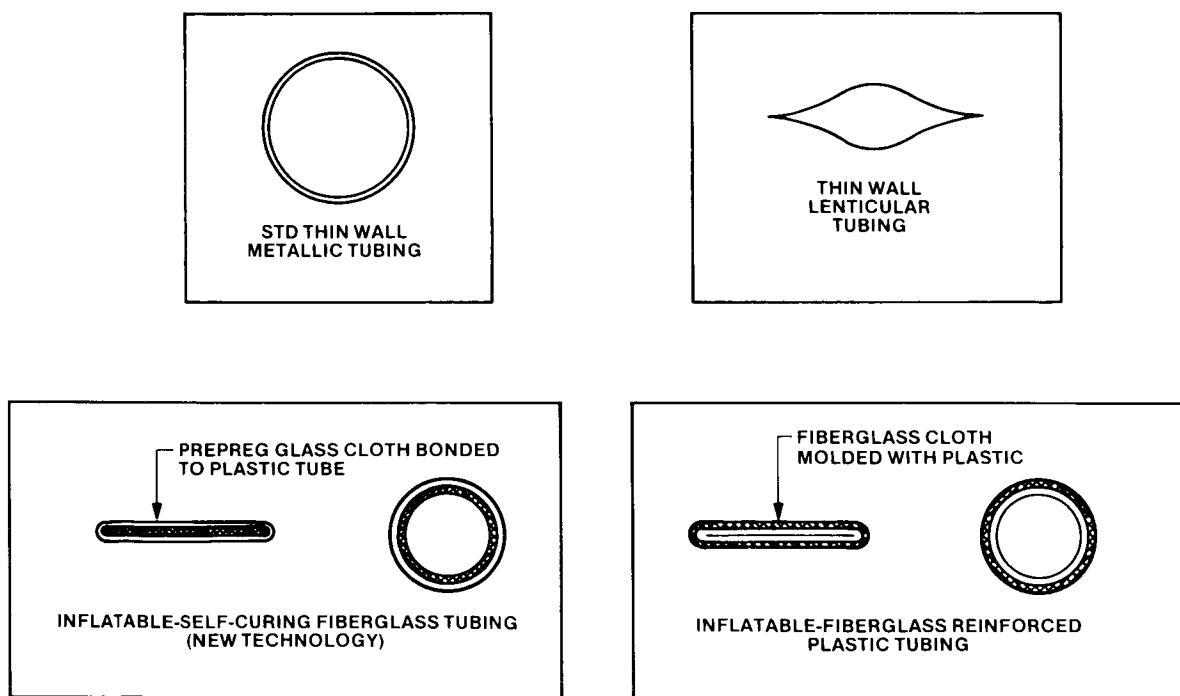

Figure 11

CABLE LAYING CONCEPT

Two basic cable storage concepts were considered: reel storage and segmented storage. Segmented storage refers to storage of individual segments of cable in lengths approximating the half-column lengths. The general arrangement of the reel storage and dispensing concept is shown in Figure 12. In general, the reel dispensers would be mounted as required at individual corners of the assembler to facilitate laying cable on either platform surface and in left- or right-hand traverses. Since the assembler has the ability to perform changes in the direction of traverses along any one of the three sides of the basic tetrahedral triangle, this property can be used to lay utilities along specified paths of the platform structure. By proper programming of the construction sequence, the partially assembled platform can have, temporarily, a free edge along the required utilities path such that the assembler can perform a cable-laying traverse. This traverse could include a number of changes of direction and would be conducted at the same time as columns are being inserted. Intersecting utility paths can be accommodated if a junction box is placed at their intersection.
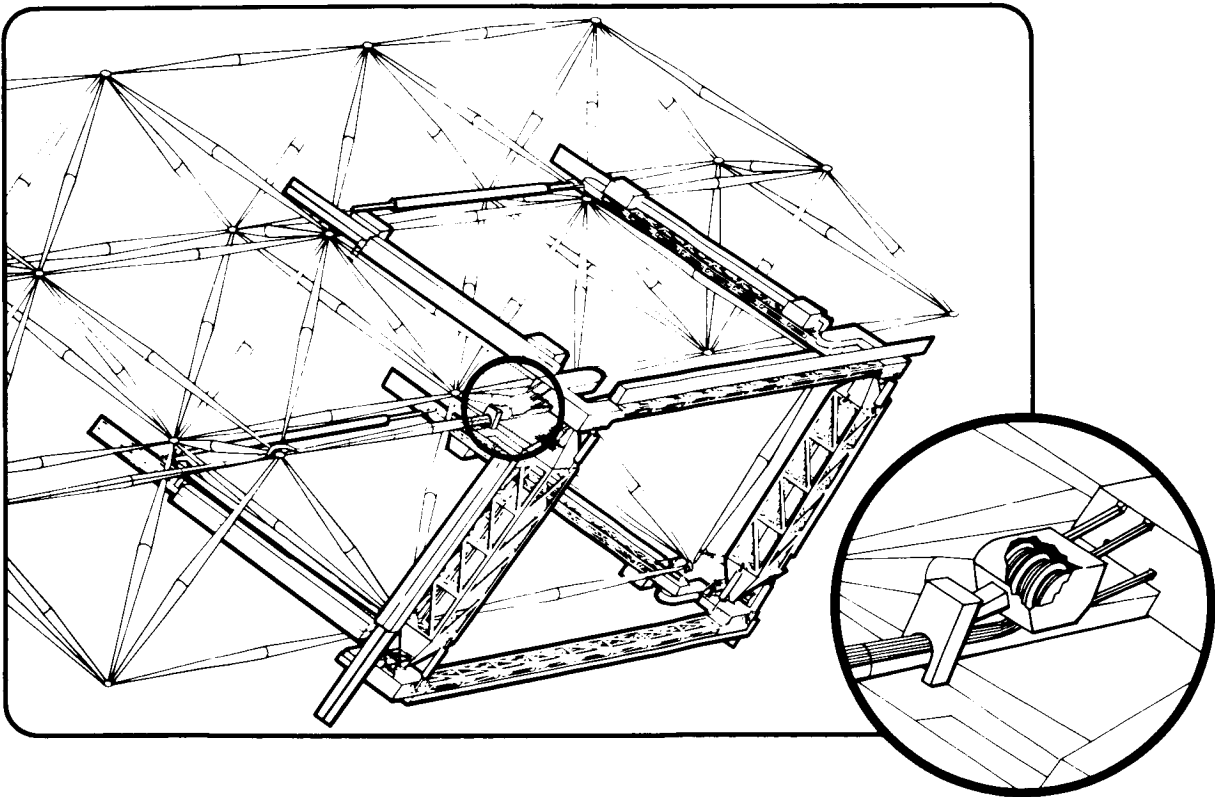

Figure 12

CABLE LAYING MECHANISM

The reel-type cable laying mechanism consists of a canister containing the cable wound continuously over one or several spools (about 80 m of flat cable per spool) and a cable guide unit which performs three additional functions: pulling the cable from the spool, straightening it, and binding it to the column. This complete system is mounted on four swinging arms which provide the necessary freedom to follow the column's surface while the assembler moves. Figure 13 shows the assembler at mid-course during a right-hand traverse between two node joints. At this point, the node joint retainer is approximately 3 m above the retainer level but the cable laying unit remains level with the columns. In the alternate traverse, the assembler swings in the plane of the platform and the cable laying unit uses its other degree of freedom to follow its track. The true motion of the cable laying unit is somewhat more complicated due to the geometry of the platform structure and requires combined motion of both degrees of freedom for one repetitive cycle of each traverse (See Ref. 1 for a description of the traversing motion). A preliminary estimate was made of the capacity of candidate reel storage designs. This estimate indicates that the round cable configuration shown in Fig. 10 could be stored in continuous lengths of about 700 m per meter width of drum, while the flat cable configuration would not allow more than about 500 m on the same drum width. On this basis, the round cable would appear preferable.
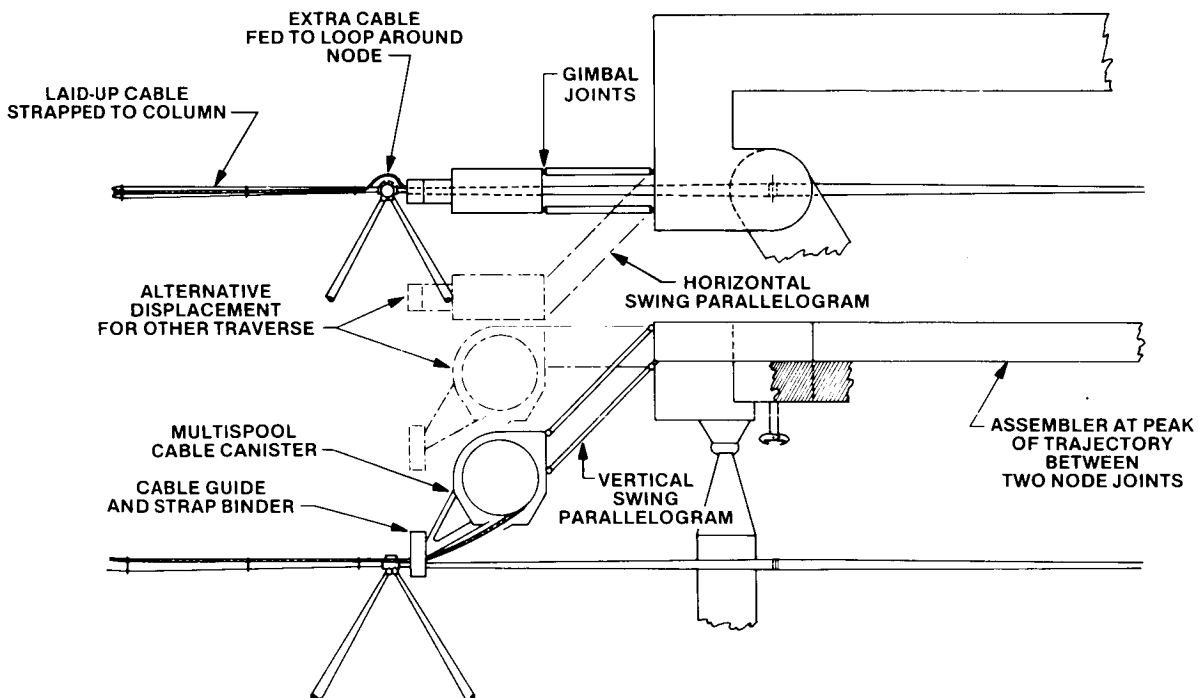

Figure 13

INSTALLATION OF SEGMENTED UTILITIES

Figure 14 shows a conceptual design for segmented cable storage in the column canisters.

With this design, the installation of cable segments is accomplished concurrently with the assembly of the half-columns. Each cable segment is individually stowed in a thin wall tube from which it is extracted by the half-column extractor system suitably modified to perform this additional function. An automatic binder attaches the cable to the first half-column. Then, as the completed column is withdrawn from the canister, additional straps are automatically placed at intervals on the other half-column. Thus, the column plus attached cable can be transported by the carrier system to the manipulator pick-up points.

Although this segmented cable installation system can be mounted on anyone of the eight arms of the platform assembler, its primary utility is on the two vertical members of the assembler, where it can be used to install cables on core columns.
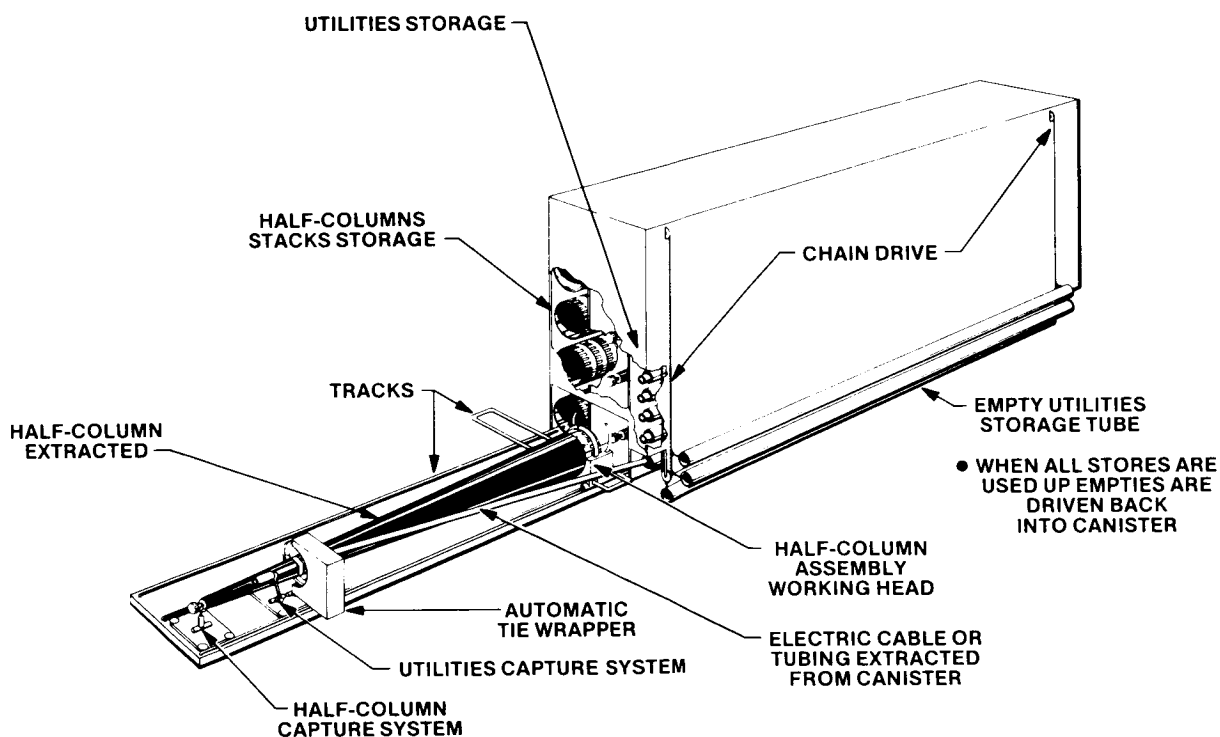

Figure 14

ASSEMBLER DESIGN AND PERFORMANCE IMPACTS

The results of this study show that concept designs for utilities installation are available which have relatively little impact on assembler design. By storing and dispensing cables or tubing on reels or drums, a separate set of mechanisms can be used which can be attached as needed to the basic assembler structure. Similarly, for the installation of segmented utilities, a separate canister can be integrated with the column canister. Column assembler and utility installation can then be performed in parallel.

In assessing operational and performance impacts, it was found that the magnitude of these impacts depended on whether utilities installation was performed concurrent with or in series with the platform assembly process. If utilities are required to be installed around the periphery of a completed platform, the operations can be performed serially. In this case, the utilities installation time is additive to that for platform assembly and is minimal. A greater impact is observed if utilities are installed in parallel with platform assembly operations. In this case, two primary impacts are foreseen. One of these is a reduction in the area of a platform which can be constructed from a single STS load of materials; this area reduction is due to the added space required in the Orbiter for carrying utilities. As shown in Fig. 15, this effect is small for utilities installation across and around the periphery of a platform, ranging from 1% to 4% decrease in area. However, a large impact on construction time is observed, with estimated increases of from 23% to 34%. The absolute values of construction times with utilities for the example shown range from 48 to 69 hours.

ASSEMBLER DESIGN

- MINIMAL HARDWARE DESIGN IMPACT
  - REEL-WOUND UTILITIES USE DEDICATED MECHANISM
  - CANISTER FOR SEGMENTED UTILITIES INTEGRATED WITH COLUMN CANISTER
- ADDED SOFTWARE

ASSEMBLER OPERATION/PERFORMANCE

- UTILITY INSTALLATION EITHER CONCURRENT WITH OR SEPARATE FROM PRIMARY ASSEMBLY PROCESS
- ADDITION OF UTILITY INSTALLATION
  - INCREASES OVERALL ASSEMBLY TIME
  - REDUCES AREA OF PLATFORM WHICH CAN BE BUILT FROM A SINGLE STS LOAD

COLUMN LENGTH (m)	NUMBER OF COLUMNS PER STS LOAD *	PLATFORM AREA WITHOUT UTILITIES (m²)	WITH UTILITIES ADDED	
			AREA CHANGE (%)	CONSTRUCTION TIME CHANGE (%)
4	4,200/4,158	6.5×10^3	-1	+23
10	3,000/2,940	2.9×10^4	-2	+30
20	2,700/2,592	1.0×10^5	-4	+34

* WITHOUT UTILITIES/WITH UTILITIES

Figure 15

UTILITY INSTALLATION SUMMARY

The studies performed on assembler utility installation have resulted in the conclusions summarized below. The installation of candidate utilities can be implemented using existing state-of-the-art technology by adding on devices or modifying the baseline assembler design. Proper programming of utility installation allows for compatible assembly operational sequences for a variety of platform sizes and shapes, with minimal impact on assembler design and operation. The study results also show that a postulated utilities network installation on candidate platforms requires little Orbiter payload bay volume and thus imposes only a small reduction in the size of the platform which can be produced from a single STS load. However, the amount of total construction time required can be increased significantly, depending on the extent of the required utilities. In addition, the complexity and development requirements of automated connection devices makes it desirable to use astronaut EVA to perform utilities hookup tasks.

This study has resulted in the identification of feasible designs for storage and dispensing of cables and tubing by two means: continuous reels or segment dispensers. Existing devices for cable binding can be adapted to perform this task automatically during utility installation. Finally, an investigation of the use of column-integrated conductors in composite columns has shown that this approach requires considerable manufacturing technology development and is not practical with current materials and column designs.

- **ASSEMBLER UTILITY INSTALLATION:**
  - USES EXISTING TECHNOLOGY
  - IS COMPATIBLE WITH ASSEMBLY SEQUENCES
  - IS ADAPTABLE TO RANGE OF PLATFORM SIZES, SHAPES
  - HAS MINIMAL IMPACT ON ASSEMBLER DESIGN, OPERATION
  - HAS NEGLIBIBLE EFFECT ON AREA OF PLATFORM ASSEMBLED PER STS LOAD
  - INCURS AN INCREASE IN ASSEMBLY TIME IN PROPORTION TO AMOUNT AND LOCATION OF UTILITIES
  - REQUIRES EVA FOR COUPLING, CONNECTIONS

- **APPLICABLE DESIGNS AND MECHANISMS INCLUDE:**
  - REEL STORAGE AND DISPENSING
  - CANISTER STORAGE
  - BINDING MECHANISMS

- **COLUMN-INTEGRATED CONDUCTORS ARE IMPRACTICAL AND DIFFICULT TO IMPLEMENT**

Figure 16

REFERENCES

1. G. G. Jacquemin, R. M. Bluck, G. H. Grotbeck, and R. R. Johnson: "Development of Assembly and Joint Concepts for Erectable Space Structures," NASA CR-3131 (to be published).

2. K. A. Bloom, "Space Construction and Utility Distribution," Large Space Systems Technology - 1979, NASA CR-2118, 1980, pp. 287-301.

3. A. LeFever, "Space Platform Utilities Distribution Study," Final Report, Contract NAS 1-15322, NASA CR-159272, July 1980.

ACKNOWLEDGEMENTS

FREE-FLYING SOLAR REFLECTOR SPACECRAFT

John M. Hedgepeth
Astro Research Corporation
Carpinteria, California

BASELINE CONFIGURATION OF A SOLAR REFLECTING SATELLITE

Since 1978, Astro has been working for NASA LaRC on "Design Requirements for Large Space Structures." Some results have been reported in refs. 1 and 2. Other results are being published. Some will be presented at the forthcoming AIAA Second Conference on Large Space Platforms in February 1981. The present paper gives results of investigations of requirements and design concepts for large solar-reflecting spacecraft. The emphasis is on the 1-kilometer-diameter self-contained spacecraft that can be packaged and launched in the Space Shuttle shown in Figure 1.
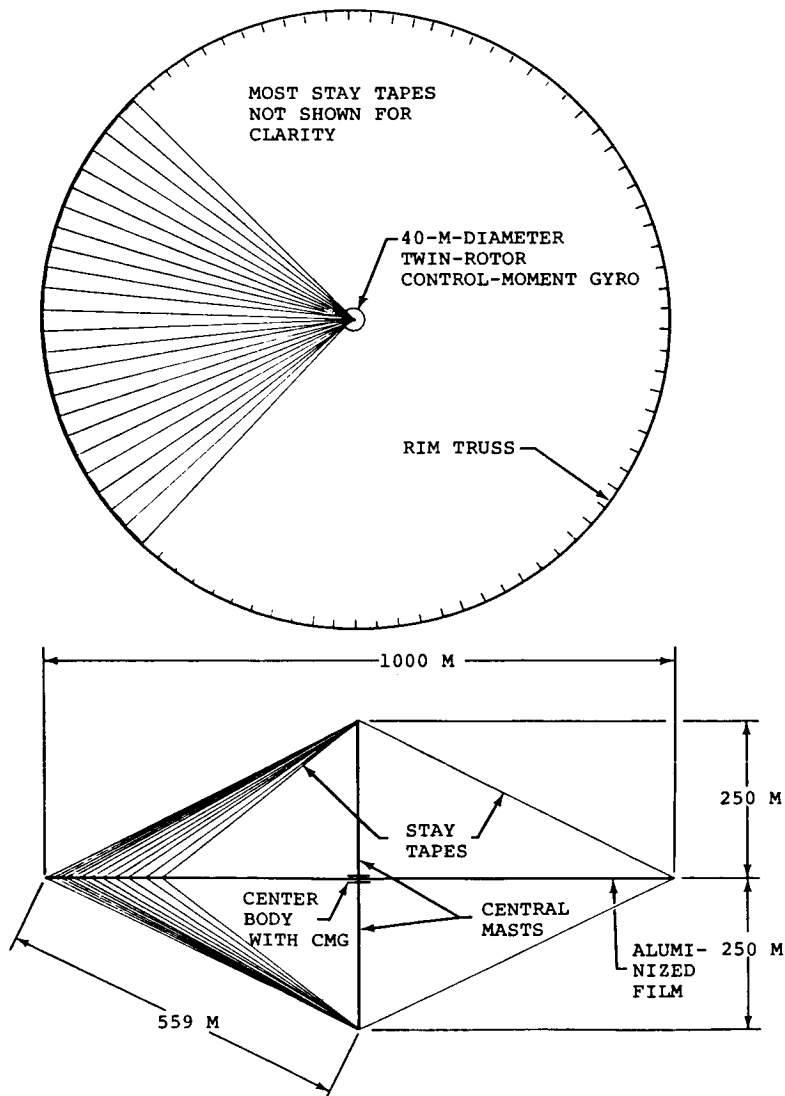
Figure 1.

CIRCULAR SOLAR-REFLECTING SATELLITE

The structure of the spacecraft is similar to that previously reported in ref. 3. Some details are shown on figure 2. The configuration consists of a compression rim stabilized by stays coming from each end of the central compression hub. The stays are stowed on reels on the ends of the hub. The hub consists of two Astromasts which are deployed after launch. The reflector membrane is a 2-micron-thick Kapton film with a vapor-deposited aluminum coating. With seams and joints, the average weight of the film is 4 g/m^2. The feasibility of this type of film was demonstrated in 1977 during work on solar sailers. Note that expansion compensators will be needed at the attachment between the film (which is assumed to have a dimensional stability of ±0.5 percent) and the relatively stable graphite/epoxy rim structure.
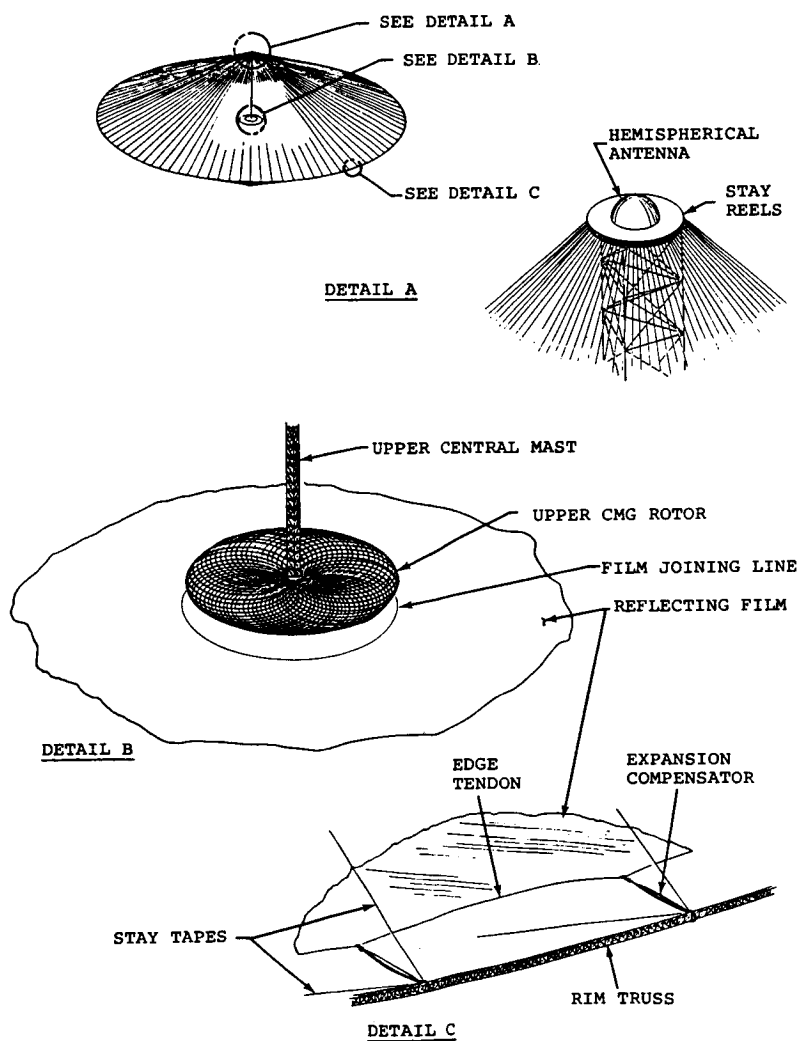

Figure 2.

CLOSEUP OF CENTER BODY SHOWING TWIN-ROTOR CONTROL-MOMENT GYRO

The "muscle" for the attitude control system is a pair of counter-rotating control-moment gyros with deployable flywheels. The requirements for control capability are obtained for the SOLARES mission in which the satellite is rotated so as to reflect the sunlight to a fixed point on the Earth as it passes near it. The torques and angular impulses required are large enough that exorbitant masses would be needed if the flywheels were small enough to be contained within the Shuttle. Hence, deployable flywheels are necessary. Even with the large diameter available with deployable flywheels, the electrical power required to accelerate the flywheels used as momentum wheels is unacceptably large. Hence, the control-moment-gyro approach was selected and is schematically shown in figure 3.
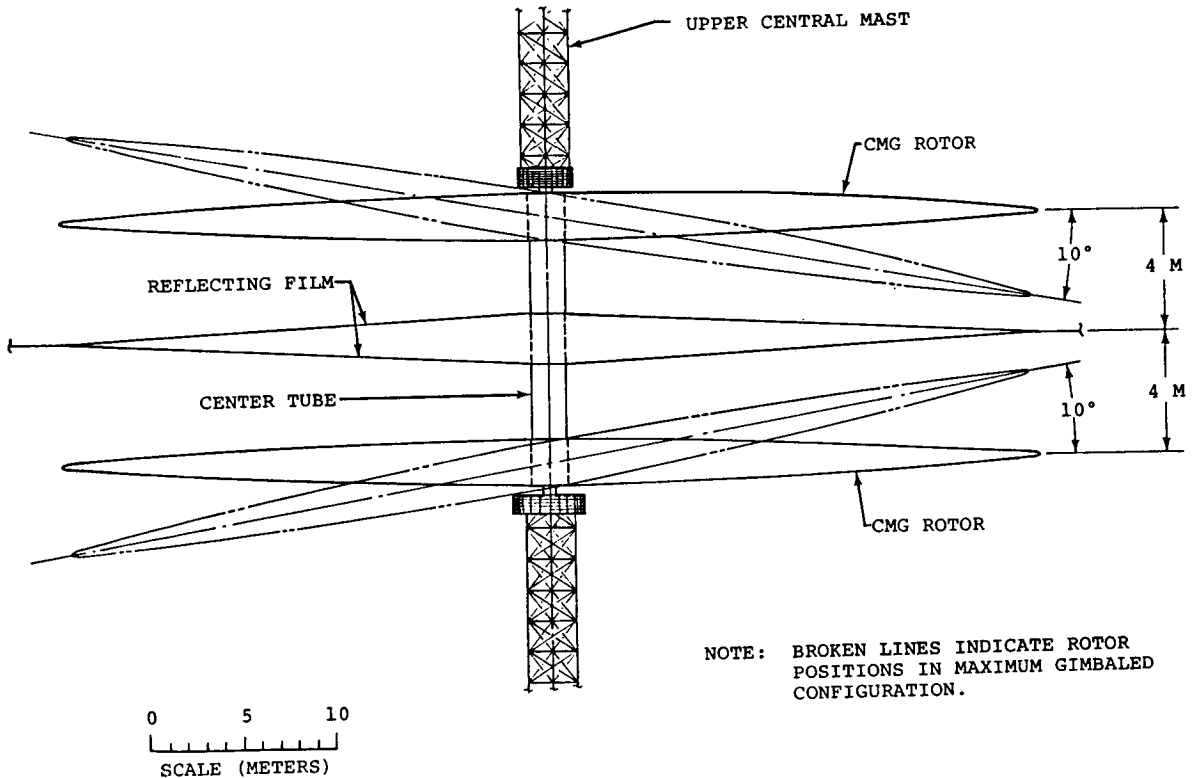

Figure 3.

DEPLOYABLE FILAMENTARY FLYWHEEL FOR CONTROL-MOMENT GYRO

Deployable flywheels were studied over 10 years ago and reported in ref. 4. They are composed of many filaments in the pattern shown in figure 4. This pattern is basically selected to put the filaments in a state of uniform tension. Note that a typical filament runs from one end of the hub out to the rim and then to the other end of the hub. The resulting wheel should have sufficient depth to ensure that it behaves essentially as a rigid body. Clearly, further work needs to be done on these types of control devices.
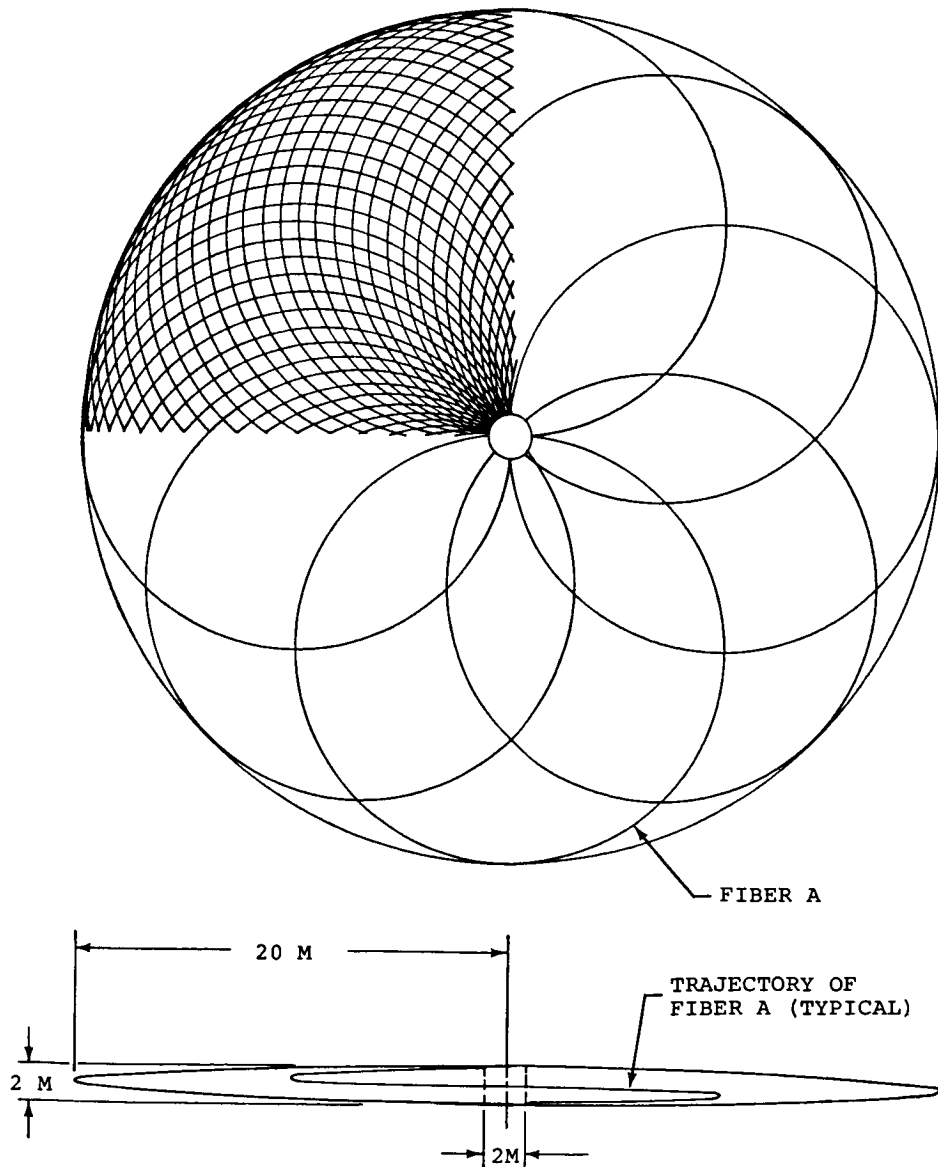
Figure 4.

MASS SUMMARY FOR BASELINE
1-KILOMETER-DIAMETER REFLECTOR SATELLITE
(flight condition)

A mass breakdown for the 1-kilometer-diameter satellite is shown in figure 5. Note that the mass of the reflector membrane which we consider to be the payload is slightly more than 3000 kg. An objective of the study was to determine whether the mass of the supporting structure could be made as light as that. In the earlier results (ref. 3), the structural mass was only about 2800 kg. Attention in the current study to the packaging and deployment requirements resulted in an increase of the structural mass to almost 3400 kg. As can be seen, the mass of the control system including a low torque electromagnetic loop system for desaturating the control-moment gyros and controlling orientation about the axis of symmetry is about 2400 kg. Including reasonable masses for other support systems, the total unit mass of the spacecraft is less than 12 g/m^2, well into the ultralightweight range.

ITEM	MASS (KG)	
STRUCTURAL COMPONENTS		
EDGE TENDONS (90)	12	
CORNER HARDWARE (90)	330	
RIM TRUSS	1760	
RIM HINGES AND MOTORS (6)	30	
STAY TAPES, FRONT AND BACK (180)	367	
TAPE REELS	42	
CENTRAL MASTS (500 M)	241	
STORAGE CANISTERS AND MECHANISMS	552	
CENTER BODY	48	
		3382
REFLECTOR MEMBRANE		
AREA = 785,400 M^2 @ 4 GM/M^2	3142	
		3142
CONTROL SYSTEM		
CONTROL-MOMENT GYRO TWIN-ROTORS	1000	
CONTROL-MOMENT GYRO SUSPENSION	1000	
MAGNETIC LOOP CONTROL (90 CIRCUITS)	335	
(FOR 2400-KM ORBIT)		2335
COMMUNICATIONS, POWER SUPPLY, AND CONTROL ELECTRONICS		
SOLAR POWER SUPPLY	60	
HEMISPHERICAL ANTENNAS (2)	20	
RATE GYROS AND SENSORS	50	
COMMUNICATIONS AND DATA HANDLING	100	
COMPUTER	46	
		376
TOTAL	9235	

Figure 5.

SEQUENTIAL ERECTION

The deployment of the structural configuration presents a very severe problem. In the past, the rim was assumed to be packaged and deployed in a zig-zag fashion in much the same manner as used in the Wire-Wheel or Hoop-Column concepts. In the present case, the difficulty is that the rim truss is over an order of magnitude larger in cross section than could be fit within the Shuttle with zigzag packaging. We deemed it unreasonable to expect that we could control the deployment of the cross section of the rim at the same time as controlling the radial deployment of the zigzag. Therefore, we reexamined the deployment and arrived at a principle of erection of large structures which is outlined in figure 6. We are convinced that all large structures must follow this principle of sequential erection.

---

1. *MOST OF THE MATERIAL IS EITHER SECURELY STOWED OR FULLY ERECTED AT ANY TIME DURING THE PERIOD OF ESTABLISHMENT.*

2. *ONLY A SMALL FRACTION OF THE MATERIAL IS IN TRANSITION AT ANY TIME.*

3. *PARTS IN TRANSITION ARE CLOSELY CONTROLLED.*

4. *STRUCTURAL PARTS IN TRANSITION ARE AVAILABLE FOR INSPECTION AND REPAIR*

Figure 6.

1-KILOMETER-DIAMETER REFLECTING SATELLITE
PACKAGED FOR SHUTTLE CARGO BAY

Figures 7 through 11 illustrate a deployment concept which obeys the principle of sequential erection. The package shown here (figure 7) is made up of three sets of containers. Each set consists of two canisters, each containing a segment of the rim truss, joined together by a rectangular bin in which the reflector membrane is stowed. Each rim-truss canister contains one-sixth of the rim and the film stowage bin is long enough to contain also the expansion compensator attachment hardware.
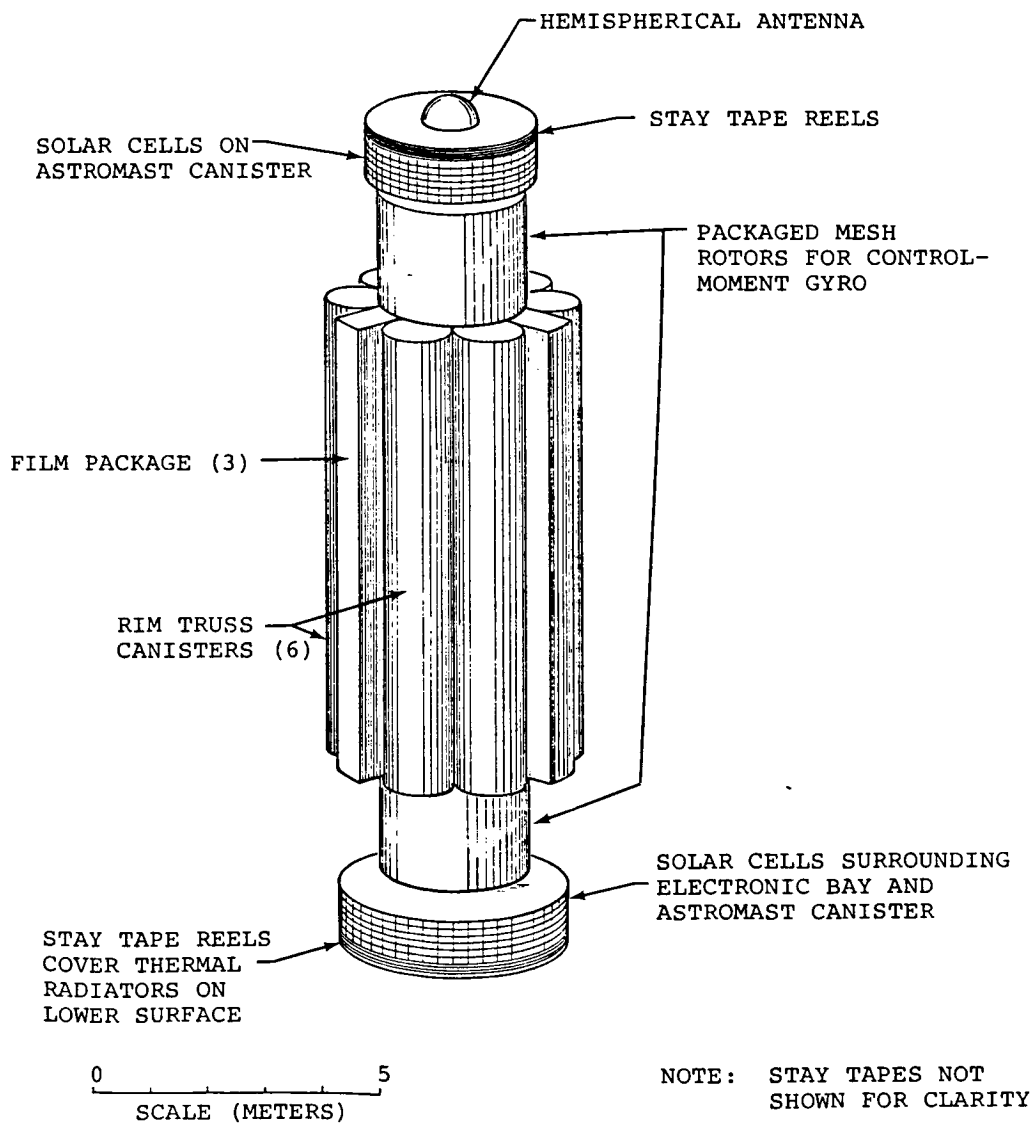
Figure 7.

FIRST PHASE OF DEPLOYMENT
SHOWING RIM-TRUSS CANISTERS AFTER 90° ROTATION

The first step in the deployment is to rotate the paired rim-truss canisters to a horizontal position (figure 8). The rim truss in this case is an Astromast, although other types of deployable trusses could be used. The tip ends of the Astromast are temporarily attached rigidly to the hub.
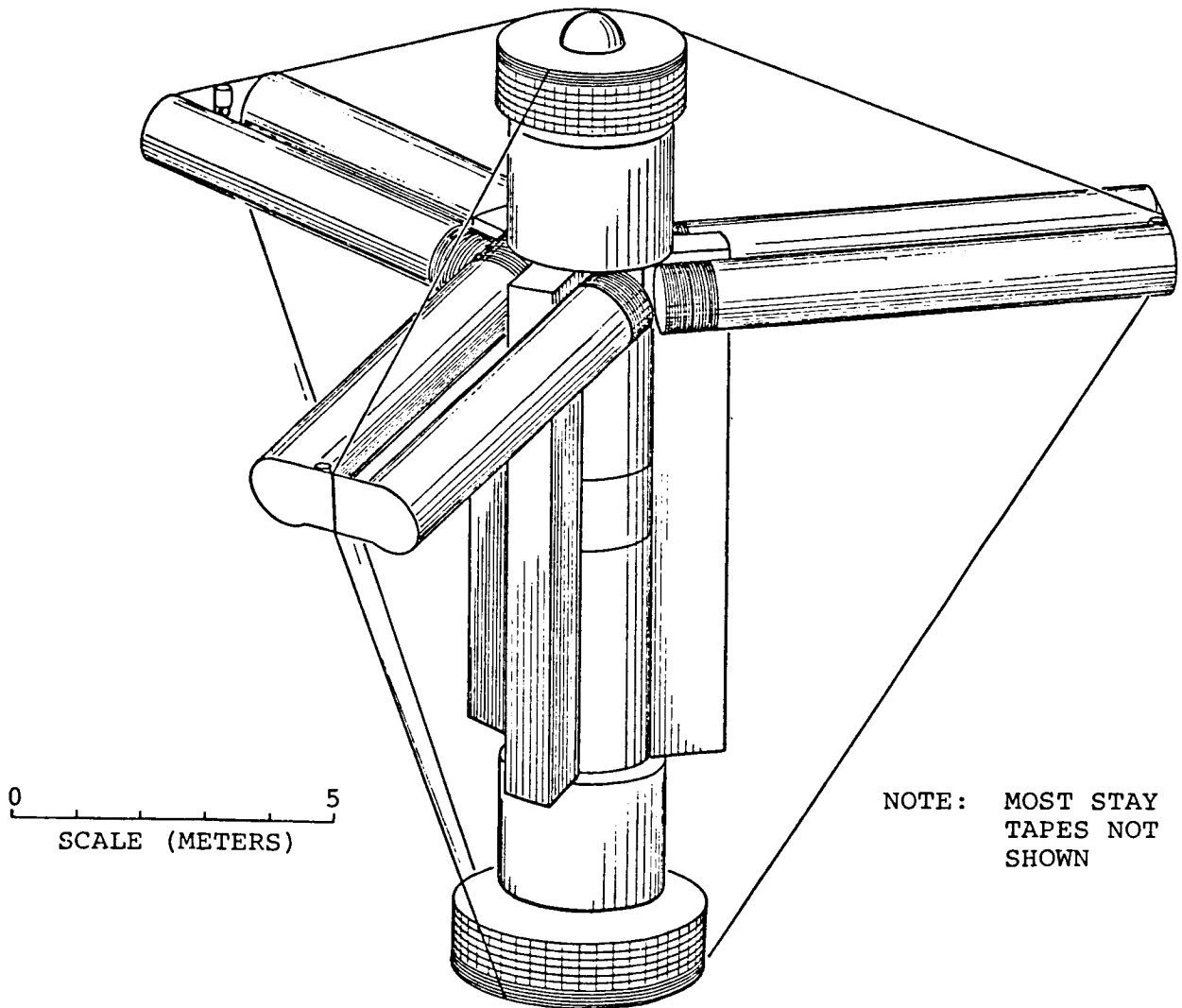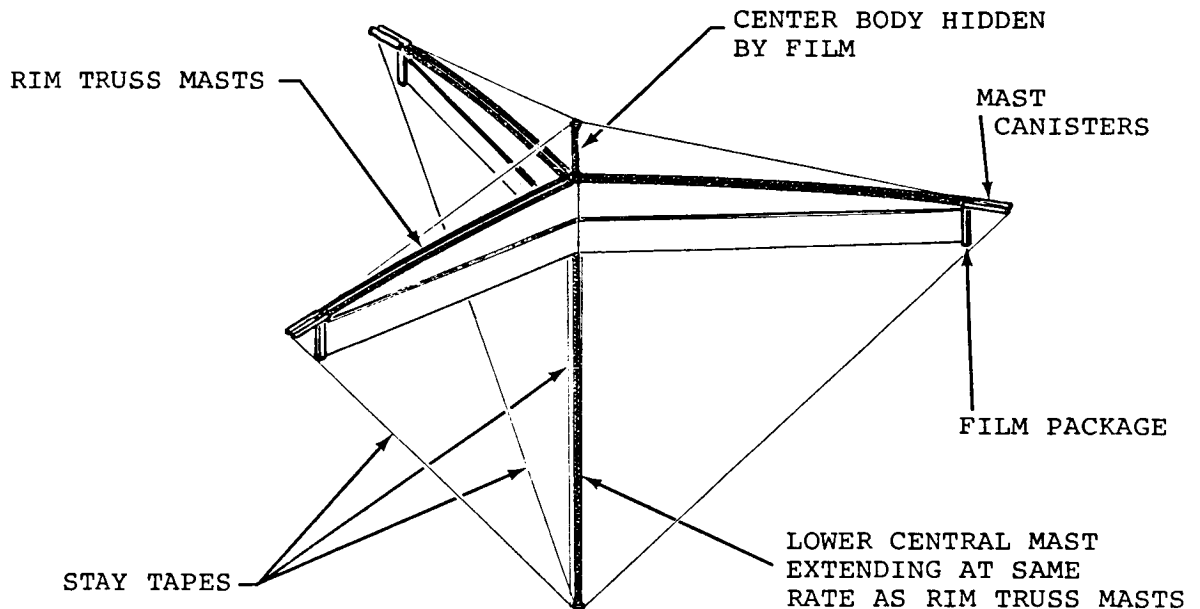

0 —————— 5
SCALE (METERS)

NOTE: MOST STAY
TAPES NOT
SHOWN

Figure 8.

SOLAR-REFLECTING SATELLITE
DURING EARLY PART OF SECOND DEPLOYMENT PHASE

Deployment continues by extending the pairs of Astromasts, transporting canisters outwards in pairs accompanied by the film bins (figure 9). As the film bins move outward, the membrane is allowed to unfold from the bin. Whenever a station on the rim is reached where an attachment of the membrane is required, an appropriate joint is made.
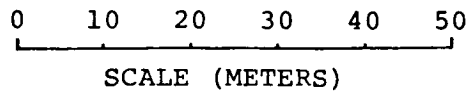
RIM TRUSS MASTS

CENTER BODY HIDDEN
BY FILM

MAST
CANISTERS

FILM PACKAGE

STAY TAPES

LOWER CENTRAL MAST
EXTENDING AT SAME
RATE AS RIM TRUSS MASTS

NOTE: MOST STAY TAPES
NOT SHOWN

0   10   20   30   40   50

SCALE (METERS)

Figure 9.

PROGRESSIVE DEPLOYMENT OF MASTS AND FILM IN SECOND PHASE

Deployment of the rim and the central hub continued until the rim is fully deployed as shown in figure 10.
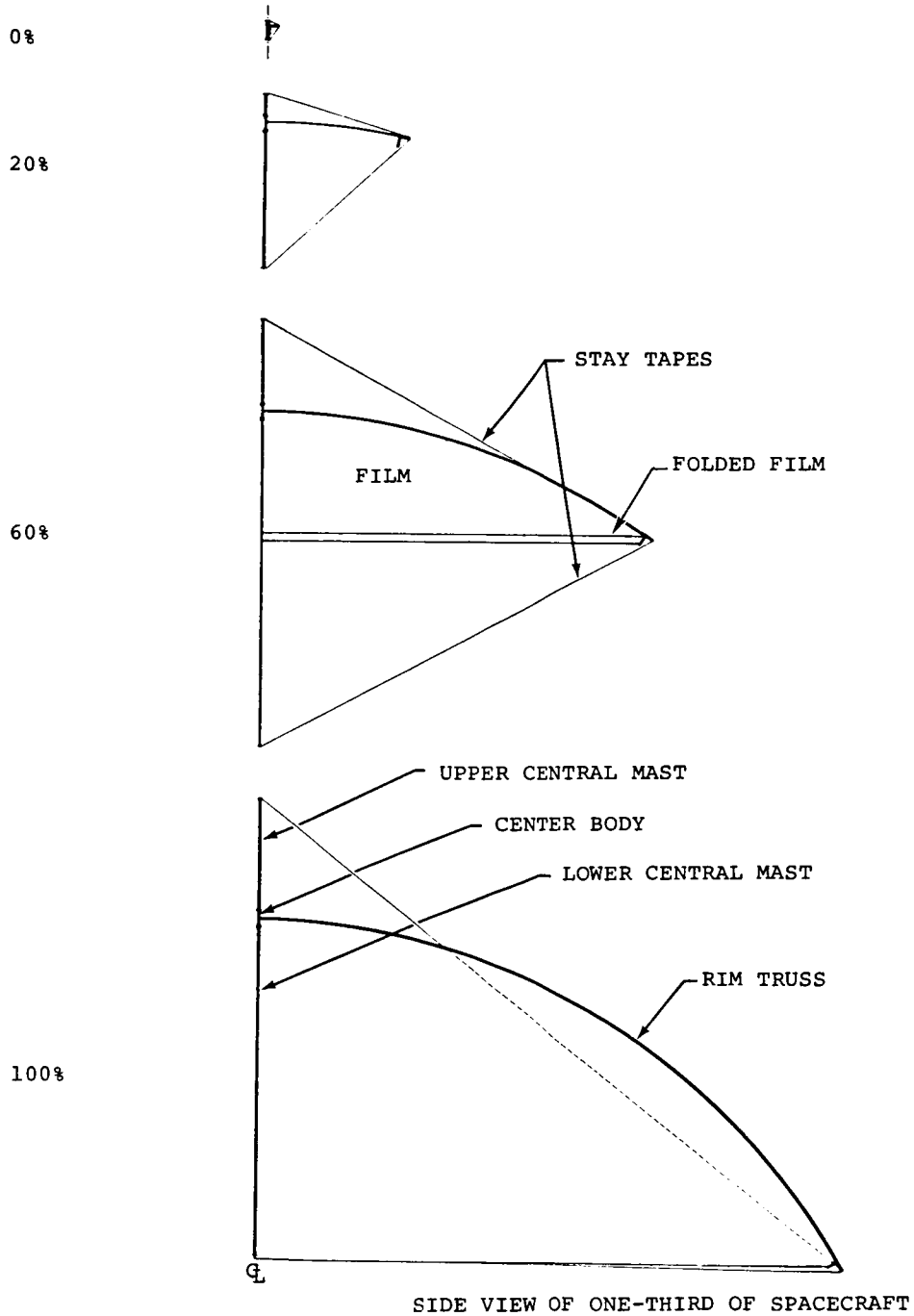
0%

20%

STAY TAPES

FILM

FOLDED FILM

60%

UPPER CENTRAL MAST

CENTER BODY

LOWER CENTRAL MAST

RIM TRUSS

100%

SIDE VIEW OF ONE-THIRD OF SPACECRAFT

Figure 10.

THIRD PHASE OF THE DEPLOYMENT SEQUENCE

The final stage of deployment is to detach the Astromast tips from the central hub and to allow the rim to hinge at six points and thereby assume its final deployed position (figure 11). This last motion is designed to be driven by synchronized electric motors at the canister base. The stay tapes are controlled properly to position the centerbody with respect to the rim during this stage.
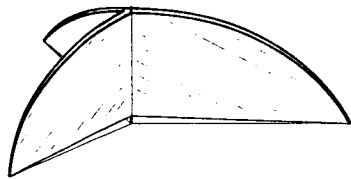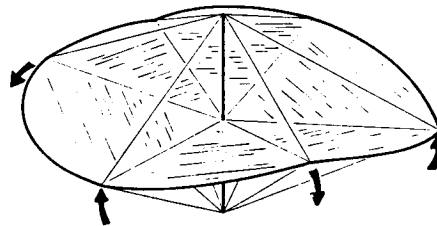
LOWER CENTRAL MAST AND RIM
TRUSSES FULLY EXTENDED

CENTRAL BODY
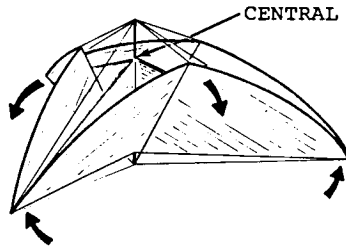
UPPER CENTRAL MAST
PARTIALLY EXTENDED

NOTE: MOST STAY TAPES
NOT SHOWN

UPPER CENTRAL
MAST NEARS
FULL EXTENSION

0   500
SCALE (METERS)

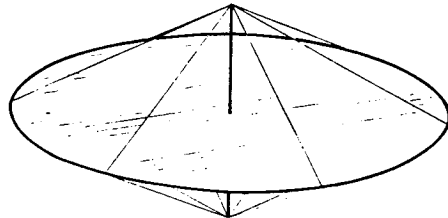FILM AND RIM
FULLY DEPLOYED
IN FINAL CONFIGURATION

Figure 11.

REFERENCES

1. Hedgepeth, John M.: Accuracy Potentials for Large Space Antenna Structures. Space Structures Session of the Society of Allied Weights Engineers 39th Annual Conference (St. Louis, MO), 12-14 May 1980, Paper No. 1375.

2. Hedgepeth, John M.: Influence of Interorbit Acceleration on the Design of Large Space Antennas. LSST/Low Thrust Propulsion Technology Information Exchange Meeting (NASA LeRC), 20-21 May 1980.

3. Hedgepeth, John M.; Knapp, Karl; and Finley, Laurence A.: Structural Design of Free-Flying Solar-Reflecting Satellites. Space Structures Session of the Society of Allied Weights Engineers 38th Annual Conference (New York, NY), 7-9 May 1979, Paper No. 1303.

4. Adams, Louis R.: Application of Isotensoid Flywheels to Spacecraft Energy and Angular Momentum Storage. NASA CR-1971, February 1972.

DESIGN CONCEPTS FOR LARGE ANTENNA REFLECTORS

John M. Hedgepeth
Astro Research Corporation
Carpinteria, California

LARGE SPACE ANTENNA REQUIREMENTS

We are performing a contractual study "Design Concepts for Large Reflector Antenna Structures," which has been underway since June. This is a report on the progress to date. The needs for large antenna structures are illustrated in figure 1, taken from work done by R.V. Powell at JPL. The lines of constant D/λ have been added to emphasize the stringency of some of the future requirements. The conclusion is that apertures from 1,000 to 10,000 wavelengths in diameter will be needed. When this is coupled with the requirement that the surface be true to a small fraction of a wavelength, the conclusion is that surface accuracies of one part in 100,000 will be needed.
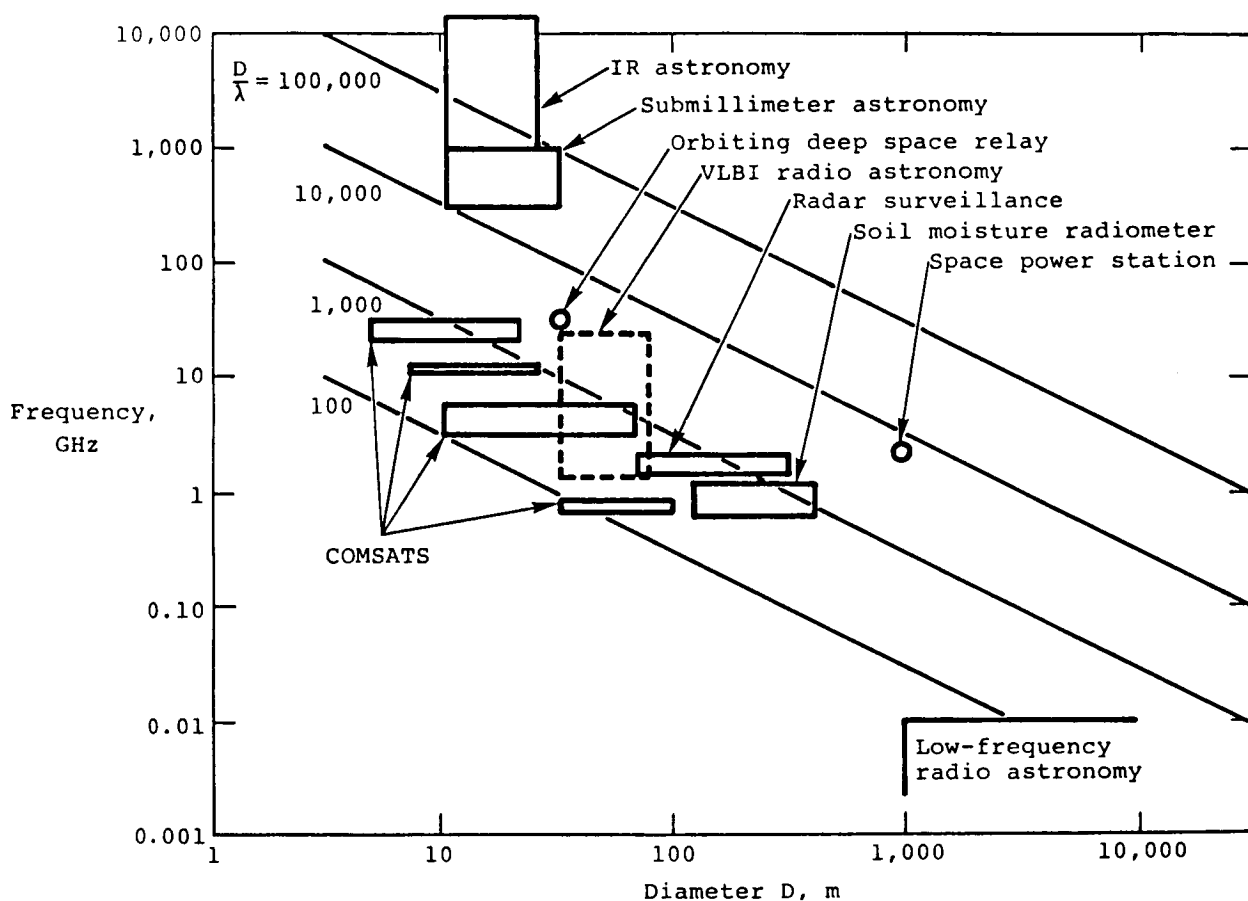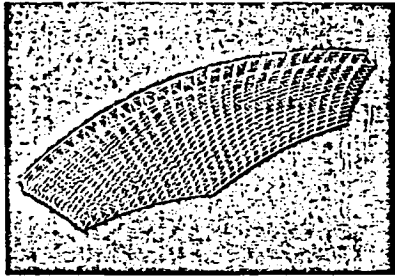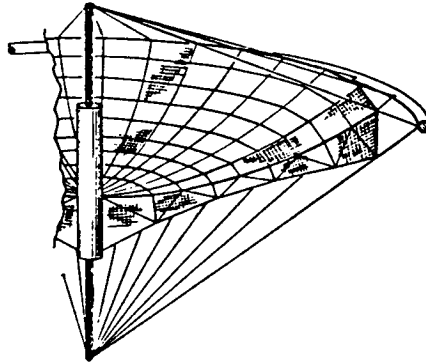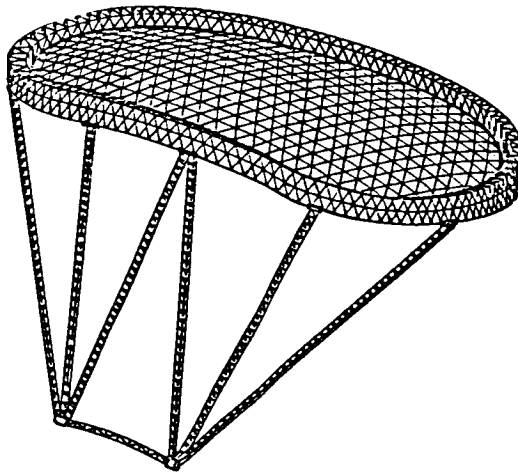

Figure 1

STRUCTURAL CONFIGURATIONS

In this study, we have confined our attention to a type of antenna reflector in which a stiff structure is constructed to hold a membrane-like reflector mesh in the correct position. An important basic restriction in our approach is that the mesh be controlled only by the structure and that no additional local shaping be employed. Furthermore, attention is confined to structures in which no adjustments would be made on assembly. Several possible configurations of this type are shown in figure 2.
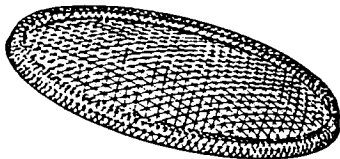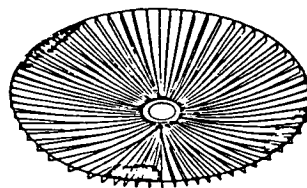

Tetrahedral truss

Pretensioned truss

Orbiting reflector
antenna

Geodesic dome

Radial rib

Figure 2

Primary attention is given to the tetrahedral-truss configuration because of its outstanding stiffness and dimensional stability. It is recognized that this type of construction is relatively complex (see figure 3), especially when the individual facets must be made small enough so that the mesh can be made flat over each facet and still approximate the desired paraboloidal surface satisfactorily.
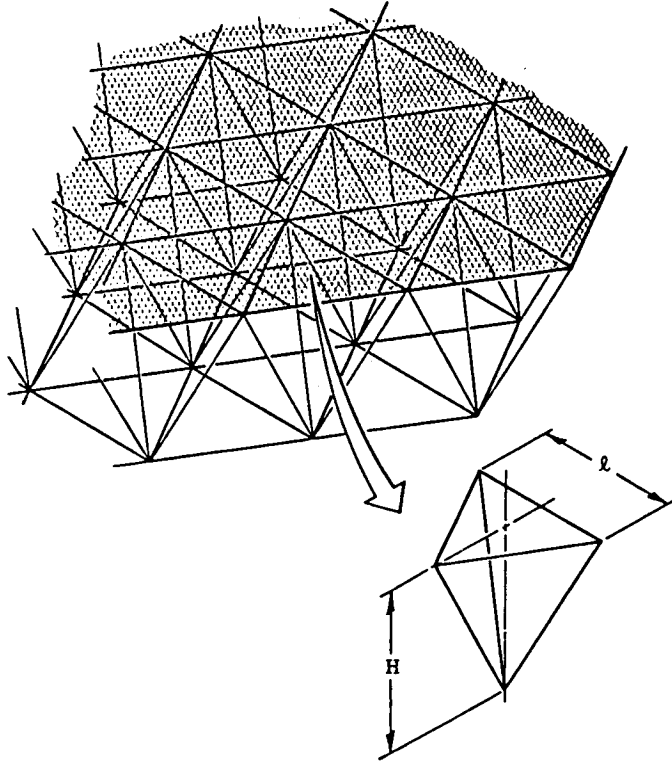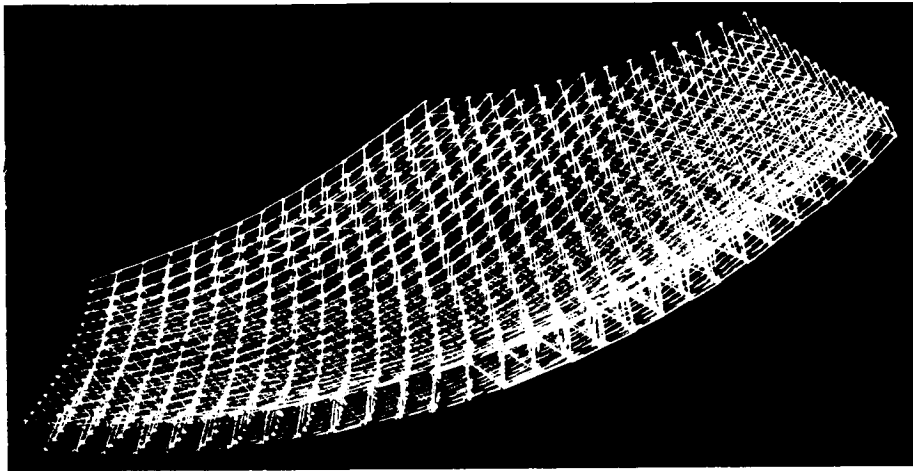

Figure 3

LIMITATIONS DUE TO FABRICATION ERRORS

Our approach is to assemble the structure from elements which are made accurately in detail and are then joined without further adjustment. The effects of the resulting tolerance buildup have been carefully analyzed and reported in ref. 1. Figure 4, taken from that reference, shows the limitations on size due to this tolerance buildup. The achievable diameter-to-wavelength ratio is plotted versus the root-mean-square of the unit length error of the constituent members. We feel that a value of σ_ϵ of 10^{-5} is achievable with careful tooling without inordinate cost increases. Note that the tetrahedral truss is markedly superior to other configurations and that diameters up to 10,000 wavelengths are achievable.
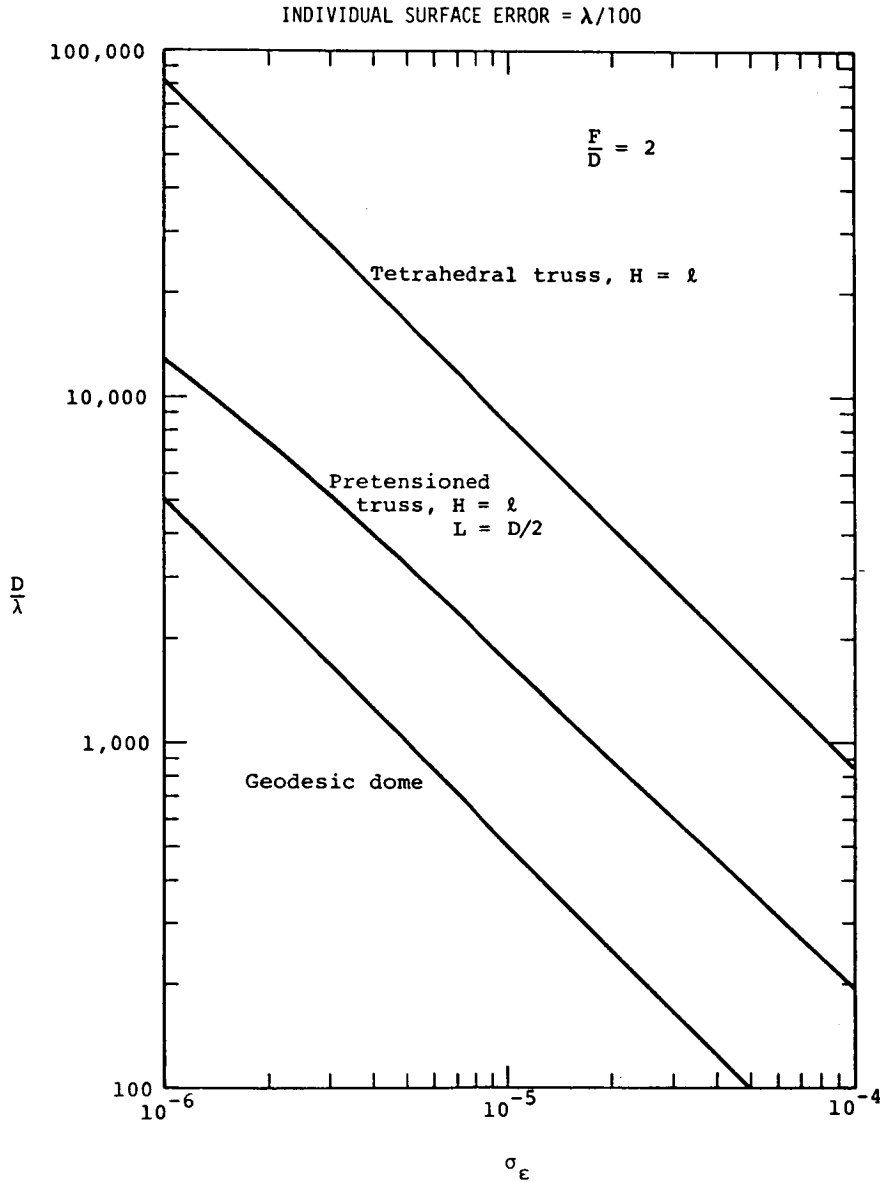
INDIVIDUAL SURFACE ERROR = $\lambda/100$

Figure 4

LIMITATIONS DUE TO THERMAL STRAINS

Similarly, the influence of steady-state thermal effects was investigated in ref. 1 for a uniform tetrahedral truss. The summary results shown in figure 5 are plotted against the parameter $\alpha_T T_{max}$. For an α_T of 0.1×10^{-6}/K, a value of this parameter of 3×10^{-5} is appropriate. The results show that the most important static thermal effect is that of self shading. The size potential is around 10,000 wavelengths.
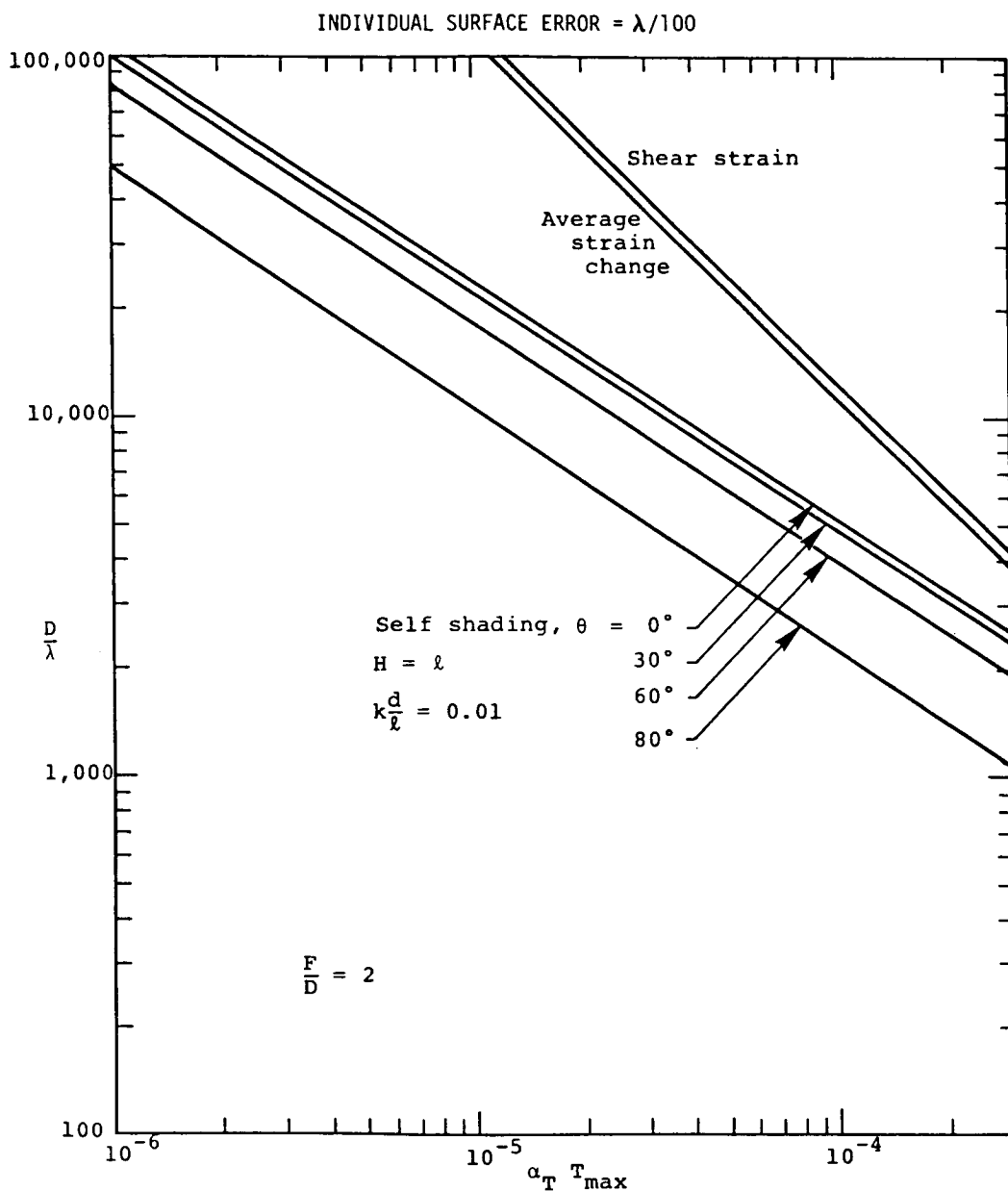
INDIVIDUAL SURFACE ERROR = $\lambda/100$

Figure 5

200-METER-DIAMETER DEPLOYABLE ANTENNA

An example antenna configuration which would meet accuracy requirements appropriate for L-band use is shown in figure 6. In this case, the cell size is selected to give an rms error due to facet flattening of 2 mm. The strut diameter is selected large enough so that the deflection of the strut under the mesh tension loads of 2.5 N/m are very small. The natural frequency of the resulting reflector structure is about 1 Hz. Similarly, the resulting structure has a significant capacity for withstanding interorbit acceleration as discussed in ref. 2. The same situation pertains to station keeping loads. Note that the structure is quite complex, being composed of about 1000 facets.
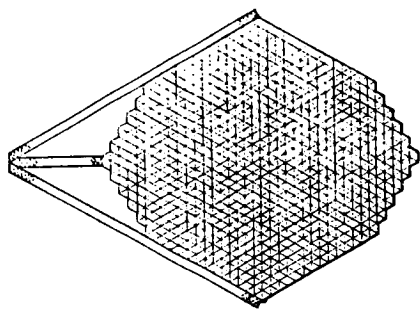
CELL SIZE = 7 m

DEPTH = 7 m

STRUT DIAMETER = 40 mm

REFLECTOR MASS = 6500 kg

VIBRATION FREQUENCY (REFLECTOR ONLY) $\simeq$ 1 Hz

SURFACE ERROR $\simeq$ 4 mm
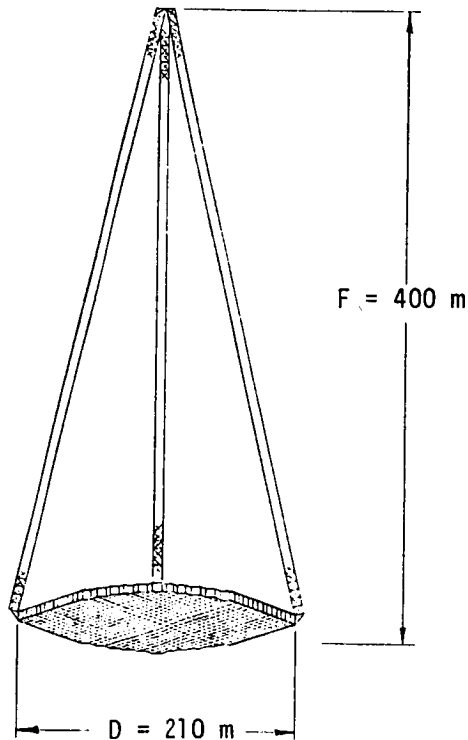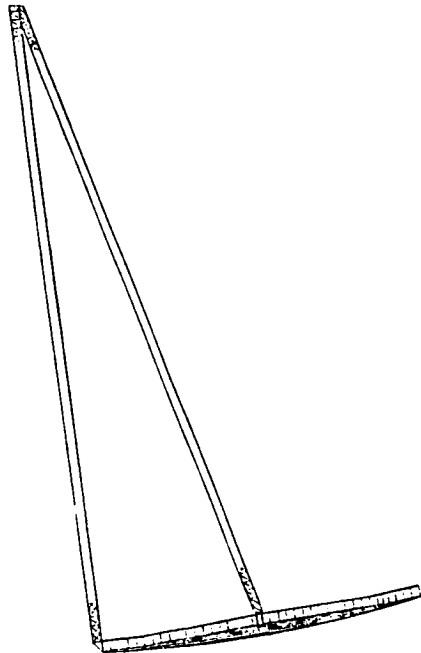
$F = 400$ m

$D = 210$ m

Figure 6

SEQUENTIAL ERECTION

Deploying the entire tetrahedral truss simultaneously is possible but is generally agreed to be difficult to make reliable. In order to achieve reliability, we must obey the principle of sequential erection shown in figure 7. In passing, note that on-orbit assembly is considered by many to be a desirable method for space erection. It follows this principle.

1. *MOST OF THE MATERIAL IS EITHER SECURELY STOWED OR FULLY ERECTED AT ANY TIME DURING THE PERIOD OF ESTABLISHMENT.*

2. *ONLY A SMALL FRACTION OF THE MATERIAL IS IN TRANSITION AT ANY TIME.*

3. *PARTS IN TRANSITION ARE CLOSELY CONTROLLED.*

4. *STRUCTURAL PARTS IN TRANSITION ARE AVAILABLE FOR INSPECTION AND REPAIR.*

Figure 7

PARABOLOIDAL TRUSS PACKAGING

We have invented a new means of packaging and deploying tetrahedral-truss structures. The approach consists of packaging slanted truss planes on top of each other sequentially as shown in figure 8. The truss planes can then be packaged along their length one bay at a time. Models have been constructed to illustrate this process. A fortuitous feature of the paraboloidal shape is that parallel planes intersect with a paraboloid in exactly the same curve. Therefore, the truss planes can be packaged in coincidence even for curved reflectors.

UPPER CHORDS

TRUSSES
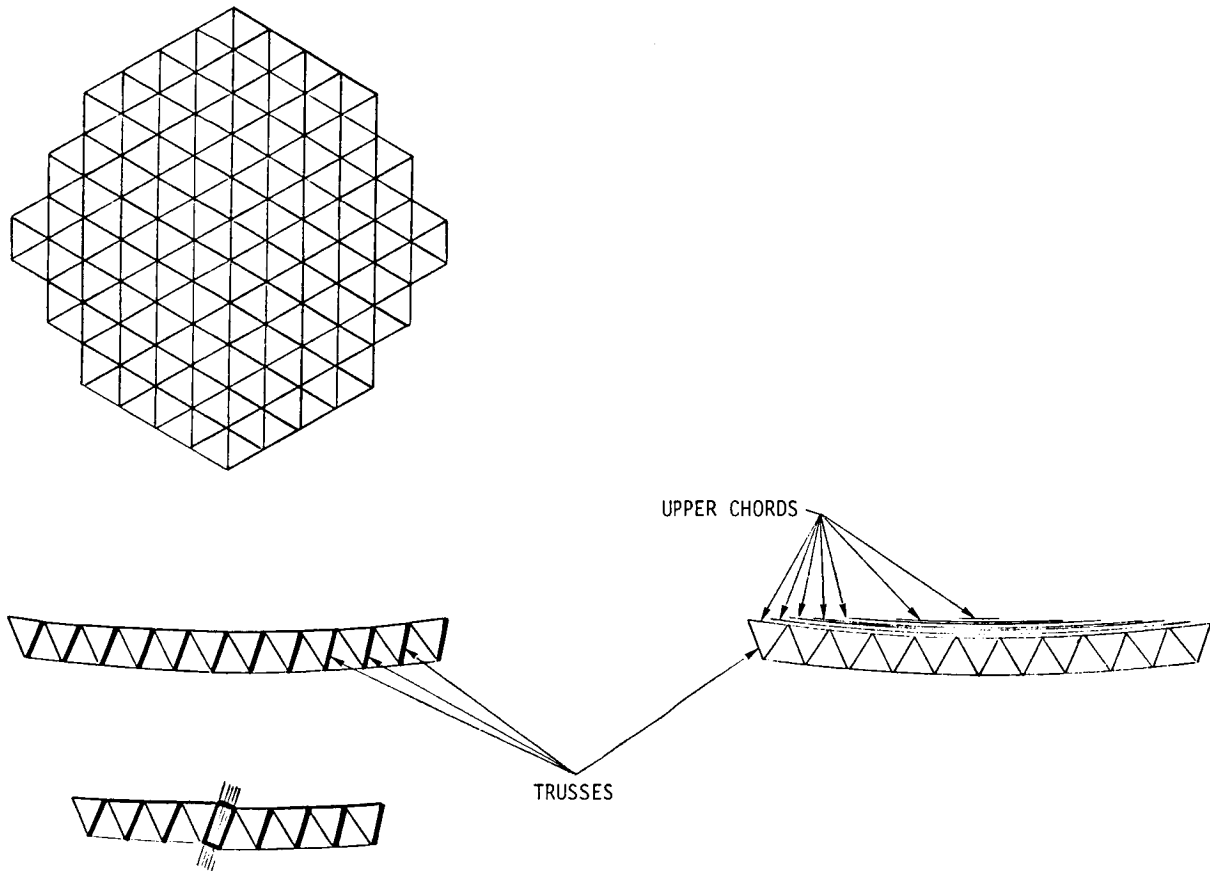
Figure 8

INITIAL DEPLOYMENT

Figures 9 through 11 illustrate the sequence of deployment. At all stages, the partially deployed structure consists of two symmetrical, fully deployed tetrahedral-truss segments which bound fully deployed truss planes. The two canisters with appropriate manipulators control the motion of the truss planes and the essentially rigid bounding tetrahedral-truss segments. In figure 9, the members which have dots in their centers are in the process of being deployed.

Figure 9

MID-DEPLOYMENT

The truss in mid-deployment is shown in figure 10.
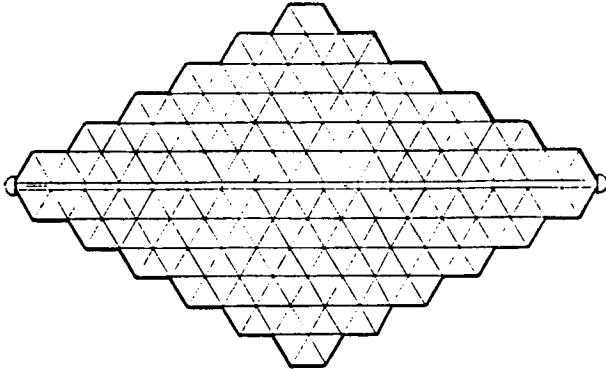
Figure 10

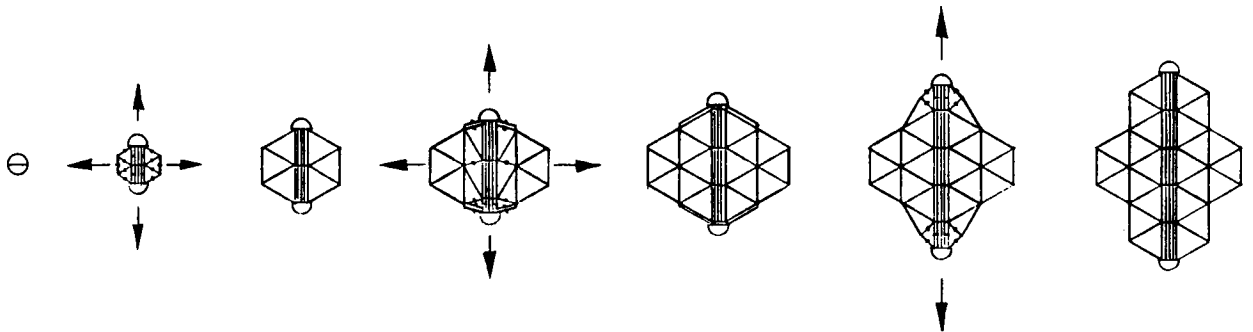The fully deployed truss has a shape which is governed in part by the character of the deployment (see figure 11).
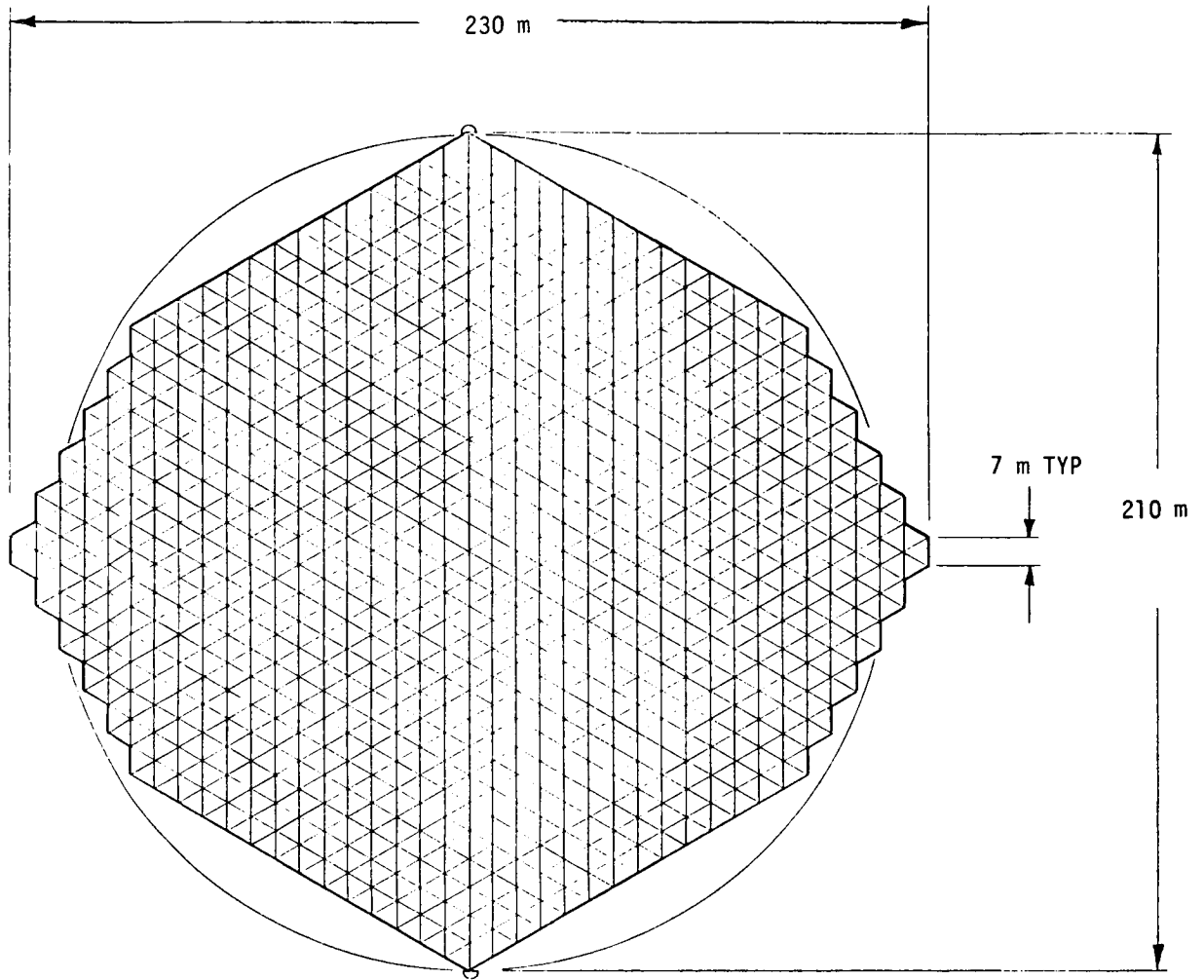
Figure 11

PACKAGED REFLECTOR

The reflector package is shown in figure 12. To this, of course, must be added the packages for the feed support which have not yet been examined.
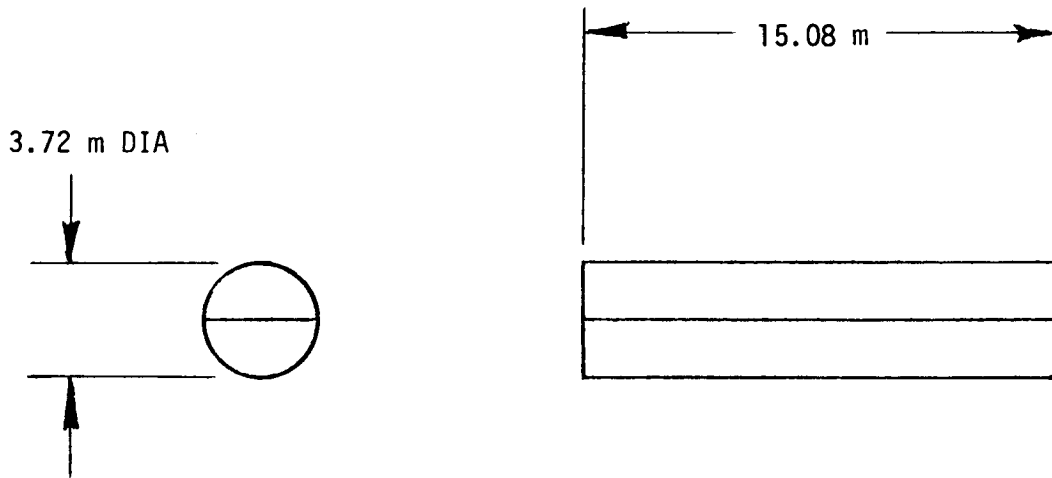
Figure 12

The details of the stowage have been examined and the package is shown in figure 13. Note that the surface members are packaged tightly without spaces, thereby maximizing the diameter of the deployed reflector possible in a single Shuttle payload.

CANISTER

3.72 m

NINE-MEMBER
MODULE (TYPICAL)

NOTE: ONLY PERIPHERAL
MODULES SHOWN.

Figure 13

116
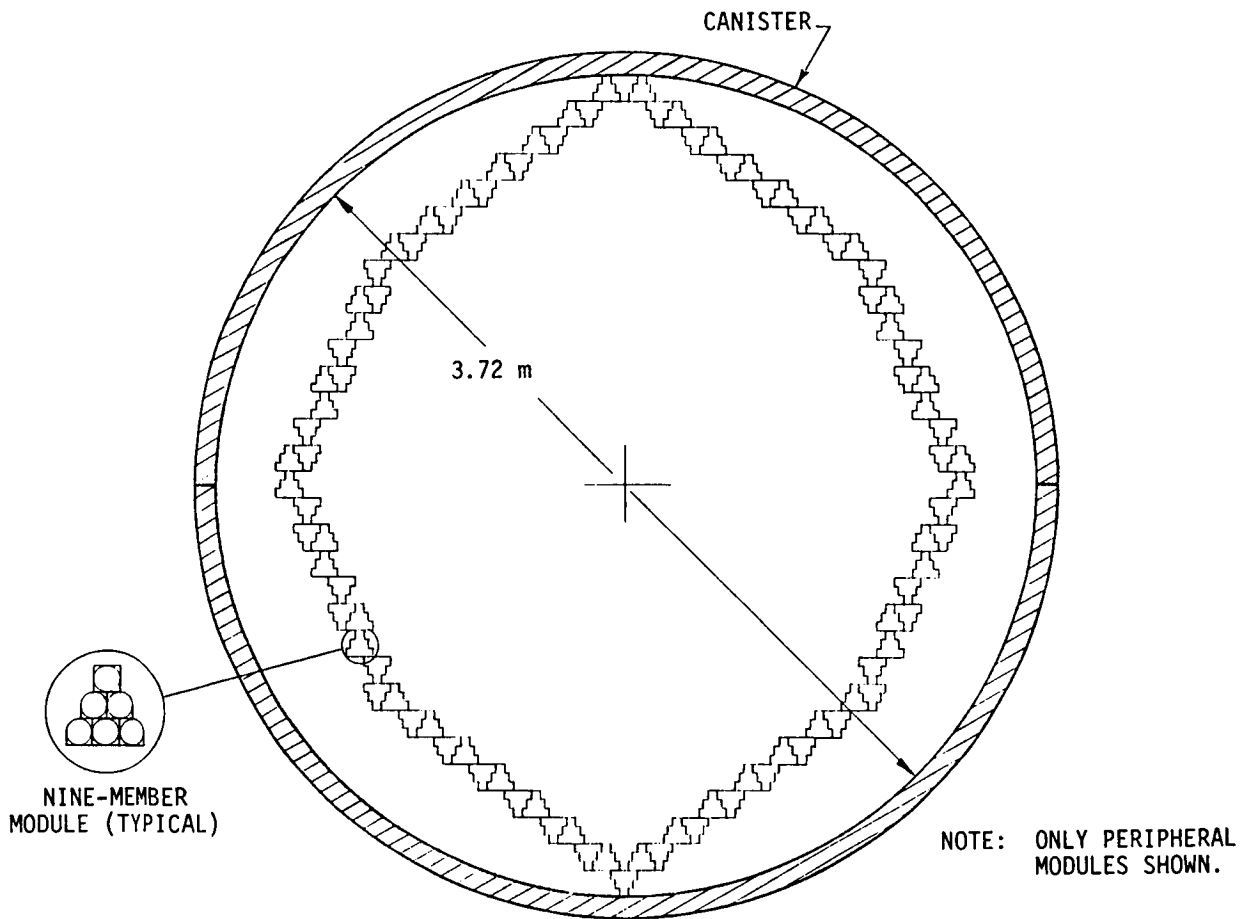
KNEE HINGE

The structure has on the order of 10,000 joints, each of which must oper-
ate successfully for a reliable deployment. Joint design is crucial, therefore,
to the success of the structure. One joint is shown in figure 14 which makes
use of an "almost-over-center" latch, developed and proved as flight hardware
on the Seasat Synthetic Aperture Radar antenna structure. This latch provided
a lockup of the many knee joints without requiring the close tolerances ordin-
arily demanded by over-center latches.
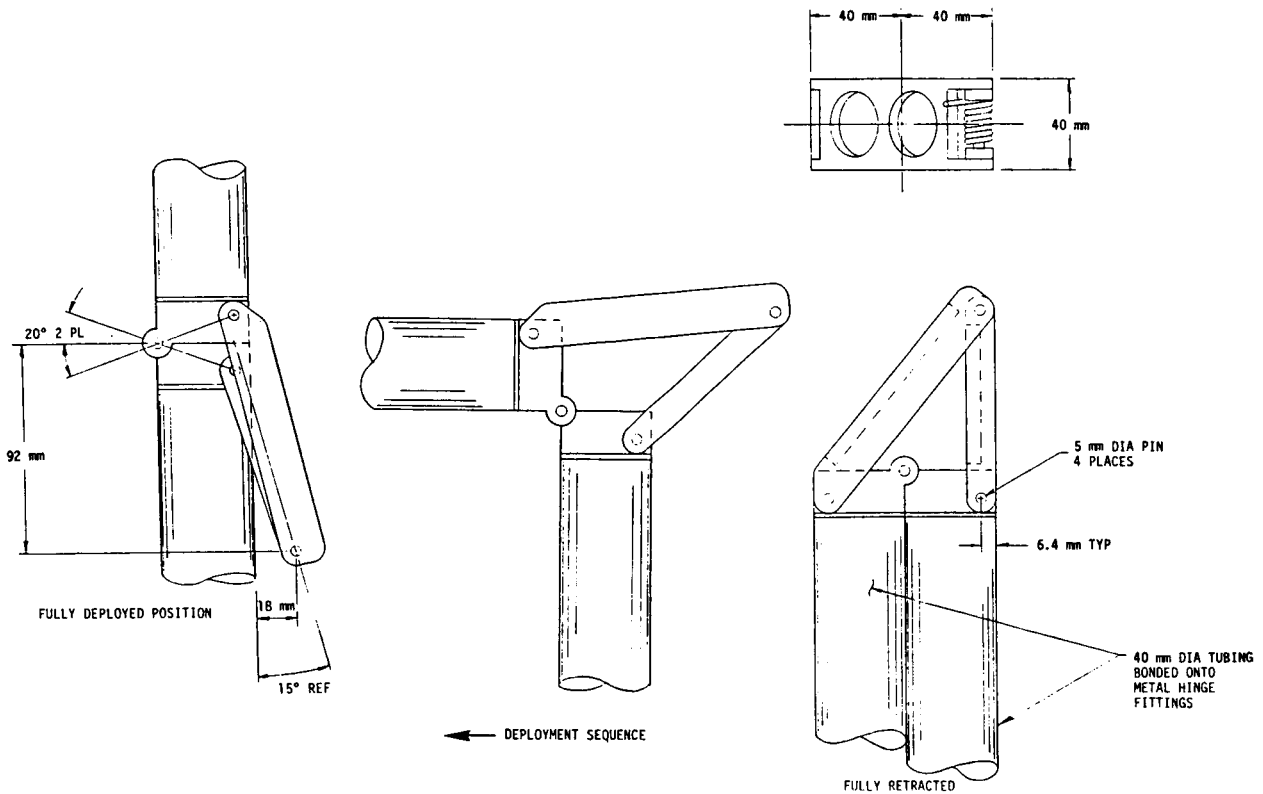
Figure 14

NINE-MEMBER JOINT - TETRAHEDRAL TRUSS

We are in process of designing other joints, the most complex of which is the nine-member joint shown in figure 15 in an obsolete form.

40 mm
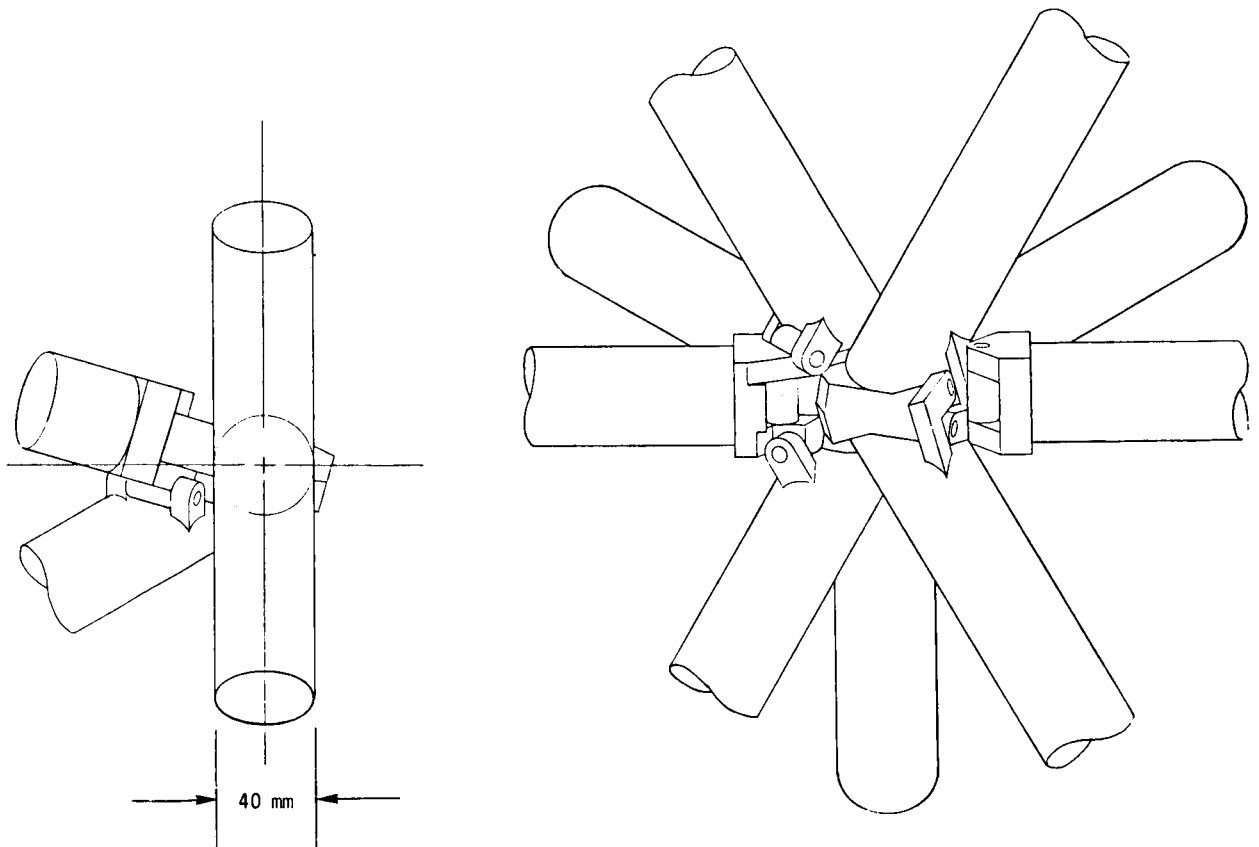
Figure 15

REFERENCES

1. Hedgepeth, John M.: Accuracy Potentials for Large Space Antenna Structures. Space Structures Session of the Society of Allied Weights Engineers 39th Annual Conference (St. Louis, MO), 12-14 May 1980, Paper No. 1375.

2. Hedgepeth, John M.: Influence of Interorbit Acceleration on the Design of Large Space Antennas. LSST/Low Thrust Propulsion Technology Information Exchange Meeting (NASA LeRC), 20-21 May 1980.

A MODULAR APPROACH TOWARD
EXTREMELY LARGE APERTURES

A. A. Woods, Jr.
Lockheed Missiles and Space Company
Sunnyvale, California

STUDY OBJECTIVES

A nine month study entitled "Development of a Deployable Module Concept for Large Reflector Application" was undertaken by Lockheed Missiles and Space Company, Inc., in September 1979. This contract was originated by Langley Research Center as a subtask of an ongoing contract in support of the development of Large Space Structures Concepts.

The subtask objectives are summarized in Figure 1. LMSC was to design a large erectable antenna using a deployable modular approach and characterize the performance of such antennas. In addition, the module deployment kinematics were to be verified by construction of a working subscale demonstration model, and on-orbit antenna assembly scenarios were to be investigated.
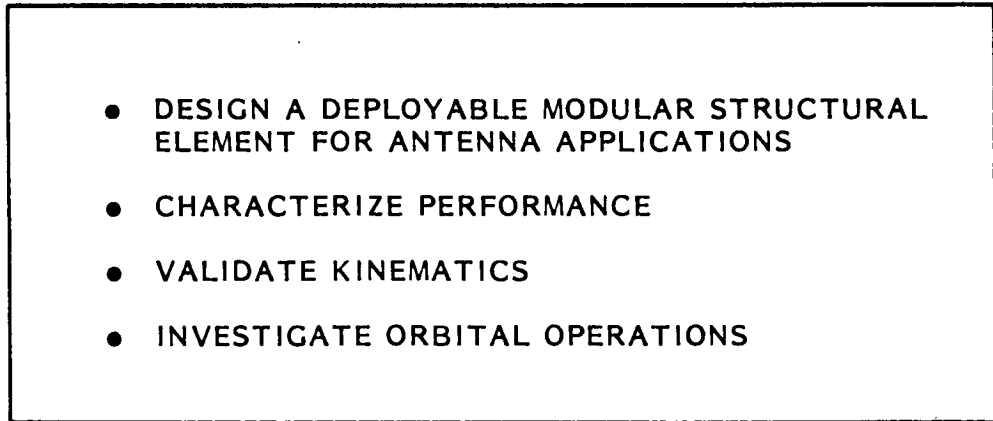
> - **DESIGN A DEPLOYABLE MODULAR STRUCTURAL ELEMENT FOR ANTENNA APPLICATIONS**
>
> - **CHARACTERIZE PERFORMANCE**
>
> - **VALIDATE KINEMATICS**
>
> - **INVESTIGATE ORBITAL OPERATIONS**

Figure 1

The final product envisioned from the study was a large parabolic reflector to be erected in lower earth orbit from up to 330 separate deployable modules transported by one STS launch. This concept is overviewed in Figure 2.
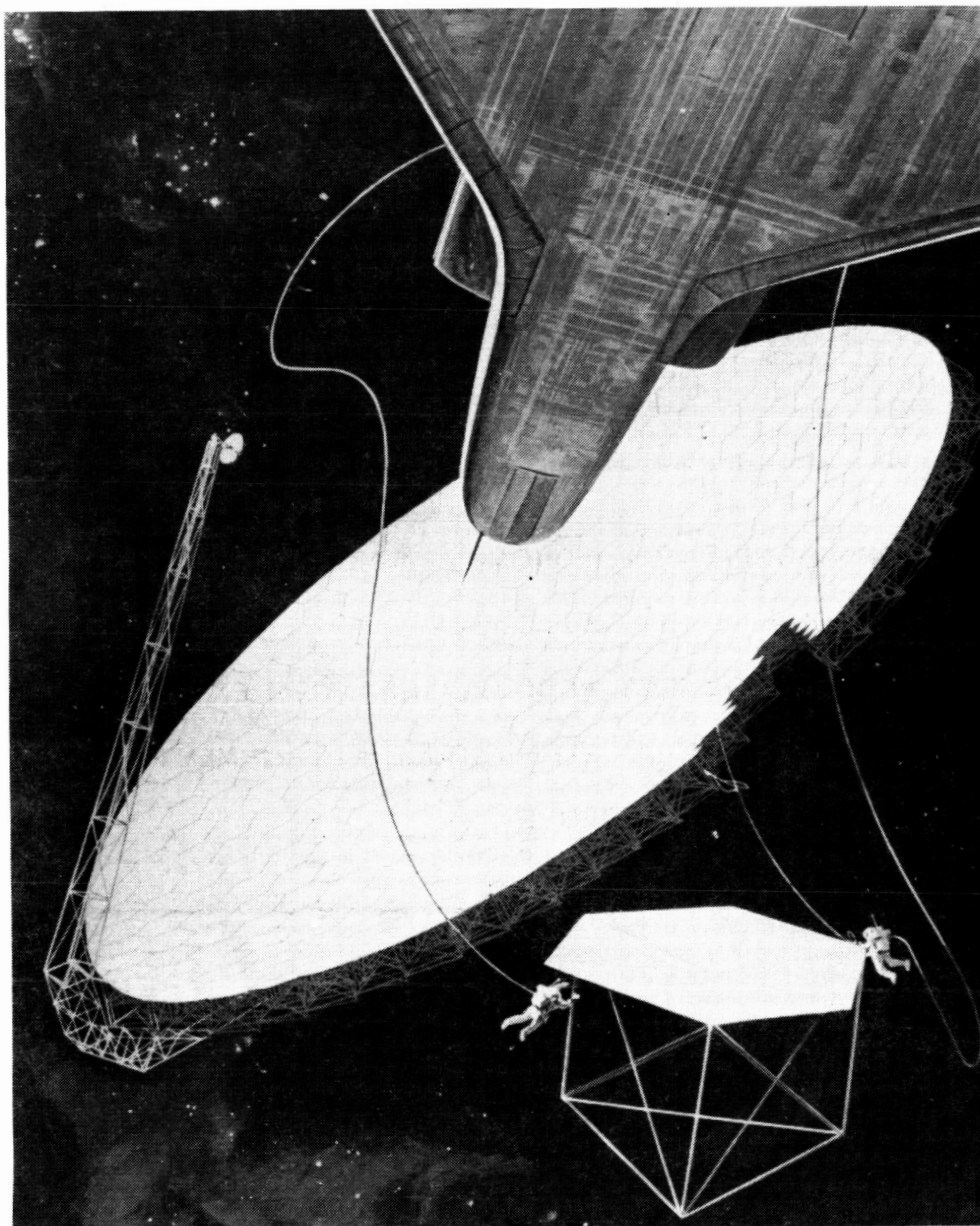
Figure 2

DESIGN REQUIREMENTS

The design constraints established for the study are listed in Figure 3. Each module was to be an autonomous deployable unit, attached to neighboring modules through three attachment points. Each module was to provide a hexagonal RF reflective surface element, independent of but adjacent to neighboring elements. The modules were to provide minimum stowed volume (maximize packing efficiency) and be capable of being deployed by an external, plug-in deployment power device.

- EACH MODULE AN AUTONOMOUS STRUCTURE

- HEXAGONAL SURFACE ELEMENT

- ORBIT DEPLOYMENT ACCOMPLISHED WITH EXTERNAL AID

- THREE POINT MODULE TO MODULE ATTACHMENT

- MINIMIZE STOWED VOLUME

Figure 3

DESIGN APPROACH

The design approach selected to satisfy the foregoing requirements consists of a reflective mesh surface supported by a small diameter (1.27 cm) thin wall (.4 mm) tubular framework. Several of the tubes contain spring powered, latching joints which allow them to be folded to reduce the stowed package size. A single central jackscrew controls all of the deployment motions, acting as both the slider link of a four bar linkage for the upper truss and as a cable reel to deploy cables which control the deployment motions of the lower structure elements. The stowed module is basically a passive device, in that external mechanical power must be supplied by a motor for deployment to occur.

- SURFACE — FOLDING HEXAGONAL TRUSS PLATE

- FRAME — FOLDED TRIANGULAR TRUSS

- STRUCTURE — 1.27 CM DIAMETER, 0.4 mm THICK GRAPHIC EPOXY TUBES

- JOINTS — SELF ACTIVATING AND LOCKING WITH TWO DEGREES OF FREEDOM

- DEPLOYMENT CONTROL — CENTRAL JACK SCREW WITH STRUCTURAL AND CABLE SYNCHRONIZATION

- DEPLOYMENT POWER — EXTERNAL PLUG IN MOTOR

Figure 4

MODULE DESIGN OVERVIEW

Figure 5 describes the basic components of a single module. An upper hexagonal truss frame supports the mesh, and structural depth is provided by a triangular lower frame cross braced to the upper frame. The folded truss elements use spring powered latching joints which provide continuous column stiffness in the deployed position. Deployment is effected by a central jack-screw in the upper space frame which opens the hexagonal frame through a four-bar linkage and simultaneously pays out cables which control the spring powered deployment motions of the lower frame members. The jackscrew is powered by a separate, plug-in motor unit which is used to deploy all individual modules.

Figure 5

126
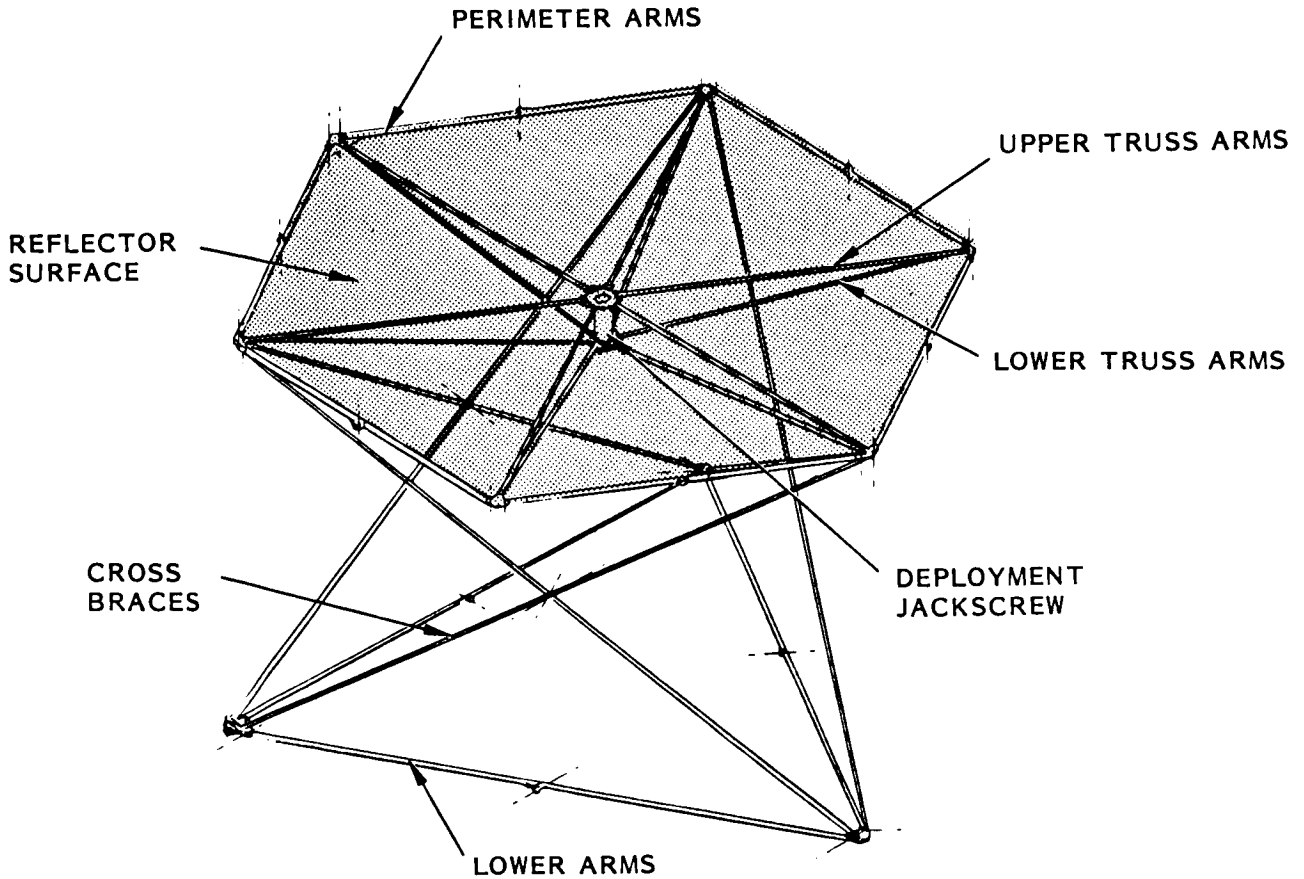
Figure 6 shows the subscale demonstration model in the stowed position. The stowed package is approximately 25 cm in diameter by 100 cm long. The separate deployment motor housing can be seen as a small rectangular box extending below the module.
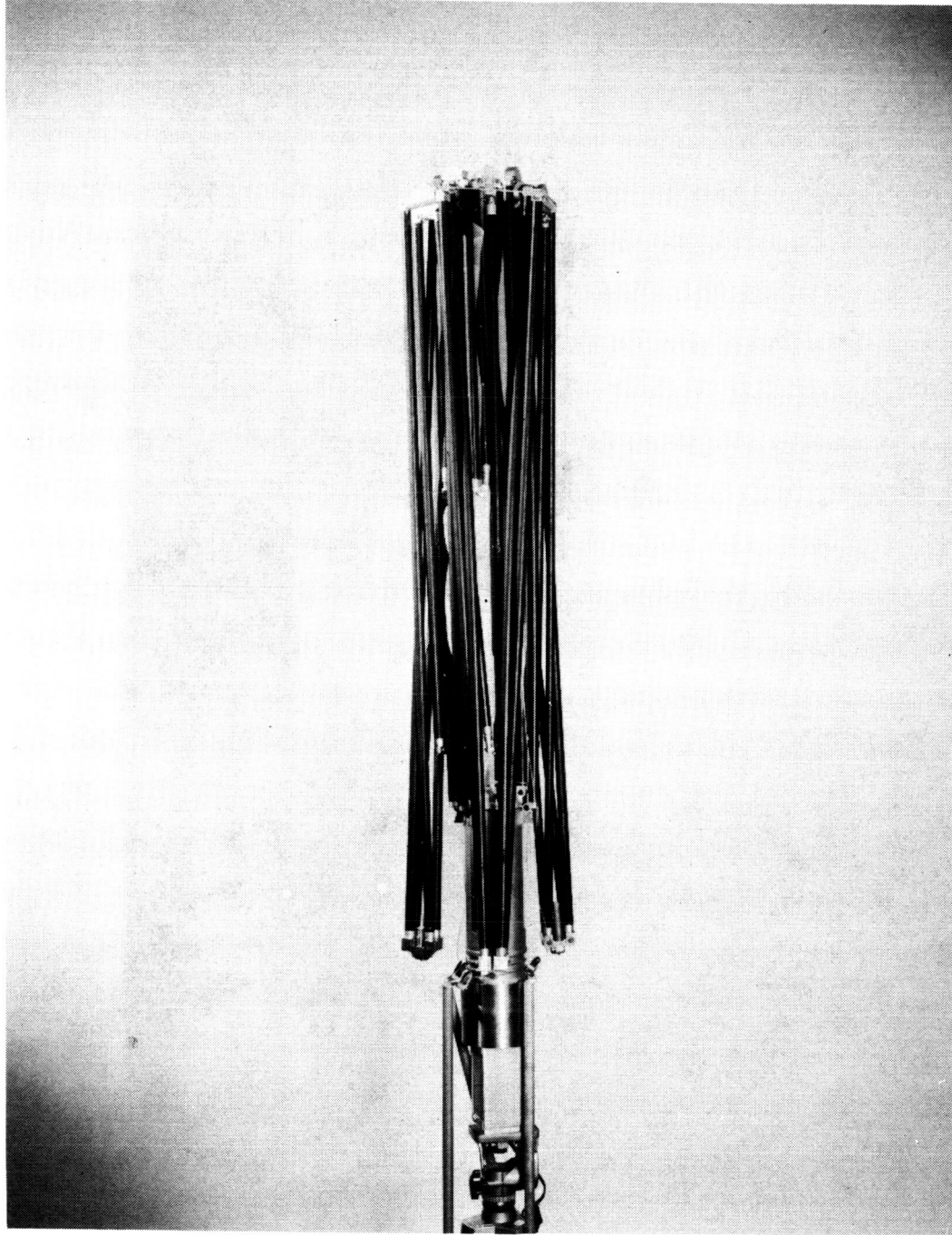
Figure 6

Figure 7 shows the demonstration model early in its deployment cycle. The cross braces are moving outward and upward and the hexagonal truss is beginning to open.
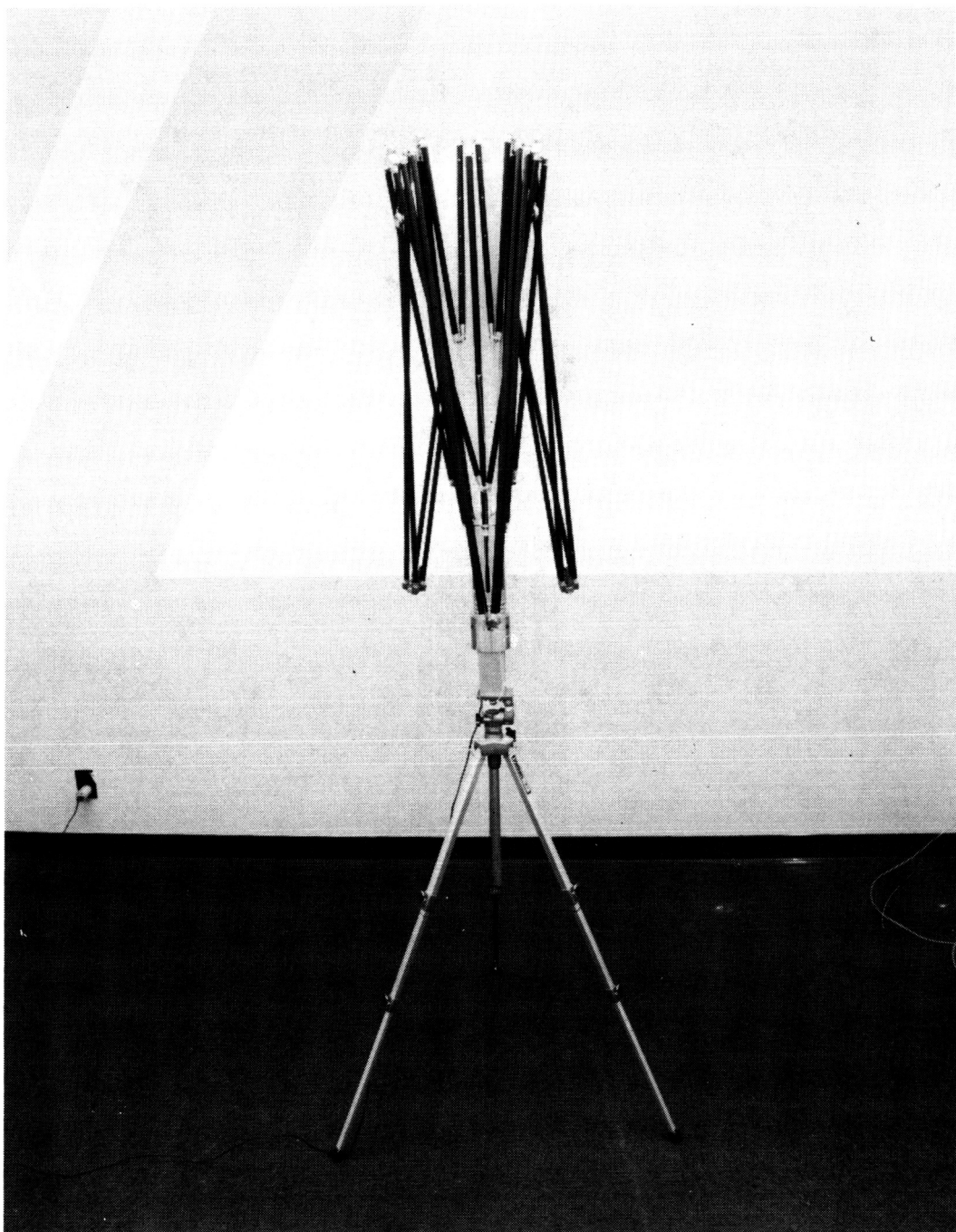
Figure 7

Figure 8 shows the model further along in its deployment motion. The upper surface has opened substantially and the cross brace center joints have reached the peak of their upward swing.
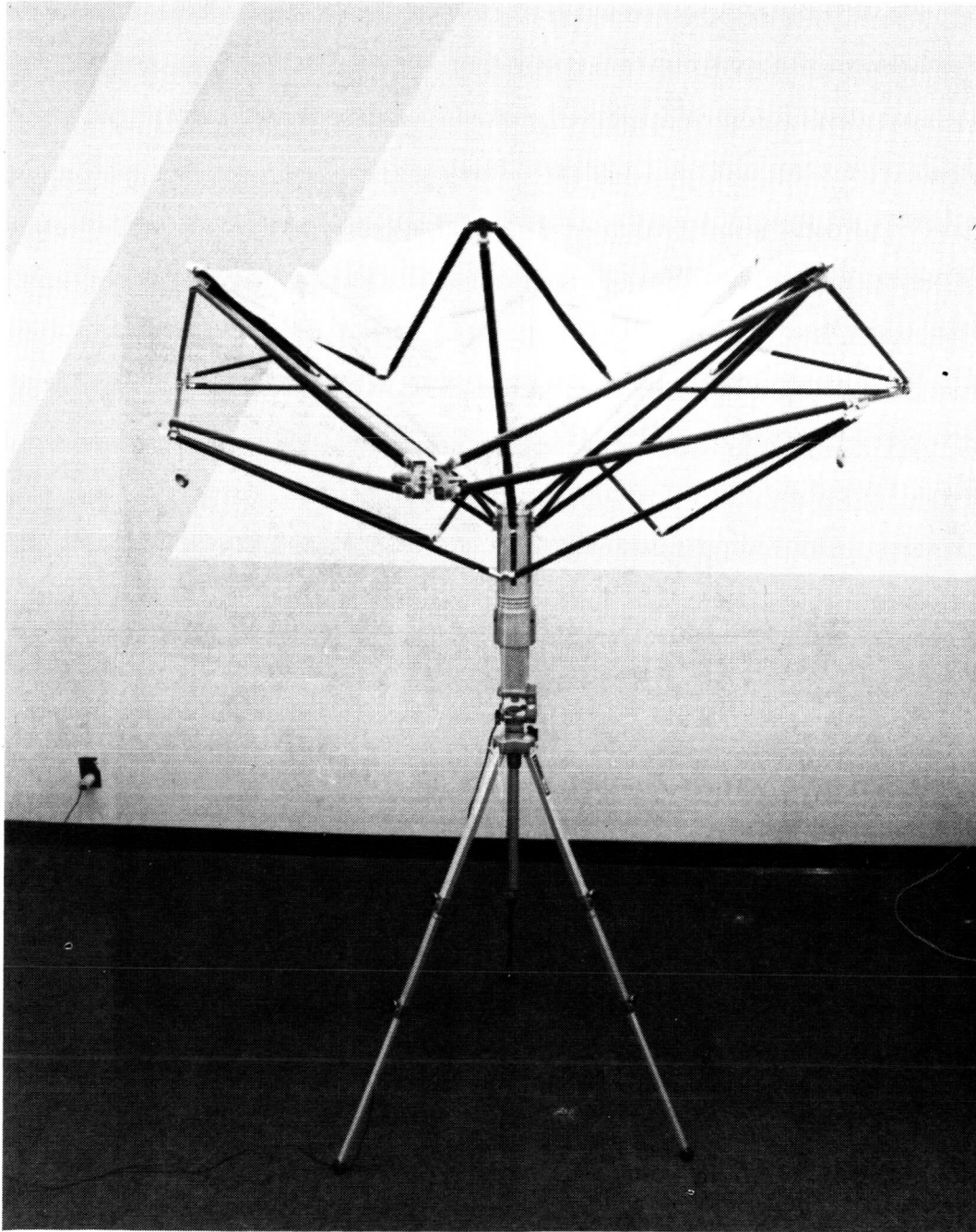
Figure 8

Figure 9 shows the model still further along in its deployment. The cross brace lower joints are separating from the upper joints deepening the structure.
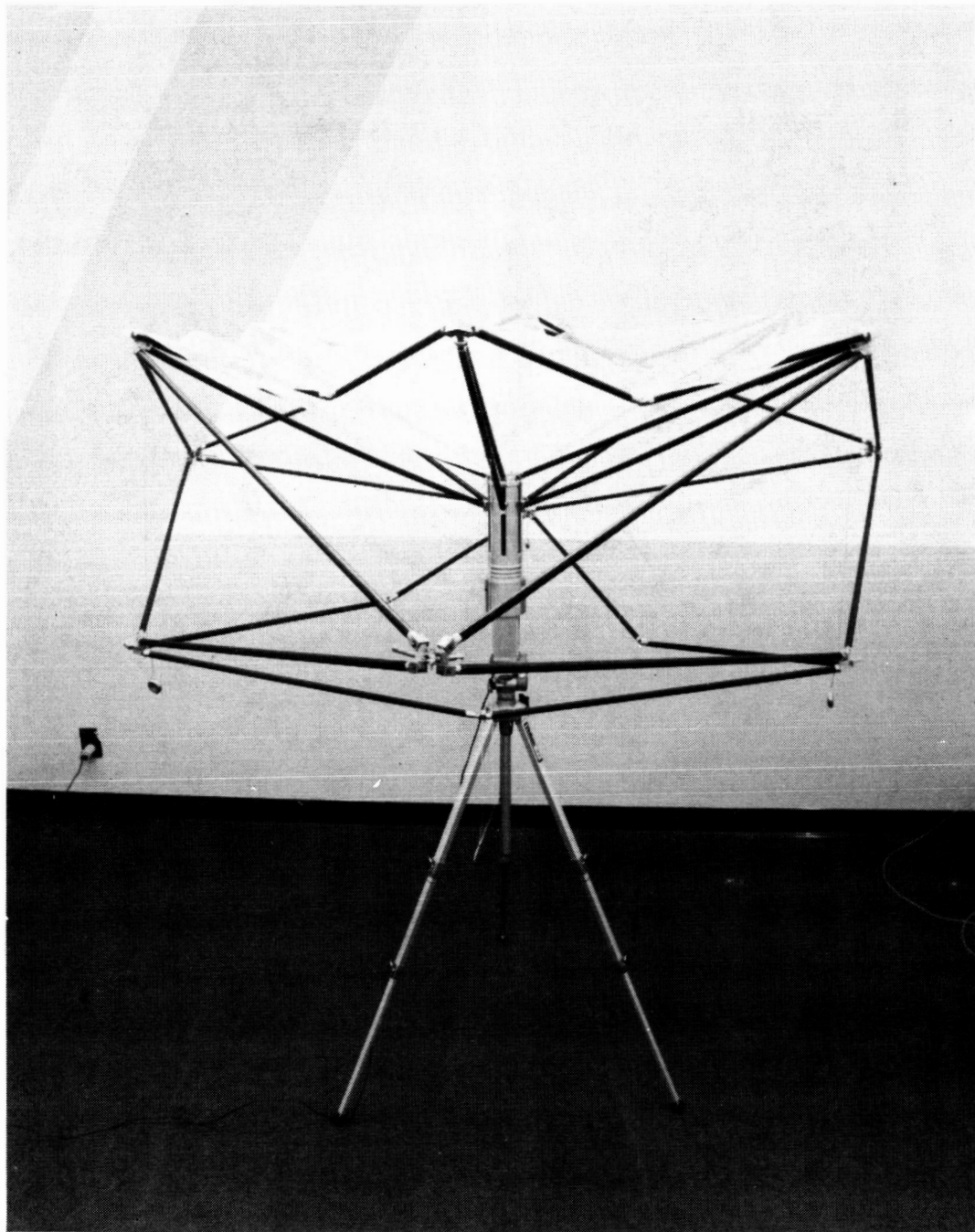
Figure 9

The fully deployed module is pictured in Figure 10. This demonstration model measures approximately 160 cm across the corners of the hexagonal reflector surface and stands approximately 135 cm high. The tubing size (1.27 cm diameter) and therefore joint sizes are full scale in the model. For a full scale module, however, the tube lengths are increased to the full length of the STS Orbiter cargo bay, resulting in a flight module measuring 28 meters across the corners of the hexagonal surface by 24 meters deep.
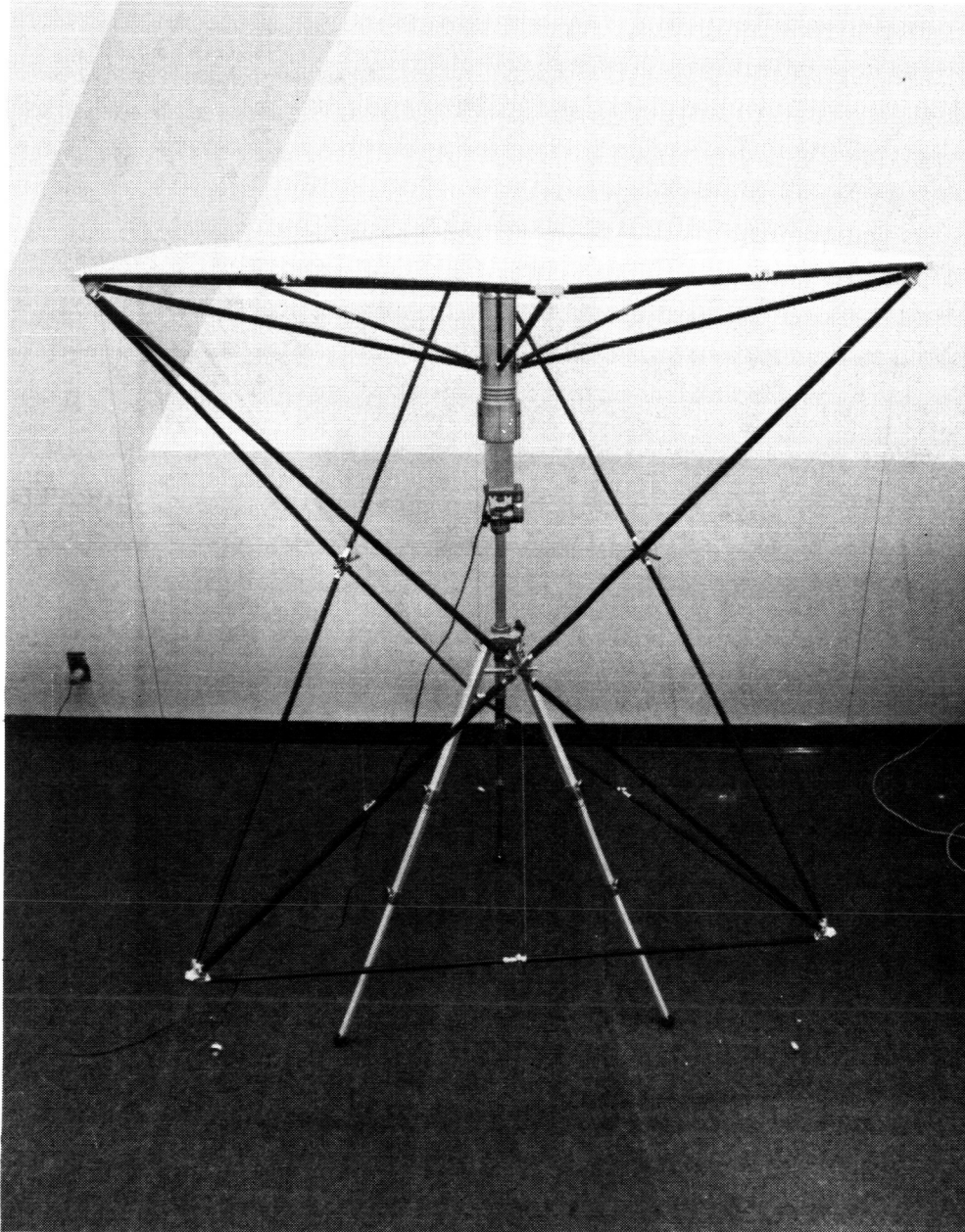
Figure 10

PERFORMANCE STUDIES

Figure 11 shows the mass of individual modules of various sizes. As the module size increases, the essentially parasitic mass of the module structure and the deployment mechanism becomes less and less significant and the module mass becomes predominantly the mass of the reflective mesh.
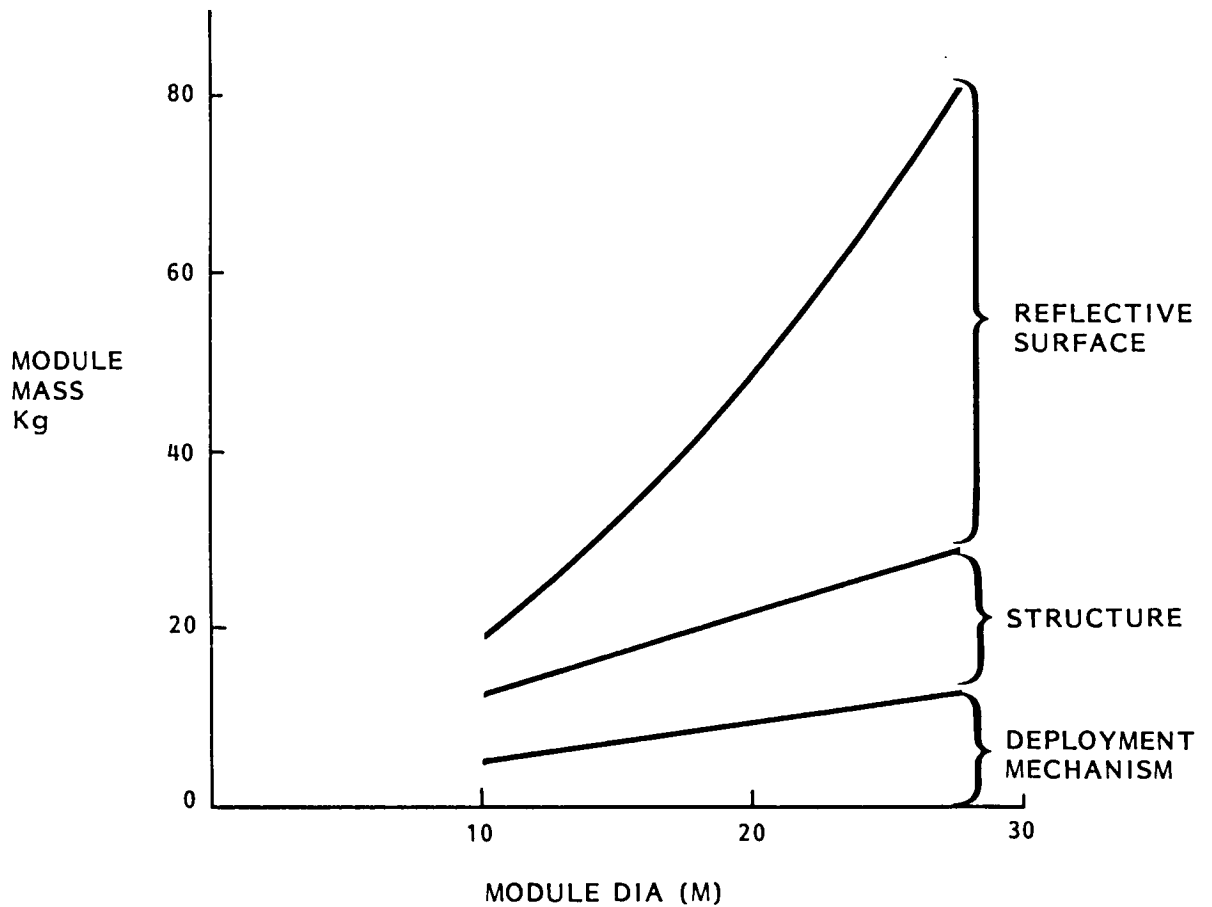
Figure 11

Figure 12 demonstrates this effect more clearly. For small modules (10 meters in diameter) the reflective mesh surface, which is for an antenna reflector the useful portion of the module, amounts to a little over one third of the total mass of the module. For a 28 meter diameter module, however, the mesh surface comprises almost two thirds of the mass of the module.
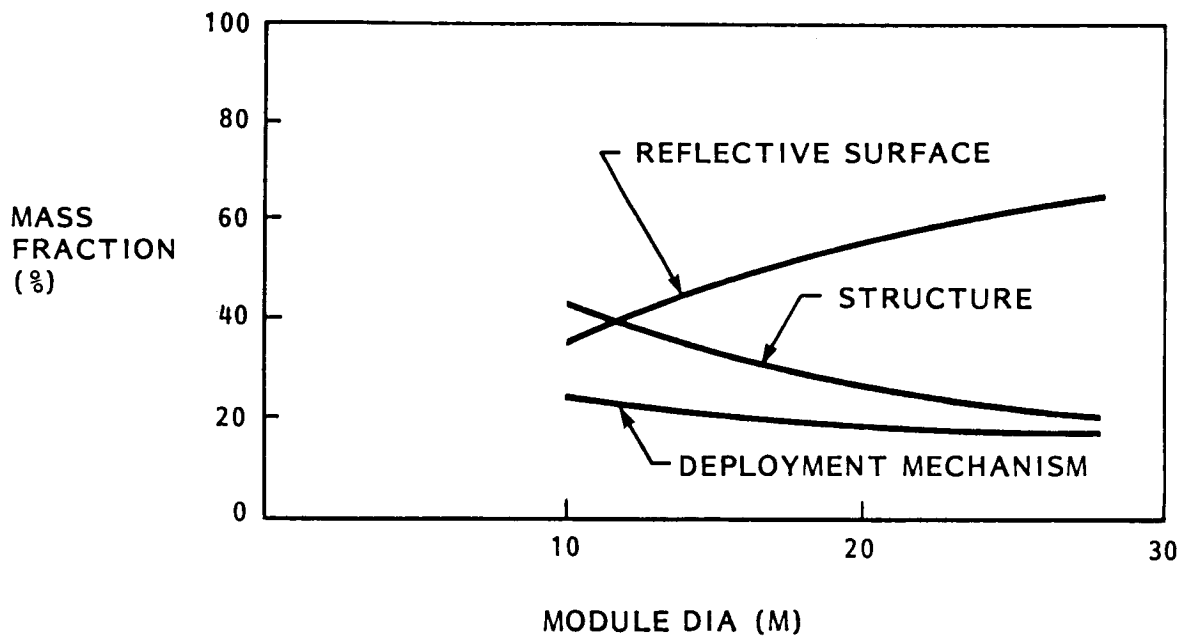
Figure 12

DEPLOYABLE MODULAR ANTENNA APPLICATION

The structural efficiency of modular antennas is fully realized in large aperture uses at moderate to mm wavelength RF frequencies. Modular antennas can be efficiently utilized through the majority of currently projected radiometry and ODSRS reflector applications when multiple shuttle flights are considered. Even with a single shuttle, the modular approach yields a significant potential for performance improvement over the current projections for mesh deployables as can be seen in Figure 13.
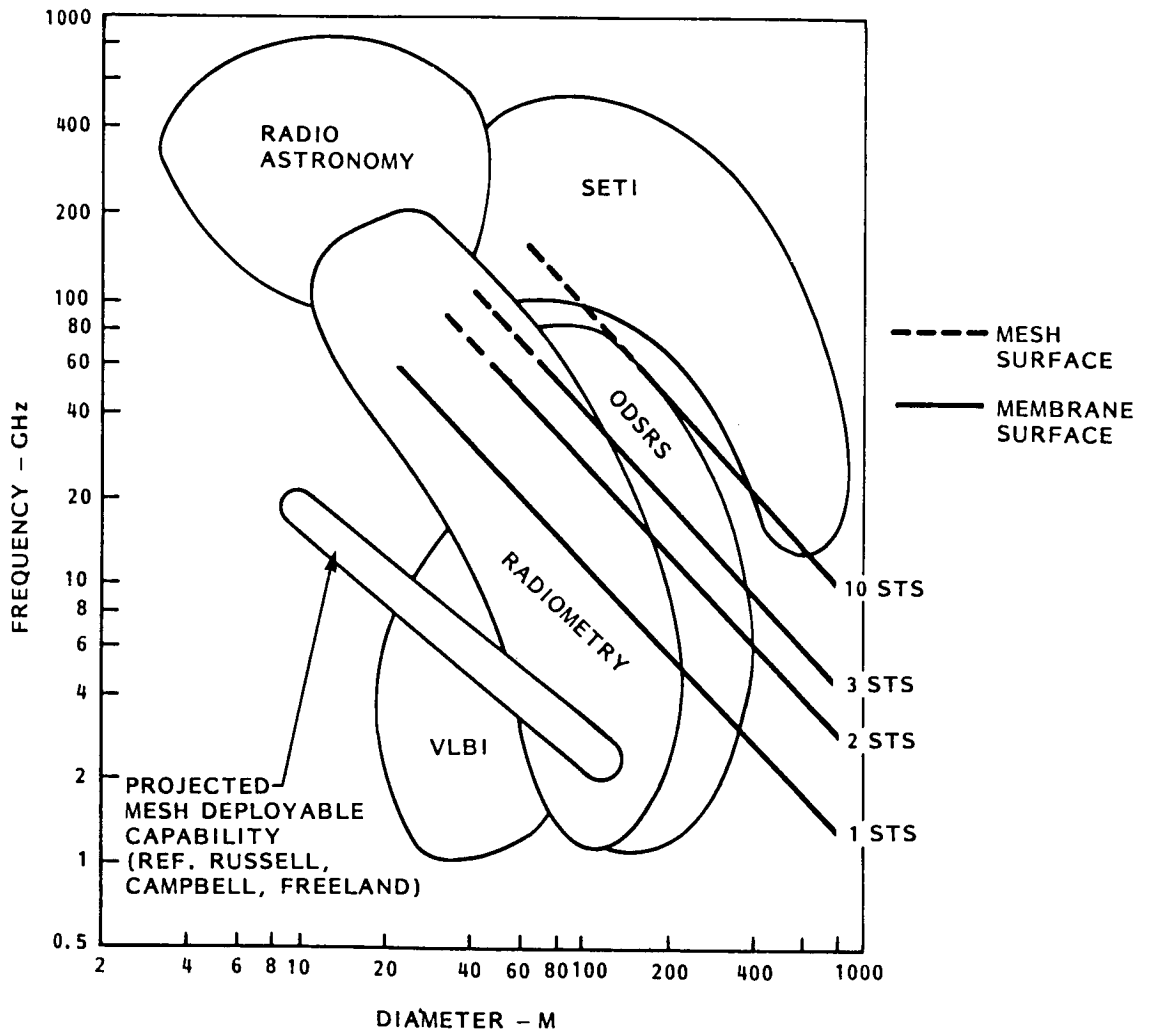
Figure 13

MODULAR ANTENNA ASSEMBLY METHODS

Figure 14 summarizes the various reflector assembly scenarios investigated during the study.

Techniques which were examined ranged from those requiring present technology STS operations with no EVA to large aperture techniques requiring development of a self contained, automated free flying assembly satellite.

```
┌─────────────────────────────────────────────────┐
│                                                 │
│    ●  STS CONTAINED WITH 2 RMS                   │
│                                                 │
│    ●  RMS/ARTICULATED BOOM FIXTURE               │
│                                                 │
│    ●  FORMATION FLYING SATELLITE                 │
│                                                 │
│    ●  FREE FLYING AUTOMATED SATELLITE            │
│                                                 │
└─────────────────────────────────────────────────┘
```

Figure 14

Reflectors of moderate size (up to approximately 70 m diameter) can be assembled directly from the Orbiter cargo bay using 2 RMS arms. One arm is used to hold and position the partially completed reflector and the other arm is used to deploy each individual module and attach it to the assembly. The entire operation can be controlled by the payload specialist working at the aft flight deck of the Orbiter. This concept is overviewed in Figure 15.
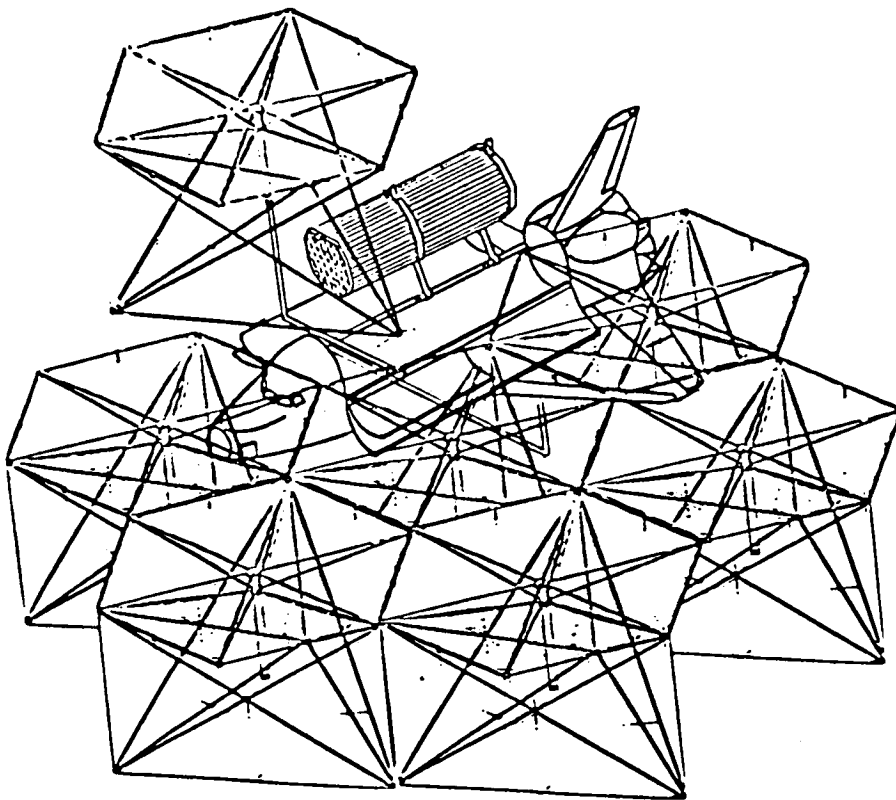
Figure 15

Figure 16 depicts assembly of a larger reflector using an articulated, extendable boom to hold the reflector for assembly. This boom is operated from inside the orbiter and is used to rotate and position the reflector to receive each module. The modules are deployed and assembled to the reflector by the Orbiter RMS. Reflector apertures up to approximately 310 meters in diameter can be assembled in one launch using this approach.
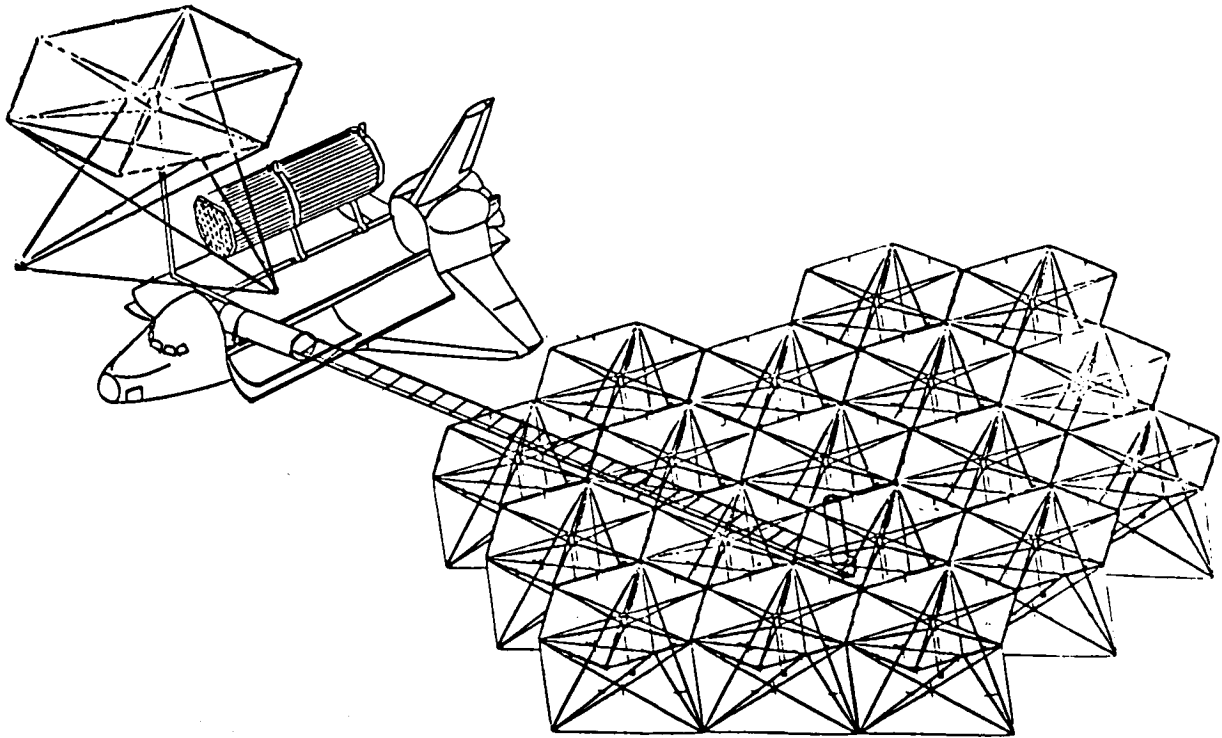
Figure 16

Large aperture antennas can be assembled only by using techniques which allow multiple resupply by the STS. One such technique is shown in Figure 17. A free flying satellite is carried to orbit with the first set of modules. After these modules are installed, the Orbiter releases the satellite and returns to Earth. Subsequent Orbiter flights rendezvous with the satellite to deliver and install additional modules.
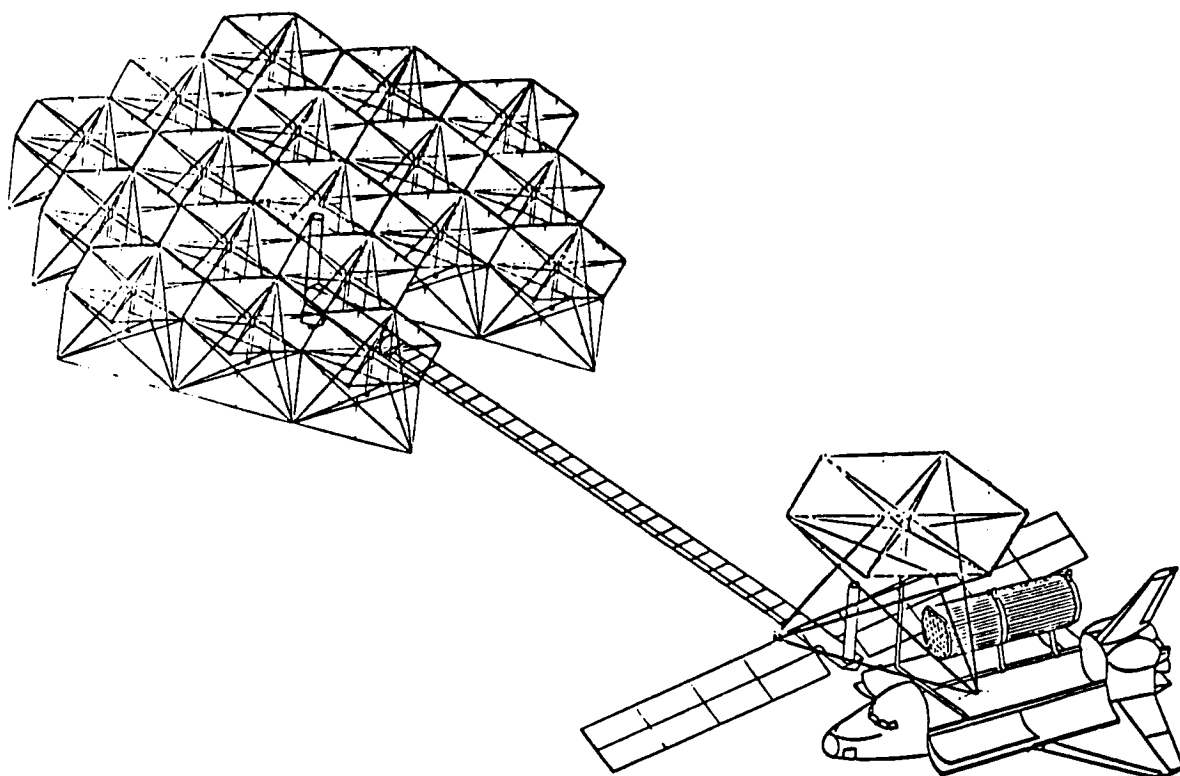
Figure 17

Figure 18 describes another reflector assembly approach for apertures requiring multiple STS launches. In the scheme, the satellite is a totally automated, self contained assembly platform. The STS ferries cargo loads of modules to orbit and delivers them to the satellite. Positioning equipment, permanently mounted on the satellite, removes the modules from their transport cannister, deploy them and attach them to the reflector.
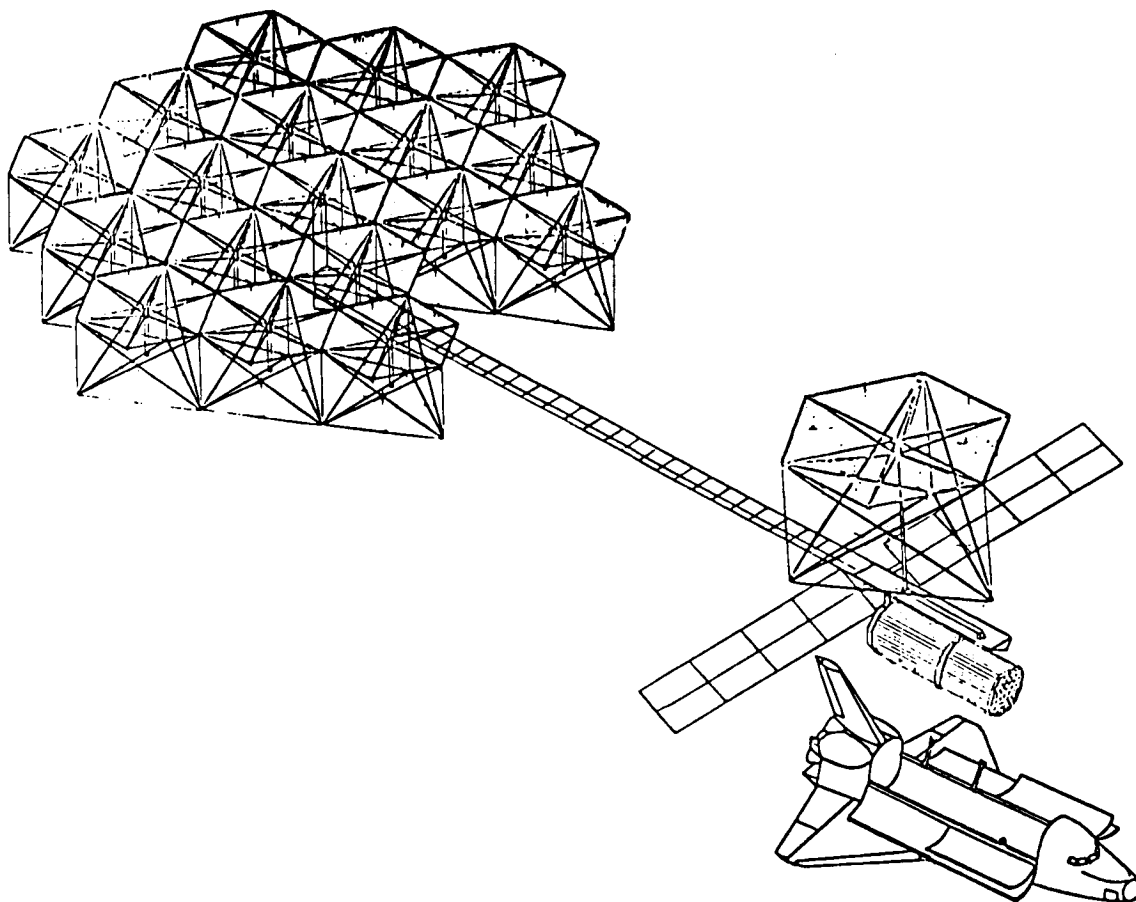
Figure 18

SIZE LIMITS OF ASSEMBLY TECHNIQUES

Figure 19 summarizes the reflector size limitations of the various assembly techniques. The approach using the RMS arms from the shuttle Orbiter is limited by the reach of the two arms, allowing a maximum size reflector of approximately 73 m diameter. The articulated boom case is limited in size by the number of modules that can be carried in the Orbiter cargo bay, with part of the volume taken up by the stowed assembly boom. The assembly satellite cases are essentially limited in size only by a number of shuttle launches devoted to the task.

- STS CONTAINED — 73 M DIAMETER

- RMS/BOOM — 310 M DIAMETER

- FORMATION SATELLITE — UNLIMITED

- AUTOMATED SATELLITE — UNLIMITED

Figure 19

STUDY CONCLUSIONS

The conclusions reached during the study are summarized in Figure 20. Modular antenna construction can provide a significant increase in reflector aperture size over deployable reflectors. The modular approach allows reflective mesh surfaces to be supported by a minimum of structure. The kinematics of the selected deployable design approach have been validated by the subscale demonstration model. Further design refinements on the module structural/joints and design optimization on intermodule joints are needed.

- MODULAR CONSTRUCTION PROVIDES A SIGNIFICANT INCREASE IN APERTURE SIZE

- APPROACH YIELDS A MINIMIZATION OF STRUCTURAL WEIGHT

- KINEMATICS ARE VALID

- JOINT AND INTER MODULE ATTACHMENT REQUIRE ADDITIONAL ACTIVITY

Figure 20

AREAS FOR FURTHER CONSIDERATION

The study concluded that work in two additional technology areas would be beneficial in developing larger reflector apertures. These study areas are summarized in Figure 21. The first area is the development of a larger deployable element, perhaps seven individual modules packaged and inter-connected to be deployed as a single unit. These large "building block" elements would then be assembled in essentially the same manner as the single modules.

The second area for research is the development of an active reflective surface, that is, surface which automatically adjusts itself on orbit to compensate for mechanical assembly tolerances and/or reflector distortions due to thermal gradient or positioning dynamic effects.

DEVELOPMENT OF A MODULAR BUILDING BLOCK

- 100 M DIAMETER BASIC ELEMENT
- MULTIPLE MODULE INTERCONNECTED
- DEPLOYED WITH SINGLE ACTUATOR
- ABILITY TO INTERCONNECT WITH OTHER 100 M ELEMENTS TO OBTAIN DESIRED SIZE

DEVELOPMENT OF ACTIVE SURFACE ELEMENT

- PRECISION HEXAGONAL SURFACE ELEMENT
- ORBITAL ATTACHMENT TO SUBSTRUCTURE
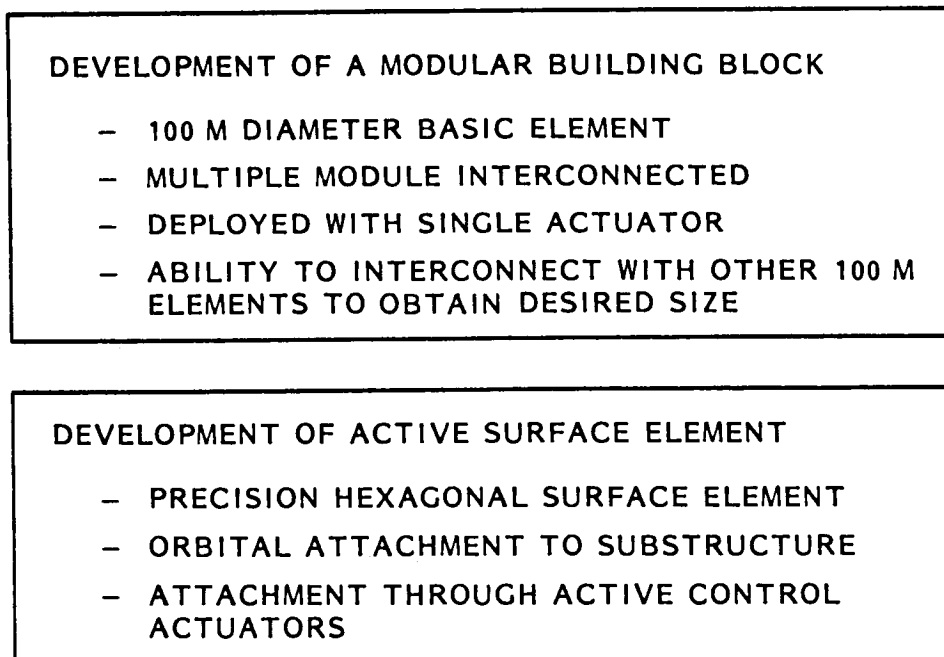- ATTACHMENT THROUGH ACTIVE CONTROL ACTUATORS

Figure 21

REFERENCE

Russel, R.; Campbell, T.; and Freeland, R.: A Technology Development Program
  for Large Space Antennas. Paper No. IAF-80A33, 31st International Aeronau-
  tical Congress of the International Astronautical Federation, Sept. 1980.

MODULAR REFLECTOR CONCEPT STUDY

D. H. Vaughan
General Dynamics Convair Division
San Diego, California

THE THREE CANDIDATE MODULAR CONCEPTS

The primary objective of this study was to investigate the feasibility of constructing large space structures, specifically a 100-meter paraboloidal R.F. reflector, by individually deploying a number of relatively small structural modules, and then joining them to form a single, large structure, in orbit.

The advantage of this approach is that feasibility of a large antenna may be demonstrated by ground and flight tests of several smaller and less costly sub-elements (modules). Thus, initial development costs are substantially reduced and a high degree of reliability can be obtained without commitment to construction of a very large system.

The three candidate structural concepts illustrated in Figure 1 are investigated:

1.   The Deployable Cell Module (DCM)

2,   The Paraboloidal Extendable Truss Antenna adapted to modular assembly (Mod-PETA)

3.   The Modular Extendable Truss Antenna (META)

DCM

Mod-PETA

META

(H)

MODULARIZED PARABOLOIDAL   (J)
ERECTABLE TRUSS ANTENNA

MODULAR ERECTABLE
TRUSS ANTENNA

DEPLOYABLE CELL MODULE
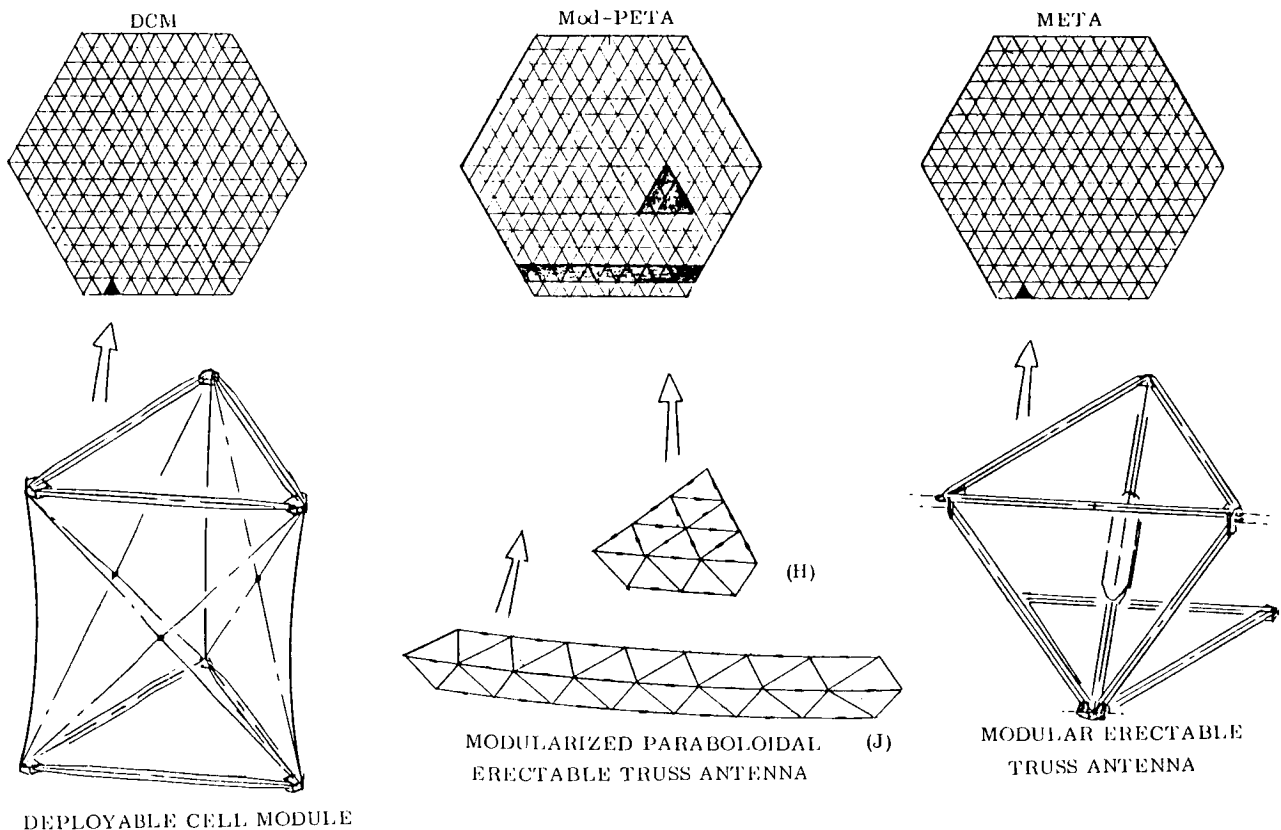
Figure 1

DCM, 100-METER, 721 MODULE REFLECTOR

The reflector configuration shown in Figure 2 is optimized for the minimum number of component structural modules.

Due to the desired paraboloidal shape of the reflector (f/d = 1.0) the component structural elements of the modules vary slightly in length. The double dimensions shown in Figures 2 and 3 indicate the limits of this variation which is generally within ± 2.06% of the median dimension. Optimization ensures that the largest module, when packaged is compatible with transverse stowage in the STS Orbiter payload bay diameter. Space is allowed for the stowage pallet, as shown in Figure 4.
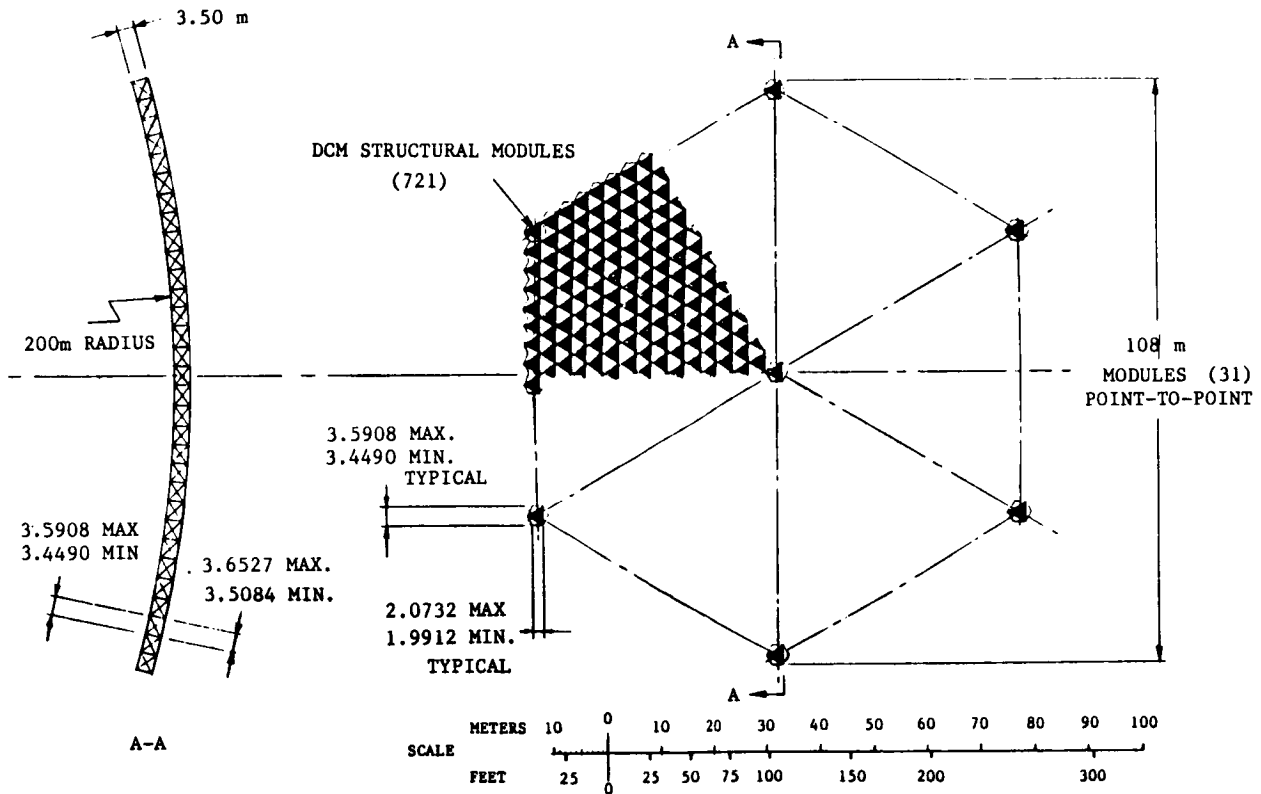
Figure 2

Figure 3 shows the typical module configuration. The two triangular frames and the six cross ties are the prime structural elements of the module. The structural performance of the total reflector is dependent on the strength and stiffness of these elements. The three prebuckled column members that separate the two triangular frames act as compression springs and provide a simple means of preloading the prime structural elements. The geometric stability of the DCM module is dependent upon this preloading, which puts the six cross ties in a state of sustained tension, and the triangular frames in sustained compression. In practice, the magnitude of this required preloading must be determined for each specific application to satisfy two critical requirements: 1) Preloading must be sufficient to ensure that the tension in the six ties remains positive for all conditions of externally applied structural loading, and 2) Preloading must not be so large as to exceed allowable column strength of the triangular frame elements (tubes) under conditions of additive applied structural loading.

Figure 3

DCM - STOWAGE OF PACKAGED MODULES
IN ORBITER PAYLOAD BAY

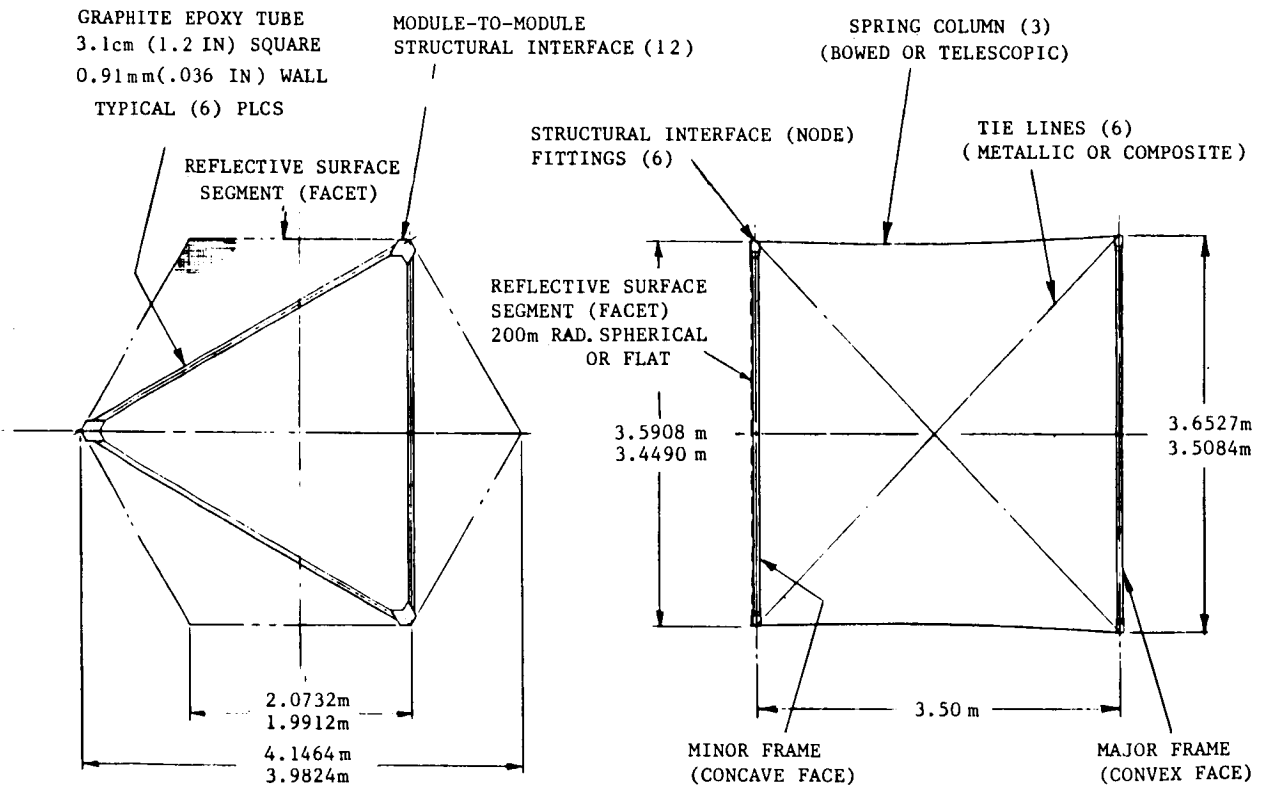The module configuration shown above in Figure 3 permits it to be mechanically folded to occupy a much lesser volume. The two, rigid, triangular frames maintain their size and shape, but when one frame is rotated, in plane, relative to the other, the three intermediate columns lean over through 90° drawing the two frames together. The overall height of the module thus shrinks from its deployed height of 3.5 meters to a packaged height of only 6.2 centimeters. This packaging capability permits 270 such modules to be stacked in a 16.7 meter increment (90%) of the Orbiter payload bay. As shown in Figure 4, each module is supported within the cradle by three "shoes" one at the bottom center line and one more on either side just above the horizontal centerline. The shoes are keyed into troughs that run the full length of the cradle, and individually engage an endless belt. In orbit the modules are dispensed one at a time from the front end of the cradle. To dispense a module the three endless belts are advanced, simultaneously, a distance equal to the overall thickness of one module. This causes the entire module stack to advance a similar distance resulting in the release of the dispensed module.
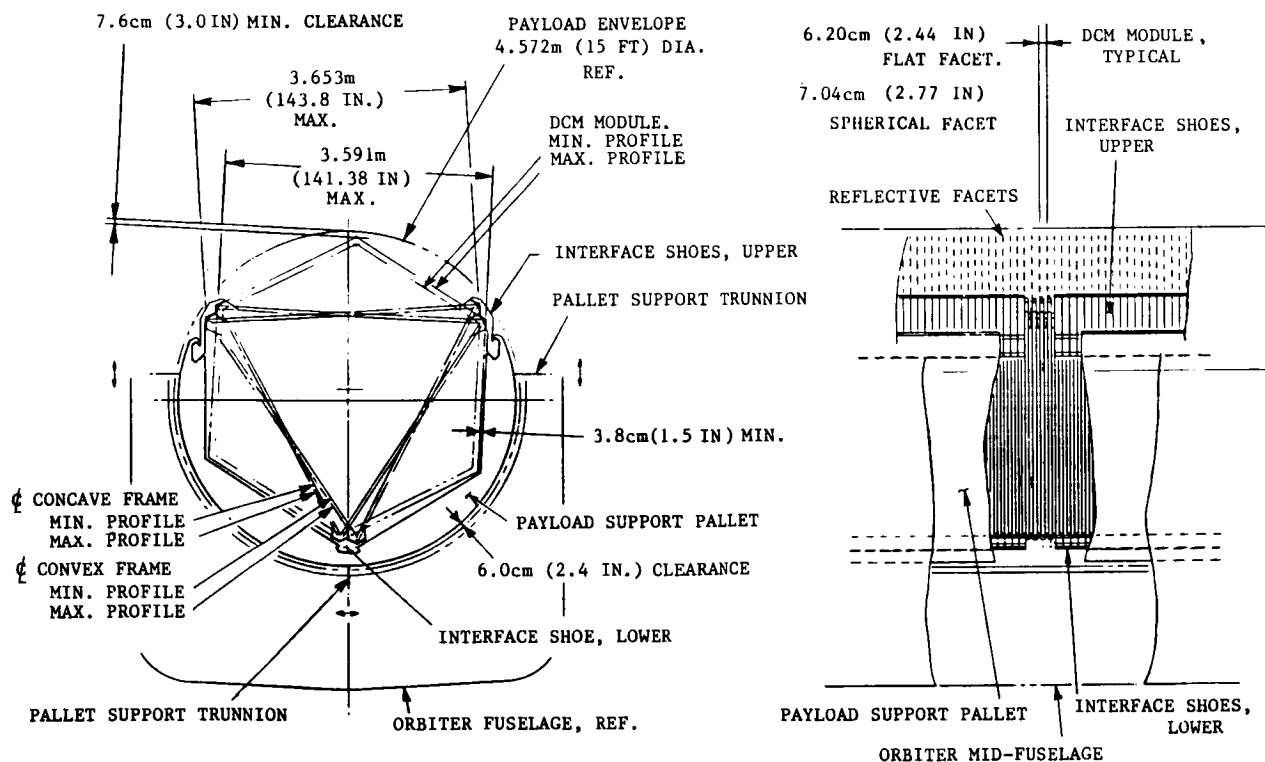

Figure 4

DCM – PAYLOAD SUPPORT PALLET (PSP) IS ELEVATED
AND SUPPORTED BY TWO ARTICULATED ARMS

The Payload Support Pallet (PSP), containing the packaged structural modules and all handling and assembly support equipment is removed as a unit from the payload bay. It is supported in an attitude and at a distance from the Orbiter that will enable observation and monitoring from the Orbiter crew compartment and that will incur minimum risk to the Orbiter.

The first stage of the in-orbit deployment sequence is release of the PSP tiedown latches and elevation of the PSP from the Orbiter bay by means of two articulating support arms (Figure 5). These arms may subsequently be locked to establish a rigid relationship between the PSP and the Orbiter. However, in order to prevent excessive loading at these support interfaces as the mass moment of the evolving structure becomes large, it may be necessary to provide a sprung (non-rigid) interface that would accommodate oscillatory movements yet maintain the mean relationship at nominal. A superimposed effect would be correction of orbital tumbling by means of the Orbiter attitude control systems.
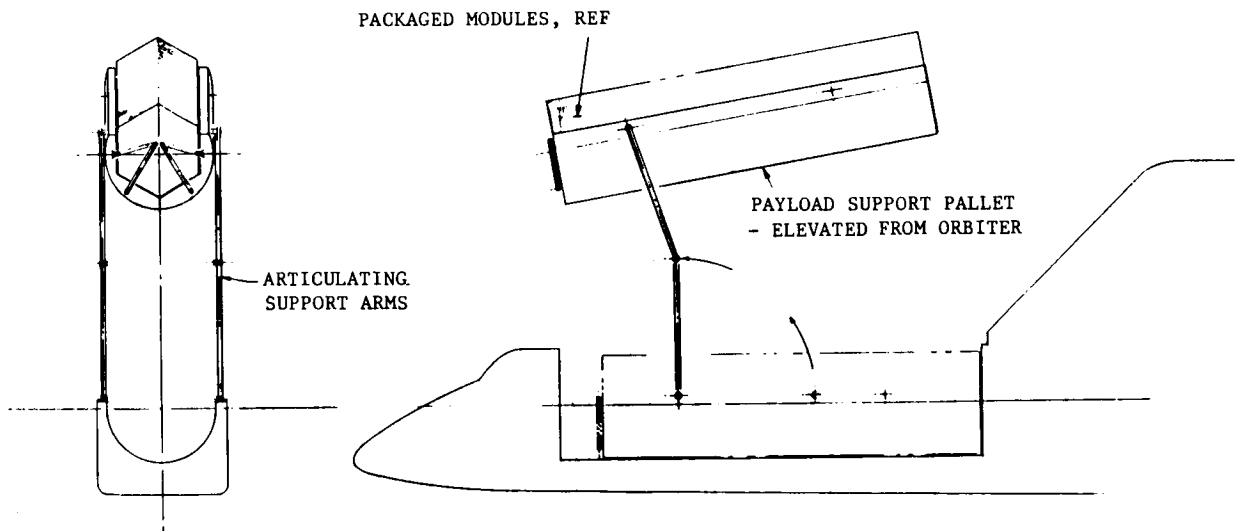
PACKAGED MODULES, REF

PAYLOAD SUPPORT PALLET
- ELEVATED FROM ORBITER

ARTICULATING.
SUPPORT ARMS

Figure 5

DCM – EFFECTOR HEADS ON THE TWO HANDLING AND JOINING ARMS (HJA)
ENGAGE, ALIGN AND JOIN MODULE NODE FITTINGS BOTH FRONT AND BACK

The individual modules are advanced to the extreme end of the PSP, as described above, and driven into deployed configuration by applying moments to the three intermediate columns.

The two HJA then engage the node fittings of the modules and position the modules side-by-side.

When the required alignment is achieved the Link Trigger Unit (LTU) rotates down to engage the node fittings and to actuate the link trigger mechanism, which effects the mechanical joining of the structural interface. The exact logic of this function is not defined but is visualized either as a latching link, built into one node fitting, which extends across the structural interface to engage the mating node fitting, or as a separate part ejected from the LTU to snap over the anchor pins in the node fittings. For the latter approach the usual undesirability of loose parts may be offset by the potential simplicity of the structural features involved.
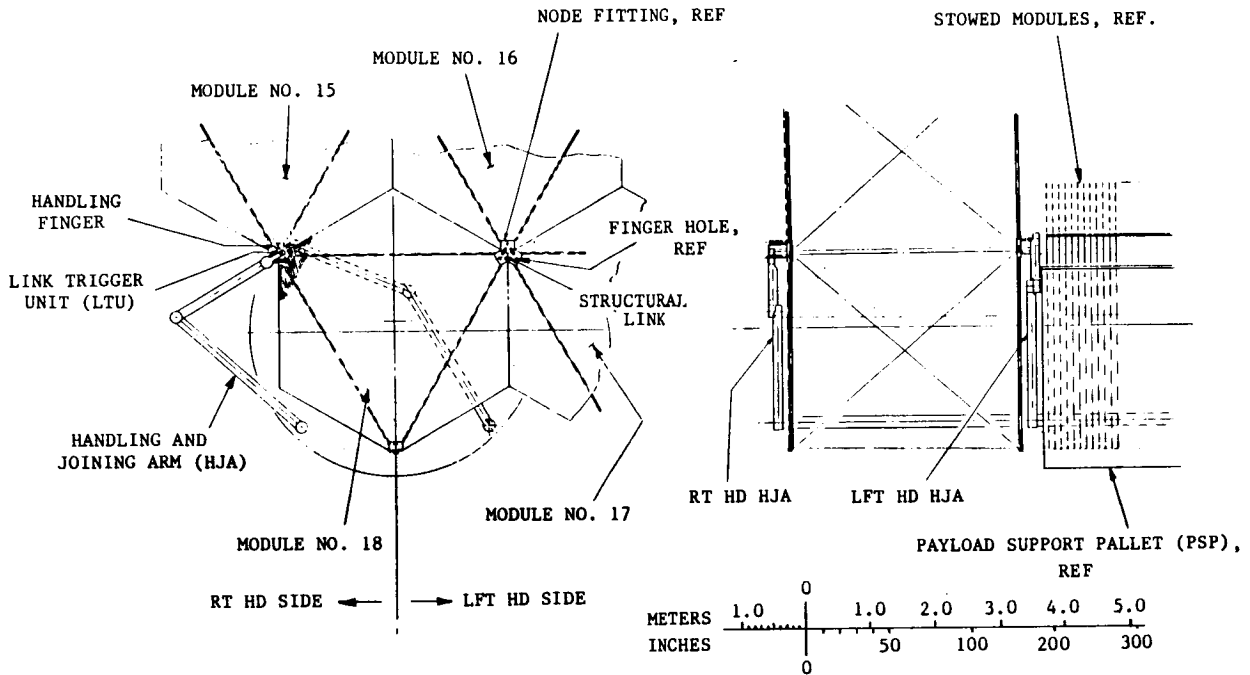
Figure 6

DCM - THE BUILD-UP PROCEEDS IN A ZIG-ZAG MANNER TO LAY DOWN
A TOTAL OF 721 MODULES IN 31 ROWS

By means of a complex sequence of motions the HJA manipulators integrate each subsequently deployed module into the evolving structure.

The total reflector structure is built-up, thus, row by row, following a zig-zag course from top to bottom.
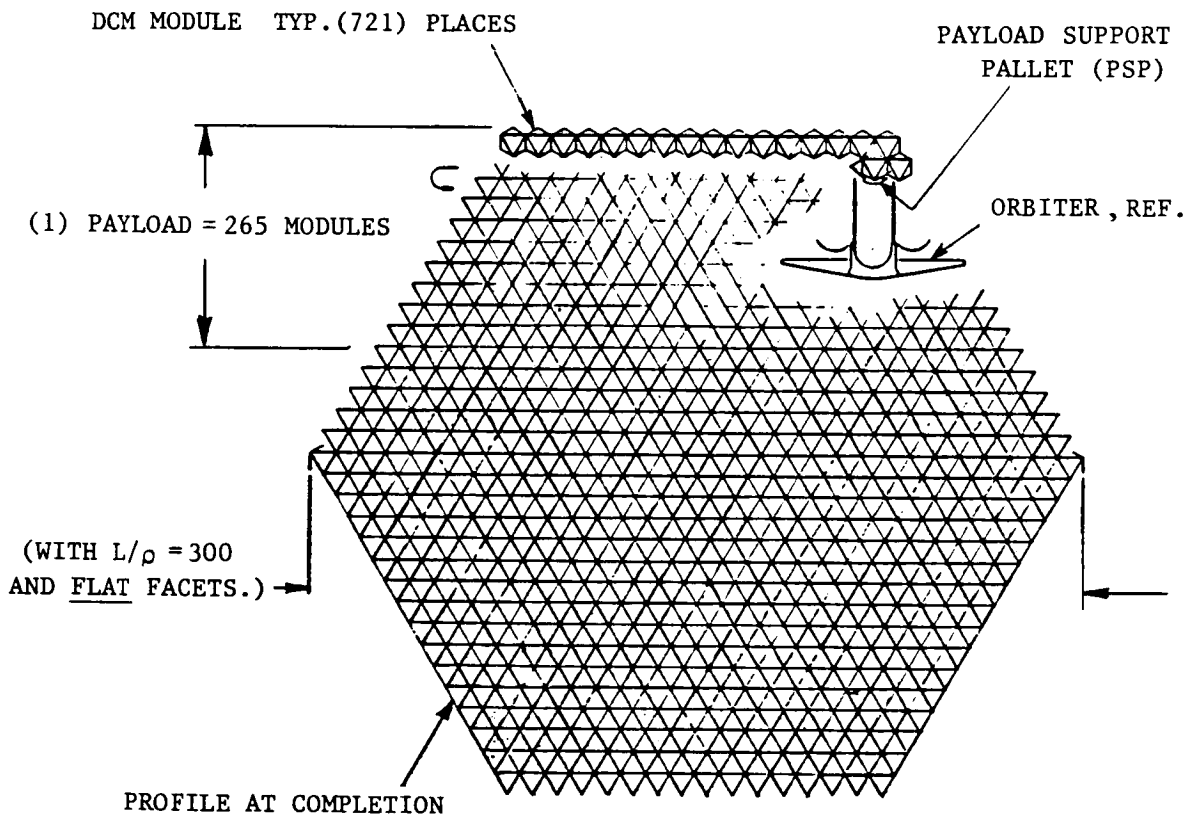
Figure 7

MOD PETA (TYPE "H") - A MODULARIZED
24 BAY "PETA" RELFECTOR CONSISTING OF 96 MODULES

The concept of deploying several such PETA structures in space, and subsequently joining them to produce a single larger structure has potential and is presented in this study as an alternative to the DCM approach.

The 100-meter, modularized PETA reflector shown in Figure 8 consists of 96 individual, triangular structural modules joined at their edges to form a single, integrated structure. In order to achieve matched geometry at the structural interfaces modules are alternately "male" and "female".
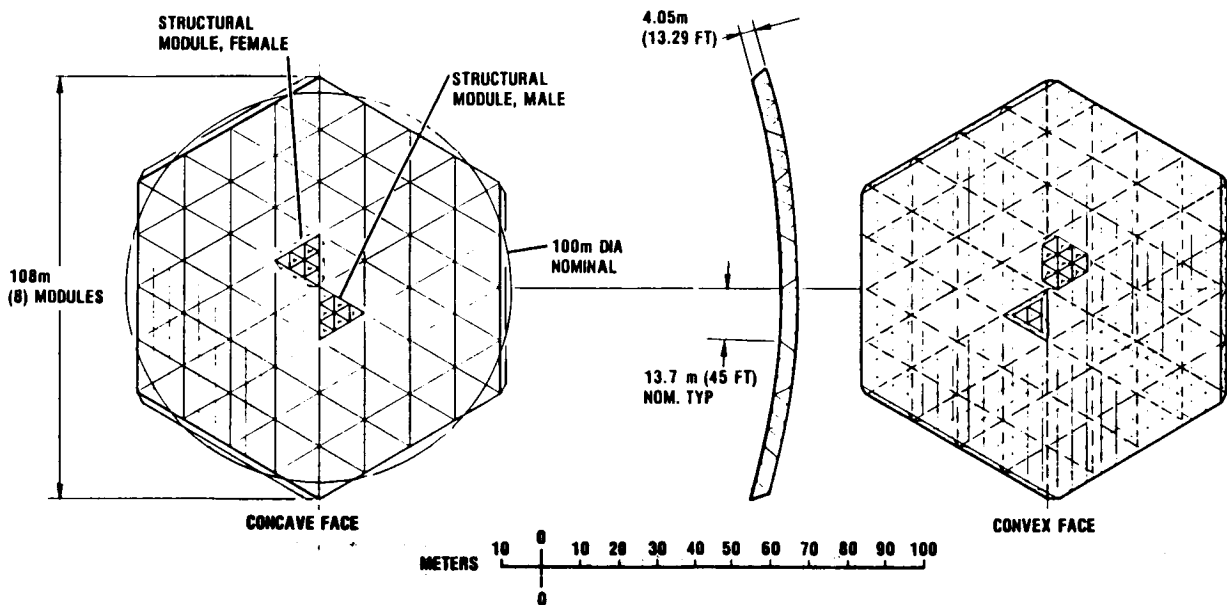
Figure 8

MOD PETA, THE ELEMENTAL TETRAHEDRAL
STRUCTURE OF SIX STRUTS

The structural system of the PETA design is, in essence, a mechanical
assembly of tubular structural members joined at their ends and arranged to
form a multiplicity of tetrahedrons. The pivotal capability of the end joints
and the mid-span hinges that are provided in certain members enable the structure
to be mechanically folded into a high density package in which all members lie
in parallel orientation (Figure 9). The mid-span hinges may be spring loaded
so that when circumferential restraints are released from the package, the
structure automatically unfolds radially until it locks-up its fully deployed
configuration.

$$\frac{\text{NODE SEPARATION DEPLOYED}}{\text{NODE SEPARATION PACKED}} = \text{DEPLOYMENT RATIO}$$
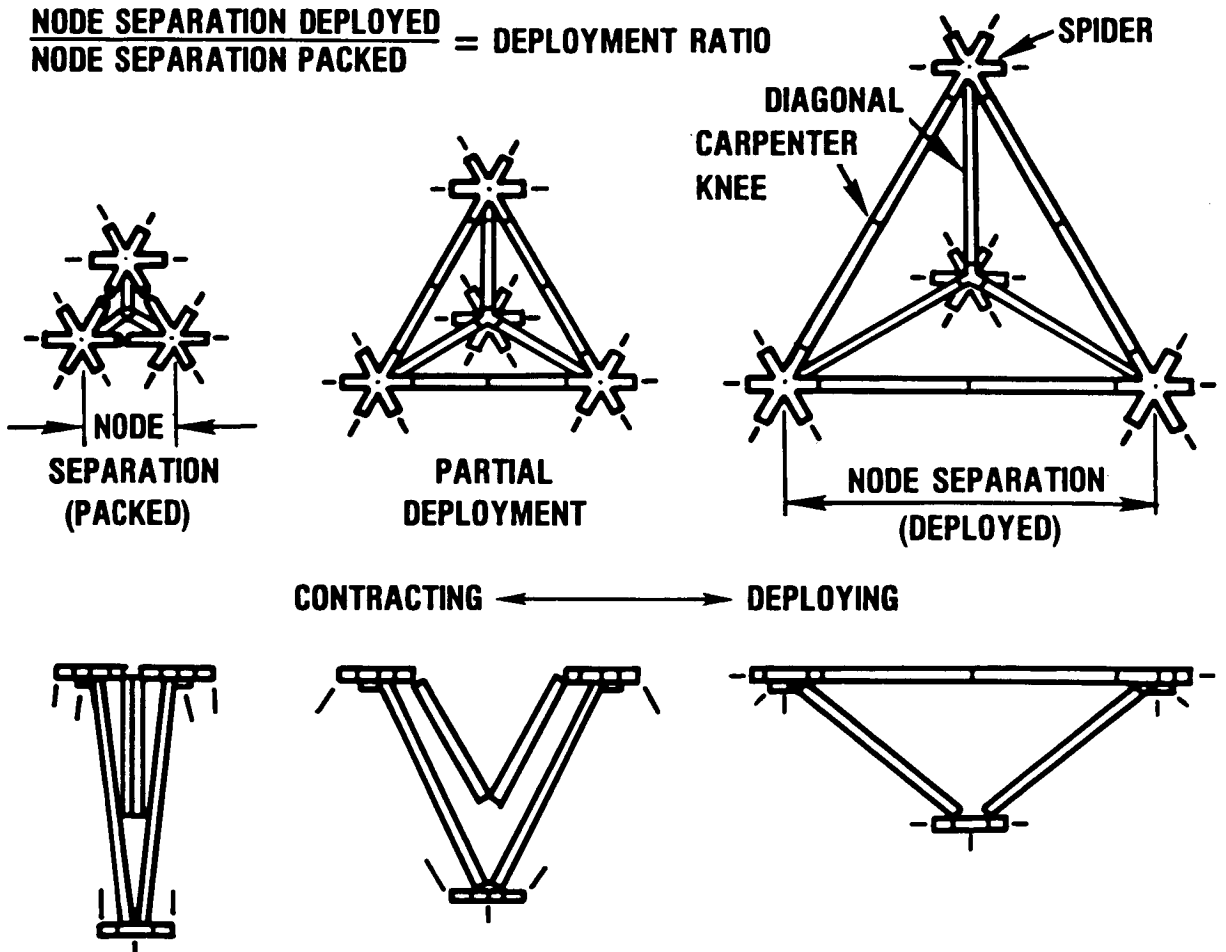
Figure 9

MOD PETA (H), MODULE STRUCTURAL DETAILS

The typical module is triangular and encompasses three bays of structure.

The concave (meshed) face of all modules is identical, but "female" modules are larger overall than the typical male module, shown below, since their side faces flare outward rather than inward.

13.7m (45 FT)
4.62m(182 IN) NOMINAL
4.71m(186 IN) NOMINAL
SURFACE STRUT CONVEX FACE TYPICAL (9) PLACES
DIAGONAL STRUT TYPICAL (18) PLACES
3.8cm (1.5 IN) SQUARE TUBE, 0.91mm (.036 IN) WALL, TYPICAL
SURFACE STRUT, CONCAVE FACE TYPICAL (18) PLACES
4.05m (13.3 FT)

Figure 10

MOD PETA (H), THE PACKAGED MODULE

The modules typically fold to approximately one fifteeth their deployed size when packaged for stowing in the Orbiter payload bay. The hexagonal node fittings meet to form solid end faces to the package; the folded "surface" struts rest securely between the parallel "core" struts, and the reflective mesh surface collects in a bundle atop the upper node fitting standoffs.

Figure 11

MOD PETA (H), STOWAGE REQUIREMENTS ARE PROPORTIONAL
TO SELECTED STRUCTURAL DEPTH

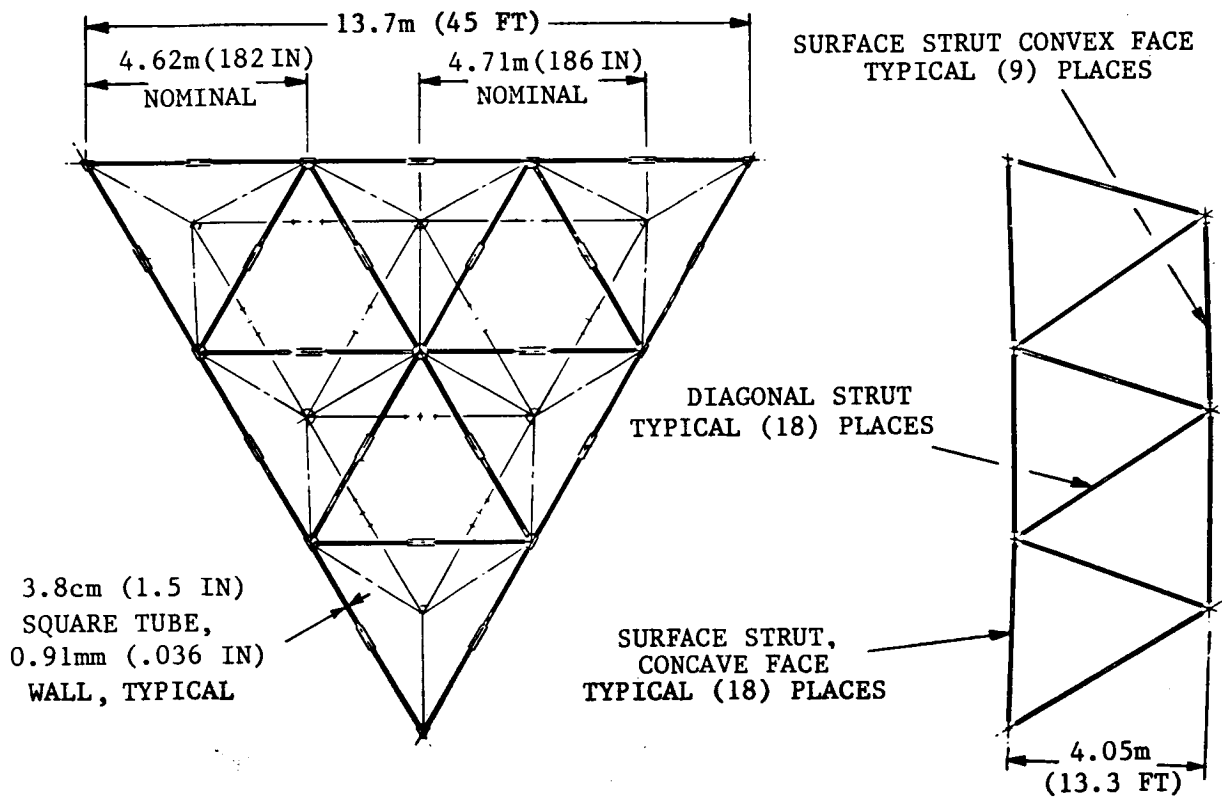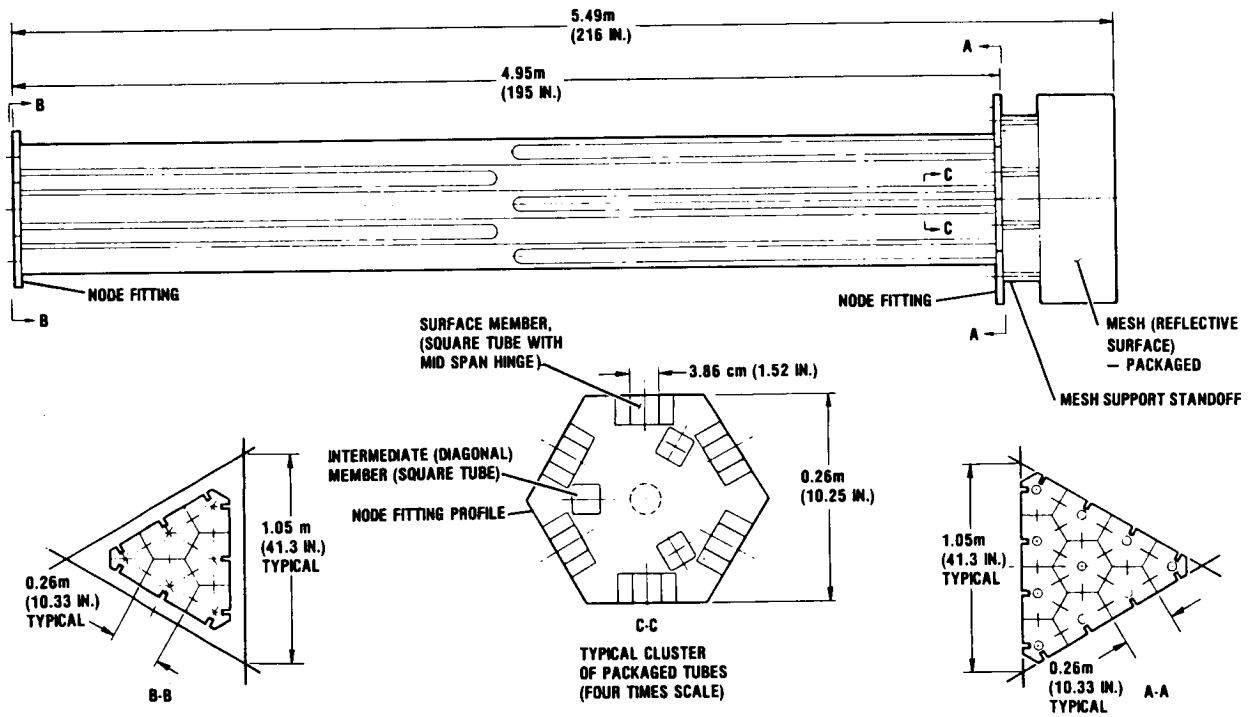As with the DCM concept studies, it is assumed that 10% of the Orbiter payload bay length is reserved for support equipment, leaving 16.46m (54 ft.) available for stowage of the packaged reflector. Thus, the PETA reflector structure, described above stows in clusters, with 24 modules per cluster. This arrangement permits three clusters to be accommodated within a single payload. A second flight is required for the fourth cluster. Total stowage space required, therefore, is equivalent to 1.3 payload bays.

It is conceivable that all four clusters can be accommodated in one payload (Study Case "D", Figure 12), by shortening each packaged module to 4.1m (162 inches). While such shortening is feasible, it must be considered that this results in corresponding reduction of deployed structural depth, structural stability (dynamic and thermal), surface shape accuracy and, therefore, potential R.F. capability.

Figure 12 presents three typical cases, Study Cases "D", "E", and "F" to illustrate the relationship between payload volume (length) and deployed structural depth, for a 100-meter structure. It will be noted that reducing structural depth also results in a significant increase in component part count due to corresponding increase in the number of structural bays.

It is seen that Orbiter flights required are 1, 2, and 4, respectively.

STUDY CASE 'D', ORBITER PAYLOADS REQUIRED (1)

STUDY CASE 'E', ORBITER PAYLOADS REQUIRED (≥2)

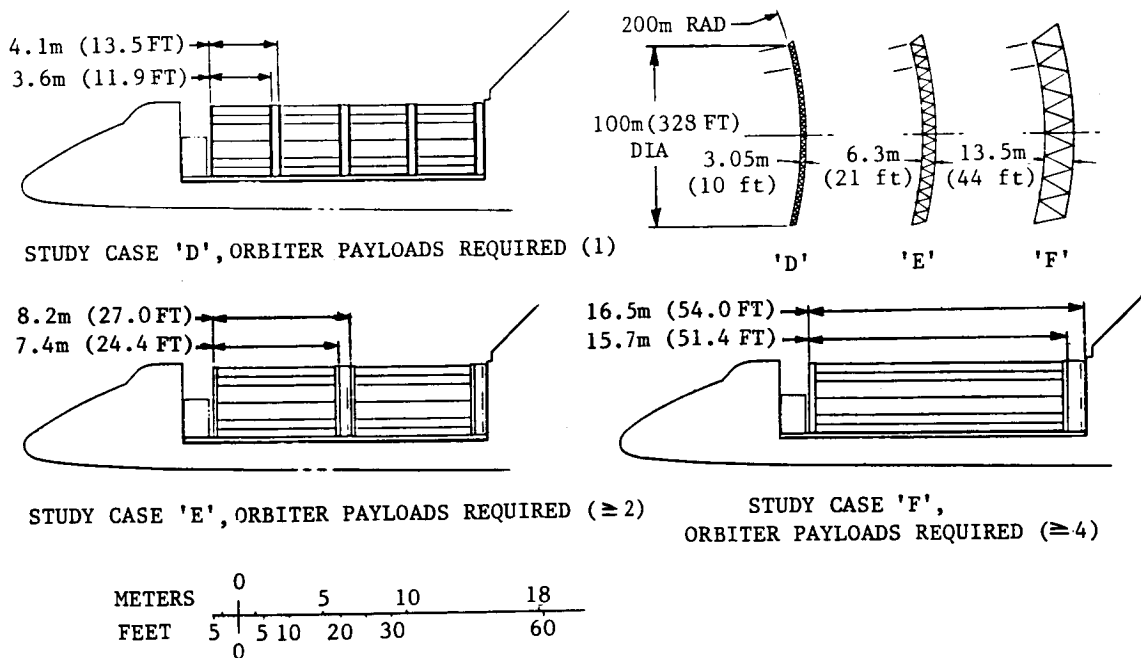STUDY CASE 'F', ORBITER PAYLOADS REQUIRED (≥4)

Figure 12

MOD PETA (J), AN ALTERNATIVE MODULE CONFIGURATION

The essential difference in this approach is that the triangular tetrahedral truss modules are replaced by high aspect ratio (beam) tetrahedral truss modules of minimum width and maximum length. The structure folds and deploys by the same basic mechanism described above in Figure 9.
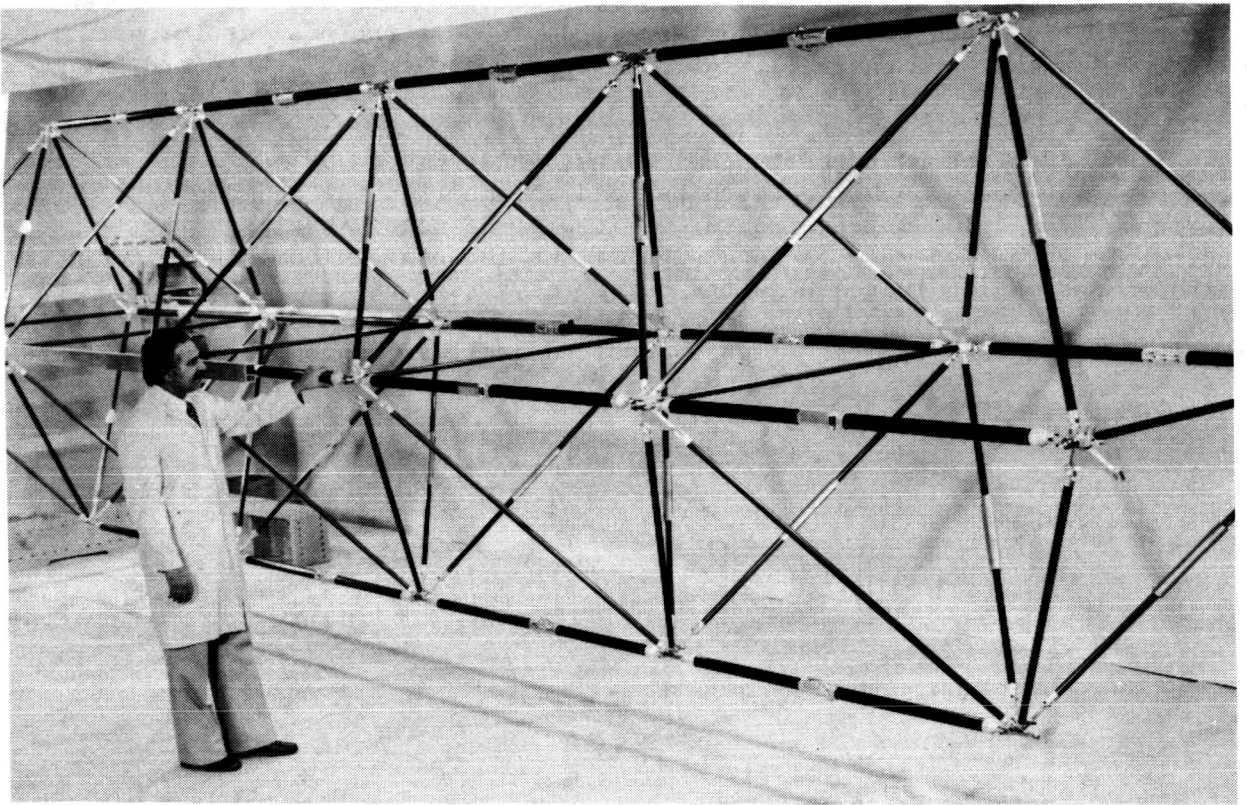
Figure 13

MOD PETA (J), CONTROLLED DEPLOYMENT OF BEAM MODULES

The mechanical sequence of deployment of the beam module is shown below. Figure 14a shows the typical "flatpack" with all tubular elements lying in parallel orientation. In Figure 14b, both the upper and lower layers of the structure transition vertically to form a diamond section shape. In Figure 14c, deployment occurs in the longitudinal direction as the structure extends bay-by-bay forming a series of tetrahedrons. In Figure 14d, the fully deployed beam (module) assumes its fully triangulated truss configuration.
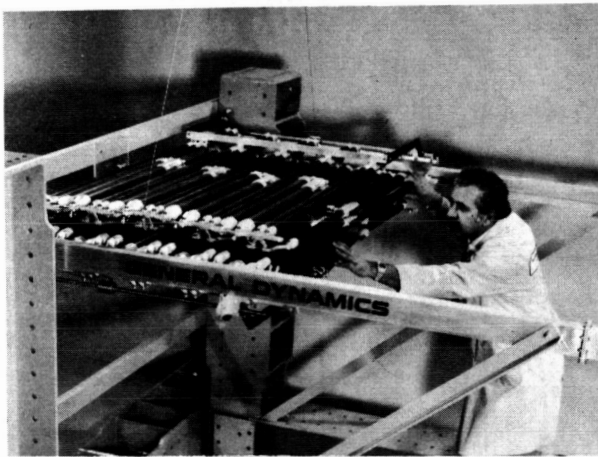
a
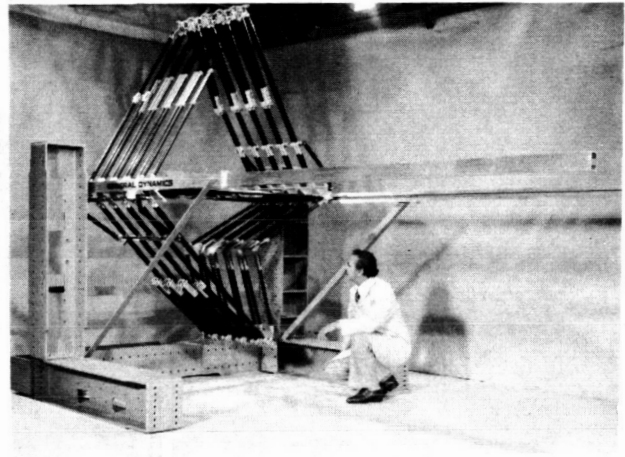
b
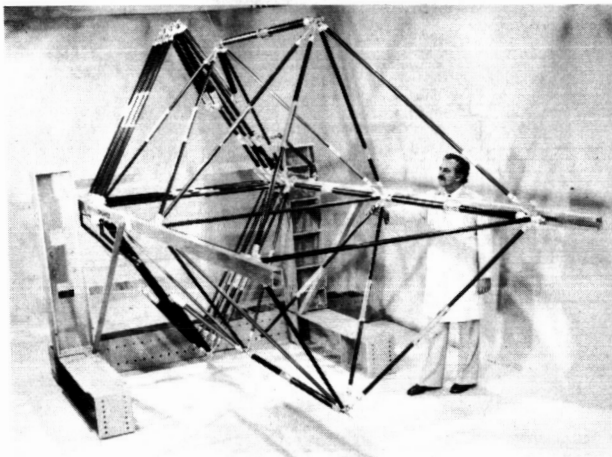
c
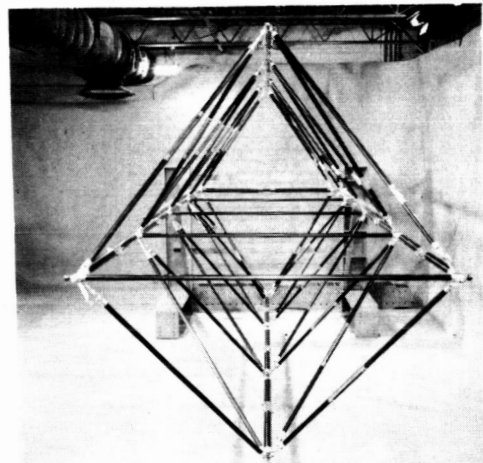
d

Figure 14

MOD PETA (J), HANDLING AND JOINING MECHANISMS (HJM) REMOVE MODULE
"FLAT-PACKS" FROM ORBITER AND HOLD THEM ERECT FOR DEPLOYMENT

For launch in the Orbiter the "flat packs" are stowed in two stacks of twelve modules each. Each stack is provided with a Handling and Joining Mechanism (HJM). These remove the modules from the payload bay one at a time, control deployment, bring the modules together, and join them.

In Figure 15, the initial stages of erection are shown. The forward HJM is seen to have engaged the second module preparatory to removing it from the payload bay. The aft HJM has already removed the first module and has positioned it ready for deployment. In the right-hand view, this module is shown supported vertically on six finger probes.
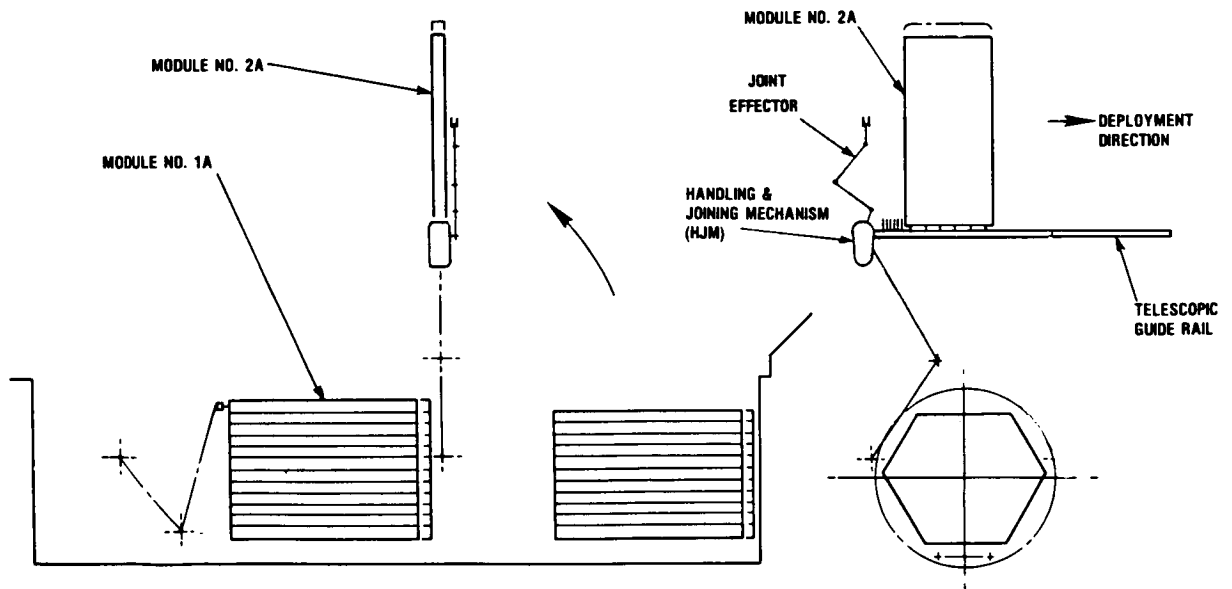
Figure 15

MOD PETA (J), MODULE DEPLOYS IN TWO PHASES, FIRST OPENING TO
A DIAMOND SECTION, THEN LONGITUDINALLY, BAY-BY-BAY

Figure 16 illustrates the first increment of deployment of the module.
This step repeats, bay-by-bay until the fully deployed module extends in canti-
lever fashion, from the guide rail. The left-hand view of Figure 16 shows the
deployed section shape of the module.

The aft HJM differs from the forward HJM in that it is provided with a
joint effector subsystem which is capable of reaching both the lower and the
upper node fittings of the modules and of performing the structural joining of
the mating node fittings, as shown in Figures 17 and 18.
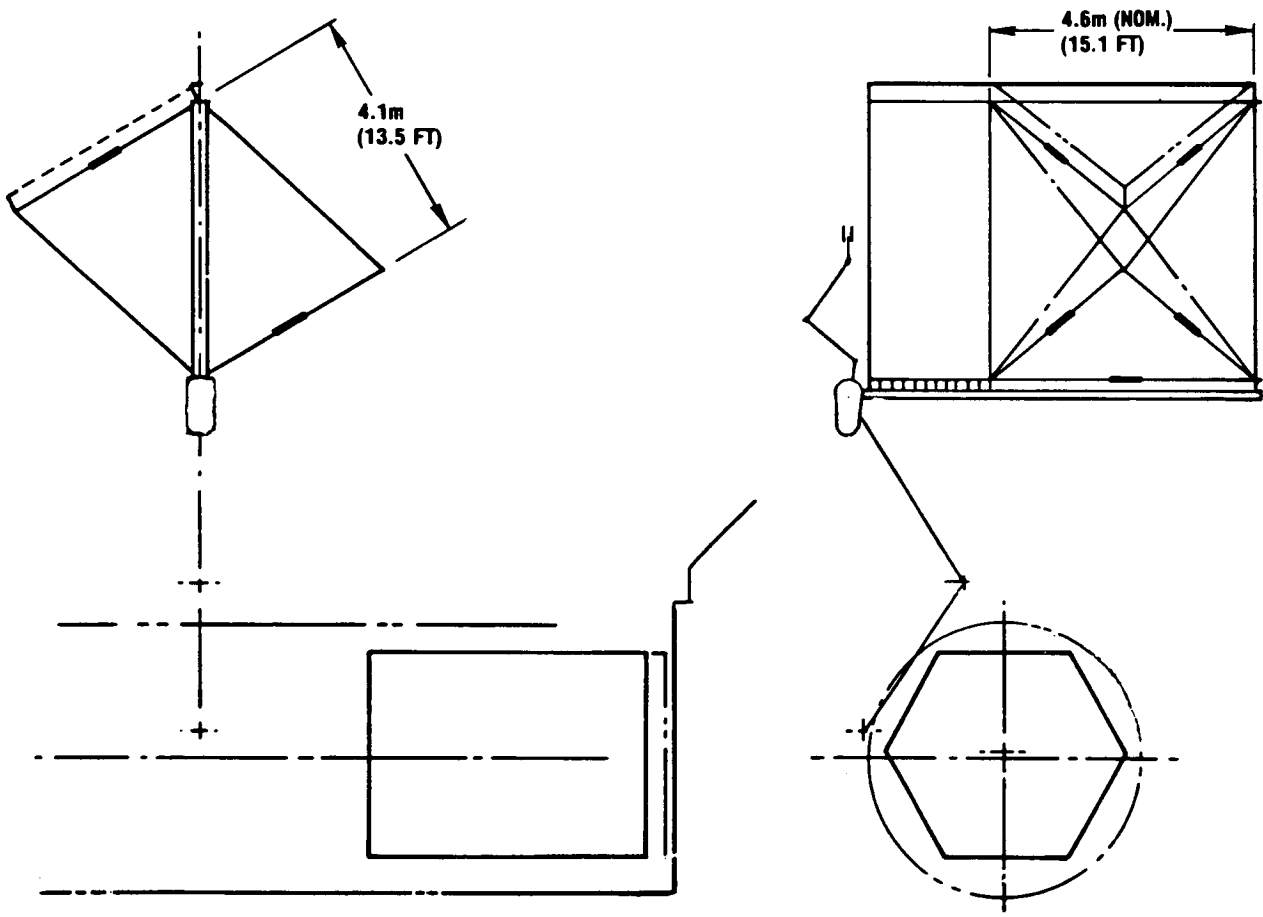
Figure 16

MOD PETA (J), INITIAL TWO MODULES DEPLOY INDIVIDUALLY, THEN JOIN

Two modules are fully deployed, one from each HJM, which then moves them into side-by-side contact for structural integration.

Joining of all node fittings along the interface is accomplished by longitudinally translating the modules across the payload bay by hand-over-hand operation of the two HJM's. As the integrated modules pass over the pay-load bay the joint effector reaches upward, into the structure, and effects the locking of the mating node fittings.
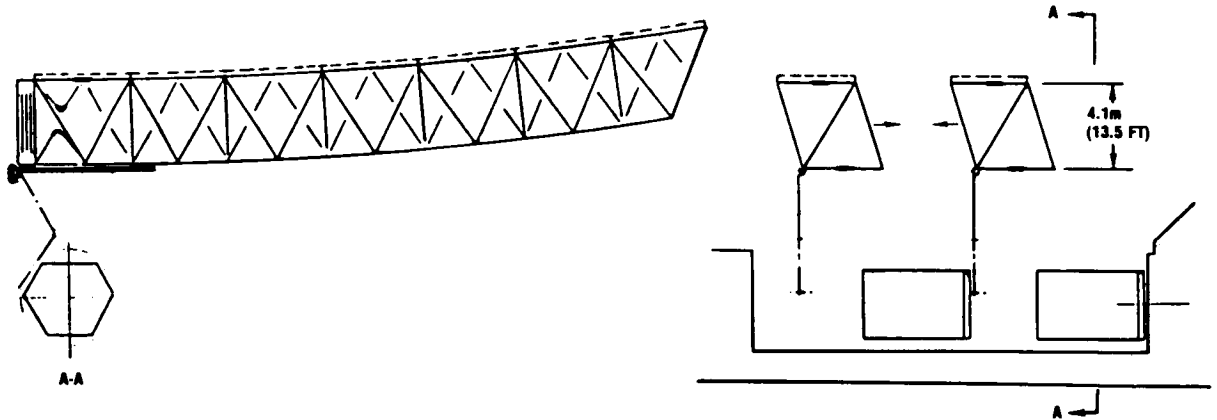
Figure 17

MOD PETA (J), HALF REFLECTOR IS ASSEMBLED BY DEPLOYING AND
JOINING THE FIRST PAYLOAD OF 24 MODULES

The third module is deployed in the opposite direction to the first two
modules and the construction thus proceeds in a zig-zag mode, as indicated in
Figure 18 where the reflector is shown a little more than quarter complete.
Thirteen modules have been deployed and joined, and the fourteenth is deployed
and about to be joined.

When twenty-four modules have been joined, the reflector is half complete
and the initial payload is exhausted.
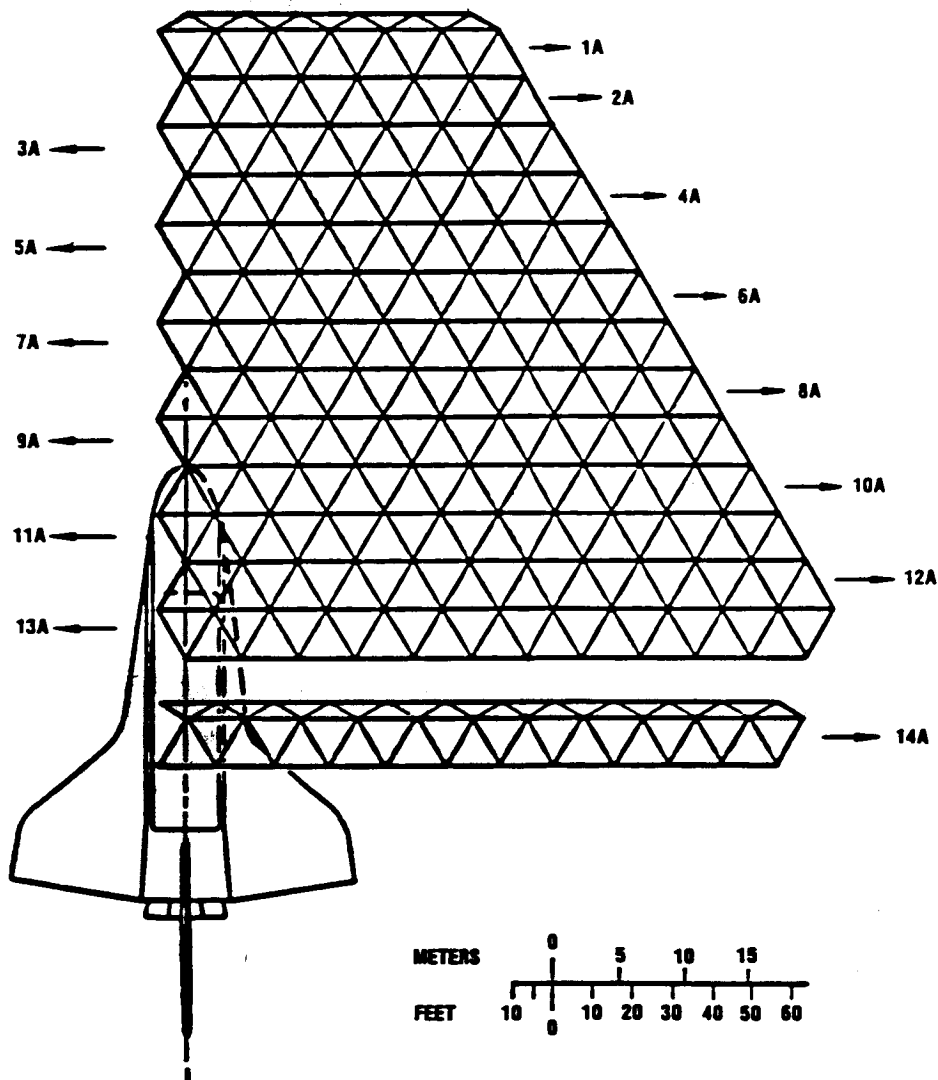
Figure 18

MOD PETA, COMPLETION OF A 100-METER PARABOLOIDAL ANTENNA

The second flight produces the second half of the structure. Integration of the two halves is a final function performed by the second flight, or integration can be performed concurrent with assembly of the second half.
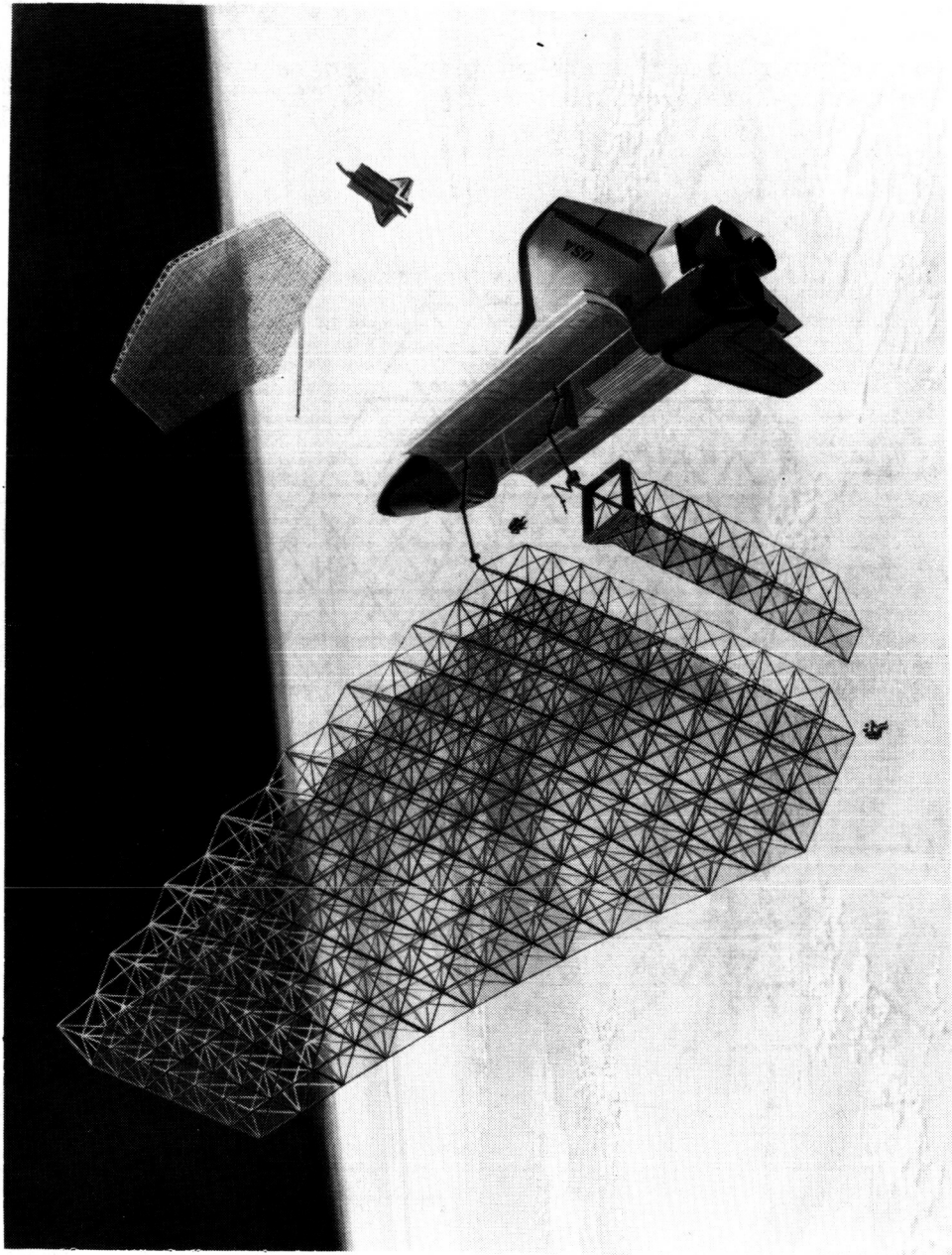
Figure 19

THE MOD PETA CONCEPT PROVIDES LARGE
STRUCTURES OF OUTSTANDING PERFORMANCE

The mode of modularization (H or J) does not significantly affect the structural characteristics of the completed Mod-PETA structure, and the estimated data presented in Figure 20 can be considered generally typical for large, hexagonal, modular Mod-PETA reflectors and platforms.

As a reflector, the structural thermal stability is more than adequate for operation at 1 GHz, but marginal at 15 GHz.
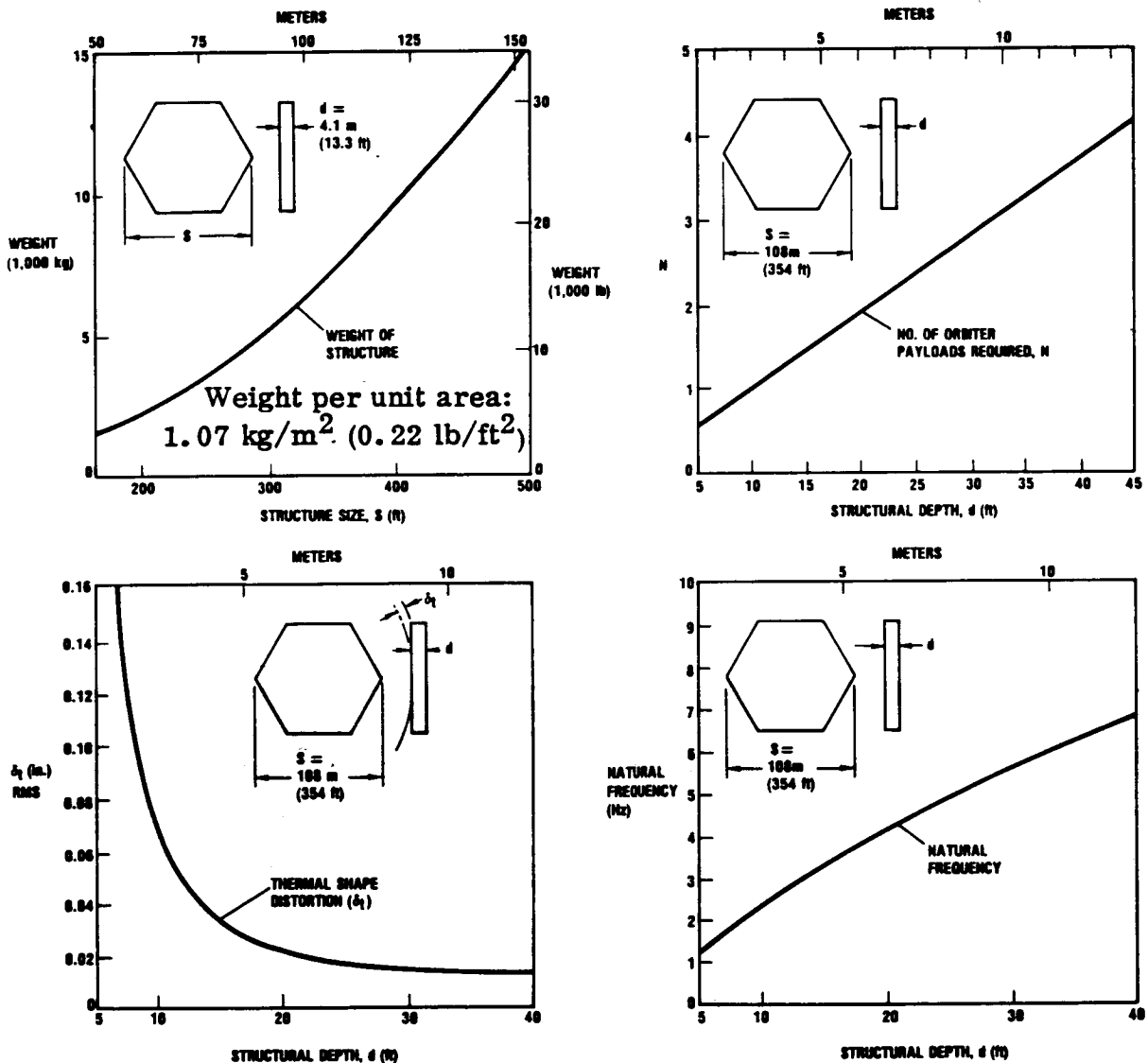
Figure 20

MOD PETA, ACHIEVABLE FIGURE ACCURACY PERMITS OPERATION AT 15 GHz

High structural shape, accuracy and stability permit operational use at high R.F. frequencies. Shape distortions result from designed approximations of the ideal reflector figure, thermal strains due to varying temperature, changes in applied structural loads, and deviations from nominal shape, during space erection, due to fit tolerances (i.e., repeatability). Initial or corrected figure accuracy is limited by the achievable accuracy of measuring the figure and effecting corrections.

Figure 21 presents the figure error budget, the RMS value of the error, and equates this to R.F. capability.

Item	δ mm (inch) RMS
1. Geometry (design)	
— Common flat facets	1.14 (0.045)
2. Thermal Strains	
— Structure	1.12 (0.044)
— Mesh system (10%)	0.11 (0.004)
3. Static Loading Strains	—
4. Measurement Accuracy	0.03 (0.001)
5. Adjustment Accuracy	0.25 (0.01)
6. Repeatability	0.76 (0.03)
Total RSS (half path error)	1.79 (0.070)
RSS correction (10%)	0.18 (0.007)
Adjusted total RSS (δ)	1.61 (0.063)
	= λ/187 at 1 GHz
	= λ/12.5 at 15 GHz

Figure 21

META, MODULAR ERECTABLE TRUSS ANTENNA

The META concept possesses a combination of the key characteristics of both the DCM and the PETA concepts. Individual modules are very similar to DCM modules in their general size and shape, in their manner of deployment, and in their reflective surface installations. The essential difference is found in the relative arrangement of their component structural elements. In META the structural component arrangement is directly related to the tetrahedral geometry of the PETA. A reflector structure assembled from META modules produces an overall structure geometry basically idential to PETA structure.

As with the DCM concept, the META modularization approach does not result in structural duplication. META has a lower part count than the DCM (6489 tubes versus 10,815 tubes and ties).

The principal disadvantages of the concept are its lower packaging density, requiring 3.9 Orbiter flights to construct the full 100-meter reflector, its high module count (721), and its relatively small structural depth, which is limited to 3.1 meters compared to 3.5 meters for the DCM.

Although mechanical movements involved in deployment of the typical META module are different from those for deploying the DCM, the overall time required to deploy/assemble the full 100-meter META structure is estimated to be similar, i.e., 240 hours, approximately.
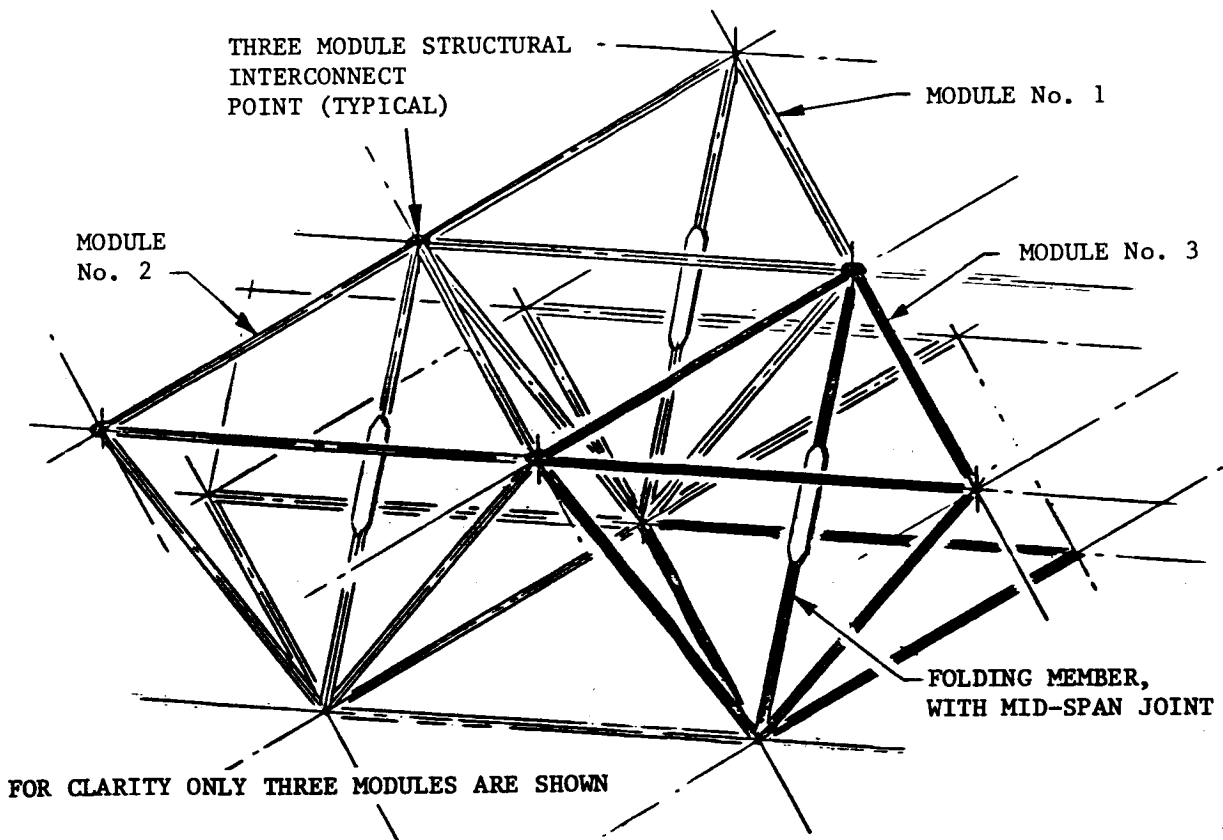

THREE MODULE STRUCTURAL INTERCONNECT POINT (TYPICAL)

MODULE No. 1

MODULE No. 2

MODULE No. 3

FOLDING MEMBER, WITH MID-SPAN JOINT

FOR CLARITY ONLY THREE MODULES ARE SHOWN

Figure 22

CONCEPT ANALYSIS OUTPUT DATA

Figure 23 presents analytical output including LASS computer program output data.

The total number of individual tubular elements in the Mod-PETA (Study Case H) is 5,440 versus 10,815 tubes and ties in the DCM. The PETA H and J require 1.3 and 2.0 Orbiter flights, respectively, versus 2.6 for the DCM. Total number of in-space structural connections to be effected for PETA (H and J) is approximately 2,200 and 900, respectively, versus 8,460 for the DCM. The total weight of PETA Study Case H is 8,125 kg (17,916 lb), versus 9,399 kg (20,725 lb) for the DCM.

Output Data	Concept Study Case			
	DCM (C)	PETA (H)	PETA (J)	META
Orbiter payloads required	2.6	1.3	2.0	3.9
Total reflector weight, kg (lb)	9399 (20,725)	8125 (17,916)	8183 (18,043)	7515 (16,573)
Structural depth, m (ft)	3.5 (11.5)	4.05 (13.3)	4.05 (13.3)	3.10 (10.17)
Fundamental frequency (f_1), hertz	1.78	2.20	2.20	1.80
Surface accuracy, RMS, mm (in.)	2.83 (0.11)	1.61 (0.063)	1.61 (0.063)	2.92 (0.114)
Surface accuracy at 1 GHz	$\lambda/107.4$	$\lambda/187$	$\lambda/187$	$\lambda/103.6$
Surface accuracy at 15 GHz	$\lambda/7.2$	$\lambda/12.5$	$\lambda/12.5$	$\lambda/6.9$
Length of packaged module, m (ft)	0.07 (0.23)	5.49 (18.0)	5.49 (18.0)	0.1 (0.34)
Surface strut column strength, newtons (lb)	2131 (480)	2895 (652)	2895 (652)	2131 (480)
Average 'concave' strut length, m (ft)	3.62 (11.8)	4.62 (15.2)	4.62 (15.2)	3.52 (11.50)
Average 'convex' strut length, m (ft)	3.68 (12.1)	4.71 (15.5)	4.71 (15.5)	3.58 (11.55)
Average 'diagonal' strut length, m (ft)	5.05 (16.6)	4.84 (15.8)	4.84 (15.8)	3.8 (12.5)
Number of surface struts	4326	3610	3361	4326
Number of 'diagonal' struts	—	1830	2112	2163
Number of cross bracing ties	4326	—	—	—
Number of spring loaded columns	2163	—	—	—
Number of 'in-space' structural connections	8460	2200	900	8460

Figure 23

COMPARATIVE ANALYSIS OF THE THREE CONCEPTS

Figure 24 presents judgment scoring of the three candidate concepts against pertinent evaluation factors. Weighting factors are presented in the final column and are applied prior to summation. In all columns, higher values indicate superiority and lower values inferiority.

The data indicates the Mod-PETA to be the superior concept despite its structural duplication and the relatively greater challenge of manipulating and joining its large modules.

Item	Concept/Study Case			Weighting Factor	Remarks
	DCM (C)	PETA (H/J)	META		
● Shape accuracy					
- as manufactured	5	5	5	8	Flat facetted surfaces on all concepts
- as assembled in space	3	7	3	5	PETA has fewer intermodular joints
- in-space correction	10	10	10	8	All concepts can be "shape tuned"
- effect of time	4	7	7	5	DCM structure is in constant stress state
● Thermal stability	9	10	8	8	META has the least structural depth
● Dynamic stability	8	10	8	8	PETA has greatest structural depth
● High strength	9	10	8	8	Tends to be proportional to structural depth
● Density of packaging	7	10	3	10	META has lowest packaging density
● Reliability of deployment	9	8	10	8	PETA modules are few but more complex
● Reliability of assembly	5	5	5	8	DCM and META very repetitive. PETA more complex
● Ease of assembly	8	5	8	10	PETA modules are large
● Minimized assembly time	5	5	5	10	All require prolonged on-orbit time
● Minimized support equipment	5	5	5	8	All concepts require sophisticated provisions
● Low cost					
- fabrication	3	7	10	8	DCM has largest component part count
- in-space assembly	7	10	3	10	PETA requires fewest orbiter flights
● Surface continuity	10	5	10	5	PETA requires surface joining at interfaces
● Low total weight	8	9	10	5	META is lightest
Total	**899**	**1000**	**892**		

Figure 24

ELECTROMAGNETIC ANALYSIS

FOR LARGE REFLECTOR ANTENNAS

M. C. Bailey

NASA Langley Research Center

Geometric-optics aperture-integration is the basic technique selected for computing the radiation pattern of a reflector antenna. Using the feed pattern as a weighting factor, together with ray-tracing, the tangential electromagnetic field is found at many points in an aperture plane parallel to the y-z plane. Numerical integration of the aperture field yields the secondary far-field radiation pattern.
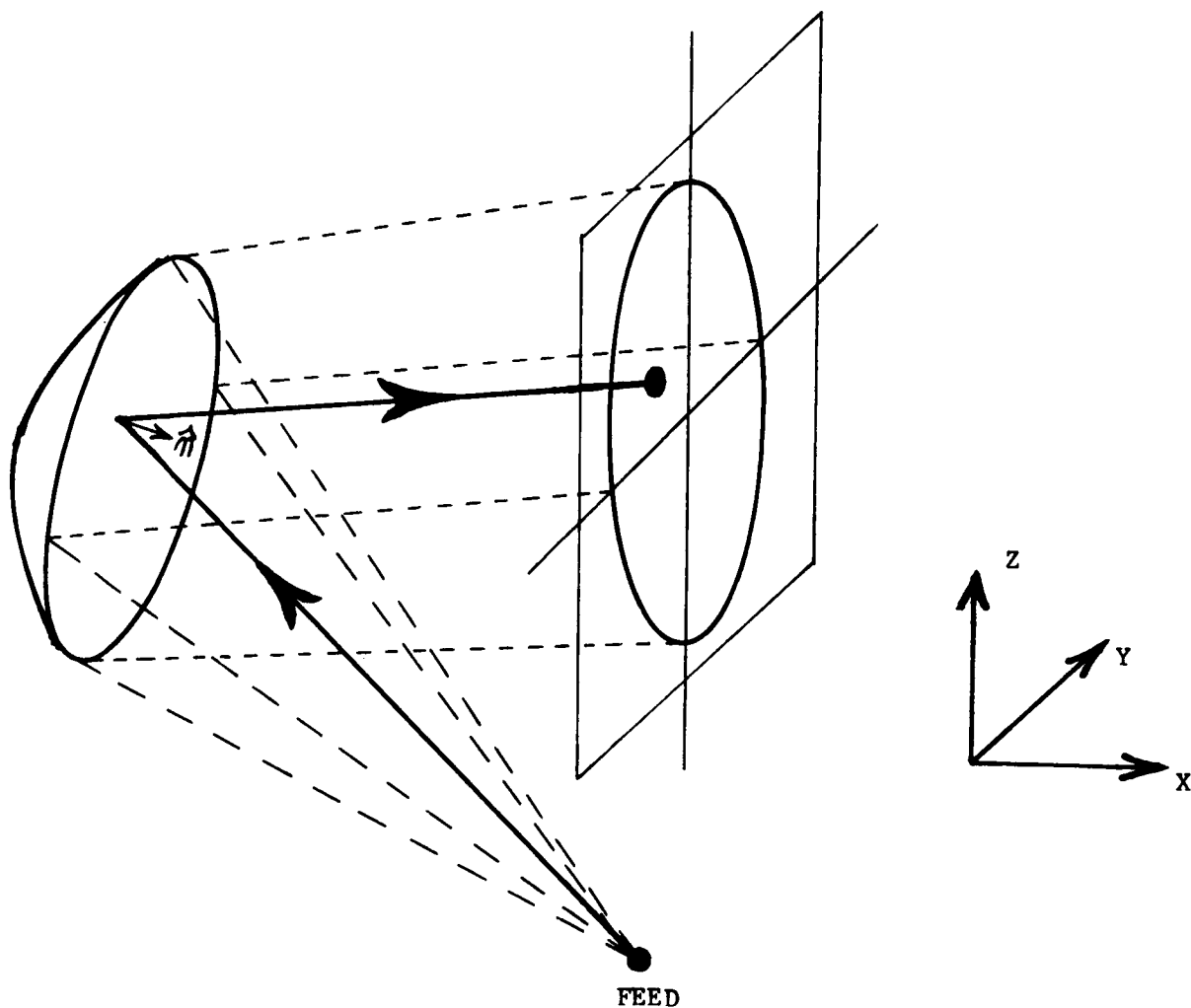
FEED

A variety of different reflector antenna geometries can be analyzed using the geometric-optics aperture-integration technique, which requires that the feed primary pattern and a description of the reflector surface be known. The present capability of the Langley computer codes for reflector antennas is listed here. Codes have been developed for reflectors whose surfaces are characterized by (a) an equation, (b) segments, (c) points in a uniform rectangular lattice arrangement, and (d) points distributed nonuniformly over the surface.

REFLECTOR ANTENNAS

ANALYTICAL SURFACE

Paraboloidal
Spherical
Ellipsoidal
Planar
Parabolic Cylinder

SEGMENTED SURFACE

Segments can be any of above analytical surfaces
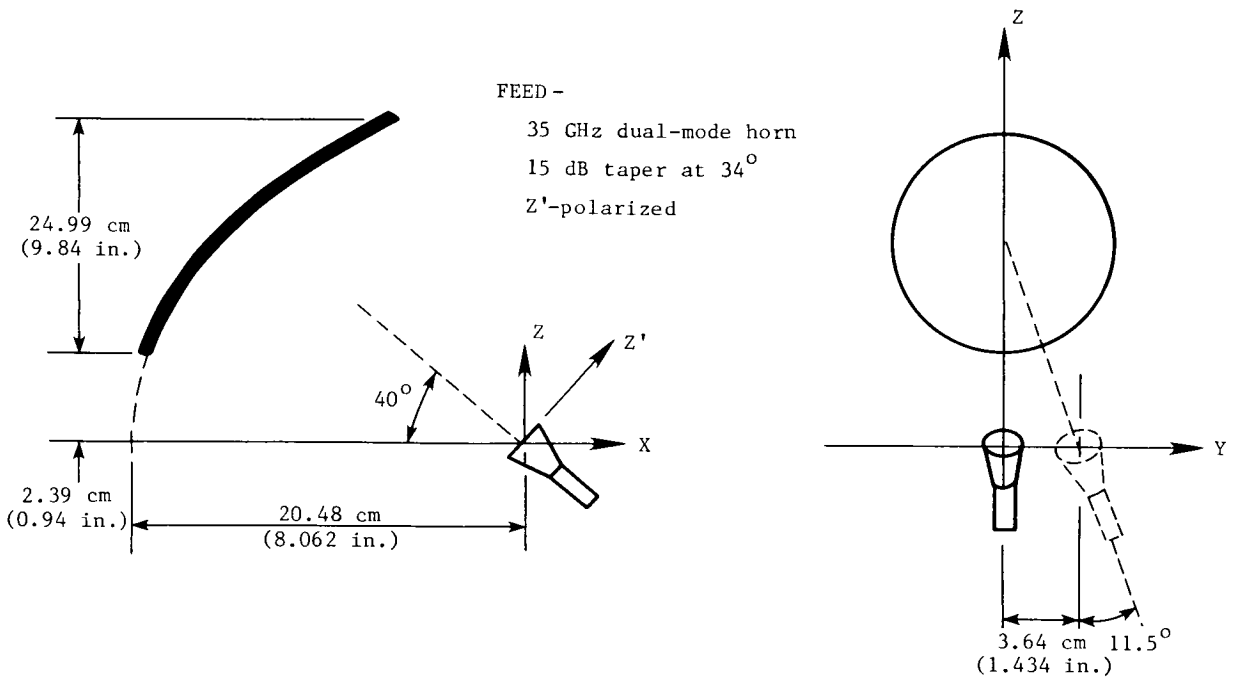
SLIGHTLY DISTORTED SURFACE

A smooth perturbation of above analytical surfaces characterized by an orderly arrangement of points

ARBITRARY SURFACE

A smooth surface characterized by an unordered arrangement of points

OFFSET PARABOLOIDAL REFLECTOR GEOMETRY

An offset paraboloidal reflector with a focal length of 20.48 cm (8.062 in.) and projected aperture diameter of 24.99 cm (9.84 in.) was fabricated and tested at 35 GHz to verify the computer code for a reflector antenna with an analytically defined surface.

FEED –

    35 GHz dual-mode horn

    15 dB taper at 34°

    Z'-polarized

24.99 cm
(9.84 in.)

2.39 cm
(0.94 in.)

20.48 cm
(8.062 in.)

40°

Z

Z'

X

Z

Y

3.64 cm   11.5°
(1.434 in.)

OFFSET PARABOLOIDAL REFLECTOR

The offset paraboloidal reflector is illuminated by a 35 GHz dual-mode horn. The horn is mounted on a 2-axis vernier positioner for precision adjustment of the feed location.

The reflector surface was measured at many points over a rectangular lattice using a 3-axis Validator. The coordinates of selected surface points were used later to verify the computer codes for reflectors characterized by ordered and unordered arrangement of points.
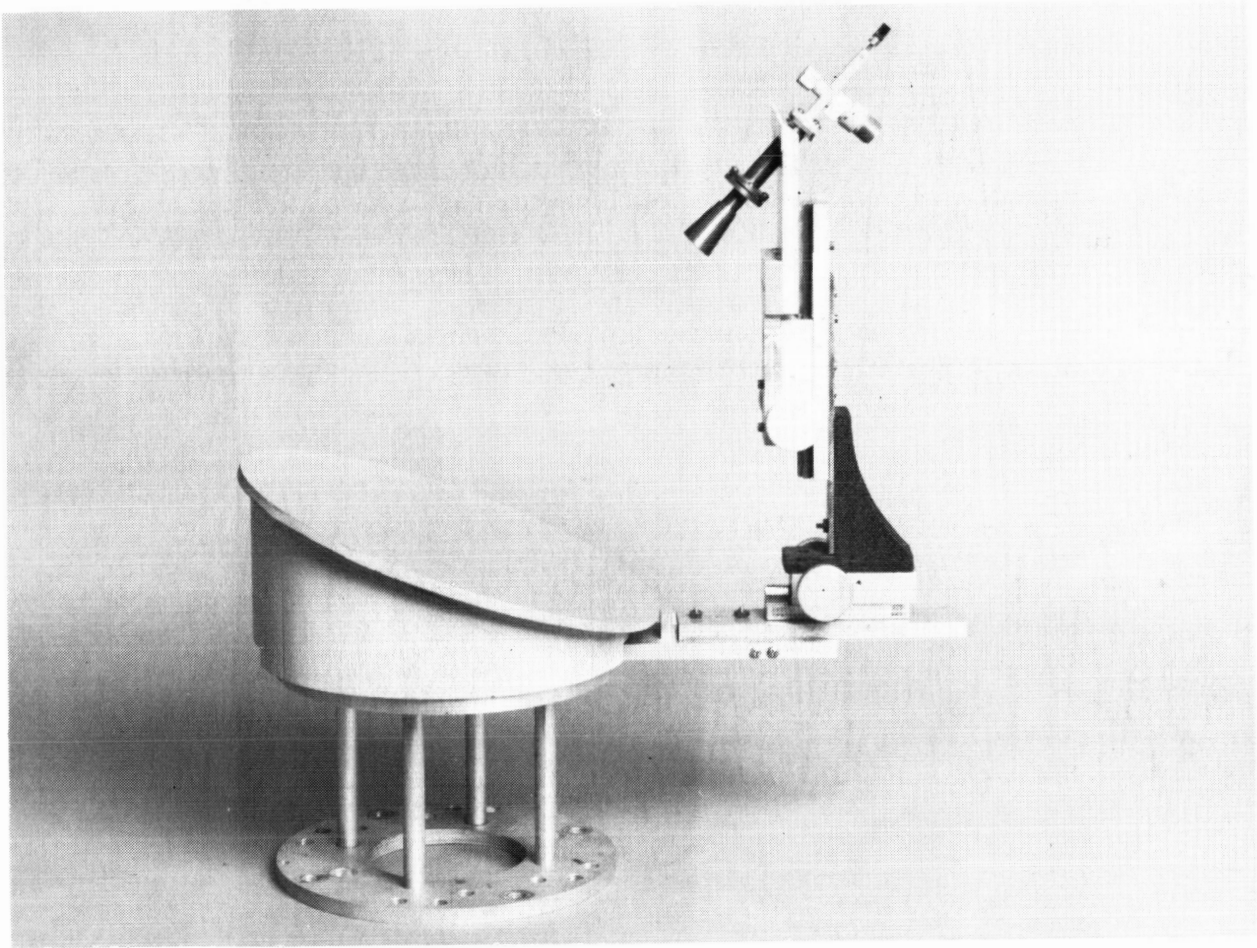
RADIATION PATTERN FOR OFFSET PARABOLOIDAL REFLECTOR

A comparison is made between the measured and calculated radiation pattern in the H-plane (x-y plane) for the offset paraboloidal reflector with the feed horn at the focal point. The calculations were obtained from the computer code for a perfect paraboloidal reflector.
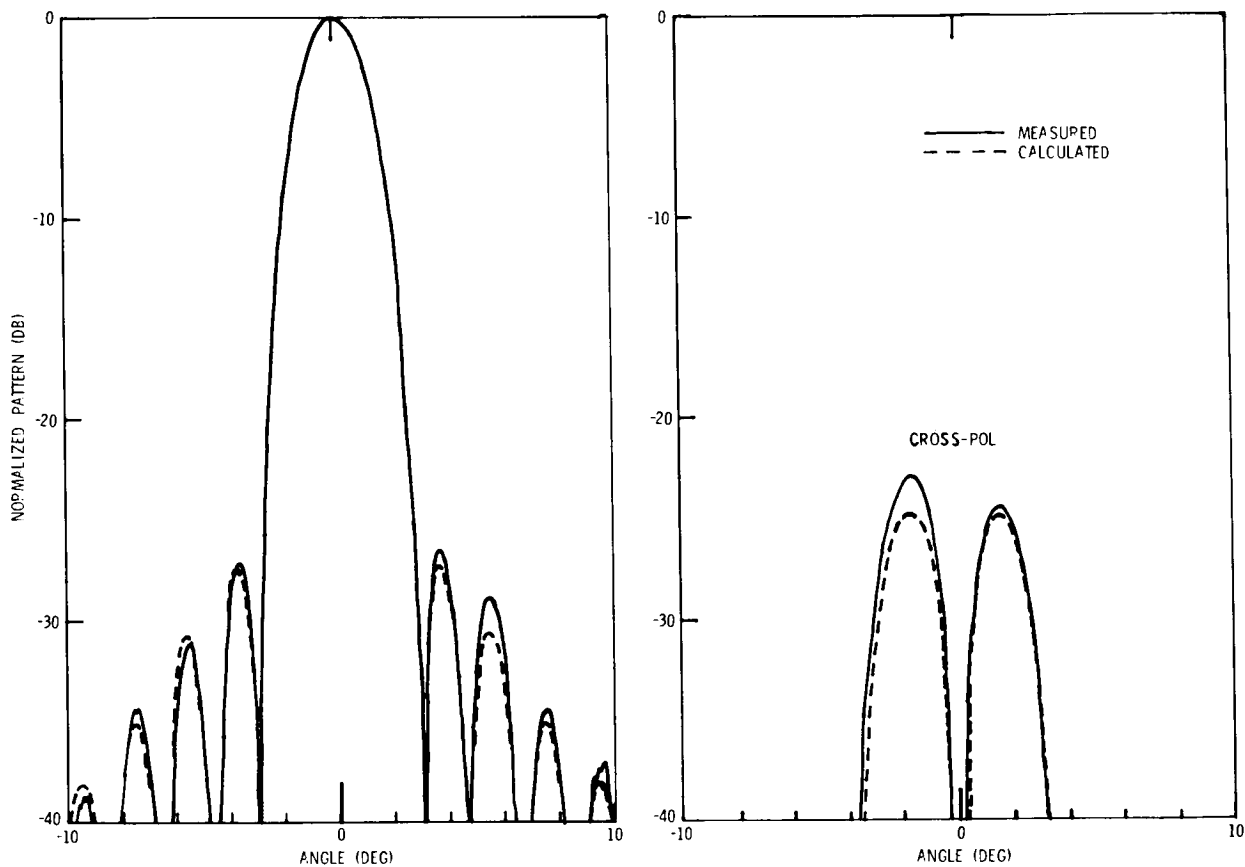
RADIATION PATTERN FOR OFFSET PARABOLOIDAL REFLECTOR (8.5° scan)

Comparison between measured and calculated patterns also verifies the computer code when the feed is laterally displaced for H-plane beam scan.
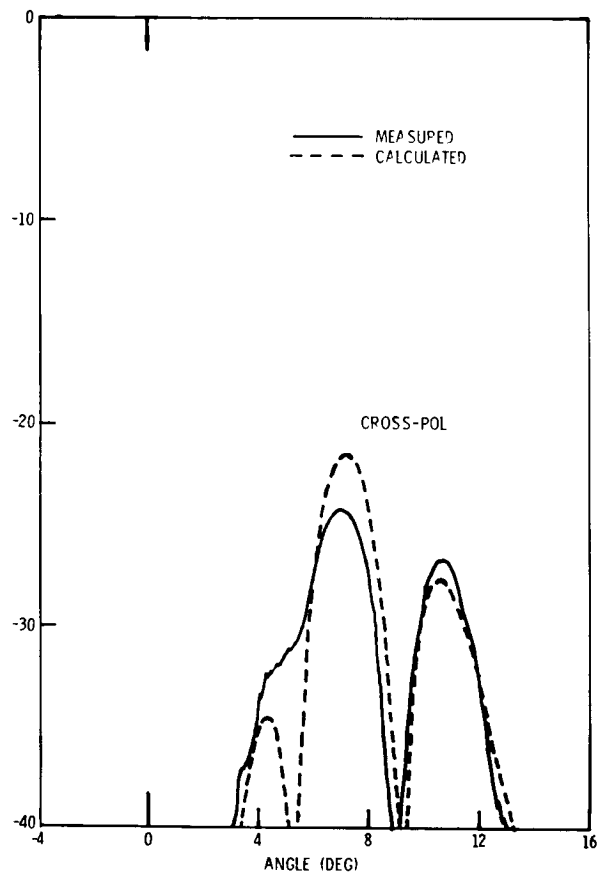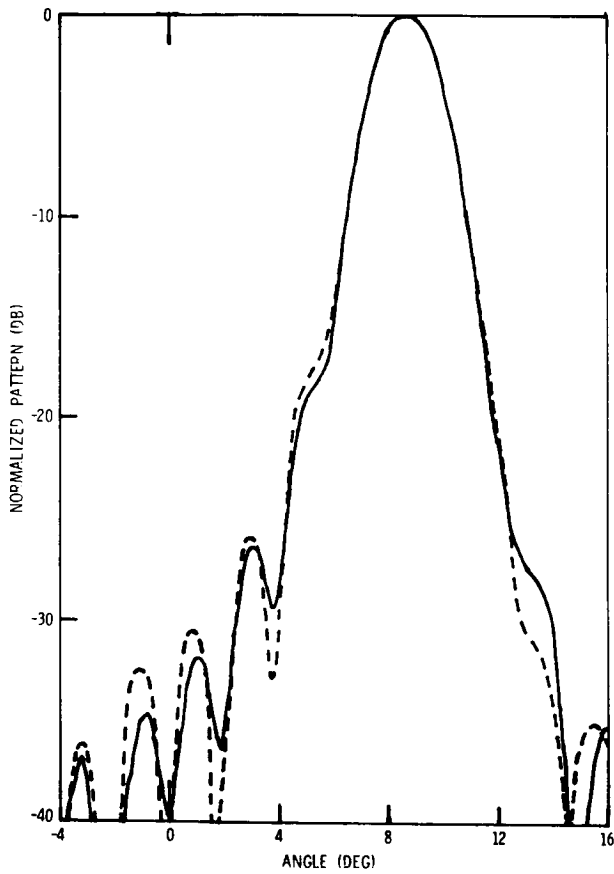
OFFSET FACETED SPHERICAL REFLECTOR GEOMETRY

An offset spherical reflector with a 60.9 cm (24 in.) radius of curvature was fabricated in which the spherical surface is approximated by 54 flat triangular segments. The faceted spherical reflector was illuminated by a 35 GHz dual-mode horn with the electric field vector polarized in the y-direction.

FEED-

35 GHz dual-mode horn

16 dB taper at 23°

Y-polarized

26.9 cm
(10.6 in.)

7.4 cm
(2.9 in.)

40°

21°

29.2 cm
(11.5 in.)

60.9 cm
(24.0 in.)

Z

X

Z

Y
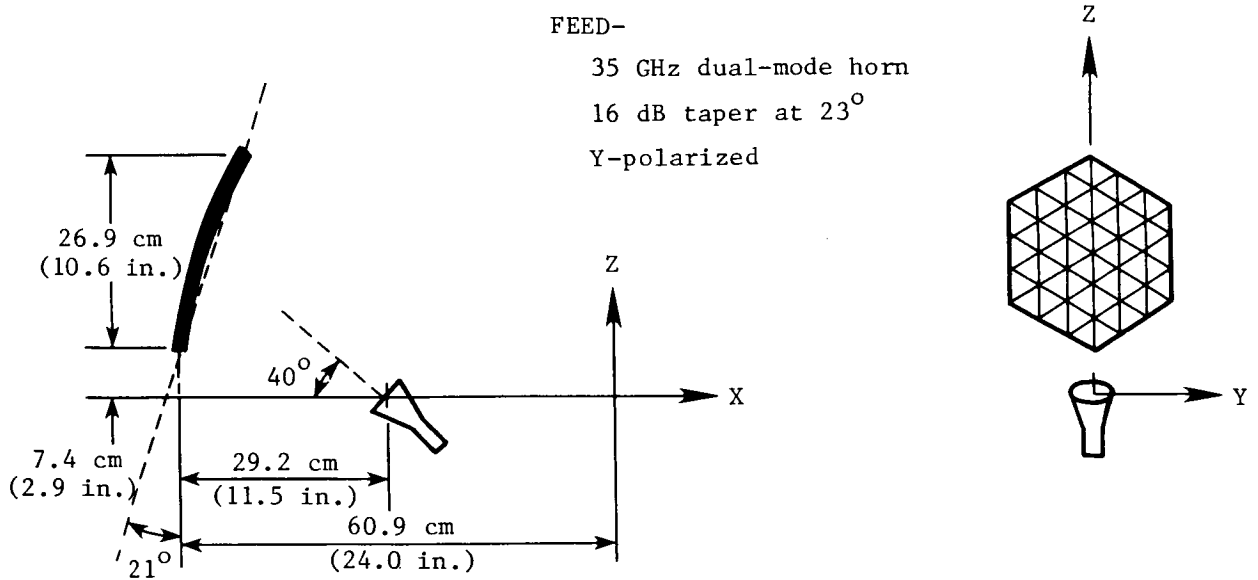
OFFSET FACETED SPHERICAL REFLECTOR

The 35 GHz faceted spherical reflector was used to experimentally verify the segmented reflector computer code for radiation pattern prediction.
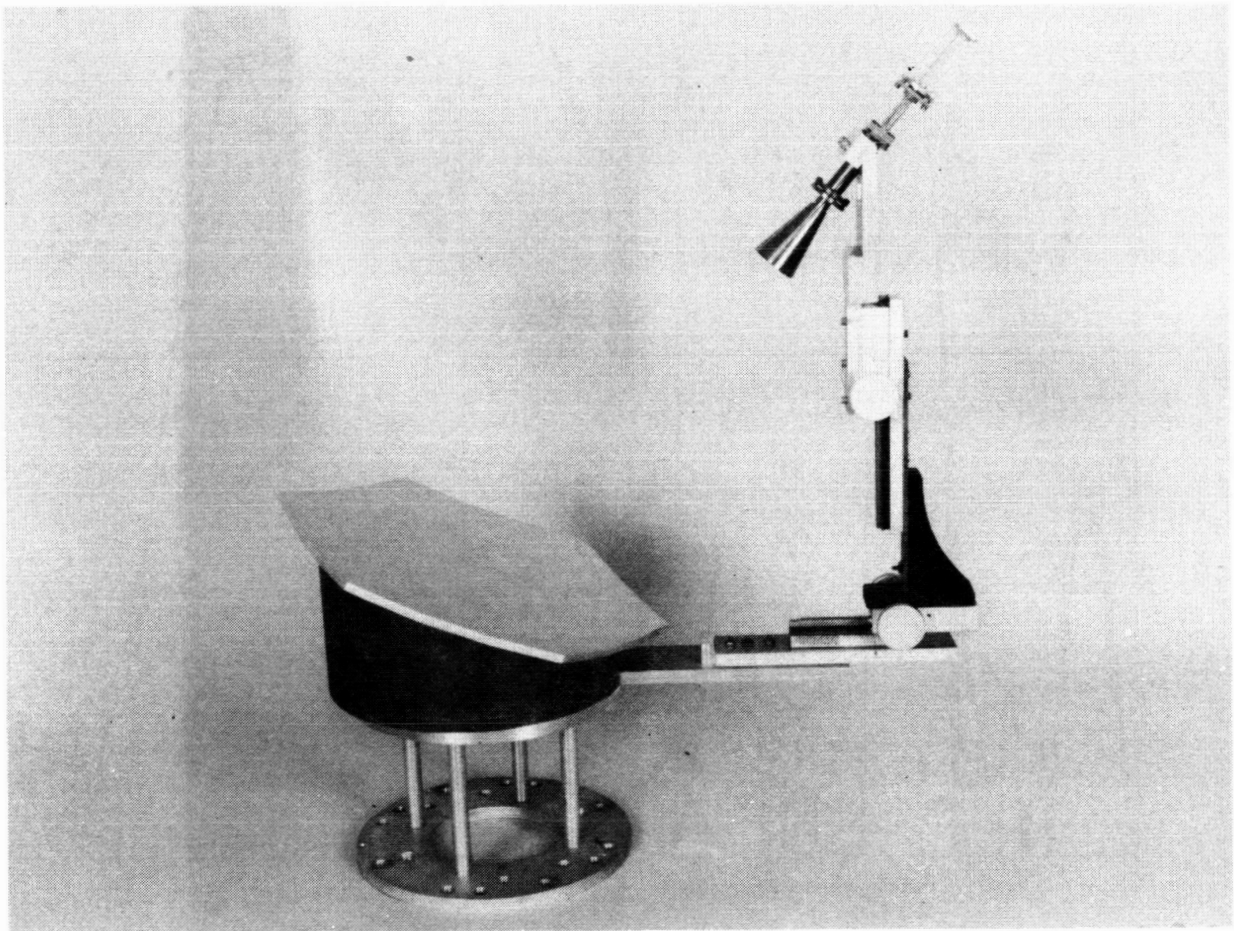
RADIATION PATTERNS FOR OFFSET FACETED SPHERICAL REFLECTOR

A comparison between the E- and H-plane calculated and measured patterns for the 35 GHz faceted spherical reflector verifies the accuracy of the computer code for segmented reflectors. The computer model also accurately predicts the occurrence of a grating lobe effect in one plane due to the periodic nature of the facets.
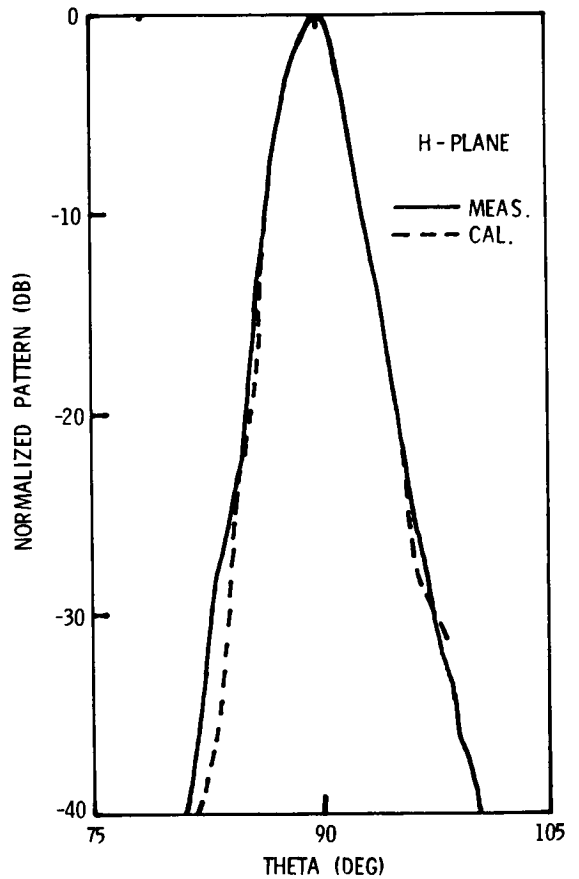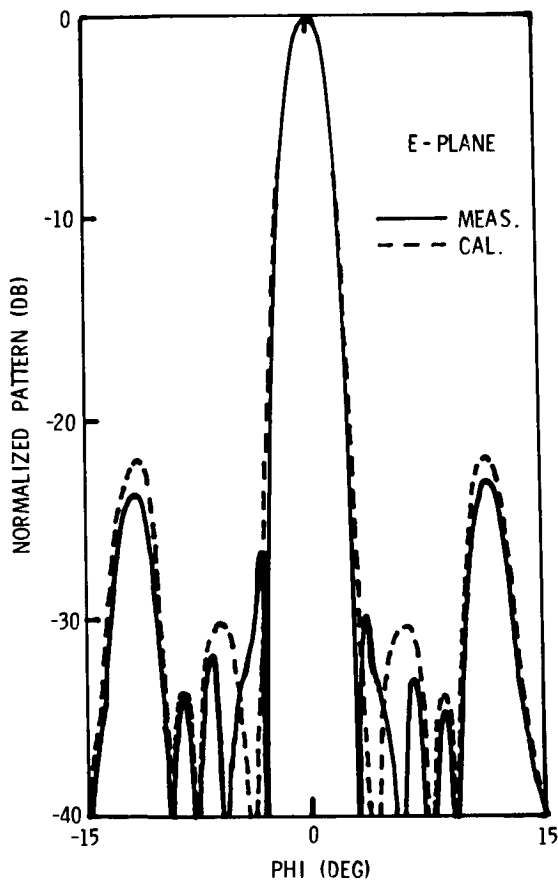
DISTRIBUTION OF POINTS USED TO
CHARACTERIZE SURFACE OF OFFSET REFLECTOR

The surface of the 35 GHz offset paraboloidal reflector was measured at 1844 points. Of these, 200 were selected as shown to be used in the computer code for an arbitrary reflector surface described by a nonuniform arrangement of points. No attempt was made to optimize the number or distribution of points, although 200 was the number selected since that appears to be a realistic number of targets for an in-orbit surface measurement system.
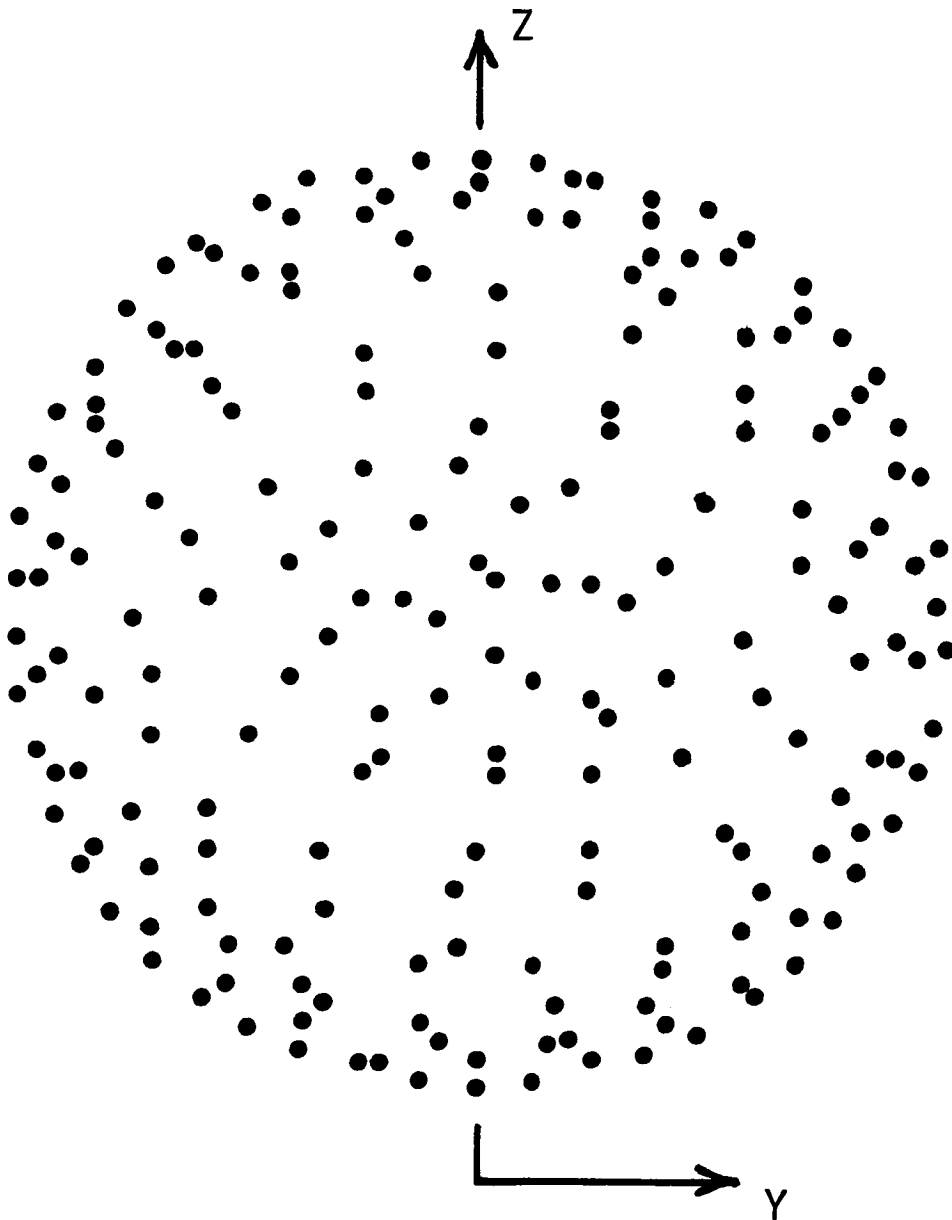
RADIATION PATTERN FOR OFFSET REFLECTOR CHARACTERIZED
BY NONUNIFORM DISTRIBUTION OF POINTS

A comparison is made between the measured E- and H- plane patterns of
the 35 GHz offset paraboloidal reflector and the calculated patterns for the
same reflector using the 200 points to describe the surface. The accuracy
of the computer prediction is quite good considering that the only descrip-
tion of the surface was the coordinates of a finite number of points on the
reflector. The results indicate the possibility of acceptable accuracy in the
prediction of electromagnetic performance for arbitrarily distorted reflectors
using the coordinates of a practical number of measured points. An
optimization of the number and distribution of points, and experimental
verification for a distorted reflector are planned.
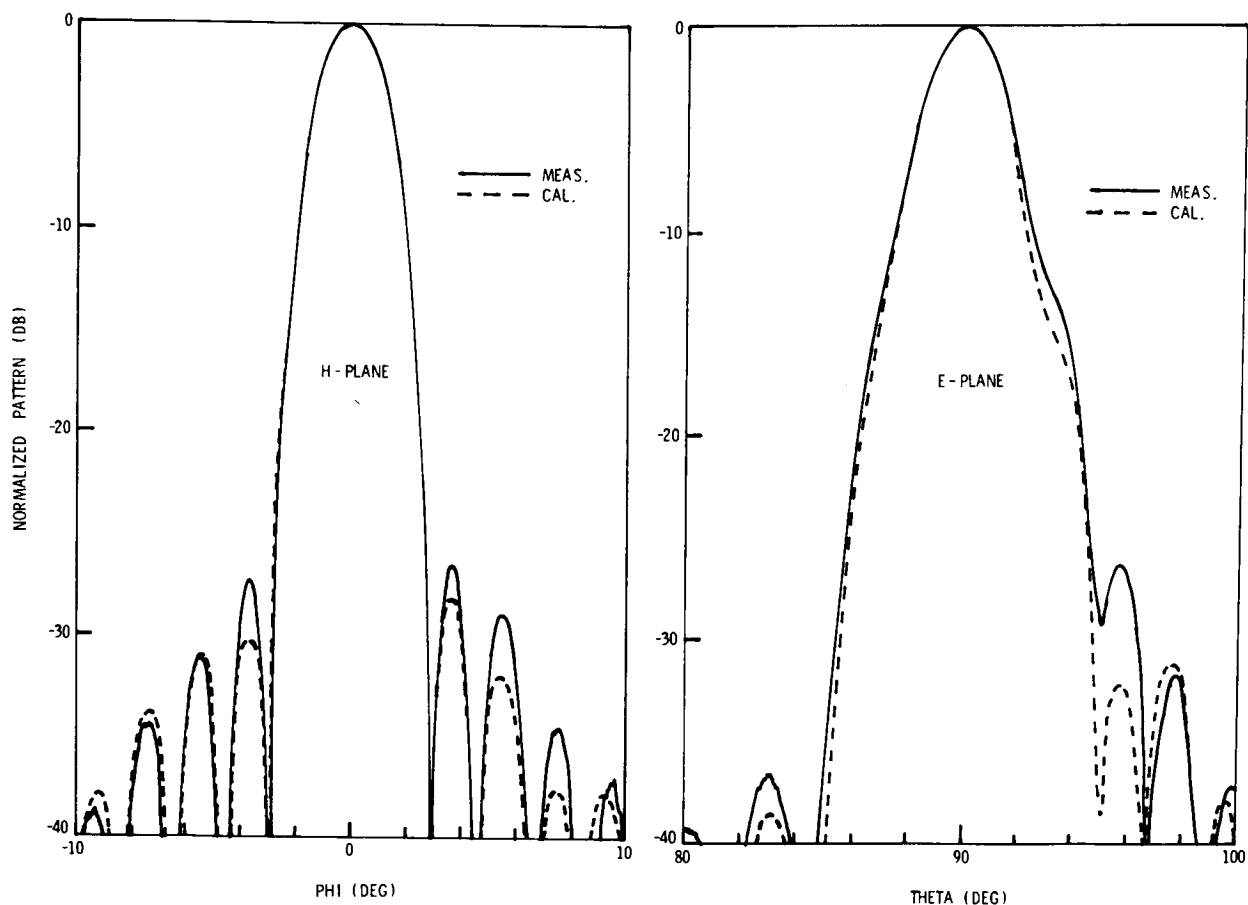
REFLECTOR ANTENNA ANALYSIS
(PLANNED ACTIVITY)

DIFFRACTION EFFECTS

    Reflector edges
Objects in aperture (cables, feed, etc.)

DUAL REFLECTORS

    Analytically defined surfaces
Surfaces characterized by finite number of points

OPTIMIZATION

    Number and distribution of points for characterizing
arbitrary (distorted) reflector surface

EXPERIMENTAL VERIFICATION

    Distorted reflector
Dual-reflector

SECOND ANNUAL TECHNICAL REVIEW ATTENDEES

NASA Headquarters
Washington, DC

R. F. Carlisle
J. D. DiBattista
F. D. Kochendorfer
S. V. Manson

NASA Langley Research Center
Hampton, VA

I. I. Akpan (ODU)
J. L. Allen, Jr.
Dr. M. S. Anderson
E. S. Armstrong
M. C. Bailey
H. T. Banks (ICASE)
L. J. Bement
D. E. Bowles
W. J. Boyer
M. L. Brumfield
Dr. J. D. Buckley
H. G. Bush
T. G. Campbell
J. E. Canady
Dr. M. F. Card
C. W. Coffee
S. R. Cole
L. J. DeRyder
R. S. Dunning
J. R. Elliott
Dr. L. B. Garrett
J. W. Goslee
W. M. Hall
H. A. Hamer
W. L. Heard, Jr.
B. B. Hefner, Jr.
W. F. Hinson
R. B. Holt
Dr. G. C. Horner
Dr. E. K. Huckins, III
R. L. James, Jr.
L. S. Keafer
C. R. Keckler
F. Kopriver III (Syst. Management Assoc.)
E. B. Lightner
M. J. Long
U. M. Lovelace
R. C. Montgomery
A. K. Noor (GWU)

NASA Langley Research Center
Hampton, VA   (Continued)

B. L. Overman
J. C. Robinson
M. T. Russell
R. A. Russell
A. A. Schy
Dr. J. D. Shaughnessy
W. S. Slemp
R. B. Spiers
Dr. O. O. Storaasli
L. W. Taylor, Jr.
J. E. Walz
Dr. D. J. Weidman
T. M. Weller

NASA Goddard Space Flight Center
Greenbelt, MD

J. Eckerman
J. P. Young

NASA Johnson Space Center
Houston, TX

L. M. Jenkins

NASA Lewis Research Center
Cleveland, OH

C. E. Provencher, Jr.
F. J. Shaker
O. F. Spurlock

NASA Marshall Space Flight Center
Huntsville, AL

Dr. J. Blair
H. J. Buchanan
E. C. Hamilton
J. K. Harrison
J. F. Macpherson
K. Smith
J. Stokes
H. H. Watters

Jet Propulsion Laboratory
Pasadena, CA

C. M. Berdahl
R. S. Edmunds
M. El-Raheb
R. E. Freeland
J. A. Garba
Dr. H. B. Garrett
Dr. E. Heer
Yu-Hwan Lin
G. Rodriguez
Dr. J. G. Smith
S. Z. Szirmay
A. F. Tolivar
W. J. Weber, III

Wright Patterson Air Force Base
WPAFB, OH

J. Pearson
Dr. L. C. Rogers
N. D. Wolf
Lt. C. J. Worsowicz

Naval Research Center
Washington, DC

K. T. Alfriend
F. L. Markley

SAMSO
Los Angeles, CA

Maj. R. Gajewski

Edwards Air Force Base
EAFB, CA

R. Preston

Howard University
Washington, DC

P. M. Bainum
P. Bofah
A. Choudhury
V. K. Kumar
A. S. S. R. Reddy

Rensselaer Polytechnic Institute
Troy, NY

A. A. Desrochers
C. G. Rubeiz

Massachusetts Institute of Technology
Lincoln Laboratory
Lexington, MA

M. Floyd
D. C. Hyland
A. N. Madiwale
G. Sarver

Massachusetts Institute of Technology
Cambridge, MA

Prof. E. F. Crawley
Dr. J. H. Lang

University of Cincinnati
Cincinnati, OH

A. H. Nayfeh

Harris Corporation
Melbourne, FL

H. L. Deffebach
J. W. Mays
D. C. Montgomery
J. W. Shipley
W. B. Stevens
M. Sullivan

Aerospace Corporation
Los Angeles, CA

G. N. Smit

Aerospace Corporation
El Segundo, CA

E. M. Polzin

Vought Corporation
Dallas, TX

W. E. Agan
G. S. Bumgarner
R. J. French
J. J. Pacey

Kentron Incorporated (LaRC)
Hampton, VA

E. P. Brien
R. E. Calleson
J. K. Jensen
R. W. LeMessurier
A. Taylor
R. E. Wallsom

Bendix Field Engineering
  Corporation (GFSC)
Greenbelt, MD

G. T. Foote

The Boeing Company
Seattle, WA

C. T. Golden
E. E. Spear
R. G. Vos
W. J. Walker

The Boeing Company
Hampton, VA

W. E. Parker

Vigyan Research Associates
Hampton, VA

S. M. Joshi

INTELSAT
Washington, DC

Dr. B. N. Agrawal
W. W. Dorsey

TRW Systems
Redondo Beach, CA

J. S. Archer
J. T. Bennett
Dr. R. Gluck
R. S. Neiswander
R. Van Vooren

Grumman Aerospace
Bethpage, NY

F. Austin
L. H. Hemmerdinger
C. A. Paez
J. L. Schultz
W. E. Simpson

Martin Marietta
Denver, CO

A. L. Brook
J. Bunting
J. V. Coyner, Jr.
C. E. Farrell
A. Fehr
W. J. Gardner
R. B. Rice, Jr.
F. R. Schwartzberg

General Dynamics/Convair
San Diego, CA

J. W. Beatty
R. H. Thomas

Lockheed Missiles and Space Company
Sunnyvale, CA

G. G. Chadwick
H. Cohan
Dr. J. Y. L. Ho
R. R. Johnson
W. B. Pruitt
R. M. Vernon
A. A. Woods

Barnes Engineering
Stamford, CT

P. W. Collyer
S. C. Spielberger
K. A. Ward

Honeywell
Minneapolis, MN

T. B. Cunningham
C. W. Farnham
C. S. Greene

Honeywell
St. Petersburg, FL

R. P. Singh

C. S. Draper Laboratories
Cambridge, MA

E. Fogel
J. G. Lin
K. Soosaar

Rockwell International
Downey, CA

H. S. Greenberg
J. A. Roebuck

Astro Research
Carpinteria, CA

J. M. Hedgepeth

MRJ, Incorporated
Fairfax, VA

R. D. Jones

The Analytic Sciences Corporation
Reading, MA

L. E. Mabius

Systems, Science and Software
La Jolla, CA

I. Katz

Systems & Applied Sciences
Riverdale, MD

J. Forbush

McDonnell Douglas
Huntington Beach, CA

F. C. Runge

General Research Corporation
Santa Barbara, CA

D. J. Mihora

General Electric
Philadelphia, PA

H. A. Brust
W. J. Downs
P. Foldes
R. V. Greco
J. J. McClinchey
A. Monfort
B. N. Ordonio

Essex Corporation (MSFC)
Greenbelt, MD

N. Shields

Scientific-Atlanta
Crofton, MD

R. Mauck

Palo Alto Research Laboratory
Lockheed Missiles and Space Company
Palo Alto, CA

M. G. Lyons

1. Report No. NASA CP-2168	2. Government Accession No.	3. Recipient's Catalog No.
4. Title and Subtitle LARGE SPACE SYSTEMS TECHNOLOGY - 1980 Volume II - Systems Technology		5. Report Date February 1981
		6. Performing Organization Code 506-62-43-05
7. Author(s) Frank Kopriver III, compiler		8. Performing Organization Report No. L-14219
		10. Work Unit No.
9. Performing Organization Name and Address NASA Langley Research Center Hampton, VA 23665		11. Contract or Grant No.
		13. Type of Report and Period Covered Conference Publication
12. Sponsoring Agency Name and Address National Aeronautics and Space Administration Washington, DC 20546		14. Sponsoring Agency Code

15. Supplementary Notes

Frank Kopriver III: Systems Management Associates, Hampton, Virginia

16. Abstract

This document is a compilation of the papers presented at the Second Annual Large Space Systems Technology (LSST) Review at the Langley Research Center. The research was supported in Fiscal Year 1980 by the LSST Program Office and the Materials and Structures Section, Research and Technology Division, of the Office of Aeronautics and Space Technology. The review provided government, university, and industry personnel with an opportunity to exchange information, to assess the present status of technology developments in large space systems, and to plan the development of new technology for large space systems. These papers were divided into three major areas of interest: (1) technology pertinent to large antenna systems, (2) technology related to large space platform systems, and (3) base technology applicable to both antenna and platform systems. Design studies, structural testing results, and theoretical applications are presented with accompanying validation data. These research studies represent state-of-the-art technology that is necessary for the development of large space systems. A total systems approach including controls, platforms, and antennas is presented as a cohesive, programmatic plan for large space systems.

17. Key Words (Suggested by Author(s)) Large space systems Space platform systems Large antenna systems	18. Distribution Statement Unclassified - Unlimited Subject Category 15	
19. Security Classif. (of this report) Unclassified	20. Security Classif. (of this page) Unclassified	21. No. of Pages 196	22. Price A09